

Daniel Kraft

A Level-Set Framework for Shape Optimisation

Dissertation

zur Erlangung des akademischen Grades

Doktor der Naturwissenschaften

an der Naturwissenschaftlichen Fakultät
der Karl-Franzens-Universität Graz

Erster Gutachter:

Ao.Univ.-Prof. Mag.rer.nat. Dr.techn. Wolfgang Ring

Institut für Mathematik und Wissenschaftliches Rechnen,
Karl-Franzens-Universität Graz

Zweiter Gutachter:

Prof. Dr. Michael Ulbrich

Lehrstuhl für Mathematische Optimierung,
Technische Universität München

Graz, am 30. November 2015

(This version includes minor corrections. The official submission was made on September 28th, 2015,
and the corresponding document can be retrieved from the library of the University of Graz.)

Abstract

The level-set method is widely employed for a range of problem settings, including shape optimisation and free-boundary problems. It allows for a natural and very flexible description of shapes and changes to them. Most of the time, however, it is applied for shape optimisation without a sound justification. In this thesis, we build a solid theoretical framework for shape optimisation using the speed method in the level-set context. Particular focus is put on the connection between the classical level-set equation and the theory of optimal control. This connection allows us to interpret the level-set equation as a Hamilton-Jacobi-Bellman equation and, in consequence, express the shape evolutions in terms of a Hopf-Lax formula. This forms a strong theoretical justification for Sethian's Fast Marching Method and our generalised Composite Fast Marching. Furthermore, based on this representation, we are also able to derive new results about shape-sensitivity analysis, non-fattening and other questions of general interest. We develop a complete gradient-descent method and apply it to image segmentation and PDE-constrained shape optimisation. In the context of this gradient descent, we also discuss ways to handle geometric constraints. The gradient descent is, however, prone to the well-known "zig-zag behaviour". To avoid this issue, we propose also a novel method that can be interpreted as a self-consistent gradient flow and is much more efficient. Main components of our numerical code are released as free software in an extension package for GNU Octave.

Keywords: Level-Set Method, Shape Optimisation, Speed Method, Hopf-Lax Formula, Fast Marching Method, Shape-Sensitivity Analysis, Geometric Constraints, PDE-Constrained Optimisation

Kurzzusammenfassung

Für viele Probleme mit freiem Rand und der Formoptimierung lässt sich die Niveaumengenmethode erfolgreich einsetzen, um auf natürliche Art und Weise Geometrien, Formen und ihre zeitliche Evolution mathematisch zu beschreiben. In den meisten Anwendungen wird die Methode allerdings ohne ausreichende theoretische Rechtfertigung benutzt. Mit dieser Arbeit möchten wir eine solide theoretische Basis für Formoptimierung mit der Geschwindigkeitsmethode und Niveaumengen schaffen. Unsere Ergebnisse basieren auf einer Interpretation der klassischen Levelset-Gleichung als Hamilton-Jacobi-Bellman-Gleichung eines Kontrollproblems, wodurch wir eine Hopf-Lax-Darstellungsformel für die geometrischen Evolutionen herleiten können. Dieses Ergebnis liefert nicht nur eine starke theoretische Grundlage für Sethians Fast-Marching-Methode und unsere verallgemeinerte Composite-Fast-Marching-Methode, sondern kann auch verwendet werden, um neue theoretische Ergebnisse zu beweisen. Im Speziellen können wir damit einen neuen Zugang zur Analyse von Formsensitivität aufbauen, neue Ergebnisse für Non-Fattening herleiten und weitere grundlegende Fragen, die sich in unserem Kontext ergeben, beantworten. Wir wenden unsere Erkenntnisse auch an, um ein vollständiges Gradientenabstiegsverfahren für Formoptimierung zu implementieren. Dieses Verfahren haben wir sowohl für Bildsegmentierung als auch Formoptimierung mit Differentialgleichungsnebenbedingungen getestet. Zusätzlich besprechen wir auch, wie man geometrische Nebenbedingungen in unser Verfahren einbauen kann, und entwickeln eine gänzlich neue, effizientere Optimierungsmethode, die als selbst-konsistenter Gradientenfluss interpretiert werden kann. Wesentliche Teile unseres numerischen Codes sind als freie Software in einem Erweiterungspaket für GNU Octave veröffentlicht.

Schlagworte: Niveaumengenmethode, Formoptimierung, Geschwindigkeitsmethode, Formsensitivität, Geometrische Nebenbedingungen, Optimierung mit Differentialgleichungsnebenbedingungen

*to my parents Monika and Jochen,
who ignited my interest in science and mathematics;*

*and to my wife Ines,
who keeps supporting me nevertheless*

Acknowledgements

I would like to thank my PhD supervisor Wolfgang Ring of the University of Graz for his support during all stages of research for this thesis. He posed the right research questions to lead me into this very fascinating and interesting field, and provided valuable insights. His detailed feedback and a thorough proofreading of my drafts allowed me to greatly clarify and improve this thesis during its preparation.

Furthermore, I am also very grateful for the support of all other members of the research training group IGDK 1754, specifically that of my co-supervisor Michael Ulbrich. Also Moritz Keuthen of the Technical University of Munich deserves a special mention, as it was a great pleasure for me to collaborate with him and share ideas on shape-optimisation topics. This work is supported by the Austrian Science Fund (FWF), the International Research Training Group IGDK 1754 and NAWI Graz.

Contents

1	Introduction	7
2	The Level-Set Method	8
2.1	The Level-Set Equation	9
2.2	Viscosity Solutions	10
2.3	The Comparison Principle	16
2.4	Perron's Method and Existence	20
2.5	Basic Solution Properties	24
3	The Hopf-Lax Representation Formula	29
3.1	Constant Speed	29
3.2	Shortest Paths	30
3.3	Mayer's Problem and the Hopf-Lax Formula	37
3.4	Representation of the Level-Set Domains	41
3.5	Numerical Time Evolution	45
3.5.1	Explicit Time Stepping	45
3.5.2	The Fast Marching Method	48
3.5.3	Initialising the Narrow Band	50
3.5.4	Composite Fast Marching	52
4	Conclusions from the Hopf-Lax Formula	57
4.1	Measure-Theoretic Non-Fattening	57
4.2	Shape Sensitivity of Domain Functionals	59
4.3	Lipschitz Continuity with Optimal Constants	62
4.4	Propagation Speed of Perturbations	67
4.5	Distances between the Evolving Surfaces	69
4.5.1	Continuity of the Hausdorff Distance	69
4.5.2	Monotonicity of the Hausdorff Distance	72
4.5.3	The Distance in Measure	74
4.6	Reachable Shapes	75
4.6.1	Density Regularity	75
4.6.2	Speed Rescaling	78
4.6.3	Hölder Continuous Speed Fields	81
5	Perimeter of the Evolving Sets for Constant Speed	86
5.1	Motivating Example for Perimeter Blow-Up	86
5.2	Auxiliary Geometric Results	89
5.3	Estimates of the Perimeter	92
5.3.1	A Bound on the Hausdorff Measure	93
5.3.2	Uniform Bounds	94
5.3.3	Geometric Regularity Properties in the Literature	98
5.4	Outlook	99
5.4.1	Showing Continuity	99
5.4.2	General Speed Fields	100
6	Gradient Descent for Shape Optimisation	102
6.1	Shape Derivatives for the Example Problem	103
6.2	Shape Gradients as Steepest-Descent Directions	104
6.3	The Gradient-Descent Method	107
6.4	Line Search with Wolfe Conditions	108
6.5	Numerical Examples for the Gradient-Descent Method	111
6.6	Geometric Constraints	114
6.6.1	Shape Projections	117
6.6.2	The Relation between Shape and Speed Projections	119
6.6.3	Numerical Experiments	124

7	Self-Consistent Gradient Flow	130
7.1	Self-Consistent Speed Fields	130
7.2	Local Existence of a Fixed Point	131
7.2.1	Lipschitz Continuity of Arrival Times	133
7.2.2	Uniform-Density Estimates	134
7.2.3	Shape-Dependent Quantities	136
7.2.4	Convergence of the Fixed-Point Iteration	139
7.3	A Strategy for Globalisation	141
7.4	Numerical Results	145
7.4.1	Demonstration in 1D	146
7.4.2	The Image-Segmentation Problem	148
7.5	Topological Derivatives	149
7.6	Boundary Length and Mean-Curvature Flow	152
8	PDE-Constrained Shape Optimisation	158
8.1	Computation of the Shape Derivative	158
8.2	Aspects of the Numerical Computation	160
8.2.1	Generation of a Triangular Mesh	160
8.2.2	FEM Discretisation of the State and Adjoint Equations	162
8.2.3	Approximation of the Shape Derivative	164
8.2.4	Discretisation of the Curvature Term	165
8.3	Numerical Results	166
8.3.1	Shape Derivative and Finite Differences	166
8.3.2	Regularisation of an Inverse Problem	168
8.3.3	Convergence of the Gradient Descent	168

1 Introduction

Shape optimisation is a beautiful field of study. It lies at the intersection of various subjects in mathematics, such as geometry, measure theory, optimisation and differential equations. This makes it particularly interesting and challenging from a theoretical point of view. The seminal research on this field has been done by Murat and Simon in [64]. Since then, of course, a wealth of applications ranging from structural optimisation to obstacle problems, computer vision and medical imaging has appeared in the literature. Let us just refer to [73], [75], [49] and [69], respectively, as some works representing these topics.

The main difficulty in shape optimisation is the fact that the concept of a “shape” is complicated and cannot be described by, say, an element of a vector space. Most optimisation methods are based on the latter. It is, thus, imperative to find a convenient way to *encode* geometric information in forms more accessible to mathematical analysis and algorithmic treatment. See Chapter 2 of [30] for a broad discussion of various methods to do so. A lot of works, particularly from engineering fields, use a (finite-dimensional) *parametrisation* of the geometry. With this approach, one can optimise the parameters with suitable schemes for finite-dimensional optimisation. This idea is employed, for instance, in [44] and [68]. These early works directly use the vertices of a triangulation of the domain as optimisation variables. More recent papers (e. g., [82]) employ more sophisticated parametrisations like splines, but are still based on the same idea. Alternatively, it is also possible to characterise a shape as the image of some reference domain under a particular *transformation*. For instance, one can choose the unit sphere as reference domain and consider all shapes that can be produced by a diffeomorphism from it. See Section 2.8 of [78] for a basic discussion. This so-called *method of mappings* leads to optimisation problems that are infinite-dimensional but still staged in a vector space. They are related to optimal-control problems in infinite dimensions, and can be solved with similar techniques. In general, let us refer to the monographs [44], [46], [68], [78] and [86] for a thorough treatment of shape optimisation in this classical context.

Both of these approaches, however, are quite limited in the range of shapes they can describe. Finite-dimensional parametrisation of the shape allows, by its very definition, only a limited number of degrees of freedom. For the transformation approach, one usually requires a certain degree of regularity of the transformation mapping, as it is not possible to solve the optimisation problem otherwise. This usually forbids changes in topology during the transformation. To gain extra flexibility, this work is focused on yet another approach: the *level-set method*. Since it was introduced by Osher and Sethian in [67], it has been widely used for shape optimisation and free-boundary problems. See, for instance, the work in [20], [66], [70], [75], [87] and a series of papers by Allaire, Jouve et al. starting with [2]. While there exists a sound and very general theory of shape evolutions in the level-set context (see [41]), the fundamental connection to shape-sensitivity analysis and optimisation has generally been neglected. Some work has been done in this direction only in recent times, see [14] and [16]. We feel, however, that there still remain a lot of open questions to address.

Consequently, it is the purpose of this work to *build a solid measure-theoretic and geometric foundation for the level-set method in the context of shape optimisation*. We start with a review of the level-set and speed methods in Chapter 2. The classical level-set equation (2) introduced there can be interpreted as the Hamilton-Jacobi-Bellman equation of an optimal-control problem. We exploit this connection in Chapter 3 to derive a *Hopf-Lax representation formula* for the time evolution of shapes in our setting. This follows the idea of Sethian’s Fast Marching Method (see [76]). Employing this result not only for numerics but also for theoretical analysis, we are able to show some new results in Chapter 4. They include, in particular, a very general framework for *shape-sensitivity analysis*. Our results need much weaker assumptions on the regularity of the involved domains and speed fields than classical approaches. This fits very well in our framework since the core advantage of the level-set method itself is precisely to allow a wider class of shapes. Chapter 5 analyses some measure-theoretic properties of our evolving domains (concerning, in particular, their perimeters). This is motivated by the shape calculus of Section 4.2. In Chapter 6, we develop a *gradient-descent method* for shape optimisation based on our level-set framework and give a numerical demonstration on a model for image segmentation. Analysis of this problem is continued in Chapter 7, where we examine a novel optimisation method that is more efficient and can be interpreted as a *self-consistent gradient flow*. Chapter 8, finally, is devoted to the study of PDE-constrained shape optimisation with our methods.

2 The Level-Set Method

This chapter is dedicated to the discussion of the basics of the *level-set method* as introduced in [67]. We use this technique to describe shapes and to evolve them over time in conjunction with the *speed method*. Most of the content of this chapter is well-known in the literature. We review it here, nevertheless, for convenience.

Definition 1. Let $\phi: \mathbb{R}^n \rightarrow \mathbb{R}$ be continuous. Interpreting ϕ as a *level-set function*, it describes the sets

$$\Omega = \{x \in \mathbb{R}^n \mid \phi(x) < 0\} = \phi^{-1}((-\infty, 0)) \quad \text{and} \quad \Gamma = \{x \in \mathbb{R}^n \mid \phi(x) = 0\} = \phi^{-1}(\{0\}).$$

We will also consider time-dependent level-set functions in the future. In this case, $\phi: \mathbb{R}^n \times [0, \infty) \rightarrow \mathbb{R}$ and we write

$$\Omega_t = \{x \in \mathbb{R}^n \mid \phi(x, t) < 0\} \quad \text{and} \quad \Gamma_t = \{x \in \mathbb{R}^n \mid \phi(x, t) = 0\}$$

for the corresponding sets at some time $t \geq 0$.

It is immediately clear that $\Omega \subset \mathbb{R}^n$ is an open set, which most often corresponds to the domain under consideration (i. e., the geometric variable to be optimised). Γ is closed, and clearly $\partial\Omega \subset \Gamma$. Note, though, that the reverse inclusion does not always hold: The function ϕ may have large regions of zero value, which do not belong entirely to the topological boundary of Ω . This effect, if it occurs, is called *fattening*. It is often undesirable in practice and will be further discussed in Section 4.1.

Given a level-set function ϕ , *unique* sets Ω and Γ are defined by Definition 1. It is important to highlight, though, that this is not entirely true the other way round: For a given domain Ω , one can always construct a level-set function that describes it. This ϕ , however, is obviously *not unique*. To get at least one possible level-set function for a given set Ω , a widely used construction is the *signed distance function* sd_Ω :

$$\text{sd}_\Omega(x) = \begin{cases} -\text{dist}(x, \partial\Omega) & \text{for } x \in \Omega^\circ, \\ 0 & \text{for } x \in \partial\Omega, \\ \text{dist}(x, \partial\Omega) & \text{for } x \notin \overline{\Omega}, \end{cases} \quad (1)$$

where $x \in \mathbb{R}^n$ and Ω is assumed to have a non-empty boundary. Here,

$$\text{dist}(x, \partial\Omega) = \inf_{y \in \partial\Omega} |x - y| = \min_{y \in \partial\Omega} |x - y|$$

is the distance of x to the boundary of Ω , either from the inside or the outside. The signed distance function sd_Ω assigns negative values to interior points of Ω , positive values to exterior points and zero to points on the topological boundary. Consequently, it is a prime candidate for the construction of a level-set function of Ω . Also note that the signed distance function of any set is always Lipschitz continuous with constant one. This elementary result can be found in (2.3) on page 268 of [30]. For a detailed discussion of distance functions in general, see also Chapters 6 and 7 of [30]. The following properties are an immediate consequence of the definition in (1):

Lemma 1. Let $A, B \subset \mathbb{R}^n$ be open and ϕ_A, ϕ_B be corresponding level-set functions. We denote the exterior of A by $A^e = \mathbb{R}^n \setminus \overline{A}$. Then

$$\phi_{A^e} = -\phi_A, \quad \phi_{A \cup B} = \min(\phi_A, \phi_B) \quad \text{and} \quad \phi_{A \cap B} = \max(\phi_A, \phi_B)$$

are level-set functions describing A^e , $A \cup B$ and $A \cap B$, respectively. The same holds for the signed distance functions.

With the help of Lemma 1, we can perform basic set operations directly on the level-set functions. This can be useful for the construction of domains in the level-set framework. Before we dive into more involved topics, we want to give two simple examples:

Example 1. For the unit ball $\Omega_1 = B_1(0) \subset \mathbb{R}^2$, the signed-distance function (and thus a possible level-set function) is

$$\text{sd}_{\Omega_1}(x, y) = \sqrt{x^2 + y^2} - 1.$$

An alternative level-set function describing the same domain is

$$\phi_1(x, y) = x^2 + y^2 - 1.$$

With similar constructions, general ellipsoids can be described.

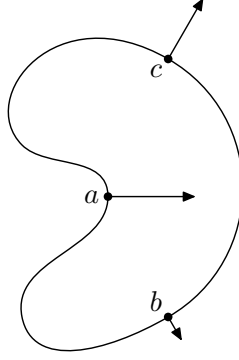


Figure 1: The speed method in normal direction. In the shown situation, $F(a) < 0 < F(b) < F(c)$.

Example 2. The unit square $\Omega_2 = (-1, 1)^2 \subset \mathbb{R}^2$ has

$$\text{sd}_{\Omega_2}(x, y) = \max(|x|, |y|) - 1$$

as its signed distance function. It is possible to construct the signed distance functions of arbitrary polygons by intersecting half spaces. For the latter, the signed distance functions are affine and can be constructed easily. This example also shows that non-smooth domains can be described perfectly well by the level-set framework.

2.1 The Level-Set Equation

In order to perform shape *optimisation*, we are not only interested in describing shapes alone: It is also important to handle *changes* to them. Various approaches exist in the literature to do that. We restrict ourselves to the so-called *speed method*, which we will adapt to fit into the level-set framework. The idea is to transform the boundary of Ω continuously according to some vector field (the “speed field”). Let us assume for our motivation that the boundary of Ω is smooth; this assumption can be dropped in the formal context that will be used afterwards. Since movements in tangential direction to the boundary do not change the geometry itself (they only lead to a reparametrisation), we are only really interested in *normal transformations* of the boundary. Because of this, we can actually use a *scalar* function $F: \mathbb{R}^n \rightarrow \mathbb{R}$ to describe the speed field. For each $x \in \mathbb{R}^n$, $F(x)$ gives the speed with which the boundary of Ω moves in normal direction when it crosses x . Positive $F(x) > 0$ means outward movement (the domain grows), while $F(x) < 0$ corresponds to local shrinking of the domain. See also Figure 1 for a schematic sketch of this situation.

We will always assume that F is Lipschitz continuous and has compact support. The latter assumption is no restriction in practice, since we are mostly interested in bounded domains anyway. This, in particular, also implies that F is bounded. We will denote the corresponding bound by \bar{F} . In other words, we assume that $|F(x)| \leq \bar{F}$ for all $x \in \mathbb{R}^n$. Lipschitz continuity will be necessary to show some results later on, and it also helps to avoid unstable situations:

Example 3. Let $\Omega_0 = (-\infty, -1)$ be the initial domain. We consider the (non-Lipschitz continuous) speed $F(x) = \sqrt{|x|}$. If we let Ω_0 evolve according to this speed field, the upper boundary moves to the right. The time it takes to reach zero can be calculated as

$$t_0 = \int_{-1}^0 \frac{1}{F(x)} dx = 2.$$

This means that Ω_t reaches an equilibrium $(\infty, 0)$ for $t \geq 2$. However, if we disturb this domain to $\Omega' = (-\infty, \epsilon)$, $\epsilon > 0$, it will continue to grow. In other words, the equilibrium is *unstable*. This is very undesirable in practice. Imposing Lipschitz continuity of F avoids this situation, as it guarantees that the moving boundary can never reach zeros of F in finite time. It is only possible to approach them as $t \rightarrow \infty$. This will be shown later in Lemma 17.

Level sets together with this speed method allow for a wide range of changes in the topology of Ω . Merging two connected components of Ω (or two holes) into one is easy. Creating a new component requires splitting it off from the existing domain, while creating a new hole is only possible by wrapping around it. These situations are harder to produce algorithmically in shape optimisation, but nevertheless supported by the underlying level-set method. Examples for both types of topology changes are shown in Figure 2. Note that these topology changes are not possible if the speed method is used in the classical setting, where the initial domain is transformed in a *diffeomorphic way* by flow maps. The regularity of these mappings forbids changes in topology. See also Section 4.6, where we discuss which shapes can be reached by our speed method from a different perspective.

So far, however, we have not discussed how the evolving domains can actually be calculated. This is, of course, a very crucial part of the full picture. Since the domain is described with the level-set method, we actually calculate the evolution of the *level-set functions* $\phi(\cdot, t)$ describing Ω_t for each $t \geq 0$. For an informal derivation (a more rigorous discussion will be done later), we follow a point $x(t) \in \Gamma_t$ as it moves according to the given speed field. Since it follows the boundary of Ω , we know that

$$\phi(x(t), t) = 0$$

must hold for all $t \geq 0$. Assuming that everything is smooth enough, we can apply implicit differentiation to this relation. This gives

$$\nabla \phi(x(t), t) \cdot \dot{x}(t) + \dot{\phi}(x(t), t) = 0.$$

Since the movement of x follows the speed field in normal direction,

$$\dot{x}(t) = F(x) \cdot \frac{\nabla \phi(x(t), t)}{|\nabla \phi(x(t), t)|}.$$

Hence, we arrive at the *level-set equation*

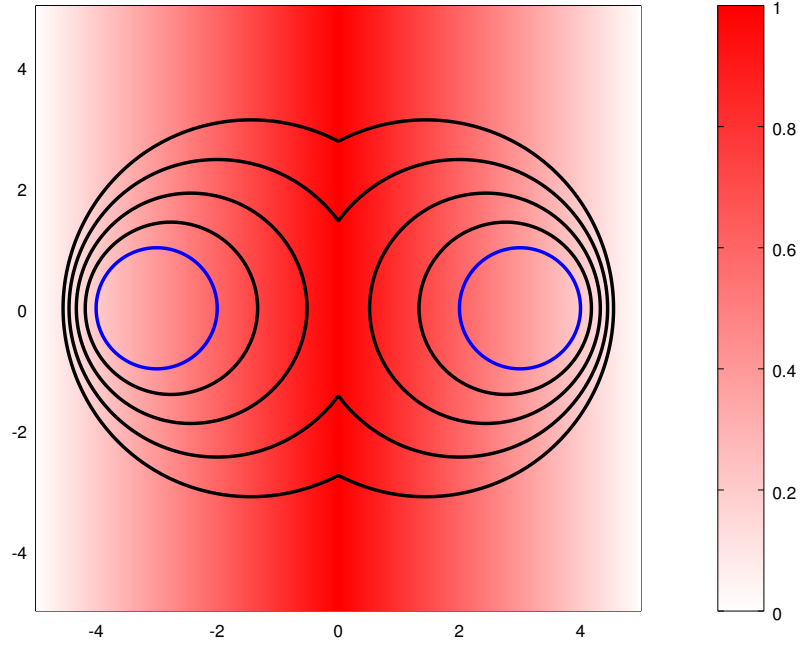
$$\dot{\phi} + F(x) |\nabla \phi| = 0. \tag{2}$$

This non-linear, first-order parabolic differential equation is one of the core subjects for discussion in the following. By solving (2) as an initial-value problem (starting with $\phi(x, 0) = \phi_0(x)$ for $x \in \mathbb{R}^n$ and ϕ_0 describing the initial geometry), we can propagate level-set functions and thus the described geometries according to a chosen speed field F . This forms a natural basis for various approaches to shape optimisation that can be developed. In the following, we will assume that ϕ_0 is Lipschitz continuous. Without losing any geometrical information, we can always choose the (Lipschitz continuous) signed distance function of the initial geometry Ω_0 as ϕ_0 to fulfil this requirement.

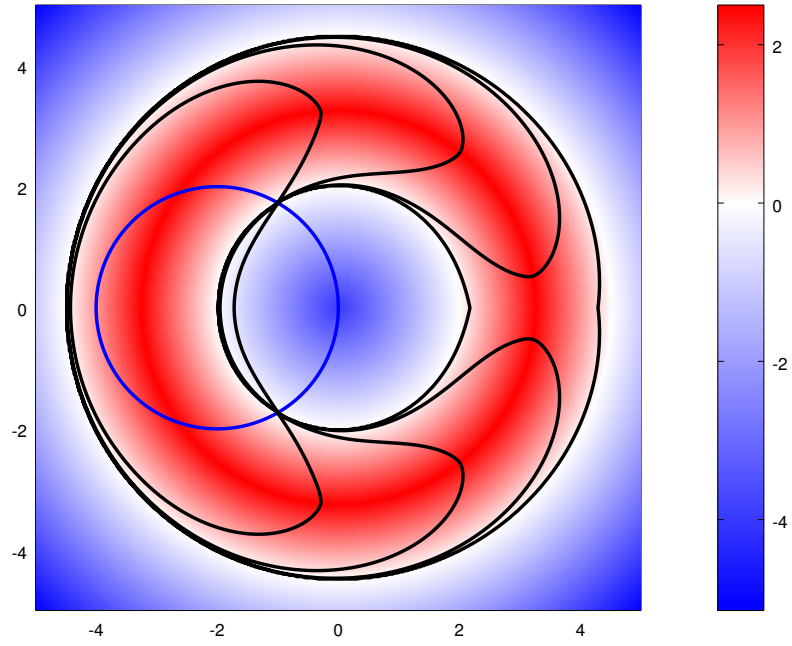
Note that the wider literature describes different variants of (2) as “level-set equation”. A common generalisation is to allow the speed F to depend on the boundary’s curvature (e. g., for mean-curvature flow problems) or other geometrical properties of Ω_t . In this context, the analogue of (2) appears already as (2.13) in [67]. See also Section 1.6 in [41]. In the context of this thesis, we will, however, always consider the level-set equation in the form (2). Allowing F to depend on space but not the geometry itself will be a natural choice and quite sufficient for the situations we are interested in below. Let us just remark that the idea investigated in Chapter 7 can be related to the evolution of Ω with respect to a shape-dependent speed field. We will, however, not use the level-set equation in this context.

2.2 Viscosity Solutions

We now analyse the level-set equation (2) in more detail. In particular, it will turn out that we can not expect classical solutions to this differential equation. Instead, the concept of *viscosity solutions* is the one that yields unique solvability of the level-set equation without requiring too much regularity for the domains we want to describe. To get there, note that signed distance functions are, in general, not differentiable (everywhere in space). They are Lipschitz continuous and thus differentiable almost everywhere according to Rademacher’s theorem (see Theorem 2 on page 81 of [37]), but they usually have kinks or other singularities on a lower-dimensional subset of \mathbb{R}^n . Furthermore, even if we exclude signed distance functions for a moment, we have to assume additional regularity of a domain in order to guarantee smooth level-set functions. We do not want to do this, since the support of less regular domains is, in fact, a big advantage of the level-set method. Hence, we can not require that ϕ should



(a) Joining components.



(b) Building a new hole.

Figure 2: Evolution of an initial domain (blue) at times $t = 1, 2, 3, 4$ (black). F is shown as a heat map in the background. See also Figure 15 and Figure 16.

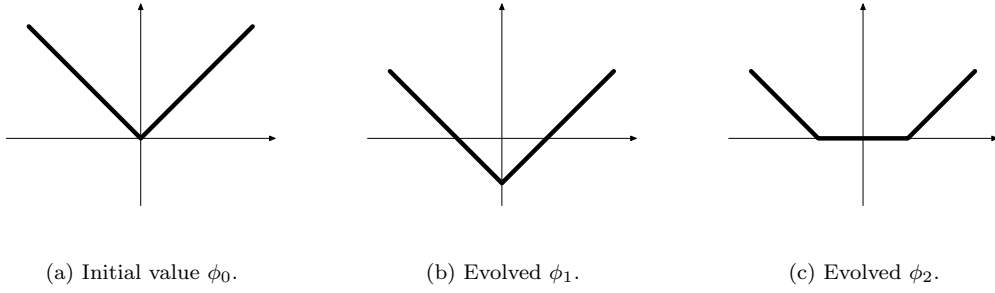


Figure 3: Two almost-everywhere solutions for the initial-value problem in Example 4.

solve (2) in every point in the classical sense. Lifting this requirement, we could demand that ϕ must solve the equation only *almost everywhere*. This seems natural, given the nature of signed distance functions. However, one can easily discover that this requirement is, on the other hand, too lenient: While almost-everywhere solutions of (2) allow non-smooth domains and signed distance functions, they are not unique. This can be seen already by a very simple example:

Example 4. Consider $n = 1$, $\phi_0(x) = |x|$ and set $F(x) = 1$. In this situation, the level-set equation (2) takes the form

$$\dot{\phi}(x, t) = -|\nabla \phi(x, t)|, \quad (3)$$

$x \in \mathbb{R}$ and $t > 0$. It is easy to see that

$$\phi_1(x, t) = |x| - t \text{ as well as } \phi_2(x, t) = \max(|x| - t, 0)$$

are differentiable almost everywhere. They satisfy the initial condition $\phi_1(\cdot, 0) = \phi_2(\cdot, 0) = \phi_0$ and, where they are differentiable, also solve (3). These functions are shown in Figure 3. Similarly, one can actually construct an arbitrary number of distinct almost-everywhere solutions of the initial-value problem defined by (3) and ϕ_0 .

The correct balance is found within the framework of *viscosity solutions*. See [25], [26] and [62]. With this solution concept, non-smooth solutions similar to signed distance functions are allowed, but we also get uniqueness for the solution of the level-set equation. (Which will be shown in Theorem 2 below.) Let us start by defining viscosity solutions:

Definition 2. Let F be given and define $Q = \mathbb{R}^n \times (0, \infty)$ to be the open space-time cylinder. We say that $\phi: Q \rightarrow \mathbb{R}$ is a *viscosity subsolution* of the level-set equation (2) if ϕ is upper semi-continuous and

$$\dot{\psi}(x, t) + F(x)|\nabla \psi(x, t)| \leq 0$$

for each test function $\psi \in C^1(Q)$ and $(x, t) \in Q$ that is a local maximum of $\phi - \psi$. Similarly, a lower semi-continuous ϕ is called a *viscosity supersolution* if

$$\dot{\psi}(x, t) + F(x)|\nabla \psi(x, t)| \geq 0$$

for each ψ and local minimum (x, t) of $\phi - \psi$. If ϕ is both a sub- and supersolution, it is called a *viscosity solution*. In this case, ϕ is continuous.

In this way, we can define a solution of the differential equation (2) without ever making use of derivatives of ϕ . To motivate Definition 2 a bit more, assume for a moment that ϕ actually *is* differentiable at some $(x, t) \in Q$. If we have ψ such that (x, t) is a local extremum of $\phi - \psi$, then

$$\dot{\psi}(x, t) = \dot{\phi}(x, t) \text{ and } \nabla \psi(x, t) = \nabla \phi(x, t)$$

due to the necessary optimality condition. Hence, if ϕ is a viscosity solution according to Definition 2, then (2) is actually fulfilled pointwise whenever ϕ is differentiable. Assuming that ϕ is differentiable almost

everywhere, this implies that viscosity solutions are a stronger concept than almost-everywhere solutions. On the other hand, they are weaker than classical solutions, unless ϕ is differentiable everywhere (in which case both concepts are equivalent).

Note that Definition 2 makes only use of the *derivatives* of the test function ψ , so that shifting ψ by a constant offset does not change anything. Because of this, we will assume, without loss of generality, that $\phi(x, t) = \psi(x, t)$ at the local extremum. Consequently, this means that ψ touches ϕ in (x, t) from above and from below if ϕ is a viscosity sub- and supersolution, respectively. See also Figure 4. Similarly, one can also require that the extrema in Definition 2 are *strict*: If $\phi - \psi$ has a (non-strict) local maximum at $(x, t) \in Q$, then $\phi - \tilde{\psi}$ has a *strict* local maximum at the same point if we define

$$\tilde{\psi}(y, s) = \psi(x, t) + (s - t)^2 + |y - x|^2.$$

The derivatives of ψ at (x, t) are not changed by the added terms. The same argument can, of course, also be applied to the case of a local minimum.

Furthermore, note that Definition 2 actually only relies on the first-order Taylor expansion of ϕ . Consequently, we can rewrite the definition to make this explicit. In order to do so, let us introduce the notion of *semijets*:

Definition 3. Let $\phi: Q \rightarrow \mathbb{R}$ and $(x, t) \in Q$. Then $D^+\phi(x, t)$ is the set of all $(p, a) \in \mathbb{R}^n \times \mathbb{R}$ such that

$$\phi(y, s) \leq \phi(x, t) + a(s - t) + p \cdot (y - x) + o(|s - t| + |y - x|) \quad (4)$$

as $(y, s) \rightarrow (x, t)$. Similarly, $(p, a) \in D^-\phi(x, t)$ if and only if

$$\phi(y, s) \geq \phi(x, t) + a(s - t) + p \cdot (y - x) + o(|s - t| + |y - x|)$$

as $(y, s) \rightarrow (x, t)$. The sets $D^\pm\phi(x, t)$ are called the *first-order (parabolic) semijets* of ϕ at $(x, t) \in Q$.

With these notions, we can now give an alternative definition of viscosity solutions. We will show in Theorem 1 that it is equivalent to Definition 2. This allows us to get rid of the auxiliary function ψ , which will be handy later on.

Definition 4. $\phi: Q \rightarrow \mathbb{R}$ is a viscosity subsolution of (2) if ϕ is upper semi-continuous and

$$a + F(x) |p| \leq 0$$

for all $(x, t) \in Q$ and $(p, a) \in D^+\phi(x, t)$. Similarly, ϕ is a viscosity supersolution if ϕ is lower semi-continuous and

$$a + F(x) |p| \geq 0$$

for all $(x, t) \in Q$ and $(p, a) \in D^-\phi(x, t)$.

If we assume again that ϕ is differentiable at some $(x, t) \in D$, then an immediate consequence of Definition 3 is that

$$D^+\phi(x, t) = D^-\phi(x, t) = \left\{ \left(\nabla\phi(x, t), \dot{\phi}(x, t) \right) \right\} \quad (5)$$

are singletons and “equal” to the classical derivative of ϕ . In this case, Definition 4 implies, as before, that (2) must be fulfilled classically at (x, t) . Note that (5) also holds in the corresponding sense if ϕ is only partially differentiable.

Example 5. To clarify the definitions above, we give an example. For simplicity, we will demonstrate the idea behind semijets for the elliptic, one-dimensional case. I. e., instead of space and time as used above for the parabolic semijets, let us assume that our function depends only on a one-dimensional space variable. This is easier to interpret, and there is no qualitative difference to the parabolic situation of the definitions above. Thus, consider the function $\phi(x) = |x|$. Since ϕ is differentiable everywhere except for $x = 0$, it is clear that

$$D^\pm\phi(x) = \{\phi'(x)\} = \begin{cases} \{-1\} & \text{if } x < 0, \\ \{1\} & \text{if } x > 0. \end{cases}$$

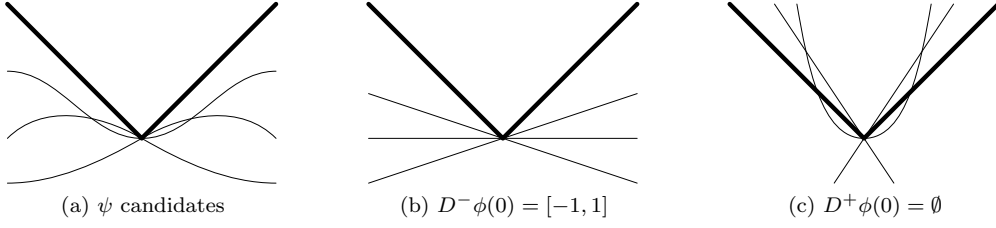


Figure 4: The semijets together with candidates for the function ψ in Definition 2 for the case of Example 5. Here, $\phi(x) = |x|$.

For $x = 0$, we have $D^-\phi(0) = [-1, 1]$. On the other hand, $D^+\phi(0) = \emptyset$. To see this, assume that $p \in D^+\phi(0)$. Then

$$\phi(x) = |x| \leq px + o(x)$$

as $x \rightarrow 0$. Dividing both sides by $|x|$ and taking the limit yields $1 \leq p$ or $1 \leq -p$, depending on the side from which x approaches zero. This, however, can not be fulfilled for both sides at the same time, leading to a contradiction. Possible functions ψ touching ϕ from below (for Definition 2) are shown in Figure 4a. It can be seen in Figure 4b that there are various elements in the semijet $D^-\psi(0)$, corresponding to lines that are entirely below the graph of ϕ . On the other hand, it is not possible to draw any straight line or smooth function that is fully *above* the graph around $x = 0$. See Figure 4c. In general, whenever ϕ has a kink, either the condition for being a subsolution or that for being a supersolution is trivially fulfilled because one of the semijets is empty.

In both definitions of viscosity solutions, the idea is that we work around the problem that derivatives of ϕ may not be defined. This is done by requiring that the differential equation must be fulfilled for some approximation of these derivatives. The approximation, in turn, is given by the semijets for Definition 4 and by a smooth function touching ϕ for Definition 2. We have not yet shown that both definitions are really equivalent. This will be done now. The argument employed is based on Section 7 of [25]. The first step is to get a better grasp of the “small-o error” in (4):

Lemma 2. *Let ϕ be upper semi-continuous, $(x, t) \in Q$ and $(p, a) \in D^+\phi(x, t)$. Then there exists a continuous, non-decreasing function $g: [0, \infty) \rightarrow [0, \infty)$ with $g(r) = o(r)$ as $r \rightarrow 0^+$ and*

$$g(r) \geq \phi(y, s) - \phi(x, t) - a(s - t) - p \cdot (y - x) \quad (6)$$

for all $(y, s) \in Q$ with $|s - t| + |y - x| \leq r$.

Proof. Motivated by (4), we define first

$$\tilde{g}(r) = \max \left\{ (\phi(y, s) - \phi(x, t) - a(s - t) - p \cdot (y - x))^+ \mid (y, s) \in Q, |s - t| + |y - x| \leq r \right\}.$$

The maximum exists, since ϕ is upper semi-continuous and the set of admissible (y, s) is compact if r is small enough. The notation h^+ denotes the positive part of an expression h , see also (23) below. Note that $\tilde{g}: [0, \infty) \rightarrow [0, \infty)$ is, by definition, non-decreasing and $\tilde{g}(r) = o(r)$ as $r \rightarrow 0^+$. It also satisfies (6) already. However, \tilde{g} is not yet necessarily continuous. Thus it remains to construct g as a continuous majorant of \tilde{g} while not violating any other of the required properties.

The idea of the construction is as follows: We divide the domain $[0, \infty)$ into a sequence of intervals, and replace \tilde{g} by its maximum value on each of these intervals (which is achieved on the right-most point since \tilde{g} is non-decreasing). This yields a step function which is still not continuous, but for which we know that the only discontinuities are jumps at the interval boundaries. We can fix these discontinuities by connecting the steps to each other with a continuous line. All of this can be done without violating the $o(r)$ requirement. This construction is sketched in Figure 5 and will now be formalised:

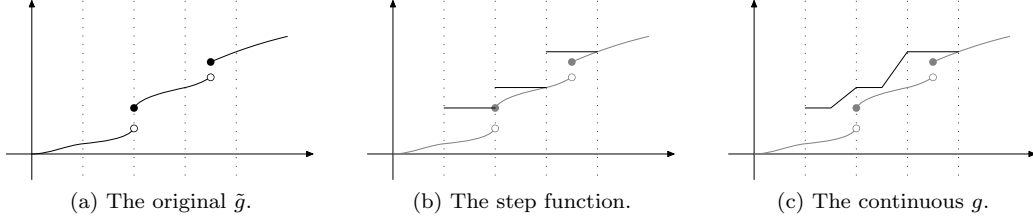


Figure 5: The construction of a continuous majorant g from the discontinuous \tilde{g} in the proof of Lemma 2.

For $k \in \mathbb{Z}$, we define $a_k = 2^k$ and $I_k = [a_k, a_{k+1}]$. This gives the following decomposition of the domain of \tilde{g} :

$$[0, \infty) = \bigcup_{k \in \mathbb{Z}} I_k \cup \{0\}$$

For I_k , we also define its midpoint $m_k = (a_k + a_{k+1})/2$. Then, set

$$g(r) = \begin{cases} 0 & \text{if } r = 0, \\ \tilde{g}(a_{k+1}) & \text{for } r \in [a_k, m_k], \\ \tilde{g}(a_{k+1}) + (\tilde{g}(a_{k+2}) - \tilde{g}(a_{k+1})) \cdot (r - m_k)/(a_{k+1} - m_k) & \text{for } r \in [m_k, a_{k+1}]. \end{cases}$$

It is easy to see that this definition yields a non-decreasing function g that is continuous on $(0, \infty)$. Furthermore, $g \geq \tilde{g}$, so that, in particular, also (6) holds. Note also

$$g(r) \leq \tilde{g}(a_{k+2}) = \tilde{g}(4a_k) \leq \tilde{g}(4r)$$

for $r \in I_k$. This implies $g(r) = o(r)$ for $r \rightarrow 0^+$, and thus also continuity at $r = 0$. Hence, the constructed g has all the required properties. \square

With this auxiliary result, we can now show that both definitions for viscosity solutions are really equivalent. This allows us to use one or the other, depending on what is more convenient at the moment. See also Remarks 2.3 in [26].

Theorem 1. *Let ϕ be upper semi-continuous and $(x, t) \in Q$. Then*

$$D^+ \phi(x, t) = \left\{ \left(\nabla \psi(x, t), \dot{\psi}(x, t) \right) \mid \psi \in C^1(Q), \phi - \psi \text{ has a local maximum at } (x, t) \right\}.$$

The analogous result holds for $D^- \phi(x, t)$ if ϕ is lower semi-continuous.

As an immediate consequence, Definition 2 and Definition 4 are equivalent.

Proof. Assume first that $\psi \in C^1(Q)$ and that $\phi - \psi$ has a local maximum at (x, t) . Without loss of generality, let $\psi(x, t) = \phi(x, t)$. If we set $p = \nabla \psi(x, t)$ and $a = \dot{\psi}(x, t)$, we have to show $(p, a) \in D^+ \phi(x, t)$. For this, we will verify that (4) holds. Since ψ is differentiable, we know that

$$\psi(y, s) = \psi(x, t) + a(s - t) + p \cdot (y - x) + o(|s - t| + |y - x|)$$

as $(y, s) \rightarrow (x, t)$. Together with

$$\phi(y, s) - \psi(y, s) \leq \phi(x, t) - \psi(x, t) = 0$$

for (y, s) close to (x, t) , this implies (4).

Now, conversely, let $(p, a) \in D^+ \phi(x, t)$. We have to construct $\psi \in C^1(Q)$ such that $\nabla \psi(x, t) = p$, $\dot{\psi}(x, t) = a$ and $\phi - \psi$ has a local maximum at (x, t) . Let g be the function constructed in Lemma 2. Define

$$G(r) = \frac{1}{r} \int_r^{2r} g(\rho) d\rho,$$

which is differentiable for $r > 0$ with

$$G'(r) = \frac{2 \cdot g(2r) - g(r)}{r} - \frac{1}{r^2} \int_r^{2r} g(\rho) d\rho \leq \frac{2 \cdot g(2r) - g(r)}{r} - \frac{g(r)}{r}.$$

Since $g(r) = o(r)$, it follows that

$$\lim_{r \rightarrow 0^+} G(r) = \lim_{r \rightarrow 0^+} G'(r) = 0$$

for $r \rightarrow 0^+$. Hence, we can continuously extend G by setting $G(0) = 0$. Furthermore, since g is non-decreasing, we see that the limit $r \rightarrow 0^+$ gives

$$0 \leq \frac{G(r) - G(0)}{r} \leq \frac{rg(2r)}{r^2} \rightarrow 0.$$

This means that also G' is continuous at $r = 0$ with respect to the (one-sided) derivative $G'(0) = 0$. This allows us to define

$$\psi(y, s) = \phi(x, t) + a(s - t) + p \cdot (y - x) + G(|s - t| + |y - x|),$$

where we know, in particular, that $\psi \in C^1(Q)$. Also, $\nabla \psi(x, t) = p$ and $\dot{\psi}(x, t) = a$ as required. Since $G(r) \geq g(r)$ and (6) holds for g , the difference $\phi - \psi$ has a local maximum at (x, t) . The result for $D^- \phi(x, t)$ can be derived by the same arguments, or by applying the shown result to $-\phi$. \square

2.3 The Comparison Principle

For the reader familiar with potential theory and harmonic functions, the terms “subsolution” and “supersolution” introduced above probably ring a bell. In this classical field, sub- and supersolutions of the Laplace equation (also called sub- and superharmonic functions) are introduced as functions that lie “below” and “above” a solution (harmonic function), respectively. These notions are useful for the investigation of the Dirichlet problem for the Laplace equation, and can also be applied to the initial-value problem associated with the heat equation. See, for instance, [36] or Section 3.3 of [45]. Very important in the study of harmonic functions as well as sub- and supersolutions are their *mean-value property*, the *maximum/minimum principles* and the *comparison principle*. As we will see in this section, a similar concept also applies to our viscosity solutions of the level-set equation. Besides showing uniqueness of the solution for the initial-value problem, the comparison principle will also be of tremendous utility for various later results:

Theorem 2. *Let $\phi, \psi: \bar{Q} \rightarrow \mathbb{R}$ be a sub- and supersolution of (2), respectively. Assume for the initial data $\phi(\cdot, 0) \leq \psi(\cdot, 0)$ on \mathbb{R}^n . Then $\phi \leq \psi$ on the whole of \bar{Q} .*

Before we prove the comparison principle in the remaining part of this section, we can use it immediately to show uniqueness for viscosity solutions of the level-set equation:

Corollary 1. *Let $\phi_0: \mathbb{R}^n \rightarrow \mathbb{R}$ be continuous. If a viscosity solution of the level-set equation (2) exists with initial value ϕ_0 , it is necessarily unique.*

Proof. Assume that $\phi, \psi: \mathbb{R}^n \rightarrow \mathbb{R}$ are two solutions with $\phi(\cdot, 0) = \psi(\cdot, 0) = \phi_0$. In this situation, the conditions of Theorem 2 are fulfilled and thus both $\phi \leq \psi$ and $\psi \leq \phi$. Hence $\phi = \psi$, showing uniqueness. \square

Let us now continue with the proof of Theorem 2. As always, recall that we assume F to be Lipschitz continuous and compactly supported. The proof technique can be considered a “standard argument” in the study of viscosity solutions, and follows the method sketched in [25]. Some details are tailored more specifically towards the concrete situation of interest to us, though. The main idea goes like this: Due to semi-continuity, the function $\phi - \psi$ attains a maximum on compact sets. Leaving aside the technical difficulty that Q is unbounded and thus not compact for a moment, we aim at showing that this maximum is non-positive. If this can, indeed, be established, the desired result $\phi \leq \psi$ is shown. To prove this, one uses a trick called *variable doubling*: Instead of looking at $\phi - \psi$ directly, we introduce

$$\Psi_\epsilon(x, y, t, s) = \frac{|x - y|^2 + (t - s)^2}{2\epsilon} \tag{7}$$

as a penalisation term and consider maxima of

$$\phi(x, t) - \psi(y, s) - \Psi_\epsilon(x, y, t, s) \quad (8)$$

for $\epsilon > 0$. In the limit $\epsilon \rightarrow 0$, the penalisation ensures that maximum points must lie on the diagonal

$$\mathcal{N} = \left\{ (x, t, y, s) \in \overline{Q}^2 \mid x = y, t = s \right\}. \quad (9)$$

This removes the “doubled” variables again. When we fix y, s or x, t , Definition 2 can be applied to (8) since Ψ_ϵ is continuously differentiable. If this is done correctly, one can derive the necessary estimates to show that the maximum must be non-positive.

We will now proceed to execute this strategy rigorously. As a first step, we show a useful result about maxima penalised by Ψ_ϵ :

Lemma 3. *Let $\Phi: \overline{Q}^2 \rightarrow \mathbb{R}$ be upper semi-continuous and bounded from above. Consider Ψ_ϵ given according to (7) and define*

$$M_\epsilon = \sup_{z \in \overline{Q}^2} (\Phi(z) - \Psi_\epsilon(z))$$

for every $\epsilon > 0$. If $(z_\epsilon)_{\epsilon > 0} \subset \overline{Q}^2$, $\epsilon \rightarrow 0$, is a family of maximising arguments with $M_\epsilon = \Phi(z_\epsilon) - \Psi_\epsilon(z_\epsilon)$, then

$$\lim_{\epsilon \rightarrow 0^+} \Psi_\epsilon(z_\epsilon) = 0.$$

Furthermore, if $\hat{z} \in \overline{Q}^2$ is an accumulation point of $(z_\epsilon)_{\epsilon > 0}$ in the limit $\epsilon \rightarrow 0$, then $\hat{z} \in \mathcal{N}$ and $\Phi(\hat{z}) \geq \Phi(z)$ for all $z \in \mathcal{N}$.

Proof. Note that \mathcal{N} defined in (9) is precisely the set of zeros of Ψ_ϵ for arbitrary ϵ . Furthermore, it is easy to see that $M_\epsilon \leq M_\mu$ if $\epsilon \leq \mu$. It follows that

$$\sup_{z \in \mathcal{N}} \Phi(z) \leq M_\epsilon \leq M_1 < \infty$$

for all $\epsilon \leq 1$. This, in turn, implies together with the monotonicity of M_ϵ that $M_0 = \lim_{\epsilon \rightarrow 0^+} M_\epsilon$ exists within the same bounds. Hence,

$$M_{2\epsilon} \geq \Phi(z_\epsilon) - \Psi_{2\epsilon}(z_\epsilon) = \Phi(z_\epsilon) - \frac{1}{2}\Psi_\epsilon(z_\epsilon) = \Phi(z_\epsilon) - \Psi_\epsilon(z_\epsilon) + \frac{1}{2}\Psi_\epsilon(z_\epsilon) = M_\epsilon + \frac{1}{2}\Psi_\epsilon(z_\epsilon).$$

This gives

$$0 \leq \Psi_\epsilon(z_\epsilon) \leq 2(M_{2\epsilon} - M_\epsilon) \rightarrow 0$$

in the limit $\epsilon \rightarrow 0^+$. Thus $\Psi_\epsilon(z_\epsilon) \rightarrow 0$.

Now, let \hat{z} be an accumulation point of $(z_\epsilon)_{\epsilon > 0}$. I. e., assume that we consider some sequence $\epsilon \rightarrow 0^+$ with $z_\epsilon \rightarrow \hat{z}$. Note that

$$\tilde{\Psi}(x, y, t, s) = \epsilon \cdot \Psi_\epsilon(x, y, t, s) = \frac{|x - y|^2 + (t - s)^2}{2}$$

is a continuous function that does not depend on ϵ any more. Thus

$$0 = \lim_{\epsilon \rightarrow 0^+} \epsilon \cdot \Psi_\epsilon(z_\epsilon) = \lim_{\epsilon \rightarrow 0^+} \tilde{\Psi}(z_\epsilon) = \tilde{\Psi}(\hat{z}).$$

This implies that $\hat{z} \in \mathcal{N}$. Finally, upper semi-continuity of Φ yields

$$\Phi(\hat{z}) \geq \limsup_{\epsilon \rightarrow 0^+} \Phi(z_\epsilon) = \limsup_{\epsilon \rightarrow 0^+} (\Phi(z_\epsilon) - \Psi_\epsilon(z_\epsilon)) = \limsup_{\epsilon \rightarrow 0^+} M_\epsilon \geq \sup_{z \in \mathcal{N}} \Phi(z).$$

□

Note that a more general version of Lemma 3 can be found as Lemma 4.1 on page 11 of [25], but the version shown above suffices for our purposes. The next step is to show comparison under additional assumptions, which remove the technical difficulties related to the unboundedness of Q . For $R > 0$, we define

$$Q_R = \{ (x, t) \in \overline{Q} \mid t < R \text{ and } |x| < R \} = B_R(0) \times [0, R).$$

Let us for the moment consider the situation only on this restricted domain. The following result contains the core idea of the comparison proof (the variable-doubling argument), without being encumbered too much by technical issues that will be resolved later:

Lemma 4. *Let $R > 0$ be fixed and $\phi, \psi: \overline{Q_R} \rightarrow \mathbb{R}$. We assume that ψ is a viscosity supersolution of (2) and that ϕ is a subsolution of*

$$\dot{\phi}(x, t) + F(x) |\nabla \phi(x, t)| + c = 0 \quad (10)$$

for some $c > 0$. Furthermore, let

$$\lim_{t \rightarrow R^-} \phi(x, t) = \lim_{|x| \rightarrow R^-} \phi(x, t) = -\infty \text{ and } \lim_{t \rightarrow R^-} \psi(x, t) = \lim_{|x| \rightarrow R^-} \psi(x, t) = \infty.$$

If $\phi(\cdot, 0) \leq \psi(\cdot, 0)$, then $\phi \leq \psi$ throughout $\overline{Q_R}$.

Proof. Choose a sequence $\epsilon \rightarrow 0^+$. For each ϵ , we consider the maximum of

$$h_\epsilon(x, y, t, s) = \phi(x, t) - \psi(y, s) - \Psi_\epsilon(x, y, t, s)$$

on the compact set $\overline{Q_R^2}$. Note that h_ϵ is upper semi-continuous even at the boundary of Q_R^2 in the context of the extended real numbers, so that we can choose maximum points $z_\epsilon = (x_\epsilon, y_\epsilon, t_\epsilon, s_\epsilon) \in \overline{Q_R^2}$ with $h_\epsilon(z_\epsilon) \geq h_\epsilon(z)$ for all $z \in \overline{Q_R^2}$. Let now $\hat{z} \in \overline{Q_R^2}$ be an accumulation point of the sequence $(z_\epsilon)_{\epsilon > 0}$. Without loss of generality, assume that $z_\epsilon \rightarrow \hat{z}$ as $\epsilon \rightarrow 0^+$ by choosing an appropriate subsequence. If we apply Lemma 3 to the upper semi-continuous function $\phi - \psi$, we find that $\hat{z} \in \mathcal{N}$. Due to the assumed divergence of ϕ and ψ for $t \rightarrow R^-$ or $|x| \rightarrow R^-$, we further know that also $\hat{z} \in Q_R^2$ must be the case. In other words, \hat{z} has the form $(\hat{x}, \hat{x}, \hat{t}, \hat{t})$ with $(\hat{x}, \hat{t}) \in Q_R$. Since the lemma also yields $\phi(y, s) - \psi(y, s) \leq \phi(\hat{x}, \hat{t}) - \psi(\hat{x}, \hat{t})$ for all other points $(y, s) \in Q_R$, it only remains to verify that $\phi(\hat{x}, \hat{t}) \leq \psi(\hat{x}, \hat{t})$ is fulfilled.

If $\hat{t} = 0$, this follows from the assumption that comparison holds for the initial data. As we will now see, this situation is, in fact, the only possibility: Assume to the contrary that $\hat{t} > 0$. Then (\hat{x}, \hat{t}) is strictly in the interior of Q_R . The same must also be true for all maximisers z_ϵ with ϵ small enough. Hence, since (x_ϵ, t_ϵ) is a local maximiser of

$$(x, t) \mapsto h(x, y_\epsilon, t, s_\epsilon) = \phi(x, t) - \psi(y_\epsilon, s_\epsilon) - \Psi_\epsilon(x, y_\epsilon, t, s_\epsilon),$$

we can use the subsolution properties of ϕ as given in Definition 2 to conclude

$$\frac{\partial \Psi_\epsilon}{\partial t} + F(x_\epsilon) |\nabla_x \Psi_\epsilon| + c = \frac{t_\epsilon - s_\epsilon}{\epsilon} + F(x_\epsilon) \frac{|x_\epsilon - y_\epsilon|}{\epsilon} + c \leq 0.$$

A similar argument applied to the local minimiser (y_ϵ, s_ϵ) of $-h(x_\epsilon, \cdot, t_\epsilon, \cdot)$ yields

$$\frac{t_\epsilon - s_\epsilon}{\epsilon} + F(y_\epsilon) \frac{|x_\epsilon - y_\epsilon|}{\epsilon} \geq 0.$$

Subtracting the second from the first inequality gives

$$(F(x_\epsilon) - F(y_\epsilon)) \frac{|x_\epsilon - y_\epsilon|}{\epsilon} \leq -c \Leftrightarrow (F(y_\epsilon) - F(x_\epsilon)) \frac{|x_\epsilon - y_\epsilon|}{\epsilon} \geq c.$$

Denoting the Lipschitz constant of F by L , we can further conclude

$$c \leq (F(y_\epsilon) - F(x_\epsilon)) \frac{|x_\epsilon - y_\epsilon|}{\epsilon} \leq |F(y_\epsilon) - F(x_\epsilon)| \frac{|x_\epsilon - y_\epsilon|}{\epsilon} \leq L \frac{|x_\epsilon - y_\epsilon|^2}{\epsilon} \leq 2L \cdot \Psi_\epsilon(z_\epsilon).$$

This, however, leads to the contradiction $0 < c \leq 0$ in the limit $\epsilon \rightarrow 0^+$, since $\Psi_\epsilon(z_\epsilon) \rightarrow 0$ by Lemma 3. \square

In order to finish the proof of Theorem 2, it remains to remove the additional assumptions made in Lemma 4. For this, we will add auxiliary terms to the original sub- and supersolution. In order to do so, we need the following result:

Lemma 5. *Let $\phi, \psi: Q \rightarrow \mathbb{R}$, $(x, t) \in Q$ and assume that ψ is differentiable at (x, t) . Then*

$$\begin{aligned} D^+(\phi + \psi)(x, t) &= D^+\phi(x, t) + \left(\nabla\psi(x, t), \dot{\psi}(x, t) \right), \\ D^-(\phi + \psi)(x, t) &= D^-\phi(x, t) + \left(\nabla\psi(x, t), \dot{\psi}(x, t) \right). \end{aligned}$$

Proof. Let $(p, a) \in D^+\phi(x, t)$. This means that

$$\phi(y, s) \leq \phi(x, t) + a(s - t) + p \cdot (y - x) + r_1(y, s).$$

Similarly, differentiability of ψ at (x, t) implies by definition

$$\psi(y, s) = \psi(x, t) + \dot{\psi}(x, t)(s - t) + \nabla\psi(x, t) \cdot (y - x) + r_2(y, s).$$

Here, $r_1(y, s)$ and $r_2(y, s)$ are both $o(|s - t| + |y - x|)$ in the limit $(y, s) \rightarrow (x, t)$. Hence,

$$(\phi + \psi)(y, s) \leq (\phi + \psi)(x, t) + \left(a + \dot{\psi}(x, t) \right) (s - t) + (p + \nabla\psi(x, t)) \cdot (y - x) + r_1(y, s) + r_2(y, s).$$

Since also $r_1(y, s) + r_2(y, s) = o(|s - t| + |y - x|)$, this yields the required

$$(p + \nabla\psi(x, t), a + \dot{\psi}(x, t)) \in D^+(\phi + \psi)(x, t).$$

The other inclusion follows by applying this result to $\phi = (\phi + \psi) - \psi$. The statement for $D^-(\phi + \psi)(x, t)$ can be deduced by an analogous argument. \square

Now, we have all the required ingredients to give the proof of Theorem 2: Let ϕ and ψ be given as sub- and supersolution of (2). Assume that, in contradiction to the comparison principle, $\phi(x, t) > \psi(x, t)$ for some $(x, t) \in \bar{Q}$. Choose $R > 0$ such that $t < R$, $|x| < R$ and $\text{supp}(F) \subset B_{R/2}(0)$. For arbitrary $c, \epsilon, \delta > 0$, we define the modified solutions

$$\begin{aligned} \tilde{\phi}(y, s) &= \phi(y, s) - 2cs - \frac{\epsilon}{R - s} - \frac{\delta}{R - |y|^2}, \\ \tilde{\psi}(y, s) &= \psi(y, s) + 2cs + \frac{\epsilon}{R - s} + \frac{\delta}{R - |y|^2}. \end{aligned}$$

Take note that they are well-defined and that the additional terms are differentiable on Q_R . Thus, Lemma 5 implies that any $(\tilde{p}, \tilde{a}) \in D^+\tilde{\phi}(y, s)$ can be written as

$$\tilde{p} = p - \frac{2\delta y}{(R - |y|^2)^2}, \quad \tilde{a} = a - 2c - \frac{\epsilon}{(R - s)^2}$$

where $(p, a) \in D^+\phi(y, s)$. Furthermore, $a + F(y)|p| \leq 0$ because ϕ is a subsolution of (2). Hence,

$$\begin{aligned} \tilde{a} + F(y)|\tilde{p}| &= a - 2c - \frac{\epsilon}{(R - s)^2} + F(y) \left| p - \frac{2\delta y}{(R - |y|^2)^2} \right| \\ &\leq a - 2c + F(y)|p| + |F(y)| \frac{2\delta |y|}{(R - |y|^2)^2} \leq -2c + |F(y)| \frac{2\delta |y|}{(R - |y|^2)^2}. \end{aligned}$$

Since $\text{supp}(F) \subset B_{R/2}(0)$, the last term on the right-hand side can be made smaller than c if only δ is chosen sufficiently small. This is possible uniformly for all $(y, s) \in Q_R$. Thus, we have shown that for arbitrary $c, \epsilon > 0$, the parameter δ can be chosen so small that $\tilde{\phi}$ is a subsolution of (10). By a similar argument, $\tilde{\psi}$ will be a supersolution of (2) for the same choice of parameters. Since $\tilde{\phi}$ and $\tilde{\psi}$ fulfil all requirements of Lemma 4, we can conclude that $\tilde{\phi}(x, t) \leq \tilde{\psi}(x, t)$ for all $c, \epsilon > 0$ and δ small enough. This, however, contradicts $\phi(x, t) > \psi(x, t)$ in the limit $c, \epsilon, \delta \rightarrow 0^+$.

2.4 Perron's Method and Existence

In the previous section, we established the comparison principle for viscosity solutions of the level-set equation. This important property ensures uniqueness of solutions. Now, we will discuss the question of *existence* of a solution. There are various approaches to show existence of viscosity solutions. The oldest is the so-called *vanishing-viscosity method*, which is the origin of the term “*viscosity solution*”. We will, however, apply an alternative strategy: Perron's method. This approach is quite flexible and can be applied to much more general equations than (2), but we will concentrate on this particular situation for our discussion. Note that Perron's method is, like the comparison principle on which it builds, also classical for harmonic functions. See, for instance, Section 3.6 of [45]. It was generalised to Hamilton-Jacobi equations and viscosity solutions by Hitoshi Ishii [48]. The presentation here follows mainly Section 4 of [26], but is simplified to the first-order case where possible.

The method works, very roughly, like this: One can show that the notion of a subsolution is stable under the supremum operation. In other words, the supremum of any family of subsolutions is itself again a subsolution. We will formalise this result as Lemma 7. On the other hand, when one has a subsolution that is not already also a supersolution, one can construct another subsolution that is strictly above it. This construction is given in the proof of Lemma 8. Taking both results together (and simplifying a bit), we can conclude that the supremum of all subsolutions gives us a solution. The final result is formulated in Theorem 3 and then applied to deduce existence for the level-set equation in Corollary 2.

As our first goal in this process, we want to show that the supremum of subsolutions gives again a subsolution. For the proof of this result, we need the following stability property of the semijet:

Lemma 6. *Let $\phi : Q \rightarrow \mathbb{R}$ be upper semi-continuous, $(x, t) \in Q$ and $(p, a) \in D^+ \phi(x, t)$. Assume that $(\phi_k)_{k \in \mathbb{N}} : Q \rightarrow \mathbb{R}$ is a sequence of upper semi-continuous functions and that $((x_k, t_k))_{k \in \mathbb{N}} \subset Q$ is a sequence of points such that $(x_k, t_k, \phi_k(x_k, t_k)) \rightarrow (x, t, \phi(x, t))$. Furthermore, let*

$$\limsup_{k \rightarrow \infty} \phi_k(y_k, s_k) \leq \phi(y, s) \quad (11)$$

for all $(y, s) \in Q$ and sequences with $(y_k, s_k) \rightarrow (y, s)$.

Then there exists a sequence $((\hat{x}_k, \hat{t}_k))_{k \in \mathbb{N}} \subset Q$ and, for each $k \in \mathbb{N}$, an element $(p_k, a_k) \in D^+ \phi_k(\hat{x}_k, \hat{t}_k)$, such that

$$(\hat{x}_k, \hat{t}_k) \rightarrow (x, t), \quad \phi_k(\hat{x}_k, \hat{t}_k) \rightarrow \phi(x, t) \quad \text{and} \quad (p_k, a_k) \rightarrow (p, a).$$

Proof. Since $(p, a) \in D^+ \phi(x, t)$, we can apply Theorem 1 to deduce that there exists $\psi \in C^1(Q)$ such that $\phi - \psi$ has a strict local maximum at (x, t) and $(p, a) = (\nabla \psi(x, t), \dot{\psi}(x, t))$. Hence, there exists $r > 0$ such that

$$\phi(y, s) - \psi(y, s) \leq \phi(x, t) - \psi(x, t)$$

for all $(y, s) \in U = \{(y, s) \in Q \mid |s - t| + |y - x| \leq r\}$. Equality holds only for $(y, s) = (x, t)$. Note that the set U is compact if r is small enough. Furthermore, we assume, without loss of generality, that $(x_k, t_k) \in U$ for all $k \in \mathbb{N}$.

For each k , choose (\hat{x}_k, \hat{t}_k) as a maximiser of $\phi_k - \psi$ over U . This can be done since ϕ_k is upper semi-continuous. We get, in particular,

$$\phi_k(x_k, t_k) - \psi(x_k, t_k) \leq \phi_k(\hat{x}_k, \hat{t}_k) - \psi(\hat{x}_k, \hat{t}_k) \quad (12)$$

for each $k \in \mathbb{N}$. Assume that we consider some convergent subsequence of $((\hat{x}_k, \hat{t}_k))_{k \in \mathbb{N}}$ with limit $(\hat{x}, \hat{t}) \in U$. Then passing to the limit inferior in (12) and using (11) yields

$$\phi(x, t) - \psi(x, t) \leq \liminf_{k \rightarrow \infty} \phi_k(\hat{x}_k, \hat{t}_k) - \psi(\hat{x}, \hat{t}) \leq \limsup_{k \rightarrow \infty} \phi_k(\hat{x}_k, \hat{t}_k) - \psi(\hat{x}, \hat{t}) \leq \phi(\hat{x}, \hat{t}) - \psi(\hat{x}, \hat{t}). \quad (13)$$

Since, on the other hand, (x, t) is the unique maximum of $\phi - \psi$ on U , we can conclude that $(\hat{x}, \hat{t}) = (x, t)$. Thus, each convergent subsequence of $((\hat{x}_k, \hat{t}_k))_{k \in \mathbb{N}}$ has the same limit (namely (x, t)), which implies that $(\hat{x}_k, \hat{t}_k) \rightarrow (x, t)$ must hold without the need for any subsequence.

Note that r is fixed and the neighbourhood U does not shrink as $k \rightarrow \infty$. This means that the maximum points (\hat{x}_k, \hat{t}_k) , converging to the “centre” of U , can not lie on the boundary except for finitely many k . This means that each (\hat{x}_k, \hat{t}_k) is a local maximiser of $\phi_k - \psi$, and thus defining

$$(p_k, a_k) = (\nabla \psi(\hat{x}_k, \hat{t}_k), \dot{\psi}(\hat{x}_k, \hat{t}_k))$$

ensures $(p_k, a_k) \in D^+ \phi_k(\hat{x}_k, \hat{t}_k)$ by Theorem 1. Since ψ is continuously differentiable, the convergence $(\hat{x}_k, \hat{t}_k) \rightarrow (x, t)$ implies $(p_k, a_k) \rightarrow (p, a)$. Finally, $\phi_k(\hat{x}_k, \hat{t}_k) \rightarrow \phi(x, t)$ follows from (13). \square

When taking the supremum of subsolutions, we have to be careful with semi-continuity. The supremum of upper semi-continuous functions need not be upper semi-continuous itself (see Example 6 below). To fix this, we need *semi-continuous envelopes*:

Definition 5. Let $\phi: Q \rightarrow \mathbb{R}$ be arbitrary. We define the lower and upper semi-continuous envelopes as

$$\begin{aligned}\phi_*(x, t) &= \lim_{r \rightarrow 0^+} \inf \{ \phi(y, s) \mid |s - t| + |y - x| \leq r \}, \\ \phi^*(x, t) &= \lim_{r \rightarrow 0^+} \sup \{ \phi(y, s) \mid |s - t| + |y - x| \leq r \}\end{aligned}$$

for $(x, t) \in Q$. It is clear that $\phi_* \leq \phi \leq \phi^*$.

If we assume that ϕ is bounded, it is easy to see that the envelopes defined in this way are, indeed, well-defined and finite. Furthermore, ϕ_* and ϕ^* are lower and upper semi-continuous, respectively. (See also (4.1) and the corresponding remarks in [26].) The need to introduce these semi-continuous envelopes is also the reason why we cannot simply take $(x_k, t_k) = (x, t)$ in the formulation of Lemma 6 and have to allow for a non-trivial sequence instead. We can give a short example that demonstrates that this technical construction is really necessary:

Example 6. For simplicity, we consider functions $\phi_k: \mathbb{R} \rightarrow \mathbb{R}$ instead of allowing for space and time. This does not change anything important for the point to be made, though. For $k \in \mathbb{N}$, define

$$\phi_k(x) = \begin{cases} 0 & \text{if } x < 1/k, \\ 1 & \text{if } x \geq 1/k \end{cases} \quad \text{and} \quad \phi(x) = \begin{cases} 0 & \text{if } x \leq 0, \\ 1 & \text{if } x > 0. \end{cases}$$

Then ϕ_k is upper semi-continuous for each k , and $\phi = \sup_{k \in \mathbb{N}} \phi_k$. However, ϕ itself is *not* upper semi-continuous! We have to consider

$$\phi^*(x) = \begin{cases} 0 & \text{if } x < 0, \\ 1 & \text{if } x \geq 0 \end{cases}$$

instead to get an upper semi-continuous “supremum function”. Because of this, note also

$$\lim_{k \rightarrow \infty} \phi_k(0) = 0 \neq 1 = \phi^*(0).$$

We really have to choose a non-trivial sequence $(x_k)_{k \in \mathbb{N}} \rightarrow 0$ to get $\lim_{k \rightarrow \infty} \phi_k(x_k) = \phi^*(0)$. One possible choice of such a sequence is $x_k = 1/k$.

We can now show that the envelope of the supremum of a family of subsolutions is, indeed, again a subsolution of the level-set equation:

Lemma 7. Let \mathcal{F} be a family of viscosity subsolutions of (2). Set $\Phi(x, t) = \sup \{ \phi(x, t) \mid \phi \in \mathcal{F} \}$ for $(x, t) \in Q$. Then Φ^* is also a viscosity subsolution of (2).

The corresponding statement also holds for the infimum of a family of supersolutions.

Proof. Let $(x, t) \in Q$. We will first show that there exists a maximising sequence $((x_k, t_k, \phi_k))_{k \in \mathbb{N}} \subset Q \times \mathcal{F}$ with $(x_k, t_k) \rightarrow (x, t)$ and $\Phi^*(x, t) = \lim_{k \rightarrow \infty} \phi_k(x_k, t_k)$. For this, choose some sequence $(\epsilon_k)_{k \in \mathbb{N}} > 0$ with $\epsilon_k \rightarrow 0$ as $k \rightarrow \infty$ and fix $k \in \mathbb{N}$. Due to Definition 5, there is $(x_k, t_k) \in Q$ with $|t_k - t| + |x_k - x| \leq \epsilon_k$ and

$$\Phi^*(x, t) - \epsilon_k \leq \Phi(x_k, t_k) \leq \Phi^*(x, t).$$

By definition of Φ , there further exists $\phi_k \in \mathcal{F}$ such that

$$\Phi(x_k, t_k) - \epsilon_k \leq \phi_k(x_k, t_k) \leq \Phi(x_k, t_k).$$

Hence

$$\Phi^*(x, t) - 2\epsilon_k \leq \Phi(x_k, t_k) - \epsilon_k \leq \phi_k(x_k, t_k) \leq \Phi(x_k, t_k) \leq \Phi^*(x, t).$$

This implies $(x_k, t_k, \phi_k(x_k, t_k)) \rightarrow (x, t, \Phi^*(x, t))$ in the limit $k \rightarrow \infty$.

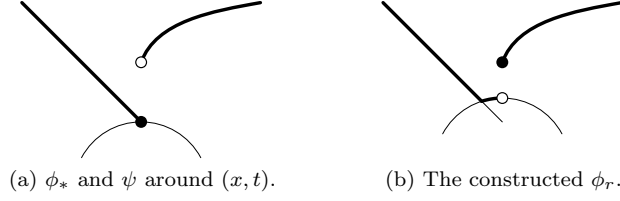


Figure 6: The construction used in the proof of Lemma 8.

Now, if $(y_k, s_k) \rightarrow (y, s)$ for $k \rightarrow \infty$ and some $(y, s) \in Q$, then clearly

$$\limsup_{k \rightarrow \infty} \phi_k(y_k, s_k) \leq \limsup_{k \rightarrow \infty} \Phi(y_k, s_k) \leq \limsup_{k \rightarrow \infty} \Phi^*(y_k, s_k) \leq \Phi^*(y, s).$$

Thus, for each $(p, a) \in D^+ \Phi^*(x, t)$, we can apply Lemma 6 with $\phi = \Phi^*$. For $k \in \mathbb{N}$, choose $(\hat{x}_k, \hat{t}_k) \in Q$ and $(p_k, a_k) \in D^+ \phi_k(\hat{x}_k, \hat{t}_k)$ according to the lemma. Since ϕ_k is a subsolution of (2), we know by Definition 4 that

$$a_k + F(\hat{x}_k) |p_k| \leq 0.$$

Passing to the limit $k \rightarrow \infty$ and using continuity of F , this yields $a + F(x) |p| \leq 0$. Hence, Φ^* is itself a subsolution of the level-set equation. \square

The next step is to show that a *maximal* subsolution must also be a supersolution. Or, in other words, if we have a subsolution that fails to be a supersolution, then we can construct another subsolution that is strictly above it. Again, we have to be careful about semi-continuity. So assume that $\phi: Q \rightarrow \mathbb{R}$ is a subsolution of the level-set equation, but that ϕ_* is *not* a supersolution. This means that there exist $(x, t) \in Q$ and $(p, a) \in D^- \phi_*(x, t)$ such that $a + F(x) |p| < 0$. The proof of the following result gives the construction of a subsolution strictly above ϕ :

Lemma 8. *Let $\phi: Q \rightarrow \mathbb{R}$ be a subsolution of (2) and assume that ϕ_* is not a supersolution. Then there exist $(x, t) \in Q$ and $r_0 > 0$ such that for each $0 < r < r_0$, we can find a subsolution ϕ_r of (2) with*

$$\sup_{(y, s) \in Q} (\phi_r(y, s) - \phi(y, s)) > 0$$

as well as $\phi_r \geq \phi$ in Q . Furthermore, the change is only local, meaning that $\phi_r(y, s) = \phi(y, s)$ for all $(y, s) \in Q$ with $|s - t| + |y - x| \geq r$.

Proof. Let $(x, t) \in Q$ and $(p, a) \in D^- \phi_*(x, t)$ be given as in the discussion above, i. e., $a + F(x) |p| < 0$. According to Theorem 1, there exists $\psi \in C^1(Q)$ such that $\phi_* - \psi$ has a strict local minimum at (x, t) and with $(p, a) = (\nabla \psi(x, t), \dot{\psi}(x, t))$. Assume, without loss of generality, that $\psi(x, t) = \phi_*(x, t)$. Then we can find $r_1 > 0$ small enough such that $\phi_*(y, s) \geq \psi(y, s)$ whenever $|s - t| + |y - x| \leq r_1$, with equality only for $(y, s) = (x, t)$. Furthermore, continuity of F and the derivatives of ψ implies that there exists another neighbourhood $\{(y, s) \in Q \mid |s - t| + |y - x| \leq r_2\}$, $r_2 > 0$, where

$$\dot{\psi}(y, s) + F(y) |\nabla \psi(y, s)| \leq 0 \tag{14}$$

holds. We choose $r_0 = \min(r_1, r_2, t/2)$. The last condition ensures that this common neighbourhood lies strictly inside of Q .

Now, let $0 < r < r_0$ be given arbitrarily and define the compact set

$$U = \left\{ (y, s) \in Q \mid \frac{r}{2} \leq |s - t| + |y - x| \leq r \right\}.$$

Since $\phi_* - \psi$ is lower semi-continuous, we can define

$$\delta = \min_{(y, s) \in U} (\phi_*(y, s) - \psi(y, s)).$$

Note that $\delta > 0$, since $(x, t) \notin U$ is a *strict* minimum of this function with minimal value zero. This definition ensures that

$$\psi_\delta(y, s) = \psi(y, s) + \delta \leq \phi_*(y, s) \leq \phi(y, s) \quad (15)$$

for all $(y, s) \in U$. Due to (14), ψ_δ is a classical solution and thus also a viscosity subsolution of (2) at least locally around (x, t) . Thus, Lemma 7 implies that

$$\phi_r(y, s) = \begin{cases} \max(\phi(y, s), \psi_\delta(y, s)) & \text{if } |s - t| + |y - x| \leq r, \\ \phi(y, s) & \text{else} \end{cases} \quad (16)$$

is a viscosity subsolution of (2). See also Figure 6b for a sketch of this construction. Note that (15) implies that the two cases in the definition of ϕ_r “overlap” on the set U . This guarantees that ϕ_r is really a viscosity solution even at the interface between the two regions.

The only remaining thing to show is $\sup(\phi_r - \phi) > 0$. Roughly speaking, we expect this supremum to be at least δ as the difference between ψ_δ and ϕ_* at (x, t) . However, a closer investigation is necessary since $\phi(x, t)$ could be strictly larger than $\phi_*(x, t)$. Thus, let $((x_k, t_k))_{k \in \mathbb{N}} \subset Q$ be a minimising sequence such that $(x_k, t_k) \rightarrow (x, t)$ and $\phi(x_k, t_k) \rightarrow \phi_*(x, t)$. Since $\psi(x, t) = \phi_*(x, t)$ and ψ is continuous, it follows that

$$\phi(x_k, t_k) < \psi(x_k, t_k) + \delta = \psi_\delta(x_k, t_k)$$

for all k sufficiently large. Consequently, $\phi_r(x_k, t_k) = \psi_\delta(x_k, t_k)$ by definition in (16). Hence

$$\lim_{k \rightarrow \infty} (\phi_r(x_k, t_k) - \phi(x_k, t_k)) = \lim_{k \rightarrow \infty} (\psi_\delta(x_k, t_k) - \phi(x_k, t_k)) = \psi(x, t) + \delta - \phi_*(x, t) = \delta.$$

This, finally, shows $\sup_{(y, s) \in Q} (\phi_r(y, s) - \phi(y, s)) \geq \delta > 0$. \square

We are now able to formulate and proof Ishii’s version (see [48]) of Perron’s method, which is the main result of this section:

Theorem 3. *Let the initial level-set function $\phi_0: \mathbb{R}^n \rightarrow \mathbb{R}$ be given. Assume that $\phi, \psi: \overline{Q} \rightarrow \mathbb{R}$ are a sub- and supersolution of the level-set equation, respectively, and that they satisfy the initial condition*

$$\phi_*(\cdot, 0) = \psi^*(\cdot, 0) = \phi_0. \quad (17)$$

Then the function

$$\Phi: \overline{Q} \rightarrow \mathbb{R}, \quad \Phi(x, t) = \sup \left\{ \tilde{\phi}(x, t) \mid \phi \leq \tilde{\phi} \leq \psi \text{ and } \tilde{\phi} \text{ is a subsolution of (2)} \right\} \quad (18)$$

solves the initial-value problem (2) with initial data ϕ_0 in the viscosity sense.

Proof. Note that Φ exists, since the set in (18) is not empty (it contains, in particular, ϕ). Observe further that

$$\phi_* \leq \Phi_* \leq \Phi \leq \Phi^* \leq \psi^*.$$

For $t = 0$, this implies with (17) that

$$\Phi_*(x, 0) = \Phi(x, 0) = \Phi^*(x, 0) = \phi_0(x)$$

must hold for all $x \in \mathbb{R}^n$. Hence, Φ as defined in (18) satisfies the initial condition. Lemma 7 implies that Φ^* is a subsolution of (2). Due to the comparison principle (Theorem 2), this further implies $\Phi^* \leq \psi$. Hence, Φ^* is itself admissible in the supremum in (18), which yields $\Phi = \Phi^*$. Thus, Φ is already upper semi-continuous and itself a subsolution to the level-set equation.

Assume now for a moment that Φ_* is *not* a supersolution of (2). In that case, Lemma 8 allows us to find some small $r > 0$ and another subsolution ϕ_r strictly above Φ . If r is chosen small enough, ϕ_r satisfies the initial condition. Thus comparison implies $\phi_r \leq \psi$, which means that ϕ_r is admissible for the supremum in (18). This, in turn, leads to $\Phi \geq \phi_r$, which contradicts $\sup(\phi_r - \Phi) > 0$. We conclude that Φ_* must be a supersolution of the level-set equation. Invoking comparison one final time, this yields $\Phi \leq \Phi_* \leq \Phi$, which shows that Φ is also lower semi-continuous and thus a supersolution itself. \square

In order to show the existence of a solution of the level-set equation (2), it now suffices to construct a subsolution and a supersolution that satisfy the initial condition:

Corollary 2. *Let $F, \phi_0: \mathbb{R}^n \rightarrow \mathbb{R}$ be Lipschitz continuous and F have compact support. Then there exists a unique viscosity solution $\phi: \bar{Q} \rightarrow \mathbb{R}$ of the level-set equation (2) satisfying $\phi(\cdot, 0) = \phi_0$ on \mathbb{R}^n .*

Proof. Uniqueness was already established in Corollary 1. We will now show existence. Denote the Lipschitz constant of ϕ_0 by L and define

$$\phi(x, t) = \phi_0(x) - \bar{F}Lt, \quad \psi(x, t) = \phi_0(x) + \bar{F}Lt.$$

Recall that we use \bar{F} to denote a bound for $|F|$. It is easy to see that ϕ and ψ are continuous (even differentiable with respect to t) and satisfy $\phi(\cdot, 0) = \psi(\cdot, 0) = \phi_0$. Thus, (17) holds and the result follows from Theorem 3 if we can show that ϕ and ψ are a sub- and supersolution of (2), respectively. For this, let $(x, t) \in Q$ and choose $(p, a) \in D^+\phi(x, t)$. Differentiability of ϕ with respect to t implies that $a = \dot{\phi}(x, t) = -\bar{F}L$ must hold (recall (5)).

To get a hold on $|p|$, define $y_\tau = x - \tau p$. Then, by definition of $D^+\phi(x, t)$, it follows that

$$\phi(y_\tau, t) - \phi(x, t) \leq p \cdot (y_\tau - x) + o(\tau) = -\tau |p|^2 + o(\tau)$$

for all $\tau \in \mathbb{R}$. Using the definition of ϕ , this further implies

$$\limsup_{\tau \rightarrow 0^+} \frac{\phi(y_\tau) - \phi(x)}{\tau} \leq -|p|^2$$

in the limit $\tau \rightarrow 0^+$. Lipschitz continuity of ϕ_0 yields $|\phi_0(y_\tau) - \phi_0(x)| \leq L|p|\tau$, so that

$$|p|^2 \leq -\limsup_{\tau \rightarrow 0^+} \frac{\phi(y_\tau) - \phi(x)}{\tau} \leq \liminf_{\tau \rightarrow 0^+} \frac{|\phi_0(x) - \phi_0(y_\tau)|}{\tau} \leq L|p|.$$

Hence $|p| \leq L$. Taking all together, we conclude

$$a + F(x)|p| = -\bar{F}L + F(x)|p| \leq -\bar{F}L + \bar{F}|p| \leq 0.$$

This shows that ϕ is, indeed, a subsolution. With a similar argument, one can also show that ψ is a supersolution of (2). \square

2.5 Basic Solution Properties

Above, we have introduced the level-set equation (2). With the appropriate concept of viscosity solutions, we have established that the equation admits a unique solution ϕ that describes the time evolution of the level-set function. In this section, we will derive some basic but very useful properties of the solution ϕ . Recall that we are actually interested in the evolving geometry $\Omega_t = \phi(\cdot, t)^{-1}((-\infty, 0))$ and not the detailed level-set function itself. However, in order to use the level-set approach, we have to choose *some* level-set function ϕ_0 that represents the initial geometry Ω_0 . Consequently, the question arises how much influence this ambiguous choice of ϕ_0 has on the resulting evolution of Ω . We will see in Corollary 3 that ϕ_0 influences $\phi(\cdot, t)$, but that Ω_t only depends on Ω_0 and not the particular form of ϕ_0 . This is, of course, a very good justification for using the level-set method to describe propagating geometries. The proof of this important property follows [41], where it is found in Theorem 4.2.8 on page 172. The second main result of this section, Theorem 5, will allow us to consider only speed fields $F \geq 0$ in the following. Any evolution with a general speed field can always be expressed in terms of evolutions where the speed is non-negative. The latter have the desirable property that the evolution of Ω_t is monotone (i. e., $\Omega_t \subset \Omega_s$ for $t < s$), which simplifies many considerations.

The first step towards Corollary 3 is to show that the level-set equation is invariant under a change of variables. To motivate this result, assume for a moment that $\theta \in C^1(\mathbb{R})$ is increasing and ϕ a classical solution of (2). Since $\theta' \geq 0$ in this case, the chain rule for $\tilde{\phi} = \theta \circ \phi$ implies

$$\dot{\tilde{\phi}} + F(x) |\nabla \tilde{\phi}| = \theta'(\phi) \dot{\phi} + F(x) |\theta'(\phi) \nabla \phi| = \theta'(\phi) \cdot (\dot{\phi} + F(x) |\nabla \phi|) = 0.$$

This shows that also $\tilde{\phi}$ is a solution of (2) in this situation. Dropping the assumptions of differentiability and formulating everything in the correct viscosity-solution framework, this statement reads as:

Lemma 9. *Let $\theta: \mathbb{R} \rightarrow \mathbb{R}$ be continuous and non-decreasing. Assume that $\phi: Q \rightarrow \mathbb{R}$ is a viscosity sub- or supersolution of (2). Then also $\theta \circ \phi$ is a sub- or supersolution.*

Proof. We show the result for ϕ being a subsolution. For supersolutions, an analogous argument can be applied. As a first step, assume that $\theta \in C^1(\mathbb{R})$ with $\theta' > 0$. This implies that its inverse $h = \theta^{-1}$ exists and also satisfies $h \in C^1(\theta(\mathbb{R}))$ as well as $h' > 0$, where $\theta(\mathbb{R})$ is an open interval. Assume $(x, t) \in Q$ and $\psi \in C^1(\mathbb{R})$ such that $(\theta \circ \phi) - \psi$ has a local maximum at (x, t) . Without loss of generality, we may assume that the maximal value is zero. In other words, $(\theta \circ \phi)(y, s) \leq \psi(y, s)$ for all (y, s) in a neighbourhood of (x, t) , with equality for $(y, s) = (x, t)$. Applying the strictly monotone inverse h on a neighbourhood of $\theta(\phi(x, t))$, this implies $\phi(y, s) \leq (h \circ \psi)(y, s)$. With the notation $\tilde{\psi} = h \circ \psi$, it follows that $\phi - \tilde{\psi}$ has a local maximum at (x, t) . Since $\tilde{\psi}$ is continuously differentiable and ϕ is a subsolution of the level-set equation, Definition 2 implies that

$$\dot{\tilde{\psi}}(x, t) + F(x) \left| \nabla \tilde{\psi}(x, t) \right| = h'(\psi(x, t)) \cdot \left(\dot{\psi}(x, t) + F(x) |\nabla \psi(x, t)| \right) \leq 0.$$

Thus $\dot{\psi}(x, t) + F(x) |\nabla \psi(x, t)| \leq 0$, which shows that $\theta \circ \phi$ is, indeed, a subsolution.

Secondly, if θ is not differentiable, we can always find a sequence $(\theta_k)_{k \in \mathbb{N}} \subset C^1(\mathbb{R})$ of smooth functions with $\theta'_k > 0$ that approximates θ from below. To do this, we can proceed as follows: In a first step, we apply some standard mollifier to θ . It is easy to see that this preserves monotonicity. Secondly, we shift the resulting function down, so that it is below θ . Finally, we can enforce *strict* monotonicity by adding a smooth, bounded, strictly increasing function (like arctan) to it. This all can be done in such a way that we get $\theta = \sup_{k \in \mathbb{N}} \theta_k$ and thus also $\theta \circ \phi = \sup_{k \in \mathbb{N}} (\theta_k \circ \phi)$. By the first part of the proof, $\theta_k \circ \phi$ is a subsolution for every $k \in \mathbb{N}$. According to Lemma 7, this implies that also the supremum $\theta \circ \phi$ must be a subsolution. (Note that the semi-continuous envelope is not necessary here since the supremum is continuous anyway.) \square

Next comes an observation: Let Ω_1, Ω_2 be two domains and ϕ_1, ϕ_2 corresponding level-set functions. While the ordering $\phi_1 \leq \phi_2$ immediately implies $\Omega_2 \subset \Omega_1$, the reverse is, in general, not true. The inclusion of the sets contains much less information than a strict pointwise ordering of the level-set functions. Note, however, that this additional information contained in the level-set functions has no meaning from a geometric point of view. Consequently, it is not of interest to us. If we allow to rescale the level-set functions provided that the domains are not affected, we can ensure also the reverse implication. The construction of a suitable change of variables is our next step:

Lemma 10. *Let $\phi_1, \phi_2: \mathbb{R}^n \rightarrow \mathbb{R}$ be continuous. Assume that the inclusion*

$$\Omega_2 = \phi_2^{-1}((-\infty, 0)) \subset \phi_1^{-1}((-\infty, 0)) = \Omega_1 \quad (19)$$

holds and that Ω_2 is bounded. Then there exists $\theta: \mathbb{R} \rightarrow \mathbb{R}$ non-decreasing and continuous such that $\theta(0) = 0$ and $\theta \circ \phi_1 \leq \phi_2$ on \mathbb{R}^n , while preserving the sub-zero level set of ϕ_1 , i. e.,

$$(\theta \circ \phi_1)^{-1}((-\infty, 0)) = \Omega_1. \quad (20)$$

Proof. We define $\theta(\sigma) = 0$ for $\sigma \geq 0$ and

$$\theta(\sigma) = \inf (\{\sigma\} \cup \{\phi_2(x) \mid x \in \mathbb{R}^n, \sigma \leq \phi_1(x) < 0\}) \quad (21)$$

for $\sigma < 0$. As we will see below, this function has all required properties except, possibly, continuity. Since ϕ_2 is continuous and the set Ω_2 , where it is negative, bounded, we find that ϕ_2 is bounded from below. Consequently, the infimum in (21) is always well-defined. It is obvious from the definition that θ is non-decreasing. Let now $x \in \mathbb{R}^n$ be arbitrary. If $\phi_1(x) \geq 0$, the assumption (19) implies that also $\phi_2(x) \geq 0$. In this case

$$\theta(\phi_1(x)) = 0 \leq \phi_2(x)$$

is trivially fulfilled. Otherwise, for $\phi_1(x) < 0$, the value $\phi_2(x)$ is admissible for the infimum in (21) when choosing $\sigma = \phi_1(x)$. Hence, also in this case $\theta(\phi_1(x)) \leq \phi_2(x)$. The equality (20) is clear by definition of θ , since $\theta(\sigma) < 0$ is equivalent to $\sigma < 0$.

The only thing that is still missing is continuity of θ . And in fact, θ as defined may be discontinuous. We can, however, show continuity at zero: Assume that θ is discontinuous at $\sigma = 0$. Obviously, since θ

is constantly zero for $\sigma \geq 0$, the discontinuity must happen from the left. This means that there exists a sequence $(\sigma_k)_{k \in \mathbb{N}} < 0$ with $\sigma_k \rightarrow 0^-$ and such that $\theta(\sigma_k) \rightarrow -\epsilon < 0$. Furthermore, according to (21), there exists also a matching sequence $(x_k)_{k \in \mathbb{N}} \subset \mathbb{R}^n$ such that $\phi_1(x_k) \rightarrow 0^-$ and $\phi_2(x_k) \rightarrow -\epsilon$. Since this sequence lies in the bounded set Ω_2 , it has an accumulation point \hat{x} in this set's closure. By switching to an appropriate subsequence, we may assume $x_k \rightarrow \hat{x}$ as $k \rightarrow \infty$. Using continuity of ϕ_1 and ϕ_2 , it follows that

$$\phi_1(\hat{x}) = \lim_{k \rightarrow \infty} \phi_1(x_k) = 0 \quad \text{and} \quad \phi_2(\hat{x}) = \lim_{k \rightarrow \infty} \phi_2(x_k) = -\epsilon.$$

This, however, means that the point \hat{x} contradicts the inclusion (19). Finally, to get continuity on $(-\infty, 0)$, we can apply the same idea as in the proof of Lemma 2 (see Figure 5) to construct a continuous minorant of θ that still satisfies all other conditions. \square

Recall our goal of showing that the evolved shapes depend only on the initial *geometry* but not the concrete level-set function ϕ_0 . In order to do so, we would like to establish that an inclusion that holds for the initial sets is preserved throughout the propagation in time. Using the previous results, this can now be deduced:

Theorem 4. *Let $\phi_1, \phi_2: Q \rightarrow \mathbb{R}$ be viscosity solutions of the level-set equation (2). Assume that $\phi_1(\cdot, 0)^{-1}((-\infty, 0))$ is bounded. If the inclusion*

$$\phi_1(\cdot, t)^{-1}((-\infty, 0)) \subset \phi_2(\cdot, t)^{-1}((-\infty, 0))$$

holds for the initial time $t = 0$, then it also holds for all $t \geq 0$.

Proof. Let θ be as in Lemma 10 such that $(\theta \circ \phi_2)(\cdot, 0) \leq \phi_1(\cdot, 0)$. Then $\theta \circ \phi_2$ is also a viscosity solution of (2) according to Lemma 9. Thus, by the comparison principle (Theorem 2), the inequality $\theta \circ \phi_2 \leq \phi_1$ holds throughout Q . Let $(x, t) \in Q$ with $\phi_1(x, t) < 0$. Then also $\theta(\phi_2(x, t)) < 0$, which implies $\phi_2(x, t) < 0$ since $\theta(0) = 0$ and θ is non-decreasing. This finishes the proof. \square

Applying this preservation of inclusions twice immediately leads to the desired result:

Corollary 3. *Let $\phi_1, \phi_2: Q \rightarrow \mathbb{R}$ be two viscosity solutions of the level-set equation. Assume that they describe the same set $\Omega_0 \subset \mathbb{R}^n$ at time $t = 0$ and that Ω_0 is bounded. Then also the geometries described by all evolved level-set functions coincide.*

In the second half of this section, we will now show some very basic but still important properties of solutions of the level-set equation. This will culminate in Theorem 5, which shows that one can solve the equation for the regions $F^{-1}((-\infty, 0))$, $F^{-1}(\{0\})$ and $F^{-1}((0, \infty))$ separately and later combine the solutions. This approach has certain advantages both for theoretical considerations as well as for numerical solvers, which we will exploit later on. The first property we consider is monotonicity of the solution with respect to the speed. Interpreting (2) as a classical equation for a moment, it can be written as $\dot{\phi} = -F(x)|\nabla\phi|$. This motivates us to expect that $\phi(x, \cdot)$ is either monotonically increasing or decreasing in time for fixed $x \in \mathbb{R}^n$, depending on the sign of $F(x)$.

Lemma 11. *Let ϕ_0 be given. Then $\phi: Q \rightarrow \mathbb{R}$ defined by $\phi(x, t) = \phi_0(x)$ solves (2) for $F = 0$.*

Proof. Let $(p, a) \in D^+\phi(x, t)$ for some $(x, t) \in Q$. Then

$$\phi(y, s) - \phi(x, t) \leq a(s - t) + p \cdot (y - x) + o(|s - t| + |y - x|) \quad (22)$$

for all $(y, s) \in Q$ by (4). Consider, in particular, $y = x$ and a sequence $(s_k)_{k \in \mathbb{N}} > 0$ with $s_k \rightarrow t$. The left-hand side of (22) vanishes since ϕ is constant in time, so that we can rearrange the relation to read

$$0 \leq a \frac{s_k - t}{|s_k - t|} + \frac{o(|s_k - t|)}{|s_k - t|}.$$

For s_k converging to t from above, this gives $0 \leq a$ in the limit. For $s_k \rightarrow t^-$ from below, it follows that $0 \leq -a$, thus $a = 0$ must necessarily hold. Hence $a + F(x)|p| = 0 \leq 0$ is satisfied, and ϕ is, indeed, a viscosity subsolution of (2). In the same way, one can also show that it is a supersolution. \square

Using the comparison principle, we can now deduce that a larger speed implies a smaller level-set function. This, in turn, corresponds to a larger domain, as one would expect:

Lemma 12. *Let $F_1 \geq F_2$ in \mathbb{R}^n and let $\phi_1, \phi_2: Q \rightarrow \mathbb{R}$ be solutions of the level-set equation (2) for $F = F_1$ and $F = F_2$, respectively. Assume that we have $\phi_1(x, 0) = \phi_{1,0}(x)$ and $\phi_2(x, 0) = \phi_{2,0}(x)$ initially. If $\phi_{1,0} \leq \phi_{2,0}$ on \mathbb{R}^n , then $\phi_1 \leq \phi_2$ on the whole of Q .*

Proof. We shall show that ϕ_1 is a viscosity subsolution of (2) also with speed $F = F_2$. Then the claim immediately follows by comparison (recall Theorem 2). So let $(p, a) \in D^+ \phi_1(x, t)$ for some $(x, t) \in Q$. This implies

$$a + F_2(x) |p| \leq a + F_1(x) |p| \leq 0,$$

since ϕ_1 is a solution of the equation with $F = F_1$. Thus it is really also a subsolution with $F = F_2$. \square

Lemma 13. *Let $F \geq 0$ and $\phi: Q \rightarrow \mathbb{R}$ solve (2). Then $t \mapsto \phi(x, t)$ is decreasing on $[0, \infty)$ for each fixed $x \in \mathbb{R}^n$. If $F \leq 0$ instead, then $t \mapsto \phi(x, t)$ is increasing in time. Furthermore, in these situations, the sets Ω_t described by $\phi(\cdot, t)$ as a level-set function grow and shrink in time, respectively.*

Proof. Let $F \geq 0$ and $s \geq 0$ be given. We have to show $\phi(x, s) \geq \phi(x, t)$ for all $x \in \mathbb{R}^n$ and $t > s$. If $s > 0$, we can shift the initial time to s and use $\phi(\cdot, s)$ as initial function, so assume $s = 0$ without loss of generality. By Lemma 11, we know that $\tilde{\phi}(x, t) = \phi(x, 0)$ solves (2) with speed $\tilde{F} = 0$. Since $F \geq 0 = \tilde{F}$, Lemma 12 implies that $\phi(x, t) \leq \tilde{\phi}(x, t) = \phi(x, 0)$ for all $t \geq 0$. For the case $F \leq 0$, a similar argument applies. The last statement follows now immediately. \square

Note that, due to the concept of viscosity solutions we use, the level-set equation has no time-reversal symmetry. To see this, consider that a connected component of the domain that disappears cannot be restored by reversing the time direction. However, there exists an interesting symmetry property with respect to sign changes in F and ϕ , which will be useful later. The geometrical interpretation of this symmetry is that instead of letting a domain, say, grow, we can equivalently let its complement shrink.

Lemma 14. *Let ϕ be the solution of (2) for some F and initial value ϕ_0 . Then $-\phi$ solves the equation for $-F$ and with initial data $-\phi_0$.*

Proof. The initial condition is obviously satisfied. Choose $(x, t) \in Q$ and let $(p, a) \in D^+(-\phi)(x, t)$. Then

$$(-\phi)(y, s) \leq (-\phi)(x, t) + a(s - t) + p \cdot (y - x) + o(|s - t| + |y - x|)$$

holds for all $(y, s) \in Q$. Turning around the signs, this is equivalent to

$$\phi(y, s) \geq \phi(x, t) - a(s - t) - p \cdot (y - x) + o(|s - t| + |y - x|).$$

Hence, $(-p, -a) \in D^- \phi(x, t)$. Since ϕ is a supersolution of (2), this implies that

$$-a + F(x) |p| = -a + F(x) |p| \geq 0 \Leftrightarrow a - F(x) |p| \leq 0.$$

Thus $-\phi$ is a subsolution when the speed is $-F$. By the same argument, one can also show that $-\phi$ is a supersolution. \square

Before we proceed to the main result, let us introduce notation for the positive and negative parts of an expression $h \in \mathbb{R}$:

$$h^+ = \max(h, 0), \quad h^- = \max(-h, 0) \tag{23}$$

It is immediately clear from the definition that both parts are non-negative and that the decompositions $h = h^+ - h^-$, $|h| = h^+ + h^-$ hold. Furthermore, at most one of h^+ and h^- can be non-zero.

Theorem 5. *For a general Lipschitz continuous $F: \mathbb{R}^n \rightarrow \mathbb{R}$, define the open sets $\Omega^+ = F^{-1}((0, \infty))$ and $\Omega^- = F^{-1}((-\infty, 0))$. Let ϕ^\pm solve the level-set equation with speeds F^+ and $-F^-$, respectively, and the same initial data ϕ_0 . Then*

$$\phi(x, t) = \begin{cases} \phi^+(x, t) & \text{for } x \in \Omega^+, \\ \phi^-(x, t) & \text{for } x \in \Omega^-, \\ \phi_0(x) & \text{if } F(x) = 0 \end{cases} \tag{24}$$

solves (2) with speed F and initial data ϕ_0 .

Furthermore, $\phi^+ \leq \phi_0 \leq \phi^-$ throughout Q , and $\phi^\pm(x, t) = \phi_0(x)$ for all $x \notin \Omega^\pm$ and $t \geq 0$.

Proof. The relation $\phi^+ \leq \phi_0 \leq \phi^-$ follows immediately from Lemma 12 since $-F^- \leq 0 \leq F^+$ and ϕ_0 is the solution for $F = 0$ by Lemma 11. It is clear that ϕ , as defined in (24), satisfies the initial condition $\phi(x, 0) = \phi_0(x)$, since this condition is imposed on both of ϕ^\pm .

The next step is to show $\phi^+(x, t) = \phi_0(x)$ for all $x \notin \Omega^+$ and $t > 0$. For this, define

$$\tilde{\phi}(x, t) = \begin{cases} \phi^+(x, t) & \text{for } x \in \Omega^+, \\ \phi_0(x) & \text{if } F(x) \leq 0. \end{cases}$$

Take note that $\phi^+ \leq \tilde{\phi} \leq \phi_0$ since $\phi^+ \leq \phi_0$. Because $\Omega^+ = F^{-1}((0, \infty))$ is open, it follows that $\tilde{\phi}$ is upper semi-continuous: Let $(x, t) \in Q$ be arbitrary and choose a sequence $((x_k, t_k))_{k \in \mathbb{N}} \subset Q$ such that $(x_k, t_k) \rightarrow (x, t)$ for $k \rightarrow \infty$. If $x \in \Omega^+$, then $x_k \in \Omega^+$ for large enough k . Consequently,

$$\limsup_{k \rightarrow \infty} \tilde{\phi}(x_k, t_k) = \limsup_{k \rightarrow \infty} \phi^+(x_k, t_k) = \phi^+(x, t) = \tilde{\phi}(x, t)$$

by continuity of ϕ^+ . If, on the other hand, $x \notin \Omega^+$, then

$$\limsup_{k \rightarrow \infty} \tilde{\phi}(x_k, t_k) \leq \limsup_{k \rightarrow \infty} \phi_0(x_k, t_k) = \phi_0(x, t) = \tilde{\phi}(x, t)$$

since $\tilde{\phi} \leq \phi_0$ is always the case and ϕ_0 is continuous.

We proceed to show that $\tilde{\phi}$ is a subsolution of (2) with F^+ . This will then imply $\tilde{\phi} \leq \phi^+$ by comparison (see Theorem 2) and thus further $\phi^+ = \tilde{\phi}$. Let $(x, t) \in Q$ and $(p, a) \in D^+ \tilde{\phi}(x, t)$. If $x \in \Omega^+$, then note that $\tilde{\phi} = \phi^+$ in a neighbourhood of (x, t) since Ω^+ is open. Thus (p, a) is also in $D^+ \phi^+(x, t)$, which implies $a + F^+(x) |p| = 0 \leq 0$ since ϕ^+ is the solution for F^+ . Assume now $x \in \mathbb{R}^n \setminus \Omega^+$, i. e., $F(x) \leq 0$. This implies $F^+(x) = 0$ and thus $\tilde{\phi}(x, t) = \phi_0(x)$ constantly in time. In this case, we can show that $a = 0$ with the same argument as in the proof of Lemma 11. Hence also $a + F^+(x) |p| = 0 \leq 0$, which shows that $\tilde{\phi}$ is, indeed, a subsolution of (2) with speed F^+ . Similarly, one can show that $\phi^-(x, t) = \phi_0(x)$ for all $x \notin \Omega^-$ and $t > 0$.

It remains to verify that ϕ as defined in (24) is actually a solution of (2) with speed F . Take note that with the considerations above, we have already shown that ϕ is continuous since they imply, in particular, that $\phi^+(x, t) = \phi^-(x, t) = \phi_0(x)$ whenever $F(x) = 0$ and ϕ^\pm as well as ϕ_0 are continuous. With the same argument that was used above for $\tilde{\phi}$, one can now also show that ϕ itself is both a sub- and supersolution of (2), finishing the proof. \square

As a final remark, let us emphasise again that Theorem 5 allows us to reduce a general speed to the two situations $F \geq 0$ and $F \leq 0$. These are much simpler, as they imply a monotone evolution of the domain (see Lemma 13). Furthermore, by means of the symmetry shown in Lemma 14, the case $F \leq 0$ can itself be reduced to $F \geq 0$. Thus, it is most of the time enough to consider only non-negative speeds. We will often exploit this simplification in the following chapters.

3 The Hopf-Lax Representation Formula

As we have seen above in Chapter 2, the viscosity solutions of the level-set equation (2) are of fundamental importance for our purposes. Using concepts from optimal-control theory, one can interpret the level-set equation as the Hamilton-Jacobi-Bellman equation of a particular control problem (Mayer's problem, see Section III.3 of [6] and Section 3.3). In this chapter, we will discuss this connection. This will allow us to express the solution ϕ of the level-set equation via the *Hopf-Lax formula* (33). Using this representation, one can go further and deduce similar formulas for the described domains themselves. As we will see in Subsection 3.5.4, this allows for efficient computation of the evolved domains. Moreover, it is also useful for theoretical considerations. We will be able to draw important conclusions from this representation later on in Chapter 4. The main results of this chapter are based on our publication [56].

3.1 Constant Speed

To motivate the discussion that follows, we will first consider the easier case of a constant speed, i. e., $F = 1$ throughout \mathbb{R}^n . In this case, the argument is simple and we can clearly show the basic idea behind the Hopf-Lax formula. Let $\Omega_0 \subset \mathbb{R}^n$ be some initial geometry. We assume that Ω_0 is open and bounded as always. Furthermore, recall (1) and let sd_{Ω_0} denote the signed distance function of Ω_0 . Intuitively, the situation with $F = 1$ means that the boundary of the initial geometry grows over time with constant speed in normal direction. If we consider a point $x \notin \Omega_0$, it will be reached by the advancing front Γ_t precisely at time $\text{sd}_{\Omega_0}(x)$. In other words, it makes sense to conjecture that

$$\Gamma_t = \text{sd}_{\Omega_0}^{-1}(\{t\}) \quad \text{and} \quad \Omega_t = \text{sd}_{\Omega_0}^{-1}((-\infty, t)). \quad (25)$$

A more general version of this formula, valid for arbitrary speed fields, will be formulated and shown later in Corollary 5. For now, we will argue that the level-set equation in our special case of constant speed is solved by

$$\phi(x, t) = \inf \{ \phi_0(y) \mid |x - y| \leq t \}. \quad (26)$$

This is a special form of the Hopf-Lax formula (33). As we will see for the general case in Theorem 7, the form (26) implies (25). Note that our illustrative argument below will only show that ϕ given by (26) is a viscosity *supersolution* of the level-set equation. The proof that it is also a subsolution will be deferred until Lemma 31, where the general case is treated. It is easy to see that $\phi(\cdot, 0) = \phi_0$ and also that ϕ is continuous.

The main idea of our argument is to consider shifts of the initial function ϕ_0 in some given direction: Let $h \in \mathbb{R}^n$ and define

$$\bar{\phi}_h(x, t) = \phi_0(x - th).$$

It is well known (and can be easily shown) that this function solves the linear transport equation

$$\dot{\phi}(x, t) + h \cdot \nabla \phi(x, t) = 0 \quad (27)$$

if we assume sufficient smoothness and classical solutions. Even for non-smooth functions, this is still true in the viscosity sense:

Lemma 15. *The function $\bar{\phi}_h$ is a viscosity solution of (27).*

Proof. It is clear that $\bar{\phi}_h$ is continuous. Choose $(x, t) \in Q$ and let $(p, a) \in D^+ \bar{\phi}_h(x, t)$. Then

$$\phi_0(y - sh) - \phi_0(x - th) \leq a(s - t) + p \cdot (y - x) + o(|s - t| + |y - x|)$$

in the limit $(y, s) \rightarrow (x, t)$. Let $s \rightarrow t$ and choose y such that $y - x = (s - t)h$. This makes the left-hand side of the inequality above disappear. Dividing by $|s - t|$ yields

$$0 \leq a \frac{s - t}{|s - t|} + p \cdot h \frac{s - t}{|s - t|} + \frac{o(|s - t|)}{|s - t|} \rightarrow \pm(a + p \cdot h)$$

in the limit $s \rightarrow t^\pm$. Consequently, $a + p \cdot h = 0 \leq 0$ must be the case. This shows, in particular, that $\bar{\phi}_h$ is a viscosity subsolution of (27). Using an analogous argument, one can show that it is also a supersolution. \square

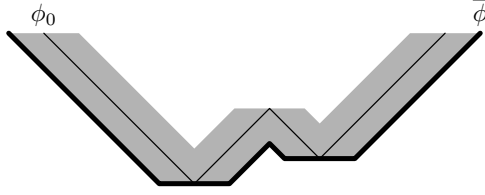


Figure 7: The infimum (lower envelope) of shifts of ϕ_0 in all directions $|h| \leq 1$. This illustrates (28) in the one-dimensional case.

For the level-set equation with $F = 1$, this result implies that all functions $\bar{\phi}_h$ with $|h| \leq 1$ are viscosity *supersolutions*: If $(x, t) \in Q$ and $(p, a) \in D^-\bar{\phi}_h(x, t)$, then

$$0 = a + p \cdot h \leq a + |p| |h| \leq a + |p|$$

as in the proof above (and making use of the Cauchy-Schwarz inequality). Note also that the infimum over shifts in all possible directions h with $|h| \leq 1$ results precisely in the Hopf-Lax formula (26) defining ϕ , as will be shown shortly in Lemma 16. See (28) and the corresponding sketch in Figure 7. This construction can also be compared to Huygens' principle for wave propagation. Using Lemma 7, we can then conclude that also ϕ is a supersolution of the level-set equation.

Lemma 16. *Let ϕ be given by (26). Then, for all $(x, t) \in \bar{Q}$,*

$$\phi(x, t) = \inf_{|h| \leq 1} \bar{\phi}_h(x, t). \quad (28)$$

Proof. For simplicity, we denote the infimum in (28) by $\bar{\phi}$ and will show $\phi = \bar{\phi}$. Fix $(x, t) \in \bar{Q}$. Note that the infimum defining $\phi(x, t)$ in (26) is actually attained. Hence, there exists $y \in \mathbb{R}^n$ with $|x - y| \leq t$ such that $\phi(x, t) = \phi_0(y)$. When we define $h = (x - y)/t$, this direction satisfies $|h| \leq 1$ and is thus admissible in the infimum in (28). In addition, this choice yields

$$\bar{\phi}_h(x, t) = \phi_0(x - th) = \phi_0(y) = \phi(x, t).$$

This implies $\bar{\phi}(x, t) \leq \phi(x, t)$, since the infimum is at most the value for this particular h .

The other way round, also the infimum in (28) is attained. So pick h_0 with $|h_0| \leq 1$ such that $\bar{\phi}(x, t) = \bar{\phi}_{h_0}(x, t) = \phi_0(x - th_0)$. Then $y = x - th_0$ satisfies $|x - y| \leq t$ and is admissible in (26). Hence, $\phi(x, t) \leq \phi_0(y) = \bar{\phi}(x, t)$. This finishes the proof. \square

3.2 Shortest Paths

In the special situation described in Section 3.1, the signed distance function sd_{Ω_0} played an important role for the Hopf-Lax formula (26). Let us now consider more general speed fields F , where we still assume $F \geq 0$ throughout this section. For this, we have to define a generalised metric instead of the Euclidean distance. It will turn out that we need the *shortest path length* between two points when the speed of movement is non-uniform and given by F . The current section is devoted to the discussion of this generalised distance function. Its analysis is a classical topic in the theory of optimal control, where this specific problem is termed *time-optimal control*:

$$\min \{t \mid \xi \in W^{1,\infty}([0, t], \mathbb{R}^n), \xi(0) = x, \xi(t) = y \text{ and } |\xi'(\tau)| \leq F(\xi(\tau)) \text{ for almost all } \tau \in [0, t]\}, \quad (29)$$

where x and y are some fixed points between which we are looking for the F -induced distance. Note that this is not the form of the distance as we will use it below, which is formulated in Definition 7. Both approaches can be related to each other with arguments similar to those we present in Section 3.3. Following the classical arguments, one can see that the minimal time from some source $y \in \mathbb{R}^n$ to other points x is the viscosity solution of the *Eikonal equation*

$$F(x) |\nabla d_y(x)| = 1, \quad d_y(y) = 0. \quad (30)$$

(Where the notion of a viscosity solution in the stationary case is defined similarly to Definition 4 for the parabolic situation.) This equation is the Hamilton-Jacobi-Bellman equation of the time-optimal control problem (29). See, for instance, Section IV.2 of [6] for a thorough discussion of these matters. We will, instead, focus here on a fundamental analysis of the shortest paths ξ themselves. The results derived will turn out to be useful later on. A presentation of optimal-control theory, dynamic programming and viscosity solutions of Hamilton-Jacobi-Bellman equations will be given later for the level-set equation itself in Section 3.3.

Note that there exists a vast literature about this problem, specifically for the case that $F \geq \underline{F} > 0$ throughout \mathbb{R}^n . See, for instance, [6], [17] and [62]. If the speed is bounded away from zero, the Hamiltonian $H(x, p) = F(x) |p|$ of the corresponding optimal-control problem is *strictly* convex. This is a frequently assumed property. See, for instance, Theorem 5.3 on page 132 of [62] for an early result. In our case, since we only have $F \geq 0$, the Hamiltonian is convex but not necessarily strictly so. As done in Theorem 5, we set $\Omega^+ = F^{-1}((0, \infty))$. Since nothing interesting happens for the time evolution on $\mathbb{R}^n \setminus \Omega^+$ according to the theorem, let us focus our attention on Ω^+ throughout this section. However, even on this set, $F > 0$ does still not imply the existence of a uniform and positive lower bound on F . With the help of Lemma 17, we will, nevertheless, still be able to reduce our situation to the classical one, so that we can apply Lions' result: Lipschitz continuity of F implies that every path going near the boundary of Ω^+ becomes “very long” (by travel time, since the speed is almost zero there). Thus, we will see that those paths can not contribute as *shortest paths* and can be ignored. This allows us to effectively assume a lower bound on F when considering the problem locally, which is enough to characterise the viscosity solution of (30).

As a first step, let us clearly define what we mean by the “paths” (and their lengths) that we already mentioned above in an informal way:

Definition 6. Let $C \subset \Omega^+$ be a connected component and $x, y \in C$. A *path* connecting x and y is a function $\xi \in W^{1,\infty}([0, 1], \mathbb{R}^n)$ with $\xi(0) = x$, $\xi(1) = y$ and $\xi(t) \in C$ for all $t \in [0, 1]$. We write $X_{\text{ad}}(x, y)$ for the set of all such paths from x to y .

For $\xi \in X_{\text{ad}}(x, y)$, the *Euclidean arc length* is defined as

$$|\xi| = \int_0^1 |\xi'(t)| \, dt$$

in the usual way. We can also define the corresponding *F-induced length* of ξ as

$$l(\xi) = \int_0^1 \frac{|\xi'(t)|}{F(\xi(t))} \, dt. \quad (31)$$

By the Sobolev embedding theorem (see, for instance, Theorem 6 on page 270 of [36]), each path $\xi \in X_{\text{ad}}(x, y)$ is continuous. Furthermore, by the continuity of F also $F \circ \xi$ is continuous, and thus this function attains a minimum on the compact interval $[0, 1]$. Since ξ maps into C , this minimum must actually be strictly positive. Thus, (31) is well-defined with $0 \leq l(\xi) < \infty$. Also note that using the fundamental theorem of calculus, one can easily show that the straight line

$$S_{xy}(t) = x + t(y - x)$$

between x and y has the shortest possible Euclidean arc length: Let $\xi \in X_{\text{ad}}(x, y)$, then

$$|\xi| = \int_0^1 |\xi'(t)| \, dt \geq \left| \int_0^1 \xi'(t) \, dt \right| = |\xi(1) - \xi(0)| = |x - y| = |S_{xy}|.$$

Another key observation is that one can always reparametrise a given path ξ such that $|\xi'(t)| = |\xi|$ is constant for all $t \in [0, 1]$. This corresponds to a parametrisation by arc length followed by a rescaling of the time interval from $[0, |\xi|]$ back to $[0, 1]$. It is easy to see that this operation does not change any geometrical properties and leaves, in particular, $|\xi|$ and $l(\xi)$ invariant. In the following, we will most of the time assume, without loss of generality, that this is done for the considered paths. With this assumption, the path length (31) becomes

$$l(\xi) = \int_0^1 \frac{|\xi|}{F(\xi(t))} \, dt. \quad (32)$$

Finally, note that paths $\xi \in W^{1,\infty}([0, 1], \mathbb{R}^n)$ are Lipschitz continuous. We denote the optimal Lipschitz constant by

$$\text{Lip}(\xi) = \sup_{t \neq s \in [0, 1]} \left| \frac{\xi(t) - \xi(s)}{t - s} \right|.$$

For paths reparametrised by arc length in the way described above, it follows easily that $\text{Lip}(\xi) = |\xi|$.

Definition 7. For $x \in \mathbb{R}^n$, we set $d(x, x) = 0$. For $y \neq x$, if there exists a connected component $C \subset \Omega^+$ with $x, y \in C$, we define

$$d(x, y) = \inf_{\xi \in X_{\text{ad}}(x, y)} l(\xi).$$

Otherwise, we set $d(x, y) = \infty$.

This defines a generalised distance $d(x, y) \in [0, \infty]$ between any two points x and y . This distance corresponds to the “shortest travel time” between the points under the speed field F . If the points are not in the same connected component of Ω^+ , then each path between them must necessarily pass through intermediate points z with $F(z) = 0$, which justifies the definition of $d(x, y) = \infty$ in this case. This will be further clarified by the following result:

Lemma 17. *Let $C \subset \Omega^+$ be a connected component, $X \subset C$ be compact, and choose $M > 0$. Then there exists $\underline{F} > 0$ such that for all $x \in X$, $y \in C$ and $\xi \in X_{\text{ad}}(x, y)$, the condition $F(\xi(t)) \leq \underline{F}$ for some $t \in [0, 1]$ necessarily implies $l(\xi) \geq M$.*

Proof. Let $\xi \in X_{\text{ad}}(x, y)$ and assume that $F(\xi(t_0)) \leq \underline{F}$ for some $\underline{F} > 0$ and $t_0 \in [0, 1]$. From Lipschitz continuity, we get

$$F(\xi(t)) \leq \underline{F} + |\xi| L_F |t - t_0|.$$

But this also implies

$$\frac{|\xi|}{F(\xi(t))} \geq \frac{|\xi|}{\underline{F} + |\xi| L_F (t_0 - t)}$$

for all $t \in [0, t_0]$. Hence

$$l(\xi) \geq \int_0^{t_0} \frac{|\xi|}{F(\xi(t))} dt \geq |\xi| \int_0^{t_0} \frac{1}{\underline{F} + |\xi| L_F (t_0 - t)} dt = \frac{\log(|\xi| L_F t_0 + \underline{F}) - \log(\underline{F})}{L_F}.$$

Now assume $F(z) \geq F_0 > 0$ for all $z \in X$, which is possible by compactness of X . This implies, in particular, $F(x) \geq F_0$. Again by Lipschitz continuity, we have

$$F_0 \leq F(x) = F(\xi(0)) \leq \underline{F} + |\xi| L_F t_0 \Rightarrow |\xi| L_F t_0 \geq F_0 - \underline{F} \geq \frac{F_0}{2}$$

if only \underline{F} is chosen at most $F_0/2$. In particular, $|\xi| L_F t_0$ is bounded away from zero with a constant depending only on X . But this gives further

$$l(\xi) \geq \frac{\log(|\xi| L_F t_0) - \log(\underline{F})}{L_F} \geq \frac{\log(F_0/2) - \log(\underline{F})}{L_F},$$

which can be made arbitrarily large by choosing \underline{F} small enough. The proof is now finished if we note that the choice of \underline{F} for the claim to be satisfied only depends on X and F but not the particular x, y or ξ under consideration. \square

Lemma 17 can be interpreted as a coercivity result: Since path lengths become infinite when approaching the boundary of Ω^+ , such paths can never be relevant for the determination of *shortest paths* and, consequently, the distance $d(\cdot, \cdot)$. This allows us to restrict ourselves to *compact* subsets of Ω^+ in these situations. As a first application of this feature, let us show the existence of a path with minimal length if x and y are in the same connected component (i. e., $d(x, y) < \infty$). For this, we make use of the theorem of Arzelà-Ascoli (see Appendix C.7 of [36]) to get compactness, and use Lipschitz estimates to show lower semi-continuity. To be precise:

Lemma 18. *Let $x, y \in \mathbb{R}^n$ with $d(x, y) < \infty$. Let $\xi \in X_{\text{ad}}(x, y)$, $(\xi_k)_{k \in \mathbb{N}} \subset X_{\text{ad}}(x, y)$ and $L > 0$ be a uniform Lipschitz constant for all ξ_k . Assume $\xi_k \rightarrow \xi$ uniformly and that all ξ_k are parametrised by arc length. (We do not assume this to be true for ξ .) Then also ξ is Lipschitz continuous and we have*

$$|\xi| = \int_0^1 |\xi'(t)| dt \leq \text{Lip}(\xi) \leq \liminf_{k \rightarrow \infty} \text{Lip}(\xi_k) \leq L.$$

Proof. For simplicity, assume that $\lim_{k \rightarrow \infty} \text{Lip}(\xi_k)$ exists. (If that is not the case, choose a subsequence that converges to the limit inferior.) Fix $t \neq s$ and note that

$$\left| \frac{\xi(t) - \xi(s)}{t - s} \right| = \lim_{k \rightarrow \infty} \left| \frac{\xi_k(t) - \xi_k(s)}{t - s} \right| \leq \lim_{k \rightarrow \infty} \text{Lip}(\xi_k).$$

Since this is true for arbitrary t and s , it also holds in the supremum to give $\text{Lip}(\xi) \leq \lim_{k \rightarrow \infty} \text{Lip}(\xi_k)$. The remaining estimates follow immediately. \square

Lemma 19. *Let $x, y \in \mathbb{R}^n$ and $d(x, y) < \infty$. Then there exists $\xi \in X_{\text{ad}}(x, y)$ such that $d(x, y) = l(\xi)$.*

Proof. By definition of $d(x, y)$, we can find a minimising sequence $(\xi_k)_{k \in \mathbb{N}}$ with $l(\xi_k) \rightarrow d(x, y)$. Assume that each ξ_k is parametrised by arc length. This implies that there exists a uniform Lipschitz constant L for all ξ_k , since each has Lipschitz constant $\text{Lip}(\xi_k) = |\xi_k|$. The arc lengths $|\xi_k|$, in turn, are bounded uniformly because the sequence minimises $l(\xi_k)$ and

$$\frac{\text{Lip}(\xi_k)}{F} \leq \int_0^1 \frac{|\xi_k|}{F(\xi_k(t))} dt = l(\xi_k).$$

By the theorem of Arzelà-Ascoli, there exists a continuous path ξ that is the uniform limit of a subsequence of $(\xi_k)_{k \in \mathbb{N}}$. Without loss of generality, assume that the subsequence is $(\xi_k)_{k \in \mathbb{N}}$ itself, so that $\xi_k \rightarrow \xi$ uniformly. Furthermore, also ξ is Lipschitz continuous with Lipschitz constant L by Lemma 18. Thus $\xi \in X_{\text{ad}}(x, y)$. Note that, in particular, the image of ξ has to lie inside of $C \subset \Omega^+$. If this were not the case, then Lemma 17 would imply that the sequence $(\xi_k)_{k \in \mathbb{N}}$ has unbounded path lengths. This would contradict the assumption that it is a minimising sequence. By definition of $d(x, y)$, it is clear that $l(\xi) \geq d(x, y)$. It remains to show that also $l(\xi) \leq d(x, y) = \lim_{k \rightarrow \infty} l(\xi_k)$ holds.

For this, define $g(\tau) = 1/F(\xi(\tau))$. Since the image of ξ lies inside of Ω^+ , we know that $F \circ \xi$ is bounded away from zero. Hence, g is Lipschitz continuous with some constant L_g . Assume that we have some partition \mathcal{I} of $[0, 1]$ into intervals $I_i = [t_i, t_{i+1}]$ and that \mathcal{I} has fineness $h = \sup_i (t_{i+1} - t_i)$. Choose $\epsilon > 0$ arbitrary and pick $K \in \mathbb{N}$ such that $\text{Lip}(\xi; I_i) \leq \text{Lip}(\xi_k; I_i) + \epsilon$ for all intervals $I_i \in \mathcal{I}$ and $k \geq K$. This is possible due to Lemma 18 (applied to the intervals I_i instead of $[0, 1]$). Finally, since $\xi_k \rightarrow \xi$ uniformly, we also have the uniform convergence $g_k = 1/(F \circ \xi_k) \rightarrow g$. Hence, we may assume $g(\tau) \leq g_k(\tau) + \epsilon$ for all $\tau \in [0, 1]$ and $k \geq K$.

Now, using again the estimates in Lemma 18, we get:

$$\int_0^1 g(\tau) |\xi'(\tau)| d\tau \leq \sum_{I_i \in \mathcal{I}} \sup_{\tau \in I_i} g(\tau) \cdot (t_{i+1} - t_i) \cdot \text{Lip}(\xi; I_i) \leq \sum_{I_i \in \mathcal{I}} \sup_{\tau \in I_i} g(\tau) \cdot \left(\int_{I_i} |\xi'_k(\tau)| d\tau + (t_{i+1} - t_i)\epsilon \right)$$

Since g is Lipschitz continuous, we also know that

$$\sup_{\tau \in I_i} g(\tau) \leq \inf_{\tau \in I_i} g(\tau) + hL_g.$$

Furthermore, clearly

$$\inf_{\tau \in I_i} g(\tau) \int_{I_i} |\xi'_k(\tau)| d\tau \leq \int_{I_i} g(\tau) |\xi'_k(\tau)| d\tau \leq \int_{I_i} (g_k(\tau) + \epsilon) |\xi'_k(\tau)| d\tau.$$

All that taken together yields

$$\begin{aligned} \int_0^1 g(\tau) |\xi'(\tau)| d\tau &\leq \sum_{I_i \in \mathcal{I}} \left(\int_{I_i} (g_k(\tau) + \epsilon) |\xi'_k(\tau)| d\tau + hL_g \int_{I_i} |\xi'_k(\tau)| d\tau + (t_{i+1} - t_i)\epsilon \|g\|_\infty \right) \\ &= \int_0^1 g_k(\tau) |\xi'_k(\tau)| d\tau + (\epsilon + hL_g) |\xi_k| + \epsilon \|g\|_\infty. \end{aligned}$$

Recall that ϵ and \mathcal{I} were arbitrary. Thus, also h can be made small. Note that $|\xi_k|$ is bounded for $k \rightarrow \infty$. This now implies the claim, since

$$l(\xi) = \int_0^1 g(\tau) |\xi'(\tau)| d\tau \leq \liminf_{k \rightarrow \infty} \int_0^1 g_k(\tau) |\xi'_k(\tau)| d\tau = \lim_{k \rightarrow \infty} l(\xi_k) = d(x, y).$$

□

We continue by deriving some fundamental properties of and estimates for the path lengths and the distance function $d(\cdot, \cdot)$:

Lemma 20. *Let $x, y \in \mathbb{R}^n$ be arbitrary. Then*

$$|x - y| \leq \bar{F} \cdot d(x, y).$$

Proof. For $d(x, y) = \infty$ and for $x = y$, the claim is obvious. Thus, assume that x and y are in the same connected component of Ω^+ and let $\xi \in X_{\text{ad}}(x, y)$. Then

$$l(\xi) = \int_0^1 \frac{|\xi|}{F(\xi(x))} dt \geq \frac{|\xi|}{\bar{F}} \geq \frac{|x - y|}{\bar{F}},$$

where we have used the assumption of a reparametrised ξ and (32). □

This result gives an important estimate relating $d(x, y)$ and $|x - y|$. If we use Lipschitz continuity of F in addition, also more precise estimates are possible especially for points close to each other. In particular, we get the following localised version of Lemma 20:

Lemma 21. *Let $x \in \Omega^+$ and $y \in \mathbb{R}^n$. Then,*

$$|x - y| \leq \frac{F(x)}{L_F} \left(e^{L_F d(x, y)} - 1 \right).$$

If, furthermore, $L_F |x - y| < F(x)$, then also

$$\begin{aligned} d(x, y) \leq l(S_{xy}) &\leq \frac{1}{L_F} \log \frac{F(x)}{F(x) - L_F |x - y|}, \\ |x - y| &\geq \frac{F(x)}{L_F} \left(1 - e^{-L_F d(x, y)} \right). \end{aligned}$$

As before, $S_{xy} \in X_{\text{ad}}(x, y)$ denotes the straight line between x and y .

Proof. If $d(x, y) = \infty$, the first claim is clear. For the remaining case, we choose $\xi \in X_{\text{ad}}(x, y)$ arbitrarily. Let ξ be parametrised by its arc length $|\xi|$. Then $|\xi| \geq |x - y|$ and Lipschitz continuity of F implies

$$F(\xi(t)) \leq F(x) + L_F |\xi(t) - x| = F(x) + L_F \left| \int_0^t \xi'(\tau) d\tau \right| \leq F(x) + L_F t |\xi|$$

for all $t \in [0, 1]$. This yields

$$l(\xi) = \int_0^1 \frac{|\xi|}{F(\xi(t))} dt \geq \int_0^1 \frac{|\xi|}{F(x) + L_F t |\xi|} dt = \frac{1}{L_F} \log \frac{F(x) + |\xi| L_F}{F(x)} \geq \frac{1}{L_F} \log \left(1 + \frac{|x - y| L_F}{F(x)} \right),$$

which also holds in the infimum over all possible paths ξ . Thus

$$e^{L_F d(x, y)} \geq 1 + \frac{|x - y| L_F}{F(x)},$$

which further implies the first estimate.

For the second estimate, note that $d(x, y) \leq l(S_{xy})$ as well as $|S_{xy}| = |x - y|$. Lipschitz continuity tells us that

$$F(S_{xy}(t)) \geq F(x) - L_F |S_{xy}(t) - x| = F(x) - L_F t |x - y|,$$

and by our assumption this expression is guaranteed to be positive for all $t \in [0, 1]$. This implies also, in particular, that S_{xy} lies entirely inside of Ω^+ . Thus we find

$$d(x, y) \leq l(S_{xy}) = \int_0^1 \frac{|S_{xy}|}{F(S_{xy}(t))} dt \leq \int_0^1 \frac{|x - y|}{F(x) - L_F t |x - y|} dt = \frac{1}{L_F} \log \frac{F(x)}{F(x) - L_F |x - y|}.$$

The third estimate is just an equivalent reformulation of the second one. \square

The following is a variant of Theorem 5.1 on page 117 of [62], adapted for our problem (30):

Lemma 22. $d(\cdot, \cdot)$ defines a metric on each connected component of Ω^+ .

Proof. By Definition 7, $d(x, x) = 0$ for each $x \in \mathbb{R}^n$. Let $C \subset \Omega^+$ be a connected component, $x, y \in C$ and $x \neq y$. For each $\xi \in X_{\text{ad}}(x, y)$, we can define $\xi_c(t) = \xi(1 - t)$, which yields $\xi_c \in X_{\text{ad}}(y, x)$ with $l(\xi) = l(\xi_c)$. Hence $d(x, y) = d(y, x)$ holds also in this case. Let now $z \in C$ be given in addition. We use Lemma 19 to choose $\xi_1 \in X_{\text{ad}}(x, z)$ and $\xi_2 \in X_{\text{ad}}(z, y)$ with

$$l(\xi_1) + l(\xi_2) = d(x, z) + d(z, y).$$

Let us define ξ as the concatenation of ξ_1 and ξ_2 with subsequent reparametrisation. Consequently, $\xi \in X_{\text{ad}}(x, y)$ and

$$d(x, y) \leq l(\xi) = l(\xi_1) + l(\xi_2) = d(x, z) + d(z, y).$$

It remains to verify that we also have non-degeneracy in the form of

$$d(x, y) = 0 \Rightarrow x = y.$$

This, however, follows directly from Lemma 20. \square

Lemma 23. Let $X \subset \Omega^+$ be compact and convex. Then

$$d(x, y) \leq L |x - y|$$

for all $x, y \in X$, where $L = 1/\underline{F}$ and $\underline{F} > 0$ is the minimum of F over X .

Proof. Let $\underline{F} > 0$ be the minimum of F on the compact set X and choose $x, y \in X$. We consider the straight line S_{xy} as particular path in $X_{\text{ad}}(x, y)$. Convexity ensures that $S_{xy}(t) \in X$ for all $t \in [0, 1]$. The claim now follows with

$$d(x, y) \leq l(S_{xy}) = \int_0^1 \frac{|S_{xy}|}{F(S_{xy}(t))} dt \leq \frac{|x - y|}{\underline{F}}.$$

\square

Lemma 24. $d(\cdot, \cdot)$ is continuous in both arguments on each connected component of Ω^+ .

Proof. Let $C \subset \Omega^+$ be a connected component and $x \in C$. By symmetry according to Lemma 22 it is sufficient to show that $d_x = d(\cdot, x)$ is continuous on C . First, we show that d_x is continuous at x itself. For this, let $(x_k)_{k \in \mathbb{N}} \subset C$ with $x_k \rightarrow x$ as $k \rightarrow \infty$ and pick $\delta > 0$ such that $\overline{B_\delta(x)} \subset C$. This is possible since C is open. Assume for simplicity and without loss of generality that $|x_k - x| < \delta$ for all $k \in \mathbb{N}$. Since $\overline{B_\delta(x)}$ is compact and convex, we can apply Lemma 23 in order to deduce

$$0 \leq d_x(x_k) = d(x_k, x) \leq L |x_k - x|$$

for some constant L . Since the right-hand side vanishes with $x_k \rightarrow x$, we find that also the limit $d_x(x_k) \rightarrow 0 = d_x(x)$ must hold. This shows continuity of d_x at x .

Now let $x, y \in C$ be arbitrary. We will show that $d_y = d(\cdot, y)$ is continuous at x . For this, choose $\epsilon > 0$. From the previous argument, we know that there exists $\delta > 0$ such that $d(x, x') < \epsilon$ if only $|x' - x| < \delta$. Applying the triangle inequality and the reverse triangle inequality from Lemma 22 for some intermediate point $x' \in B_\delta(x)$, we get

$$d(x, y) \leq d(x, x') + d(x', y) \Rightarrow d(x', y) \geq d(x, y) - d(x, x') \geq d(x, y) - \epsilon$$

and

$$d(x', y) \leq d(x', x) + d(x, y) \leq d(x, y) + \epsilon.$$

Hence we find $|d(x', y) - d(x, y)| < \epsilon$ whenever $|x' - x| < \delta$, which is the claimed continuity. \square

After this quite general discussion, let us get back to the task of solving (30). For the case of a strictly positive, uniform lower bound $F \geq \underline{F} > 0$, this is well-understood. In order to reduce our more general problem to the known results, we will make use of Lemma 17. As a first step, let us introduce a sequence of *cut-off speeds*:

Definition 8. For given $\underline{F} > 0$, we define $\tilde{F}(x) = \max(F(x), \underline{F})$. The notation $l_{\underline{F}}(\xi)$ and $d_{\underline{F}}(x, y)$ will be used for path lengths and distances according to Definition 6 and Definition 7, respectively, based on \tilde{F} instead of the original F .

Note that \tilde{F} has no longer compact support, but this is no problem since \tilde{F} is still bounded as long as the original speed field F is bounded. This guarantees that all arguments go through nevertheless. The distance $d_{\underline{F}}(x, y)$ is equivalent to $L(x, y)$ given in (47) on page 116 of [62] when using $n(x) = 1/\tilde{F}(x)$. Theorem 5.1 on page 117 of [62] will be the main tool on which we build our results. There, it is shown that $d_{\underline{F}}(\cdot, y)$ is a viscosity solution of (30) if the speed F is replaced by \tilde{F} . We will now work on reducing our situation to the case where the result of [62] is applicable.

Lemma 25. *Let $C \subset \Omega^+$ be a connected component and $X \subset C$ be compact. Then there exists $\underline{F} > 0$ such that $d(x, y) = d_{\underline{F}'}(x, y)$ for all $\underline{F}' \in (0, \underline{F}]$ and $x, y \in X$.*

Proof. Let \tilde{F} be the cut-off speed for some $\underline{F} > 0$. Then clearly $F(x) \leq \tilde{F}(x)$, which implies $l_{\underline{F}}(\xi) \leq l(\xi)$ for every path ξ . Hence also $d_{\underline{F}}(x, y) \leq d(x, y)$. It remains to show that our assumptions actually imply equality. Furthermore, if we show the result for a single \underline{F} as cut-off threshold, it must also hold for all smaller thresholds. This is the case because $\underline{F}' \leq \underline{F}$ implies $d(x, y) = d_{\underline{F}'}(x, y) \leq d_{\underline{F}}(x, y) \leq d(x, y)$. Thus, it remains to show that $d(x, y) \leq d_{\underline{F}}(x, y)$ holds for some threshold $\underline{F} > 0$.

Set $M = \max_{x, y \in X} d(x, y)$, which is well-defined and finite because of Lemma 24 and since X is compact. We now apply Lemma 17 for this M to get a corresponding positive threshold \underline{F} . We can assure $F(x) > \underline{F} > 0$ for all $x \in X$ by decreasing \underline{F} further as necessary. Now, assume that $d_{\underline{F}}(x, y) < d(x, y)$ for some $x, y \in X$. Choose a minimising path $\xi \in X_{\text{ad}}(x, y)$ with $l_{\underline{F}}(\xi) = d_{\underline{F}}(x, y)$. Consequently,

$$l_{\underline{F}}(\xi) < d(x, y) \leq l(\xi).$$

This, however, implies that there exists $t \in [0, 1]$ with $F(\xi(t)) < \underline{F}$. If that would not be the case, then $F(\xi(t)) = \tilde{F}(\xi(t))$ for all $t \in [0, 1]$ and thus the lengths would have to coincide. Define now

$$t_0 = \inf \{t \in [0, 1] \mid F(\xi(t)) \leq \underline{F}\} = \min \{t \in [0, 1] \mid F(\xi(t)) \leq \underline{F}\},$$

which is well-defined because the set is non-empty and $F \circ \xi$ is continuous. Furthermore, we have $F(\xi(t)) \geq \underline{F}$ for all $t \in [0, t_0]$ and, consequently, $F(\xi(t)) = \tilde{F}(\xi(t))$. Also, $t_0 > 0$ because $x \in X$ and thus $F(\xi(0)) = F(x) > \underline{F}$. Define now a new path $\xi_1(t) = \xi(t/t_0)$. We have $\xi_1 \in X_{\text{ad}}(x, \xi(t_0))$ and $l(\xi_1) = l_{\underline{F}}(\xi_1)$ because F equals \tilde{F} along the path. Since $F(\xi_1(1)) = \underline{F}$, we can apply Lemma 17 now to ξ_1 to deduce $l(\xi_1) \geq M$. This is a contradiction, since

$$l_{\underline{F}}(\xi) \geq l_{\underline{F}}(\xi_1) = l(\xi_1) \geq M$$

and we know $l_{\underline{F}}(\xi) < d(x, y) \leq M$. □

Theorem 6. *Let $C \subset \Omega^+$ be a connected component and $y \in C$ be fixed. Then $d_y(\cdot) = d(\cdot, y)$ is a viscosity solution of (30) in $C \setminus \{y\}$.*

Proof. Note that d_y is continuous on C by Lemma 24, and that the boundary condition is satisfied because of $d_y(y) = d(y, y) = 0$. It remains to show that d_y satisfies $F(x)|\nabla d_y(x)| = 1$ in the viscosity sense. For this, let $x \in C \setminus \{y\}$ be fixed and $p \in D^+ d_y(x)$. Now choose $Y \subset C$ compact, connected, with smooth boundary and such that $x, y \in Y^\circ$. Choose \underline{F} for Y according to Lemma 25 and such that $\underline{F} \leq \min_{z \in Y} F(z)$ in addition. Then $\tilde{F} = F$ on Y and $d_y(x') = d(x', y) = d_{\underline{F}}(x', y)$ for all $x' \in Y$. The latter property holds, in particular, also in a neighbourhood of x so that $p \in D^+ d_{\underline{F}}(x, y)$ must be true. Since $d_{\underline{F}}(\cdot, y)$ solves (30) with \tilde{F} in $Y^\circ \setminus \{y\}$ in the viscosity sense according to Theorem 5.1 on page 117 of [62], this implies $F(x)|p| = \tilde{F}(x)|p| \leq 0$. This, however, is all we need to show that d_y is a viscosity subsolution of (30) on the whole of $C \setminus \{y\}$. By a symmetric argument one can also show that it is a viscosity supersolution. □

We conclude this section with a final auxiliary result that will be useful later:

Lemma 26. *Let $X \subset \mathbb{R}^n$ be closed, $x \in X$ and assume that $d(x, y) \geq t$ for some $t \geq 0$ and all $y \in \partial X$. Then $d(x, y) > t$ for all $y \notin X$. More precisely: If $y \notin X$ and $\delta > 0$ are such that $B_\delta(y) \cap X = \emptyset$, then $d(x, y) \geq t + \delta/\bar{F}$.*

Proof. Let $y \notin X$, then there exists $\delta > 0$ such that $B_\delta(y) \subset \mathbb{R}^n \setminus X$ since $\mathbb{R}^n \setminus X$ is open. Consequently, $|x' - y| \geq \delta > 0$ for all $x' \in X$. Clearly, $y \neq x$ and if $x \notin \Omega^+$, $y \notin \Omega^+$ or they are not in the same connected component of Ω^+ , then $d(x, y) = \infty > t$ holds. So assume that $x, y \in \Omega^+$ are in the same connected component and choose $\xi \in X_{\text{ad}}(x, y)$. Since ξ is continuous, the set $\xi^{-1}(X) \subset [0, 1]$ is closed and since it is also bounded, it is compact. Define thus

$$t_0 = \max \{t \in [0, 1] \mid \xi(t) \in X\} \quad \text{and} \quad y_0 = \xi(t_0).$$

Then $y_0 \in X$ and, furthermore, $y_0 \in \partial X$ since every sequence $(\xi(t_k))_{k \in \mathbb{N}}$ with $t_k \rightarrow t_0^+$ from above is in $\mathbb{R}^n \setminus X$ and converges to y_0 . Denote the two parts of ξ up to and starting at y_0 by ξ_1 and ξ_2 , respectively. Then $\xi_1 \in X_{\text{ad}}(x, y_0)$, $\xi_2 \in X_{\text{ad}}(y_0, y)$ and $l(\xi) = l(\xi_1) + l(\xi_2)$. Since $y_0 \in \partial X$, we know by our assumption that $l(\xi_1) \geq d(x, y_0) \geq t$. Furthermore, Lemma 20 implies that

$$l(\xi_2) \geq d(y_0, y) \geq \frac{|y_0 - y|}{\bar{F}} \geq \frac{\delta}{\bar{F}}.$$

Both estimates together imply $l(\xi) \geq t + \delta/\bar{F}$. Since ξ was arbitrary, also $d(x, y) \geq t + \delta/\bar{F} > t$ follows by taking the infimum over all possible paths. \square

Note that Lemma 26 can be interpreted as a variant of the classical *minimum principle*: If $x \in \mathbb{R}^n$ is fixed and $Y \subset \mathbb{R}^n$ open with $x \notin Y$, then $d(x, \cdot)$ attains its minimum over \bar{Y} at ∂Y . (The complement $\mathbb{R}^n \setminus Y$ takes the role of the closed set X in the lemma.) A corresponding maximum principle does, however, not hold in general: If $F(y)$ is very small or even zero, then all paths connecting x to y may have a larger length than paths “circling around” y . In this case, $d(x, y)$ can, indeed, have a local maximum at y . See also [7], where a more general result is derived for viscosity solutions. The Eikonal equation, in particular, is covered by Example 5. A discussion of the classical minimum and maximum principles for harmonic functions can be found in Section 2.5 of [45].

3.3 Mayer’s Problem and the Hopf-Lax Formula

We are now ready to derive a general form of (26) for the case of $F \geq 0$. The basic idea that is illustrated in Figure 7 can still be applied. However, instead of shifts along straight lines (which are the shortest paths for $F = 1$), we have to consider the shortest paths introduced in Section 3.2. The *Hopf-Lax formula* then becomes:

$$\phi(x, t) = \inf \{\phi_0(y) \mid d(x, y) \leq t\} = \min \{\phi_0(y) \mid d(x, y) \leq t\} \quad (33)$$

Existence of a minimiser follows from continuity of ϕ_0 and $d(\cdot, \cdot)$. The aim of this section is to prove that the formula gives, indeed, the viscosity solution of the level-set equation (2). This will be done with tools from the theory of optimal control. We mainly follow the arguments outlined in Section III.3 of [6]. In the literature, the considered situation is usually more general than what we need, though. Thus, the discussion below is tailored (and simplified) specifically to our needs.

In the previous Section 3.2, we considered the paths $\xi \in X_{\text{ad}}(x, y)$ introduced in Definition 6. In particular, among the fixed quantities were both ends x, y of the path, and we were interested in the path lengths $l(\xi)$. For the current considerations, this changes. The new question is: *Which points y are reachable from a given source x in a fixed time t ?* To accommodate for this change, we introduce a new set of paths:

Definition 9. Let $x \in \mathbb{R}^n$ and $t \geq 0$. We define

$$S_t(x) = \{\xi \in W^{1,\infty}([0, t]) \mid \xi(0) = x \text{ and } |\xi'(\tau)| \leq F(\xi(\tau)) \text{ for almost all } \tau \in [0, t]\}.$$

The set of all possible *end points* $\xi(t)$ that can be reached with some $\xi \in S_t(x)$ is usually called the *reachable set* from x in time t ,

$$R_t(x) = \{\xi(t) \mid \xi \in S_t(x)\}.$$

If $F(x) = 0$, then $S_t(x) = \{\xi_0\}$, where ξ_0 is the path that is constant at x , i. e., $\xi_0(\tau) = x$ for all τ . Consequently, $R_t(x) = \{x\}$. Furthermore, for $\xi \in S_t(x)$ the path length can be estimated by

$$l(\xi) = \int_0^t \frac{|\xi'(\tau)|}{F(\xi(\tau))} d\tau \leq \int_0^t 1 d\tau = t.$$

Using these paths, we can now introduce the so-called *Mayer problem*: Find ξ minimising

$$V(x, t) = \inf_{\xi \in S_t(x)} \phi_0(\xi(t)) = \inf_{y \in R_t(x)} \phi_0(y). \quad (34)$$

This is a classical example problem in the field of optimal control. See, for instance, the introductory discussion on page 147 of [6]. Given some fixed $x \in \mathbb{R}^n$ and $t \geq 0$, the minimal value that can be achieved is denoted by $V(x, t)$. The function V is called the *value function* of the Mayer problem. One can immediately see from the definition that $V(x, t) = \phi_0(x)$ for all $t \geq 0$ and all x with $F(x) = 0$, and that $V(x, 0) = \phi_0(x)$ for all $x \in \mathbb{R}^n$. We will see below that the level-set equation is precisely the *Hamilton-Jacobi-Bellman equation* of this Mayer problem. Its value function V solves this equation in the viscosity sense, and we will see that V coincides with our Hopf-Lax formula (33). For this, we have to relate $S_t(x)$, $R_t(x)$ and $X_{\text{ad}}(x, y)$:

Lemma 27. *Let $x \in \mathbb{R}^n$ and $t \geq 0$. Then*

$$R_t(x) = \{y \in \mathbb{R}^n \mid d(x, y) \leq t\}.$$

Consequently, if ϕ is defined by the Hopf-Lax formula (33), then $V = \phi$ holds.

Proof. Let $y \in R_t(x)$. Then there exists $\xi \in S_t(x)$ with $\xi(t) = y$. Since $l(\xi) \leq t$, this yields $d(x, y) \leq t$. (After rescaling the time to the reference interval $[0, 1]$, we have $\xi \in X_{\text{ad}}(x, y)$.) Conversely, let $y \in \mathbb{R}^n$ with $d(x, y) \leq t$ be given. According to Lemma 19 there exists $\xi \in X_{\text{ad}}(x, y)$ with $l(\xi) = d(x, y) \leq t$. As before, we can assume that $|\xi'(\tau)| = |\xi|$ for all $\tau \in [0, 1]$ by reparametrising ξ according to the arc length. Consider now the initial-value problem

$$s(0) = 0, \quad \dot{s}(\tau) = \frac{1}{|\xi|} F(\xi(s(\tau))).$$

Since F and ξ are Lipschitz continuous, the Picard-Lindelöf theorem implies that there exists a unique solution s . Because its derivative is always non-negative, s is increasing. Thus, the solution exists at least until time τ_0 , where $s(\tau_0) = 1$ holds. (For $\tau > \tau_0$, the function s is not defined any more because ξ lives only on the interval $[0, 1]$.) We set $\tilde{\xi}(\tau) = \xi(s(\tau))$ for $\tau \in [0, \tau_0]$. Note that this construction ensures $\tilde{\xi} \in S_{\tau_0}(x)$. Furthermore, since $\tilde{\xi}(\tau_0) = \xi(1) = y$, we have just rescaled time without changing the path itself. Thus

$$t \geq l(\xi) = l(\tilde{\xi}) = \int_0^{\tau_0} \frac{|\xi'(s(\tau))\dot{s}(\tau)|}{F(\xi(s(\tau)))} d\tau = \int_0^{\tau_0} 1 d\tau = \tau_0.$$

Hence, we can extend $\tilde{\xi}$ to a path in $S_t(x)$ by adding a constant piece at the beginning or end. This finally implies $y \in R_t(x)$. It remains to verify that $V = \phi$, but this follows immediately since the already shown statement makes (33) and (34) equivalent. \square

Similarly to Lemma 19, we can again show that the infimum in (34) is actually a minimum and that an optimal path exists:

Lemma 28. *Let $x \in \mathbb{R}^n$ and $t \geq 0$ be given. Then $R_t(x)$ is compact and there exists $\xi \in S_t(x)$ with $V(x, t) = \phi_0(\xi(t))$. In other words, the infimum in (34) is actually attained.*

Proof. Closedness of $R_t(x)$ follows from Lemma 27 and the fact that $d(\cdot, \cdot)$ is continuous. The reachable set must also be bounded, since $y \in R_t(x)$ with $y = \xi(t)$ and $\xi \in S_t(x)$ yields

$$|y - x| \leq \bar{F} \cdot l(\xi) \leq \bar{F}t \Rightarrow |y| \leq |x| + \bar{F}t.$$

(This follows by the same argument that we used to prove Lemma 20.) Furthermore, compactness implies that there exists a minimising $y \in R_t(x)$ with $V(x, t) = \phi_0(y)$. By definition of $R_t(x)$, there also exists $\xi \in S_t(x)$ with $\xi(t) = y$. Consequently, we have $V(x, t) = \phi_0(\xi(t))$, which finishes the proof. \square

A very important property of the value function is the so-called *dynamic programming principle*:

Lemma 29. *Let $x \in \mathbb{R}^n$ and $t \geq 0$ be arbitrary. Then*

$$V(x, t) = \inf_{\xi \in S_h(x)} V(\xi(h), t - h) \quad (35)$$

for all $h \in [0, t]$.

Proof. Lemma 28 allows us to choose an optimal path $\bar{\xi} \in S_t(x)$ such that $V(x, t) = \phi_0(\bar{\xi}(t))$. We can split the path at time h into a piece $\bar{\xi}_1 \in S_h(x)$ and the remaining part $\bar{\xi}_2 \in S_{t-h}(\bar{\xi}_1(h))$. Since $\bar{\xi}_1$ is admissible for the infimum in (35) and $\bar{\xi}_2$ a particular path in the infimum that defines $V(\bar{\xi}(h), t - h)$, we find that

$$V(x, t) = \phi_0(\bar{\xi}(t)) \geq \inf_{\xi_1 \in S_h(x)} \inf_{\xi_2 \in S_{t-h}(\xi_1(h))} \phi_0(\xi_2(t - h)) = \inf_{\xi \in S_h(x)} V(\xi(h), t - h)$$

must hold. For the reverse inequality, let $(\xi_k)_{k \in \mathbb{N}} \subset S_h(x)$ be a minimising sequence for the infimum in (35). For each $k \in \mathbb{N}$, we can apply Lemma 28 to $V(\xi_k(h), t - h)$ to get $\tilde{\xi}_k \in S_{t-h}(\xi_k(h))$ with $V(\xi_k(h), t - h) = \phi_0(\tilde{\xi}_k(t - h))$. The concatenation of ξ_k and $\tilde{\xi}_k$ gives a path $\tilde{\xi}_k \in S_t(x)$, so that

$$V(x, t) \leq \liminf_{k \rightarrow \infty} \phi_0(\tilde{\xi}_k(t)) = \liminf_{k \rightarrow \infty} \phi_0(\tilde{\xi}_k(t - h)) = \lim_{k \rightarrow \infty} V(\xi_k(h), t - h) = \inf_{\xi \in S_h(x)} V(\xi(h), t - h).$$

□

The dynamic programming principle (35) was introduced by Bellman in the seminal article [9] and later described in his book [10]. See also [11] for a thorough discussion. The idea behind it is as follows: To evaluate the value function for some time t , we can first calculate it throughout space at a smaller time $t - h$. When this is done, we solve another optimisation problem (the infimum in (35)), but with shorter time horizon h . This allows us to combine the solutions of both smaller problems and arrive at the solution of the full problem we are interested in. The same idea, based on discrete optimisation variables, is also applied in computer science. This technique makes it possible to find efficient algorithms for a wide range of computational problems. See, for instance, Chapter 15 of [23].

In our context, however, Lemma 29 is mainly an intermediate result. The Hamilton-Jacobi-Bellman equation (which is for us the level-set equation (2)) can be seen as a differential version of the dynamic programming principle. Investigating this relation further will lead us to the conclusion that the value function V is a viscosity solution of (2). Using dynamic programming, we can derive other important properties of the value function:

Definition 10. The value function V satisfies *suboptimality* if $s \mapsto V(\xi(s), t - s)$ is increasing for every $\xi \in S_t(x)$. If a path $\bar{\xi} \in S_t(x)$ exists such that $s \mapsto V(\bar{\xi}(s), t - s)$ is actually constant, it also satisfies *superoptimality*.

It is easy to see that V should, indeed, have suboptimality: The larger s is, the longer is also the fixed initial segment of the path. Since only the remainder of the path is optimised in $S_{t-s}(\xi(s))$ to get $V(\xi(s), t - s)$, the resulting optimal value can only get worse (i. e., larger). Superoptimality is a direct consequence of the existence of an optimal path according to Lemma 28. Let us now give a formal proof of these intuitive arguments:

Lemma 30. *V satisfies sub- and superoptimality.*

Proof. We show suboptimality first. For this, let $t \geq 0$ and $\xi \in S_t(x)$ be given. Choose $0 \leq r \leq s \leq t$. According to the dynamic programming principle (35) applied to $\xi(r)$ and $h = s - r$, we know that

$$V(\xi(r), t - r) = \inf_{\tilde{\xi} \in S_{s-r}(\xi(r))} V(\tilde{\xi}(s - r), t - r - (s - r)).$$

This is, of course, at most the value achieved with a particular choice of $\tilde{\xi}$. If we use the piece of ξ restricted to the time interval $[r, s]$ as $\tilde{\xi}$, we have $\tilde{\xi}(s - r) = \xi(s)$ and thus

$$V(\xi(r), t - r) \leq V(\xi(s), t - s).$$

This shows suboptimality.

For superoptimality, let $\bar{\xi} \in S_t(x)$ be the optimal path from Lemma 28, such that $V(x, t) = \phi_0(\bar{\xi}(t))$. We have to show that $s \mapsto V(\bar{\xi}(s), t - s)$ is constant. By suboptimality, we have for arbitrary $s \in [0, t]$:

$$V(x, t) = V(\bar{\xi}(0), t - 0) \leq V(\bar{\xi}(s), t - s) \leq V(\bar{\xi}(t), 0) = \phi_0(\bar{\xi}(t)) = V(x, t)$$

Hence, equality holds throughout, and superoptimality is shown. \square

Another important fact is continuity of the value function. We will see later in Theorem 11 and Theorem 13 that ϕ defined by the Hopf-Lax formula is, in fact, Lipschitz continuous. Thus, let us postpone the proof of continuity until then. For now, let us check all other requirements of Definition 2. This can now be done based on sub- and superoptimality:

Lemma 31. *V is a viscosity subsolution of (2).*

Proof. Let $(x, t) \in Q$ and $\psi \in C^1(Q)$ be such that $V - \psi$ has a local maximum at (x, t) . Consider first the case $F(x) = 0$: In this situation, $V(x, \cdot)$ is constant in time. Thus, based on the same argument as (5), $\dot{\psi}(x, t) = 0$ must hold as a necessary optimality condition. But then, clearly $\dot{\psi}(x, t) + F(x) |\nabla \psi(x, t)| = 0$ is also true. So assume $F(x) > 0$ now. Choose $0 < h < t$ and $\xi \in S_h(x)$ arbitrarily for a moment. Then $V(x, t) \leq V(\xi(h), t - h)$ by dynamic programming (or suboptimality), and

$$V(\xi(h), t - h) - \psi(\xi(h), t - h) \leq V(x, t) - \psi(x, t)$$

since (x, t) is a local maximum. Taking both inequalities together, we arrive at

$$\psi(x, t) - \psi(\xi(h), t - h) \leq V(x, t) - V(\xi(h), t - h) \leq 0. \quad (36)$$

Let $p \in \mathbb{R}^n$ be such that $p \cdot \nabla \psi(x, t) = -|\nabla \psi(x, t)|$ as well as $|p| = 1$. (Normalising the gradient if it is non-zero and choosing an arbitrary vector if it is zero.) Choose ξ as the solution of

$$\xi(0) = x, \quad \xi'(\tau) = F(\xi(\tau)) \cdot p$$

for $\tau \in [0, h]$ and note that this implies, in particular, $\xi \in S_h(x)$. Since ψ and ξ are continuously differentiable, we can write

$$0 \geq \psi(x, t) - \psi(\xi(h), t - h) = \dot{\psi}(x, t) \cdot h - \nabla \psi(x, t) \cdot \xi'(0) \cdot h + o(h) = h \cdot \left(\dot{\psi}(x, t) + F(x) |\nabla \psi(x, t)| + \frac{o(h)}{h} \right).$$

Dividing by h and taking $h \rightarrow 0^+$, this yields the necessary inequality to show that V is, indeed, a viscosity subsolution of (2). \square

Lemma 32. *V is a viscosity supersolution of (2).*

Proof. Let this time $(x, t) \in Q$ and $\psi \in C^1(Q)$ be such that $V - \psi$ has a local minimum at (x, t) . Using superoptimality and proceeding similarly to the proof of Lemma 31, we can conclude as an analogue to (36) that

$$0 \leq \psi(x, t) - \psi(\xi(h), t - h)$$

for $0 < h < t$. In this case, $\xi \in S_h(x)$ is not arbitrary but instead the *particular* path for which superoptimality holds.

Since ψ is continuously differentiable and ξ is absolutely continuous, $\psi \circ \xi$ is absolutely continuous as well. Furthermore, we have the almost-everywhere derivative

$$\frac{\partial}{\partial h} (\psi(x, t) - \psi(\xi(h), t - h)) = \dot{\psi}(\xi(h), t - h) - \nabla \psi(\xi(h), t - h) \cdot \xi'(h).$$

Hence, according to Theorem 7.20 on page 148 of [74],

$$\psi(x, t) - \psi(\xi(h), t - h) = \int_0^h \left(\dot{\psi}(\xi(s), t - s) - \nabla \psi(\xi(s), t - s) \cdot \xi'(s) \right) ds.$$

Since $|\xi'(s)| \leq F(\xi(s))$, we get

$$0 \leq \psi(x, t) - \psi(\xi(h), t - h) \leq \int_0^h \left(\dot{\psi}(\xi(s), t - s) + F(\xi(s)) |\nabla \psi(\xi(s), t - s)| \right) ds.$$

Note that the integrand is continuous. Thus dividing by h and letting $h \rightarrow 0^+$ leads to

$$0 \leq \dot{\psi}(x, t) + F(x) |\nabla \psi(x, t)|,$$

which shows that V is a supersolution of the level-set equation (2). \square

Taking Lemma 31 and Lemma 32 together, we have shown that the value function V solves the level-set equation (2). In other words, the level-set equation is really the Hamilton-Jacobi-Bellman equation of Mayer's problem. But even more interesting for us is the final conclusion if we use Lemma 27 as well:

Corollary 4. *Let $F, \phi_0: \mathbb{R}^n \rightarrow \mathbb{R}$ be Lipschitz continuous and assume $F \geq 0$. Then ϕ defined by the Hopf-Lax formula (33) is the viscosity solution of the level-set equation (2) for initial data ϕ_0 .*

This formula can also be derived for the case $F \geq \underline{F} > 0$ from Theorem 3.1 on page 140 of [17]. To remove the required lower bound \underline{F} and show Corollary 4, one can then proceed with cut-off arguments as in the proof of Theorem 6. However, we believe that the derivation based directly on the Mayer problem is the most straight-forward argument. A similar derivation based on control theory is also given in [39], leading to Theorem 3.1 in the paper.

3.4 Representation of the Level-Set Domains

Based on the representation formula (33) shown for the level-set function ϕ in the previous section, we will now proceed to derive corresponding formulas describing the evolving sets Ω_t , Γ_t and $\Gamma_t \cup \Omega_t$ themselves. The crucial ingredient in those formulas is the distance between a point x and the initial set (not just a single point as given by $d(x, \cdot)$). This distance corresponds to the time it takes the evolving front to arrive at x . Roughly speaking, we are now looking at the modified Eikonal equation

$$F(x) |\nabla d_0(x)| = 1 \text{ in } C \setminus (\Gamma_0 \cup \Omega_0), \quad d_0(x) = 0 \text{ on } \Gamma_0 \cup \Omega_0. \quad (37)$$

As before, $C \subset \Omega^+$ is a connected component. In comparison to (30), we consider no longer a single point source y . Instead, the source is now the initial geometry $\Gamma_0 \cup \Omega_0$. Note, though, that we present this equation here only as a motivation for the following considerations. We will come back to it later in Section 4.1, where we build a formal connection between d_0 as defined below and (37). In the mean time, let us define the distance we need as follows:

Definition 11. Let $F \geq 0$ and denote the distance of Definition 7 by $d(\cdot, \cdot)$. For $x \in \mathbb{R}^n$, we set

$$d_0(x) = \inf_{y \in \Gamma_0 \cup \Omega_0} d(x, y), \quad d'_0(x) = \inf_{y \in \Omega_0} d(x, y).$$

If C is a connected component of Ω^+ , then d_0 is finite on the whole of C if and only if C contains a part of the initial domain $\Gamma_0 \cup \Omega_0$. If this is not the case, then the distance is infinite on the whole of C . For d'_0 , a corresponding statement is true.

Take note that it follows immediately from Definition 11 that $d_0(x) \leq d'_0(x)$ must be true for all $x \in \mathbb{R}^n$. We will show now that strict inequality can only hold if Γ_0 has non-empty interior. This is an unusual situation in applications, although we have not excluded it so far. Also note that the infimum is actually a minimum if we take it over a closed set. (The range of potential minimisers y is automatically bounded since we have $|F| \leq \bar{F}$, which means that points too far away can never minimise the distance. This follows from Lemma 20.)

Lemma 33. *Let $0 \leq F \leq \bar{F}$ and $x \in \mathbb{R}^n$ be arbitrary. Then there exist $y \in \Gamma_0 \cup \Omega_0$ and $y' \in \overline{\Omega_0}$ with $d_0(x) = d(x, y)$ and $d'_0(x) = d(x, y')$.*

Furthermore, if $\overline{\Omega_0} = \Gamma_0 \cup \Omega_0$ and either $x \in \Omega^+$ or $x \notin \Gamma_0$, then $d_0(x) = d'_0(x)$.

Proof. Let $x \in \mathbb{R}^n$ be given. Consider the case $x \notin \Omega^+$ first. If $x \in \Gamma_0 \cup \Omega_0$, then $d_0(x) = d(x, x) = 0$ and the claim is true. If this is not the case, then $d_0(x) = d(x, y) = \infty$ for all $y \neq x$ and the claim also holds. The same argument can be used for Ω_0 and d'_0 . For the second statement, we only have to consider $x \notin \Gamma_0$ since $x \notin \Omega^+$ by assumption. But then either $d_0(x) = d'_0(x) = 0$ if $x \in \Omega_0$, or otherwise $d_0(x) = d'_0(x) = \infty$ since then $x \notin \Gamma_0 \cup \Omega_0$.

Now, assume that $x \in C$ where $C \subset \Omega^+$ is a connected component. If $d_0(x) = \infty$, then also $C \cap (\Gamma_0 \cup \Omega_0) = \emptyset$ and we can choose y to be any element of $\Gamma_0 \cup \Omega_0$. The same applies if $d'_0(x) = \infty$. So assume from now on that $d_0(x)$ and $d'_0(x)$ are both finite. This together with Lemma 17 implies that there exists a compact set $X \subset C$ such that

$$d_0(x) = \inf_{y \in X \cap (\Gamma_0 \cup \Omega_0)} d(x, y), \quad d'_0(x) = \inf_{y \in X \cap \Omega_0} d(x, y). \quad (38)$$

To see this, choose $y \in C$ arbitrarily for a moment. Then $d(x, y) < \infty$. According to Lemma 17, there exists $\underline{F} > 0$ such that $d(x, \tilde{y}) > d(x, y)$ for all \tilde{y} with $F(\tilde{y}) < \underline{F}$. Thus, defining $X = F^{-1}([\underline{F}, \overline{F}])$ ensures (38). If this set is not bounded, we can, furthermore, choose some radius $R > 0$ such that $d(x, \tilde{y}) > d(x, y)$ for all \tilde{y} with $|x - \tilde{y}| > R$ based on Lemma 20. This allows us to use the compact set $X \cap \overline{B_R}(x)$ instead of X itself.

Note that $d(x, \cdot)$ is finite and continuous when restricted to X . By taking a minimising sequence and using this continuity as well as compactness of the sets $X \cap (\Gamma_0 \cup \Omega_0)$ and $X \cap \overline{\Omega_0}$, we see that the infima in (38) are actually minima. If $\overline{\Omega_0} = \Gamma_0 \cup \Omega_0$ and $y \in \Gamma_0 \cup \Omega_0$ is chosen with $d_0(x) = d(x, y)$, then

$$d_0(x) = d(x, y) \geq d'_0(x) \geq d_0(x),$$

showing equality between $d_0(x)$ and $d'_0(x)$. □

Theorem 7. *Let $F \geq 0$. Then the evolving sets can be represented as*

$$\begin{aligned} \Gamma_t \cup \Omega_t &= \{x \in \mathbb{R}^n \mid d_0(x) \leq t\}, \\ \Omega_t &= \{x \in \mathbb{R}^n \mid d'_0(x) < t\}, \\ \Gamma_t &= \{x \in \mathbb{R}^n \mid d_0(x) \leq t \leq d'_0(x)\} \end{aligned}$$

for all $t > 0$. If $\overline{\Omega_0} = \Gamma_0 \cup \Omega_0$, then the last relation states that

$$\Gamma_t = \{x \in \mathbb{R}^n \mid d_0(x) = t\} \cup (\Gamma_0 \setminus \Omega^+). \quad (39)$$

Proof. We use Corollary 4 to express ϕ by (33). Let $x \in \Gamma_t \cup \Omega_t$. By definition, this means $\phi(x, t) \leq 0$. Hence (33) implies that there exists $y \in \Gamma_0 \cup \Omega_0$ with $d(x, y) \leq t$. This, in turn, yields $d_0(x) \leq d(x, y) \leq t$. The other way round, let $d_0(x) \leq t$. By Lemma 33, there exists $y \in \Gamma_0 \cup \Omega_0$ with $d(x, y) = d_0(x) \leq t$, such that $\phi(x, t) \leq \phi_0(y) \leq 0$ by (33) and thus $x \in \Gamma_t \cup \Omega_t$.

Now assume that $d'_0(x) < t$. Applying Lemma 33 again, we find that there exists $y \in \overline{\Omega_0}$ with $d(x, y) = d'_0(x) < t$. Thus, continuity of $d(x, \cdot)$ implies that there also exists $y' \in \Omega_0$ with $d(x, y') < t$. Hence (33) yields $\phi(x, t) \leq \phi_0(y') < 0$ and, consequently, $x \in \Omega_t$. If, on the other hand, $x \in \Omega_t$ and thus $\phi(x, t) < 0$, there exists $y \in \Omega_0$ with $d(x, y) \leq t$. This implies at least $d'_0(x) \leq d(x, y) \leq t$. Let us for a moment assume that $d'_0(x) = t$. In this case, $d(x, y) = t$ must hold, and also $d(x, \tilde{y}) \geq t$ must be the case for all $\tilde{y} \in \Omega_0$. Since Ω_0 is open, there exists a small radius $\delta > 0$ such that $B_\delta(y) \subset \Omega_0$. Define $X = \mathbb{R}^n \setminus B_\delta(y)$, which is closed, and note that $x \in X$ because otherwise $x \in \Omega_0$ and this would lead to a contradiction with $0 = d(x, x) \geq t > 0$. Since $\partial X = \partial B_\delta(y) \subset \Omega_0$, we know that $d(x, \tilde{y}) \geq t$ for all $\tilde{y} \in \partial X$. This, however, implies $d(x, y) > t$ with Lemma 26, which is a contradiction. Thus we have shown that $d'_0(x) < t$ must be the case.

For the third equality, note that Γ_t and Ω_t are clearly disjoint, so that the relation

$$\Gamma_t = (\Gamma_t \cup \Omega_t) \setminus \Omega_t = \{x \in \mathbb{R}^n \mid d_0(x) \leq t \text{ and not } d'_0(x) < t\} = \{x \in \mathbb{R}^n \mid d_0(x) \leq t \leq d'_0(x)\}$$

holds. Finally, assume that we know $\overline{\Omega_0} = \Gamma_0 \cup \Omega_0$ in addition. Consider $x \in \mathbb{R}^n$. If $x \in \Gamma_0 \setminus \Omega^+$, then $\phi(x, t) = \phi_0(x) = 0$ and thus $x \in \Gamma_t$ by Theorem 5. This shows that $\Gamma_0 \setminus \Omega^+$ is always a subset of both sides of (39). Consider now the case $x \notin \Gamma_0 \setminus \Omega^+$. For these x , Lemma 33 implies that $d_0(x) = d'_0(x)$, and thus (39) holds as well. □

A part of the statement of Theorem 7 can be found already in Theorem 3.2 in [39]. Note, however, that we are not aware of any actual further conclusions derived from such a Hopf-Lax formula towards a framework for shape-sensitivity analysis or shape optimisation in general. Drawing such conclusions to derive new results in this direction is one of our main contributions, which we present in Chapter 4.

To conclude this section, we will now combine Theorem 7 with Theorem 5 to give formulas for the case of arbitrary signs of F . For this, we define $\Omega^- = F^{-1}((-\infty, 0))$ and $\Omega^z = F^{-1}(\{0\})$. We also introduce the notation

$$\Omega'_0 = \mathbb{R}^n \setminus (\Gamma_0 \cup \Omega_0) = \phi_0^{-1}((0, \infty))$$

and assume for simplicity that we are in the case $\overline{\Omega}_0 = \Gamma_0 \cup \Omega_0$. Then $\mathbb{R}^n = \Omega_0 \cup \Gamma_0 \cup \Omega'_0$ is a disjoint decomposition of \mathbb{R}^n into two open sets and the interface Γ_0 between them, which has empty interior. Next, we define a modified version of d_0 from Definition 11 for this extended situation:

$$D(x) = \begin{cases} \inf_{y \in \Gamma_0 \cup \Omega_0} d(x, y) & \text{for } x \in \Omega^+, \\ -\inf_{y \in \Gamma_0 \cup \Omega'_0} d(x, y) & \text{for } x \in \Omega^-, \end{cases} \quad (40)$$

Here, $d(\cdot, \cdot)$ is defined according to the metric discussed in Section 3.2 for the speed chosen as $|F| \geq 0$. Since there is no meaningful way to define D on Ω^z , we leave the distance undefined there. In the following, we never need the values of D on this set. On Ω^+ , where F is positive, the front moves outwards. In this case, D gives the time it takes the front to reach points outside the initial geometry. For Ω^- with negative F , the front moves inwards and D is negative *inside* the initial geometry. There, $-D$ is the time until an originally interior point is hit by the front and later no longer part of Ω_t at all. This convention for the sign of D gives it somewhat the characteristics of a signed distance function of the initial geometry (although with respect to the metric $d(\cdot, \cdot)$ induced by $|F|$ instead of the usual Euclidean distance). The composite distance D defined in this way is depicted in Figure 8. Note that D blows up towards Ω^z (the vertical line $x = 0$ in the example), which is a consequence of Lemma 17. Since this corresponds to *slow* movement of the evolving boundary, it does not create any numerical difficulties. Take note that $D = d_0$ on Ω^+ by its definition in (40). On Ω^- , the function D is defined in a similar way. This implies that most of the local properties of d_0 that we will derive in the following (e. g., Lemma 34) carry over to D .

Corollary 5. *Let F be Lipschitz continuous and have compact support. Assume that $\overline{\Omega}_0 = \Gamma_0 \cup \Omega_0$ and use the notation above. Then*

$$\begin{aligned} \Omega_t &= \{x \in \Omega^+ \mid D(x) < t\} \cup (\Omega_0 \cap \Omega^z) \cup \{x \in \Omega^- \mid D(x) < -t\}, \\ \Gamma_t &= \{x \in \Omega^+ \mid D(x) = t\} \cup (\Gamma_0 \cap \Omega^z) \cup \{x \in \Omega^- \mid D(x) = -t\}, \\ \Gamma_t \cup \Omega_t &= \{x \in \Omega^+ \mid D(x) \leq t\} \cup ((\Gamma_0 \cup \Omega_0) \cap \Omega^z) \cup \{x \in \Omega^- \mid D(x) \leq -t\} \end{aligned}$$

for all $t > 0$. Note that we no longer require that $F \geq 0$ or $F \leq 0$ throughout \mathbb{R}^n .

Proof. Since the level-set function $\phi(x, \cdot)$ is constant in time for each $x \in \Omega^z$ according to Theorem 5, it is clear that the formulas hold for those x and we only have to consider $x \in \Omega^\pm$. Let $x \in \Omega^+$. Then Theorem 5 tells us that $\phi(x, t) = \phi^+(x, t)$, where ϕ^+ solves (2) with $F^+ = \max(F, 0) \geq 0$. In particular, the evolving sets are the same as those generated by ϕ^+ when inside of Ω^+ . Take note that $D(x) = d_0(x)$ in this case, since $d(x, \cdot)$ induced by $|F|$ is the same as $d(x, \cdot)$ induced by F^+ using arguments based on Lemma 17. Hence,

$$\Omega_t \cap \Omega^+ = \{x \in \Omega^+ \mid d_0(x) < t\} = \{x \in \Omega^+ \mid D(x) < t\}$$

follows by Theorem 7 applied to F^+ . The other relations follow in the same way.

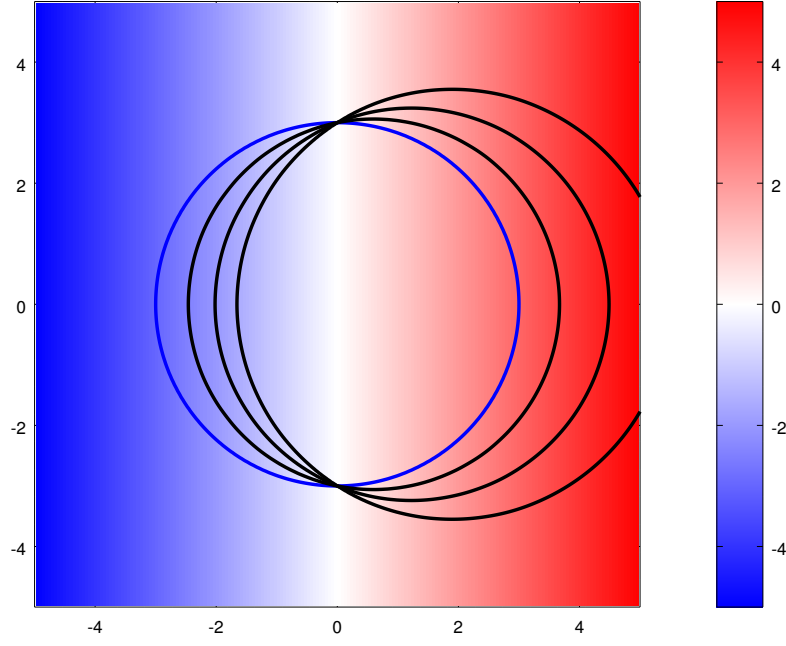
It remains to consider the case $x \in \Omega^-$. In this situation, Theorem 5 and Lemma 14 imply that $\phi(x, t) = -\phi^-(x, t)$, where ϕ^- solves (2) with $F^- = -\min(F, 0) \geq 0$ and initial data $-\phi_0$. Since this initial level-set function corresponds to the initial geometry Ω'_0 , the distance for applying Theorem 7 is $-D(x)$ in this case. This yields

$$x \notin \Omega_t \Leftrightarrow \phi(x, t) \geq 0 \Leftrightarrow \phi^-(x, t) \leq 0 \Leftrightarrow -D(x) \leq t \Leftrightarrow D(x) \geq -t.$$

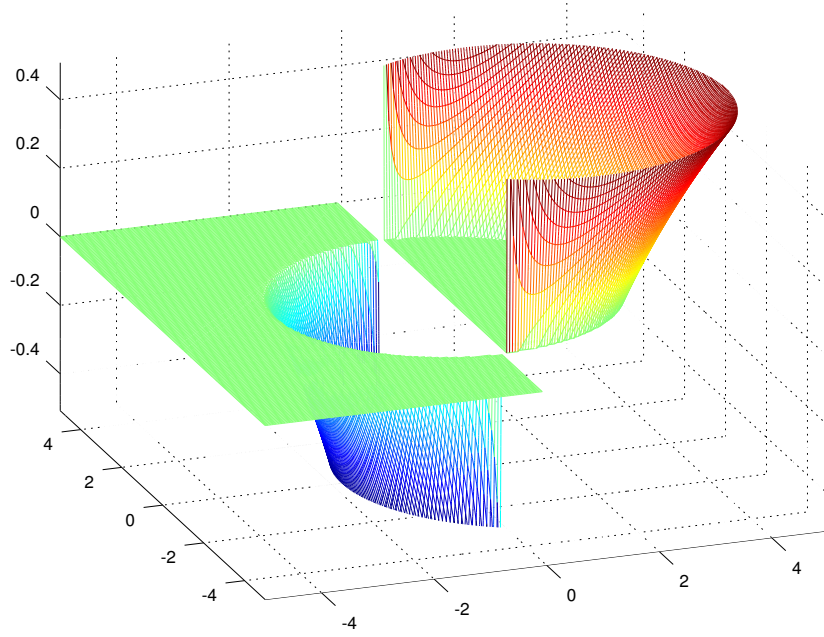
In other words,

$$\Omega_t \cap \Omega^- = \{x \in \Omega^- \mid D(x) < -t\}$$

when taking the complement. The same can be done for the other sets as well. \square



(a) The speed field, initial domain Ω_0 (blue) and resulting shape evolution (black).



(b) The composite distance D of (40).

Figure 8: Demonstration of the composite distance D of (40) and the representation formula of Corollary 5 for an example with positive and negative speeds.

The Hopf-Lax formula derived above in Corollary 5 will be used in Chapter 4 to draw some conclusions about the evolution of Ω_0 in time. Besides these theoretical purposes, it can also be employed directly for the *numerical computation* of evolved domains. This will be discussed now, particularly in Subsection 3.5.4.

3.5 Numerical Time Evolution

In the final section of this chapter, we will discuss how the time evolution of a geometry can be numerically calculated using our level-set framework. Subsection 3.5.1 briefly describes how explicit time stepping can be used together with a suitable spatial discretisation to solve (2) directly. However, it is also possible to use the Hopf-Lax formula presented before in Section 3.4 combined with the Fast Marching Method introduced by Sethian in [76]. This yields a very efficient algorithm. We present numerical examples computed with this approach in Subsection 3.5.4. The code written during this research, implementing all of the aspects discussed in the following, has been released as free software. It is available as the `level-set` package [59] for GNU Octave [35].

3.5.1 Explicit Time Stepping

The most straight-forward way to solve the level-set equation is to discretise (2) in space and time, after which standard time-stepping schemes for the solution of differential equations can be applied. It is even possible to use the simplest scheme, namely the explicit Euler method:

$$\phi_i^{k+1} = \phi_i^k - \Delta t \cdot F_i |D\phi_i^k| \quad (41)$$

Here, Δt denotes the discrete time step, ϕ_i^k is the discretised value of ϕ at time t_k and some point x_i of a spatial grid, and F_i the speed $F(x_i)$ at this grid point. For two-dimensional situations, let us use the notation x_{ij} and ϕ_{ij}^k instead. In this case, i and j correspond to row and column indices in the spatial grid, respectively. $D\phi_i^k$ is the spatial discretisation of $\nabla\phi(x_i, t_k)$. Since the level-set equation propagates a front in time, there exists an intrinsic direction for the flow of information. The discretisation scheme for $D\phi_i^k$ must be chosen carefully to respect this direction. This can be achieved with a so-called *upwind scheme*. These are commonly used in the discretisation of hyperbolic problems (like the wave equation), where a direction of propagation plays an important role as well.

To motivate this need further, consider the case of $F = 1$ and some monotonically increasing, one-dimensional initial profile ϕ_0 . One can quickly deduce from (33) that the time evolution in this case is just a shift of the profile to the right. The corresponding discrete situation is depicted in Figure 9. Since the continuous behaviour leads us to expect $\phi_i^{k+1} = \phi_{i-1}^k$ for a time step $\Delta t = h$, information should, again, be propagated from left to right. In this example, we can achieve this behaviour using *backward differences*, since then

$$\phi_i^{k+1} = \phi_i^k - \Delta t |D^- \phi_i^k| = \phi_i^k - \Delta t \cdot \frac{|\phi_i^k - \phi_{i-1}^k|}{h} = \phi_{i-1}^k.$$

Here and in the following, we use the notation

$$D^- \phi_i = \frac{\phi_i - \phi_{i-1}}{h}, \quad D^+ \phi_i = \frac{\phi_{i+1} - \phi_i}{h}$$

for backward and forward finite differences. In the two-dimensional case, $D_x^\pm \phi_{ij}$ and $D_y^\pm \phi_{ij}$ are used for the differences in x and y direction, respectively. No other spatial discretisation (e. g., the commonly used central differences) is able to reproduce the exact shift of the profile in the discrete case. Note that the direction of the differences has to be adapted if the sign of F_i changes or if the profile is (locally) decreasing instead of increasing. The simplest such upwind scheme, formulated now for a general situation in two dimensions, is the following:

$$|D\phi_{ij}| = \begin{cases} \sqrt{(\nabla_x^+ \phi_{ij})^2 + (\nabla_y^+ \phi_{ij})^2} & \text{if } F_i \geq 0, \\ \sqrt{(\nabla_x^- \phi_{ij})^2 + (\nabla_y^- \phi_{ij})^2} & \text{if } F_i \leq 0, \end{cases} \quad \text{where} \quad (42)$$

$(\nabla_x^\pm \phi_{ij})^2 = \max(D_x^\mp \phi_{ij}, 0)^2 + \min(D_x^\pm \phi_{ij}, 0)^2$ and $(\nabla_y^\pm \phi_{ij})^2$ is defined similarly.

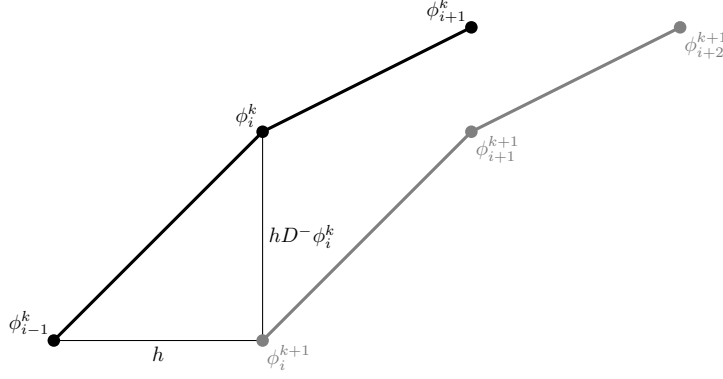


Figure 9: Application of the upwind scheme (42) leads precisely to a shift if the initial profile is monotone. This is what one expects for the exact solution as well.

For $n \neq 2$, the discretisation scheme can, of course, be generalised in the straight-forward way. This scheme is implemented in [59] and used for the demonstration in Figure 11. It is already used in [67] and discussed explicitly in Section 6.4 on page 65 of [77]. Let us remark that there exist also upwind schemes of higher order, such as those described in Section III of [67]. For simplicity, we will, however, only use the first-order scheme (42) in the following. It is sufficient for our purposes.

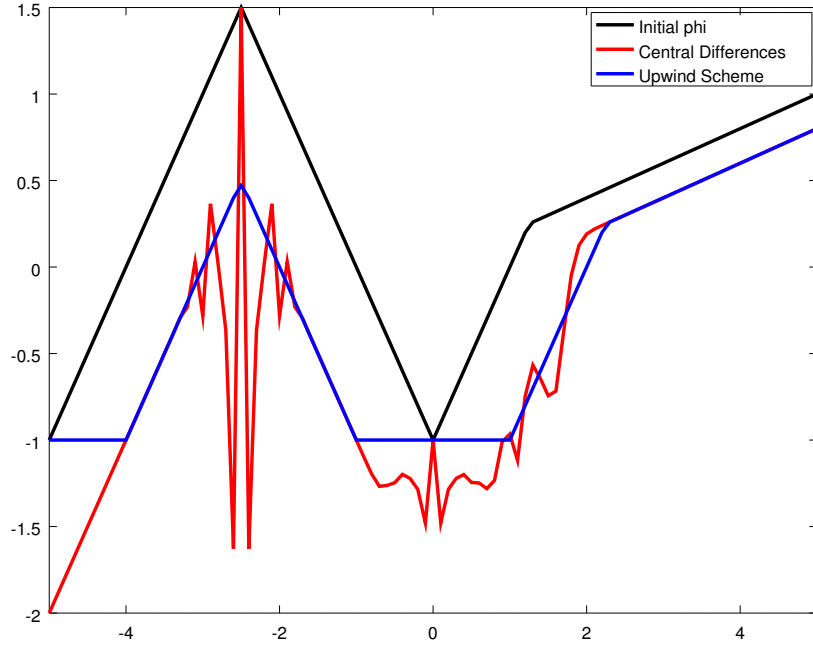
Figure 10 shows the numerical behaviour of the upwind scheme (42) in comparison to central differences in two situations. For both methods, all parameters (in particular, grid size and time step) are equal. In Figure 10a, the speed is chosen as $F = 1$. One can clearly see that the upwind scheme (blue curve) leads precisely to shifts of the initial profile (black) in the proper directions (depending on whether the profile is increasing or decreasing). The use of central differences (red line), on the other hand, leads to large, spurious oscillations in the numerics. The same can be seen in Figure 10b: Here $F = -1$ is chosen, so that the initial square shrinks over time. Again, the result with the upwind scheme is clearly far superior to the one based on central differences.

It is also important to note that the time step Δt must be chosen small enough to satisfy the Courant-Friedrichs-Lewy condition

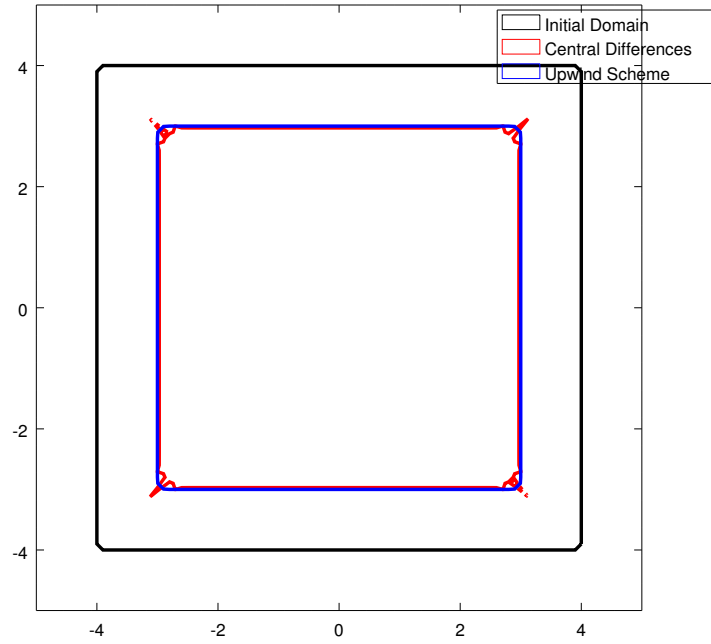
$$\Delta t \leq c \cdot \frac{h}{F n}, \quad (43)$$

where n is the space dimension and \bar{F} an upper bound for the speed. For $c \leq 1$ this condition ensures that no propagation over distances longer than a grid spacing h occurs during a single time step Δt . This is necessary for the finite-difference approximation to actually have a chance to converge to the exact solution. The original discussion of this requirement can be found in Section II.2 of [24]. For a modern reference, see Section 10.7 of [61]. The standard choice for the constant is $c = 1$, but different values can be used to fine-tune the time step in special situations.

To conclude this subsection, let us give a basic numerical example: We consider a circle as the initial domain Ω_0 and let it evolve according to the speed field $F = 1$. This simply leads to the circle's radius increasing uniformly in time, so that the exact solution is known. The Hausdorff distance (see Definition 12 below) between the exact solution and a numerical approximation obtained with the time-stepping scheme described above is plotted in Figure 11. One can clearly see that the numerical approximation converges to the exact solution if the time step is made sufficiently small. The minimal error is achieved when we choose $c \approx 3$. We are not fully sure why this is the case and why the error seems to increase back to approximately h when c is decreased further. A possible explanation is that this is an artefact from the numerical approximation of the Hausdorff distance. In particular, this approximation relies on the signed distance functions of the two sets (see [57]). The distance function of the exact solution is known precisely, but we have to approximate it for the numerical solution with the scheme described below in Subsection 3.5.2. It seems very plausible that this approximation is only accurate up to, approximately, the grid spacing h and that this leads to the observed “error” in Figure 11 for very small time steps.



(a) The level-set function ϕ for a one-dimensional situation.



(b) The evolved domain Ω_t in two dimensions.

Figure 10: Evolution of the level-set equation in time using the upwind scheme (42) (blue) as well as central differences (red) with otherwise equal parameters.

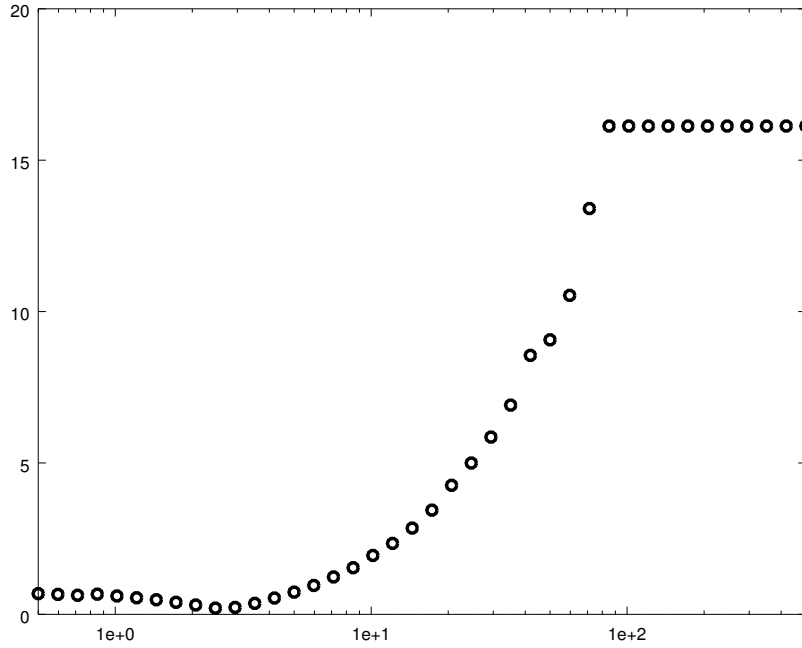


Figure 11: Difference between a circle evolved with time stepping and the exact solution. The x -axis shows the time step (actually, the choice of c in (43)). The error in the resulting shape is measured via the Hausdorff distance in units of h .

3.5.2 The Fast Marching Method

While the time stepping method described in Subsection 3.5.1 works to compute evolved geometries, we would like to take advantage of the Hopf-Lax formula shown in Theorem 7 instead. In order to do so, the main difficulty is the computation of the F -induced distance function d_0 to the initial geometry. This means that we have to solve the Eikonal equation (37) with boundary values prescribed on Γ_0 . Note that we will assume $F > 0$ throughout the current subsection. Later on in Subsection 3.5.4, we make use of Theorem 5 to discuss general speed fields. In order to arrive at a numerical approximation, we have to define again a discretisation scheme for $|\nabla d_0(x)|$. One can use (42), but it will turn out to be more convenient to use a slightly different upwind scheme. In particular, let us use

$$\max(D_x^- d_0(x_{ij}), -D_x^+ d_0(x_{ij}), 0)^2 + \max(D_y^- d_0(x_{ij}), -D_y^+ d_0(x_{ij}), 0)^2 = \frac{1}{F_{ij}^2} \quad (44)$$

together with suitable conditions for boundary values as the discrete form of (37). (As before, this equation for the two-dimensional case can be generalised to an arbitrary number of dimensions in the straight-forward way.) This scheme is used in [72], where the following convergence result is shown: The solution of (44) converges for $h \rightarrow 0^+$ to the viscosity solution of the Eikonal boundary-value problem (37). It is, again, possible to define also higher-order schemes. This is discussed in Section 8.8 of [77], but we will concentrate exclusively on the first-order scheme (44) below.

The discretisation (44) yields a quadratic equation for each grid point x_{ij} . This equation expresses $d_0(x_{ij})$ in terms of the values of d_0 at neighbouring grid points. The resulting system of equations can be solved iteratively by updating d_0 throughout the grid, using the current values for the neighbours. This method is applied in [72], and it turns out that no more changes are made after a finite number of iterations. However, one can make another observation: The upwind nature of (44) ensures a specific flow of information, similarly to the situation in Subsection 3.5.1. In particular, by construction only those neighbouring values $d_0(x_{i\pm 1, j})$, $d_0(x_{i, j\pm 1})$ actually appear in (44) whose values are less than $d_0(x_{ij})$. Furthermore, when one uses the *larger* solution of the quadratic equation, the resulting value of $d_0(x_{ij})$

will be not less than the neighbouring values used as inputs. Thus, if one chooses the right order of grid points (increasing in distance to the boundary), *a single iteration is enough!* This observation is the basis for the so-called *Fast Marching Method* introduced by Sethian in [76]. See also Chapter 8 of [77]. The implementation details used in [59] are based on the technical report [5].

Before discussing the Fast Marching Method itself, we want to introduce *Dijkstra's algorithm* [32]. This is a fundamental method to find the shortest path from some initial node x_0 to all other nodes of a graph. (Actually, the algorithm computes the *shortest distances* to all the other nodes—corresponding to the value function in optimal control. The shortest path itself can then be constructed easily in a follow-up step.) The algorithm works like this:

1. Start with some set A of nodes for which the shortest distances are already known. (Initially, this is just $A = \{x_0\}$ with distance zero.)
2. Try all edges that connect nodes in A to nodes not in A . Find the node $y \notin A$ for which the resulting distance to x_0 is smallest.
3. Add y to A and repeat until A has grown to a connected component of the graph.

With a little consideration, one can see that this algorithm works if the graph has no edges with negative weight. The distance calculated for y must, indeed, be the correct smallest possible value. In order to speed up the algorithm, note that it is not necessary to start with the search for y from scratch at every iteration: One can keep track of all points connected to A by a single edge as “candidates”. If a binary heap (see pages 144–149 of [55]) is used to store them according to their resulting distances, it is very efficient to find y (just use the heap's top element). Afterwards, when y is added to A , all new nodes that can be reached from y with a single edge are added into the heap. If some of these nodes are already there but the path via y is shorter than the previously best one, they can be “bubbled up” in the heap after decreasing their trial distance. Keeping this strategy in mind, it makes sense to divide all nodes into *three* disjoint subsets depending on their current state in the running process:

Alive Nodes for which the shortest distance is already known definitely. This is the set A from above.

Narrow Band Nodes which are already in the heap. These are the candidates for the selection of y . The name comes from the fact that they are connected to A with a single edge, thus forming a “narrow band” around the alive set A .

Far Away All other nodes, for which not even a tentative distance is known yet.

But how does all this work in our situation? Unlike shortest paths on a graph, we have no explicitly defined edges. The actual shortest path (as a continuous curve in space) connecting two arbitrary grid points will, most of the time, not go along grid lines or through other grid points. However, in some sense “implicit edges” can be defined: For each point that is a grid neighbour of the alive set, we can use (44) to compute a trial distance. In other words, the narrow band is composed of all grid neighbours of the alive set. Whenever a new point y is added to A , we add all of its neighbours in the grid (which are not yet alive) to the narrow band and recompute their distances from (44). We follow the suggestion made in [5] and only use distance values of neighbours that are already alive. All other points are assumed to have a larger distance, such that the corresponding terms in (44) vanish. As before, a binary heap can be used to keep track of all narrow-band points. An additional requirement on the used data structure is that we must be able to recalculate the distances of neighbours of a newly-alive grid point. For this to work out, one needs a way to quickly locate the heap entries corresponding to certain grid points. Thus, it is necessary to add a pointer to the heap element to each grid point's data. In the same way, each heap element must (of course) identify the grid point it corresponds to. Hence, one needs a data structure with a *two-way mapping* between heap entries and grid points.

All together, we arrive at a variant of Dijkstra's algorithm that correctly computes the shortest distances between grid points; this is the Fast Marching Method. With the suggested binary-heap technique to keep track of the narrow band, its total run-time complexity is $O(N \log N)$, where N is the total number of grid points. Considering that $O(N)$ is the minimum requirement to even *store* the distance for each grid point (let alone compute it), this is clearly a fairly efficient algorithm. See Section 4 of [76] for a proof that the distances calculated in this way actually solve our system (44) of quadratic equations. Hence, the algorithm really results in a numerical approximation for the viscosity solution of the Eikonal equation (37).

3.5.3 Initialising the Narrow Band

After introducing the basic idea of the Fast Marching Method above in Subsection 3.5.2, we have yet to discuss how the initially alive points are initialised. With them, an initial narrow band can be constructed by updating all distances for neighbours of those initially alive points with (44). This initialisation encodes the information about the initial geometry in a form that can be used and propagated by the algorithm. A possible but very crude “naive” initialisation could just add all grid points inside the initial domain Ω_0 as alive with distance zero. This, however, is obviously not a very accurate method. It is only mentioned here because we will compare it below to the more sophisticated methods that are implemented in [59]. Let us now discuss these. We assume that all information that we have about the initial geometry Ω_0 is its level-set function ϕ_0 on the grid points. With this knowledge, we can locate grid cells that are intersected by the initial boundary Γ_0 : Whenever ϕ_0 has not the same sign on all vertices of a grid cell, this cell is intersected by Γ_0 . On such a cell, we approximate ϕ_0 in an affine way in each coordinate direction. In two dimensions, this corresponds to a bilinear model. From this model, we can compute approximate intersection points between Γ_0 and the grid lines. This allows us to construct a polygonal approximation of Γ_0 . For instance, in the situation depicted in Figure 12a, this yields

$$x = \frac{\phi(c)}{\phi(c) - \phi(b)}h, \quad y = \frac{\phi(c)}{\phi(c) - \phi(d)}h \quad (45)$$

for the distances x and y to the grid point c . (Note that $\phi(c) > 0 > \phi(b), \phi(d)$ in the shown situation.) From x and y , in turn, we may estimate $d_0(c)$: This can be done in a way similar to the distance update of the Fast Marching Method. Except for pathological situations, it is plausible to assume that the proper upwind discretisation of $|\nabla d_0(c)|$ involves differences in direction towards Γ_0 . Thus, (44) becomes

$$\left(\frac{d_0(c) - d_0(b')}{x}\right)^2 + \left(\frac{d_0(c) - d_0(d')}{y}\right)^2 = \frac{1}{F(c)^2}$$

in this case. Since b' and d' are, by definition, on Γ_0 , we know $d_0(b') = d_0(d') = 0$. Hence, we can solve this equation for the unknown $d_0(c)$, which yields

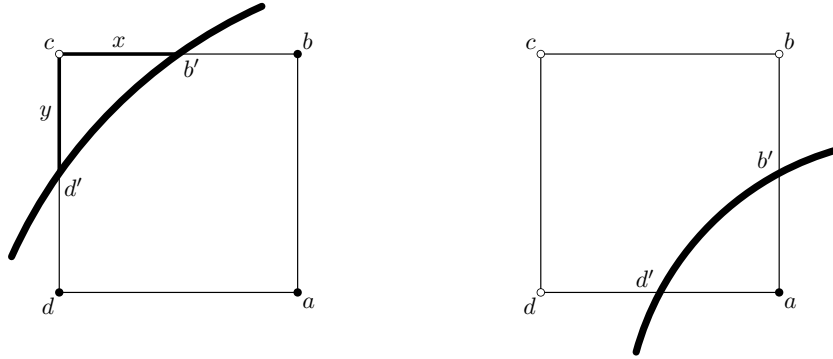
$$d_0(c)^2 \cdot \left(\frac{1}{x^2} + \frac{1}{y^2}\right) = \frac{1}{F(c)^2} \Rightarrow d_0(c) = \frac{1}{F(c)} \frac{xy}{\sqrt{x^2 + y^2}}. \quad (46)$$

Geometrically, this result for $d_0(c)$ corresponds to the altitude of the right triangle $b'-c-d'$. If we assume that Γ_0 is approximated by a straight line $b'-d'$, this is exactly what we expect. Furthermore, this method of approximating d_0 near Γ_0 is straight-forward to apply in arbitrary dimension and fits in nicely with the Fast Marching Method itself. Thus, it is used as the standard initialisation method in [59].

There are, however, situations when this method does not produce the desired result. For instance, consider Figure 12b: In this case, the standard initialisation method will set b and d to be initially alive. Let us, for the sake of simplicity in this demonstration, assume that the grid spacing is $h = 1$ and that the intersections with Γ_0 lie precisely at the midpoints of the grid edges. Furthermore, we assume $F(b) = F(c) = F(d) = 1$. In this situation, the standard initialisation method based on (44) yields $d_0(b) = d_0(d) = 1/2$. The point c , which is “diagonally away” from the initial boundary Γ_0 , is not initialised. Instead, $d_0(c)$ will be calculated from $d_0(b)$ and $d_0(d)$ during the Fast Marching procedure itself. For our example situation, one can easily see that the final result will be

$$(d_0(c) - d_0(b))^2 + (d_0(c) - d_0(d))^2 = 1 \Rightarrow d_0(c) = \frac{1}{2} + \sqrt{\frac{1}{2}}.$$

On the other hand, the *actual* distance of c , if we assume again that Γ_0 is approximated by the straight line $b'-d'$, is different: Using basic geometry, one finds that this distance is $3/\sqrt{8}$. This effect is also observed in Section 4 of [5]. There, it is attributed to the fact that the Fast Marching Method as formulated by us does not account for curvature in the front. This can be overcome by using a higher-order discretisation instead of (44). However, we suggest the following alternative initialisation method instead: Construct the boundary polygon and use it to initialise the distances for vertices of boundary grid cells. Each such point is set to be initially alive, with d_0 given by the Euclidean distance to the boundary polygon weighted by the local value of the speed field. This distance can be computed exactly



(a) Initialisation of $d_0(c)$ via (44).

(b) The case of a “diagonally away” point.

Figure 12: Initialisation of the narrow-band values for a single grid cell. Full dots are grid points inside of Ω_0 , non-filled dots are outside of the initial domain.

by looking at the edges of the boundary polygon in (at most) all four grid cells adjacent to the vertex in question. In our situation of Figure 12b, $d_0(b)$, $d_0(d)$ and $d_0(c)$ will be initialised from the edge $b'-d'$. For two space dimensions, this method is implemented in [59] and can optionally be used instead of the standard initialisation procedure.

We will now compare both methods (as well as the “naive” method described in the beginning of this subsection) to each other. For this, we chose a coarse grid so that introduced artefacts are larger. On this grid, we performed various shape evolutions utilising the different initialisation schemes. The results are shown in Figure 13 and Figure 14: The simplest situation is Figure 13a. There, the smaller black circle is propagated to grow to the larger one. Both the standard initialisation (blue) and the initialisation using the boundary polygon (green) perform very well, despite the coarse grid. Only the naive initialisation is clearly not as good, which does not come as a big surprise. For Figure 13b, the black circle was repeatedly shrunk and grown again by $h/10$. To achieve this effect, we solved the Eikonal equation (37) for alternating positive and negative speed fields. Since these evolutions cancel out exactly, the expected final result is the initial black curve itself. Note that movements of the boundary by less than a grid spacing are, of course, already a quite difficult situation for the numerical approximation. Despite this fact, both methods performed relatively well. The standard initialisation lies closer to the exact result than the initialisation from the boundary polygon, but the green curve leads to less distortions of the geometry itself. Depending on the problem, this may be a desirable property. Due to the limitations described below, this test makes no sense for the naive initialisation method. Figure 14, finally, shows the same growth as Figure 13a, but now performed as a series of 10 or 100 smaller steps. Here again, each small step moves the boundary by (much) less than a grid spacing, after which the narrow band is reinitialised for the new initial shape. Note that the naive initialisation is not able to capture any movements smaller than a grid cell at all and repeatedly cancels out all growth during the previous step, so that the only growth visible in the end is the one during the very last step alone. This explains why the red curve shows no meaningful growth with respect to the initial geometry at all. Both other methods work quite well. Figure 14b leads to a similar conclusion as Figure 13b: Initialisation from the boundary polygon gives a more faithful representation of the geometry, while the standard initialisation yields a result that is closer to the exact solution. Note, though, that the latter effect is not universal. For Figure 14a, for instance, the green curve is clearly a better approximation in all aspects than the blue one. All in all, we can conclude that both proposed initialisation methods have their merits and work quite well. Depending on the actual situation, one or the other may be more suitable. For the shape-optimisation problems solved later, the initialisation based on the boundary polygon usually performed better in our numerical experiments. For these problems, it is seemingly beneficial to avoid artificial

distortions as much as possible.

Sethian proposes an entirely different initialisation scheme in [77]: One can start from some initial level-set function ϕ_0 of Ω_0 and perform time stepping on it as described in Subsection 3.5.1. Then, for points near to the initial boundary, d_0 can be initialised by the time at which the evolving front arrives. Ideally, this only requires time stepping to be performed for a very short time interval. Afterwards, the Fast Marching Method can be used to calculate the distances of points further away from Γ_0 . We did not implement this, though, since it seems overly complicated. Furthermore, especially for a situation where the magnitude of F varies greatly, one may be forced to perform a large number of time steps. This, somehow, negates the entire purpose of Fast Marching. A further justification of our decision is the following thought: Consider again the situation of Figure 12a for the initialisation of $d_0(c)$. As before, it is plausible to assume that the upwind discretisation of $|\nabla d_0(c)|$ consists of the finite differences towards Γ_0 . In this situation, the time step (41) with the upwind discretisation (42) is given by

$$\phi^{k+1}(c) = \phi^k(c) - \Delta t \cdot F(c) \cdot \sqrt{\left(\frac{\phi^k(c) - \phi^k(b)}{h}\right)^2 + \left(\frac{\phi^k(c) - \phi^k(d)}{h}\right)^2}.$$

If we express this again by x and y of (45) and require that $\phi^{k+1}(c) = 0$, we can calculate the arrival time of the moving front at c :

$$d_0(c) = \Delta t = \frac{1}{F(c)} \frac{xy}{\sqrt{x^2 + y^2}}$$

This result, however, is precisely what one gets also from the standard initialisation (46). We would like to stress, though, that this is not a conclusive proof that Sethian's method is precisely the same as the one we propose. (Which is, depending also on the implementation details, not true in general.) But it gives a good indication that both methods are related. Given that both time stepping and the initialisation from the Fast Marching update equation (44) rely on a similar upwind discretisation, this is not surprising.

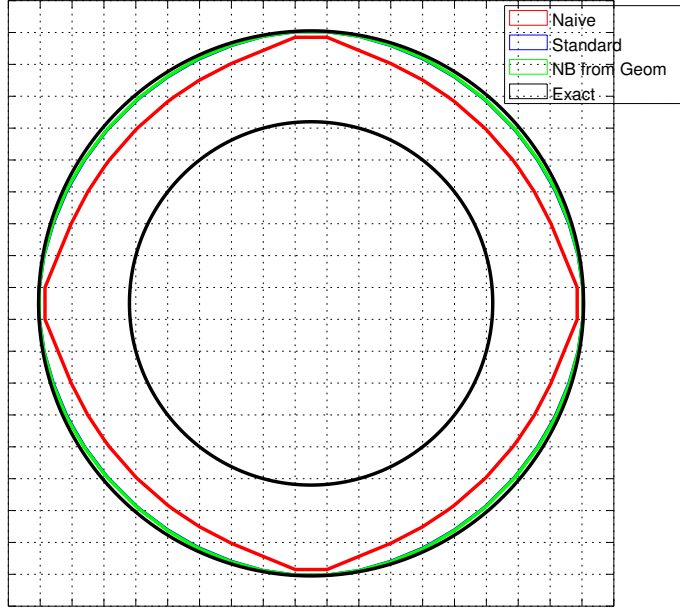
3.5.4 Composite Fast Marching

Having discussed the Fast Marching Method now in detail, we know how the Eikonal equation for d_0 can be solved numerically for the case $F > 0$. This, finally, allows us to numerically construct evolved domains Ω_t by putting all pieces of the puzzle together: Let ϕ_0 be given as a level-set function of the initial geometry Ω_0 and $F: \mathbb{R}^n \rightarrow \mathbb{R}$ as a speed field with arbitrary signs. In order to handle positive as well as negative speeds, we use Corollary 5 (based on Theorem 5) to combine results in $\Omega^+ = F^{-1}((0, \infty))$ with results in $\Omega^- = F^{-1}((-\infty, 0))$. This leads us to a *Composite Fast Marching* method. In particular, we employ Fast Marching twice: Once in Ω^+ and once in Ω^- , where $-F$ is used as a second (again positive) speed field. In this way, we are able to construct D as defined in (40) numerically on $\Omega^+ \cup \Omega^-$. Whenever a connected component of Ω^+ or Ω^- does not contain parts of Γ_0 , it may happen that Fast Marching is not able to calculate distances to all points in this connected component. If this is the case, it means that no admissible paths exist to those points. We set D to $\pm\infty$ there. This method is implemented in `ls_solve_stationary` of [59]. Let us also refer to [19], which presents a further generalisation of the Fast Marching Method to speed fields with arbitrary signs that may even depend on time. We will, nevertheless, stick to our method of handling sign changes in the speed field based on Theorem 5. Since we are not interested in time-dependent speeds, this seems more natural and easier to implement. It is, furthermore, useful for theoretical conclusions in Chapter 4 as well, not just for numerical computations.

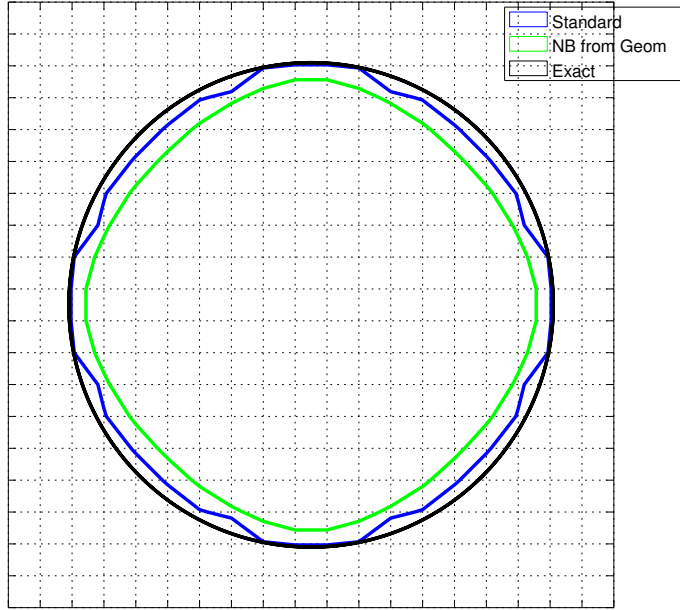
With D computed, it is straight-forward to give a level-set function $\phi(\cdot, t)$ for the evolved shape Ω_t at any time $t > 0$: Following Corollary 5, we may choose

$$\phi(x, t) = \begin{cases} D(x) - t & \text{if } F(x) > 0, \\ \phi_0(x) & \text{if } F(x) = 0, \\ D(x) + t & \text{if } F(x) < 0. \end{cases} \quad (47)$$

This is the level-set function returned by `ls_extract_solution` of [59]. Note that ϕ defined in this way may contain infinite values if D is computed as described above. Since only the sign of ϕ is relevant from the geometrical perspective of encoding Ω_t , this is fine. Also our code in [59] is designed to handle infinite values in level-set functions well. If one does not want to do that, however, it is straight-forward

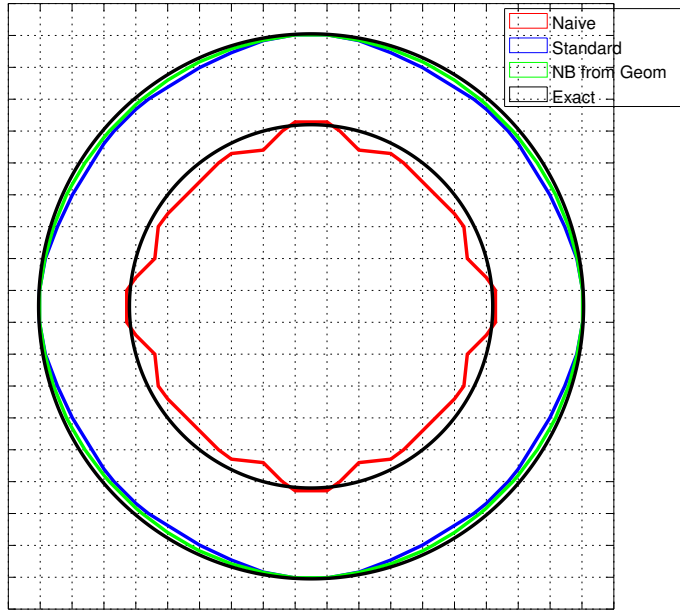


(a) Growth in a single propagation step.

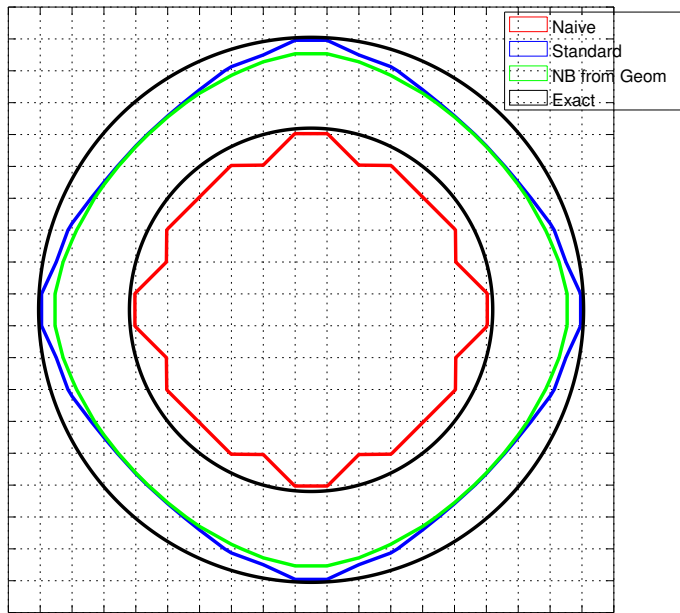


(b) 50 repetitions of shrinking and growing, cancelling each other out.

Figure 13: Demonstration how the shape evolution depends on the method used to initialise the narrow band. The black curve shows the exact initial and expected final shapes. Red is the numerical result using the “naive” initialisation and blue for the generic initialisation method based on the update equation (44). The green line shows the result if the boundary polygon is used to initialise the narrow band.



(a) Growth in 10 small steps.



(b) Growth in 100 small steps.

Figure 14: Continuation of Figure 13. We show the evolution of Figure 13a, but now the propagation is done in a series of small steps. Note that each small step moves the boundary by less than a grid spacing (especially in the bottom).

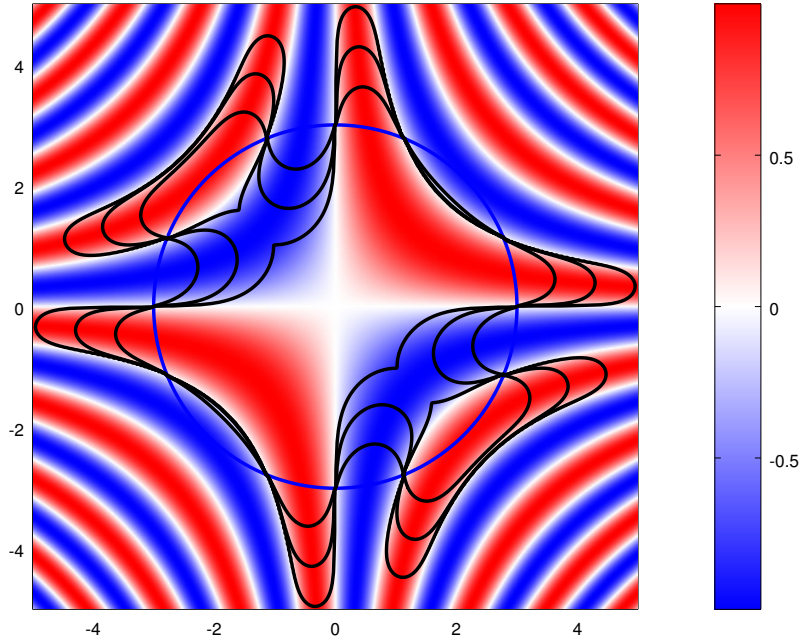
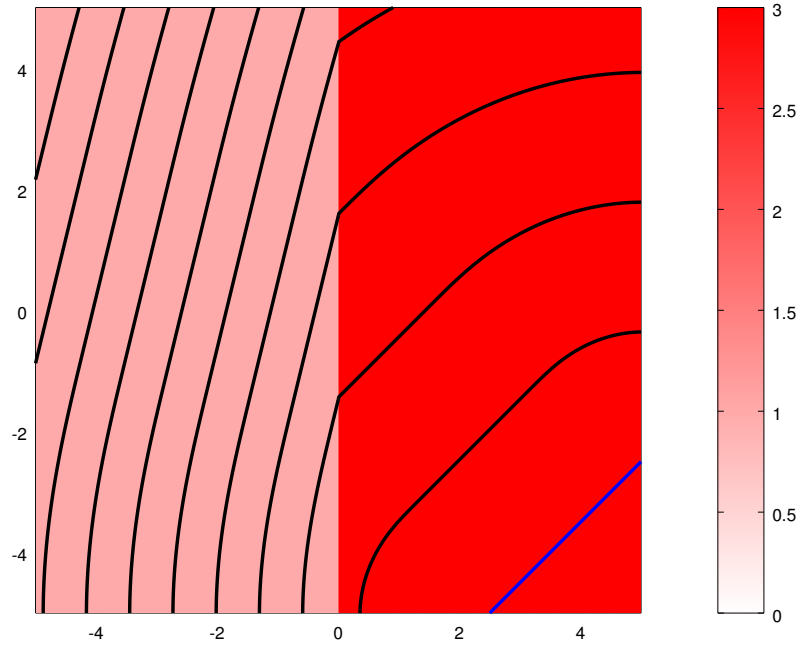


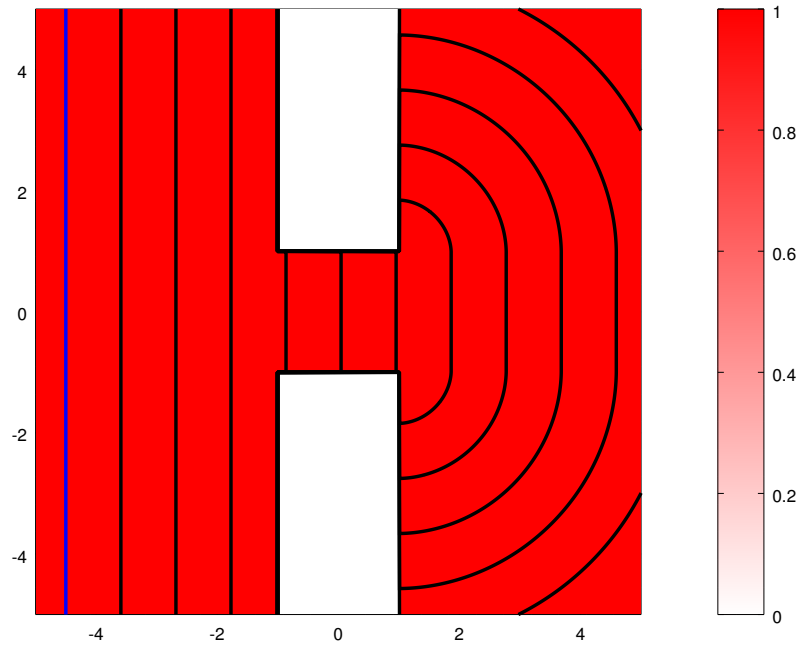
Figure 15: Evolution of a circle (blue) in a speed field with sign changes. The speed field is indicated by the colour map in the background. The black lines show the evolved shapes Ω_t for various times $t > 0$. Note the splitting of components at the last shown time. See also Figure 2.

to adapt our method in such a way that values of ϕ are always finite. Let us now also point out a very nice property of this method for evolving Ω_0 in time: The most expensive part of the calculation is the construction of D . (But also that is quite efficient with Fast Marching, as discussed in Subsection 3.5.2.) This computation does not depend on t . The explicit time is only required in the final step, when we apply (47). This last step, though, requires nothing more than a simple evaluation of (47) and is thus very cheap. Consequently, our method is especially efficient if Ω_t must be computed at multiple times t for a single speed field F . This is, for instance, the case when performing line searches during a shape-optimisation procedure such as the one discussed below in Section 6.3.

Let us now, finally, present computational results for several speed fields and geometries: Figure 2, Figure 8a, Figure 15 and Figure 16 all show geometrical evolutions calculated with our implementation of Composite Fast Marching in [59]. These examples show very well that the method is robust and flexible, so that it can handle various situations including sign changes in F . Even discontinuities of the speed field pose no numerical problems in these examples. We have to point out, though, that we have no theoretical justification for using speed fields that are not Lipschitz continuous.



(a) Refraction from thinner to denser medium.



(b) Diffraction around an obstacle.

Figure 16: Continuation of Figure 15. Movement of a front (shown in blue at the initial position) through a medium with varying speed of propagation.

4 Conclusions from the Hopf-Lax Formula

Let us now discuss some important conclusions from and applications of the Hopf-Lax representation formula shown above in Theorem 7 and Corollary 5. Equipped with this powerful tool, we are now able to derive new results about non-fattening, shape-sensitivity analysis, Lipschitz continuity of the evolved level-set function ϕ and the effect of perturbations in the speed field or initial domain. These results are published in [56] and will also be presented below. Particularly the shape calculus of Section 4.2 is very important for level-set based shape optimisation. In addition to the results also given in [56], we include considerations about the Hausdorff distance between evolved surfaces and the reachability of shapes with our speed method at the end of this chapter. They are also of particular interest for shape optimisation.

4.1 Measure-Theoretic Non-Fattening

When the level-set approach is used to describe geometries, the set Γ_t as given in Definition 1 is usually thought of as the “boundary” of the geometry one is interested in. With this interpretation, one definitely does not want Γ_t to become “fat” in any way (for instance, developing interior points or having non-zero measure). A classical result showing *non-fattening* in the former, topological sense under certain conditions is presented in [8]. We are not aware of any results with respect to the latter, measure-theoretic notion of non-fattening. Based on the representation of the evolving sets derived in Theorem 7, the issue of non-fattening can now be investigated with relative ease.

Lemma 34. *Let $\Omega^+ = F^{-1}((0, \infty))$ as before, $C \subset \Omega^+$ be a connected component and assume that d_0 is finite on C . Then d_0 is locally Lipschitz continuous on C and, in particular, differentiable almost everywhere in C . The same holds for d'_0 .*

Proof. We can assume $F \geq 0$ throughout \mathbb{R}^n without loss of generality, as we only consider Ω^+ anyway. We also restrict ourselves to d_0 here; the same arguments can be applied for d'_0 as well. Note that if local Lipschitz continuity is shown, differentiability almost everywhere follows by Rademacher’s theorem (see Theorem 2 on page 81 of [37]).

Let $X \subset C$ be compact and convex. Since F is continuous, we can introduce $\underline{F} > 0$ as the minimum of F over X . We will show now that d_0 has the Lipschitz constant $L = 1/\underline{F}$ on X . For this, let $x, y \in X$ be given. We can choose $x_0 \in \Gamma_0 \cup \Omega_0$ with $d_0(x) = d(x, x_0)$ by Lemma 33. Note also that $d_0(x) < \infty$ according to our assumption, and that $d(x, y) \leq L|x - y|$ as shown in Lemma 23. Thus, the triangle inequality implies

$$d_0(y) \leq d(y, x_0) \leq d(y, x) + d(x, x_0) \leq d_0(x) + L|x - y|.$$

If we exchange the roles of x and y , the same argument can be applied to derive an estimate the other way round. Taking both inequalities together, we get $|d_0(x) - d_0(y)| \leq L|x - y|$. \square

As a next step, recall the Eikonal equation (37) with boundary values on $\Gamma_0 \cup \Omega_0$. Without any mathematical analysis, we have used it to motivate the distance d_0 from Definition 11. Now, we will see that d_0 actually solves the equation in a certain sense. This turns out to be a useful tool for the proof of our non-fattening result Theorem 8. Of course, corresponding properties always also hold for d'_0 when the boundary values are prescribed on $\bar{\Omega}_0$ instead of $\Gamma_0 \cup \Omega_0$.

Lemma 35. *The function d_0 is a viscosity supersolution of (37).*

Proof. Recall that

$$d_0 = \inf_{y \in \Gamma_0 \cup \Omega_0} d_y$$

is defined as pointwise infimum of a family of functions $d_y(\cdot) = d(\cdot, y)$. Each d_y is a viscosity solution of (30) according to Theorem 6. Thus their infimum is also at least a viscosity supersolution of the equation. (See, for instance, Lemma 2.4.5 on page 101 of [41] for this well-known property of viscosity solutions. Compare also Lemma 7 above, which was shown for the parabolic case.) Since $d_0(x) \geq 0$ is fulfilled for all $x \in \mathbb{R}^n$, it holds, in particular, for $x \in \Gamma_0 \cup \Omega_0$. This shows that also the boundary condition is satisfied. \square

Lemma 36. *The function d_0 solves (37) almost everywhere. In particular, $F(x)|\nabla d_0(x)| = 1$ for all $x \in \Omega^+ \setminus (\Gamma_0 \cup \Omega_0)$ at which d_0 is differentiable.*

Proof. Fix $x \in \Omega^+ \setminus (\Gamma_0 \cup \Omega_0)$ such that $d_0(x) < \infty$ and $\nabla d_0(x)$ exists. Note that $F(x)|\nabla d_0(x)| \geq 1$ according to Lemma 35 and thus also, in particular, $\nabla d_0(x) \neq 0$. We have to show $F(x)|\nabla d_0(x)| \leq 1$. Define $p_0 = \nabla d_0(x)/|\nabla d_0(x)|$ and note that $|\nabla d_0(x)| = \nabla d_0(x) \cdot p_0$, which is the directional derivative of d_0 in direction p_0 . For $\epsilon > 0$, consider $\overline{B_\epsilon(x)}$. If ϵ is small enough, this is a compact and convex subset of Ω^+ , so that Lemma 34 yields that d_0 is Lipschitz continuous on $\overline{B_\epsilon(x)}$. The Lipschitz constant is $L_\epsilon = 1/\underline{F}_\epsilon$, where $\underline{F}_\epsilon = \min_{y \in \overline{B_\epsilon(x)}} F(y)$. By continuity of F , $L_\epsilon \rightarrow 1/F(x)$ as $\epsilon \rightarrow 0^+$. Hence

$$|\nabla d_0(x)| = \nabla d_0(x) \cdot p_0 = \lim_{\epsilon \rightarrow 0^+} \frac{d_0(x + \epsilon p_0) - d_0(x)}{\epsilon} \leq \lim_{\epsilon \rightarrow 0^+} \frac{|d_0(x + \epsilon p_0) - d_0(x)|}{\epsilon} \leq \lim_{\epsilon \rightarrow 0^+} L_\epsilon = \frac{1}{F(x)},$$

which completes the proof. \square

Lemma 36 will be strengthened below in Lemma 52, where we are also able to provide directional information about ∇d_0 along optimal paths. The advantage of Lemma 36, however, is that its statement is true whenever ∇d_0 exists. The later result only applies along the path, which is of no help for our analysis of non-fattening as the image of the path has measure zero.

We now need a general lemma about the measure of level sets of Lipschitz continuous functions:

Lemma 37. *Let $\Omega \subset \mathbb{R}^n$ and $f: \Omega \rightarrow \mathbb{R}$ be Lipschitz continuous. Then*

$$\text{vol}(f^{-1}(\{0\})) = \text{vol}(\{x \in \Omega \mid f(x) = 0 \text{ and } f \text{ is differentiable at } x \text{ and } \nabla f(x) = 0\}), \quad (48)$$

where $\text{vol}(\cdot)$ denotes the n -dimensional Lebesgue measure of the preimage sets.

Proof. This follows immediately from Lemma 7.7 on page 152 of [42]. \square

Lemma 37 shows that if a level set of some Lipschitz continuous function “fattens” in measure, then there must also exist a set of positive measure on which its gradient exists and vanishes. This can not happen for our case of d_0 , since we know that it solves (37) almost everywhere. This is the central argument in the proof of our main non-fattening result:

Theorem 8. *Let $\text{vol}(\Gamma_0) = 0$. Then $\text{vol}(\Gamma_t) = 0$ for all $t \geq 0$.*

Proof. Note first that $\text{vol}(\Gamma_0) = 0$ implies, in particular, $\overline{\Omega_0} = \Gamma_0 \cup \Omega_0$. If this were not the case, then Γ_0 would have interior points and thus non-zero measure. We now apply Corollary 5 to express Γ_t and calculate its measure. Note that the part $\Gamma_t \cap \Omega^z = \Gamma_0 \cap \Omega^z$ can be ignored, since it has zero measure by assumption. Thus, consider $\Gamma_t \cap \Omega^+ = D^{-1}(\{t\})$ first. Since $D = d_0$ in Ω^+ , Lemma 34 and Lemma 36 apply. These results together imply that $\nabla D(x) \neq 0$ for almost all $x \in \Gamma_t \cap \Omega^+$. Consequently, it follows from Lemma 37 that $\text{vol}(\Gamma_t \cap \Omega^+) = 0$. The same argument can also be used for $\text{vol}(\Gamma_t \cap \Omega^-)$, so that we have finally shown $\text{vol}(\Gamma_t) = 0$. \square

We conclude this section by using our representation formula to show non-fattening also in a topological sense. This result is similar to the classical result of [8]. Note, however, that our result concerns the sets for each instant in time separately, while the result of [8] considers the topological properties of the evolving sets in space-time. The property that we show is strictly stronger, although [8] considers a more general situation.

Theorem 9. *Let $F \geq 0$ and assume that $\overline{\Omega_0} = \Gamma_0 \cup \Omega_0$. Then $\overline{\Omega_t} = \Gamma_t \cup \Omega_t$ for all $t \geq 0$.*

Proof. Note that $\overline{\Omega_t} \subset \Gamma_t \cup \Omega_t$ follows immediately from Definition 1 because ϕ is continuous. Hence, we only have to show $\Gamma_t \cup \Omega_t \subset \overline{\Omega_t}$. Let us use Theorem 7 to express the evolving sets. The case $F(x) = 0$ is easy: If $x \in \Gamma_t \cup \Omega_t$, then $x \in \Gamma_0 \cup \Omega_0$ since these sets are stationary in time on Ω^z . Hence $x \in \overline{\Omega_0} \subset \overline{\Omega_t}$ by assumption. (Recall that $F \geq 0$ implies monotonic growth of the domains according to Lemma 13.)

For the remaining case, let $x \in (\Gamma_t \cup \Omega_t) \cap \Omega^+$. Since nothing is to be shown if $x \in \Omega_t$, assume that $x \in \Gamma_t$. Thus $d_0(x) = t$ by Theorem 7. Lemma 33 implies that there exists $x_0 \in \overline{\Gamma_0 \cup \Omega_0}$ with $d_0(x) = d(x_0, x) = t$. Assume that $x \notin \overline{\Omega_t}$, which means that there exists $\delta > 0$ with $\overline{B_\delta(x)} \subset \Omega^+ \setminus \Omega_t$. In other words, $d_0(y) \geq t$ for all $y \in \overline{B_\delta(x)}$. Note that this also implies $d(x_0, y) \geq t$ for all those y , since $d_0(y) \leq d(x_0, y)$. Consider now the closed set $X = \mathbb{R}^n \setminus B_\delta(x)$, for which we know $x_0 \in X$ and $d(x_0, y) \geq t$ for all $y \in \partial X = \partial B_\delta(x)$. Thus Lemma 26 implies $d(x_0, x) > t$, which is a contradiction. Hence we have shown $x \in \overline{\Omega_t}$. \square

For the case of $F \leq 0$, a similar statement can be shown by applying Lemma 14 and taking complements of all involved sets:

$$(\Gamma_0 \cup \Omega_0)^\circ = \Omega_0 \Rightarrow (\Gamma_t \cup \Omega_t)^\circ = \Omega_t$$

It is, however, not possible to get both results at the same time, and also not to get one of them for changing sign of F . This is demonstrated by the following example:

Example 7. Let $\phi_0(x) = |x| - 1$, such that $\Omega_0 = B_1(0)$ and $\Gamma_0 = \partial\Omega_0$. Choose $F \leq 0$ with compact support and Lipschitz continuous such that $F(x) = -1$ for all $x \in B_{1+\epsilon}(0)$ with some $\epsilon > 0$. Then $\Omega_t = B_{1-t}(0)$ is a shrinking circle that disappears for $t \geq 1$ entirely. This implies that we have, for $t = 1$, $\Gamma_1 \cup \Omega_1 = \{0\} \neq \overline{\Omega_1} = \emptyset$.

Similarly, if we choose Ω_0 to be $B_2(0) \setminus \overline{B_1(0)}$ and $F \geq 0$ with $\text{supp}(F) \subset B_2(0)$ and $F(x) = 1$ for all $x \in B_{1+\epsilon}(0)$, then $\Omega_t = B_2(0) \setminus \overline{B_{1-t}(0)}$ and the hole disappears at $t = 1$. In this case, $(\Gamma_1 \cup \Omega_1)^\circ = B_2(0) \neq \Omega_1 = B_2(0) \setminus \{0\}$.

4.2 Shape Sensitivity of Domain Functionals

If one considers a functional depending on the evolving sets, one is often also interested in its derivative with respect to time in the shape propagation. This leads to *shape derivatives*, which form the foundation for level-set based schemes for shape optimisation as investigated in this work. In the applied literature such as [34], [75] and [80], the shape-sensitivity formulas are not always rigorously justified or rely on smoothness assumptions on the domain which may not be fulfilled in practice. Based on our representation formula of Corollary 5, we are able to rigorously derive such a shape derivative for an important class of domain functionals. This result can be applied to the mentioned and other problems. We will do so later in Chapter 6 and Chapter 8. Note specifically that our shape calculus requires *no regularity assumptions* on the domain Ω besides being an open set and having a boundary with measure zero. We are not aware of any other result that has this feature. Recall also that we use a *scalar* speed field, which defines the direction of movement via the normal direction of the domain itself. Classical shape-sensitivity analysis as discussed, for instance, in Chapter 9 of [30] usually requires a *vector-valued* velocity field which is completely independent of the geometry. This is a much stronger assumption than ours: Consider, for instance, the simple case $F = 1$ and some initial Ω_0 that has a corner (e. g., a square). Our approach is perfectly able to handle this situation, since the scalar speed field is obviously completely smooth in this situation. A corresponding velocity field describing the same outward movement, however, must necessarily be discontinuous at the corner due to the discontinuous normal direction there. Thus, standard shape calculus is not applicable for such a propagating geometry.

In this section, we will always assume that $\text{vol}(\Gamma_t) = 0$ holds for all times as per Theorem 8. For $f \in L^1_{\text{loc}}(\mathbb{R}^n)$, we define the domain functional

$$j(t) = \int_{\Omega_t} f \, dx.$$

With the help of the co-area formula (Theorem 2 on page 117 of [37]) and Corollary 5, the functional $j(t)$ can be expressed in terms of the composite distance D defined in (40):

Theorem 10. *If Corollary 5 holds for Ω_t , then*

$$j(t) = j(0) + \int_0^t \int_{\Omega^+ \cap D^{-1}(\{s\})} F f \, d\sigma \, ds + \int_0^t \int_{\Omega^- \cap D^{-1}(\{-s\})} F f \, d\sigma \, ds \quad (49)$$

for all $t \geq 0$. Based on (40), this expression can also be written more compactly as

$$j(t) = j(0) + \int_{-t}^t \int_{D^{-1}(\{s\})} F f \, d\sigma \, ds.$$

Proof. For $t = 0$, the claim is clear. So assume $t > 0$ fixed now. We use the decomposition of Ω_t that is given in Corollary 5 as well as the representation

$$j(t) = j(0) + \int_{\Omega_t \setminus \Omega_0} f \, dx - \int_{\Omega_0 \setminus \Omega_t} f \, dx. \quad (50)$$

Note further that

$$\Omega_t \setminus \Omega_0 = \Omega^+ \cap D^{-1}((0, t))$$

is the part of Ω_t that an outward-moving boundary has created over time, while

$$\Omega_0 \setminus \Omega_t = \Omega^- \cap D^{-1}((-t, 0))$$

is the subset that an inward-moving boundary has removed from Ω_0 .

Consider the first of these sets now and recall that D is locally Lipschitz continuous on $\Omega^+ \cap D^{-1}((0, t))$ according to Lemma 34. Furthermore, $|\nabla D(x)| = 1/F(x)$ holds for almost all $x \in \Omega^+ \cap D^{-1}((0, t))$ because of Lemma 36. Let $(A_k)_{k \in \mathbb{N}}$ be a sequence of compact subsets of $\Omega^+ \cap D^{-1}((0, t))$ converging in measure to $\Omega^+ \cap D^{-1}((0, t))$ as $k \rightarrow \infty$. Such a sequence exists by regularity of the Lebesgue measure (Theorem 2.20 on page 50 of [74]). Since these sets are compact, D is Lipschitz continuous when restricted to each A_k . We define χ_k to be the characteristic function of A_k , χ that of $\Omega^+ \cap D^{-1}((0, t))$ and set $g_k = \chi_k F f$. Then $g_k \in L^1(\mathbb{R}^n)$ for each $k \in \mathbb{N}$ since F has compact support. Also, $\chi_k \rightarrow \chi$ as $k \rightarrow \infty$ in $L^1(\mathbb{R}^n)$. Hence the co-area formula yields

$$\int_{A_k} f dx = \int_{\mathbb{R}^n} |\nabla D| g_k dx = \int_{\mathbb{R}} \int_{D^{-1}(\{s\})} \chi_k F f d\sigma ds = \int_0^t \int_{A_k \cap D^{-1}(\{s\})} F f d\sigma ds.$$

Using Lebesgue's dominated convergence theorem, we can pass the limit $k \rightarrow \infty$ to obtain

$$\int_{\Omega^+ \cap D^{-1}((0, t))} f dx = \int_0^t \int_{\Omega^+ \cap D^{-1}(\{s\})} F f d\sigma ds.$$

For the set $\Omega^- \cap D^{-1}((-t, 0))$, basically the same argument can be applied when we take the correct signs into account. As above, we proceed assuming that D is Lipschitz continuous by using suitable compact cut-off sets and the dominated convergence theorem. Here, χ is the characteristic function of $\Omega^- \cap D^{-1}((-t, 0))$ and we define $g = \chi |F| f = -\chi F f$. Then $|\nabla D(x)| = 1/|F(x)| = -1/F(x)$ for almost all $x \in \Omega^- \cap D^{-1}((-t, 0))$, since $-D$ is the solution for speed $|F| = -F$ in this part of the domain according to (40). Hence, again using the co-area formula, we get:

$$\begin{aligned} \int_{\Omega^- \cap D^{-1}((-t, 0))} f dx &= \int_{\mathbb{R}^n} |\nabla D| g dx = \int_{\mathbb{R}} \int_{D^{-1}(\{s\})} \chi |F| f d\sigma ds \\ &= - \int_{-t}^0 \int_{\Omega^- \cap D^{-1}(\{s\})} F f d\sigma ds = - \int_0^t \int_{\Omega^- \cap D^{-1}(\{-s\})} F f d\sigma ds \end{aligned}$$

Using this now in (50) gives the correct term of (49). \square

As an immediate corollary of Theorem 10, the *shape derivative* of j can be calculated in direction of a particular deformation described by a speed field F . This quantity is often called *Eulerian derivative* in the literature (see Section 2.11 of [78]).

Corollary 6. *The functional j is differentiable for almost all $t \geq 0$ and the derivative is given by*

$$j'(t) = \int_{\Omega^+ \cap D^{-1}(\{t\})} F f d\sigma + \int_{\Omega^- \cap D^{-1}(\{-t\})} F f d\sigma. \quad (51)$$

Proof. This follows by using the Lebesgue differentiation theorem (Theorem 13.15 on page 278 of [85]) on j in the form of (49), where the dependence on t is only in the upper bound of the one-dimensional outer integral. The co-area formula guarantees that the integrand is really a function of $L^1(\mathbb{R})$ as is required for the differentiation theorem. \square

Note that the argument employed by the proof of Corollary 6 unfortunately only implies differentiability for *almost all* times and not full differentiability at *every* t . For this, one would have to show in addition that the derivative given in (51) can be continuously extended to all $t \geq 0$. This question will be discussed (and partially resolved) in Chapter 5 below. See also Lemma 63. For shape optimisation based on a gradient-descent scheme as investigated in Chapter 6, particularly $j'(0)$ would be interesting. It is not clear by Corollary 6 alone, though, that this derivative exists. Hence, our subsequent analysis

will be based on Theorem 10 instead of Corollary 6, so that we can formulate results that hold without an “almost all” qualification. These results state absolute continuity of the shape functionals. This, in turn, allows to deduce the existence of a weak almost-everywhere derivative in the same way as done in the proof of Corollary 6.

For the remainder of this section, we assume for simplicity that $F \geq 0$ is non-negative. It is straightforward to apply the full statement of Theorem 10 in order to generalise the results to arbitrary signs of F . For a fixed speed field F , let Ω_t and Γ_t describe the evolved domain as per Theorem 7. We consider now a more general shape functional

$$J(t) = J(\Omega_t) = \int_{\Omega_t} f(x, \Omega_t) dx. \quad (52)$$

The integrand $f(\cdot, \Omega)$ is assumed to be integrable for any fixed domain Ω . Furthermore, let us, for now, assume that it has a weak shape derivative f' in the sense that

$$f(x, \Omega_t) = f(x, \Omega_0) + \int_0^t f'(x, \Omega_s) ds \quad (53)$$

holds for all $x \in \mathbb{R}^n$ and $t \geq 0$. The function $f'(\cdot, \Omega)$ must also be integrable for all fixed domains Ω . Under these assumptions, we can derive a *total shape differential*:

Corollary 7. *Let J and f be as above. Then J is absolutely continuous, i. e.,*

$$J(t) = J(0) + \int_0^t J'(s) ds = J(0) + \int_0^t \left(\int_{\Gamma_s} F f(x, \Omega_s) d\sigma + \int_{\Omega_s} f'(x, \Omega_s) dx \right) ds. \quad (54)$$

Proof. By integrating (53) over Ω_t , we find

$$J(\Omega_t) = \int_{\Omega_t} f(x, \Omega_0) dx + \int_{\Omega_t} \int_0^t f'(x, \Omega_s) ds dx.$$

Applying Theorem 10 to the first term (where Ω_0 is now fixed) and Fubini’s theorem to the second, this further yields

$$J(\Omega_t) = J(\Omega_0) + \int_0^t \int_{\Gamma_s} F f(x, \Omega_0) d\sigma ds + \int_0^t \int_{\Omega_t} f'(x, \Omega_s) dx ds.$$

Note that this result already looks *almost* like the claimed (54). However, it has Ω_0 instead of Ω_s in the middle term and Ω_t instead of Ω_s in the last one. Consequently, it remains to show that

$$\int_0^t \int_{\Gamma_s} F (f(x, \Omega_s) - f(x, \Omega_0)) d\sigma ds = \int_0^t \left(\int_{\Omega_t} f'(x, \Omega_s) dx - \int_{\Omega_s} f'(x, \Omega_s) dx \right) ds.$$

With the corresponding shape derivatives for the differences, we can turn this equation into

$$\int_0^t \int_{\Gamma_s} F \int_0^s f'(x, \Omega_\tau) d\tau d\sigma ds = \int_0^t \int_s^t \int_{\Gamma_\tau} F f'(x, \Omega_s) d\sigma d\tau ds. \quad (55)$$

Using Fubini’s theorem again on the left-hand side and renaming s and τ on the right-hand side, this is further equal to

$$\int_0^t \int_0^s \int_{\Gamma_s} F f'(x, \Omega_\tau) d\sigma d\tau ds = \int_0^t \int_\tau^t \int_{\Gamma_s} F f'(x, \Omega_\tau) d\sigma ds d\tau.$$

Since both sides of this equation only express different ways to integrate over the same right triangle in the (s, τ) -plane, this shows that (55) and thus the claim are true. \square

Our result (54) matches the classical formulas for shape derivatives. Compare it, for instance, to (2.168) on page 113 of [78]. Note, however, that we were able to obtain it without employing domain transformations and without requiring regularity of the domain! To conclude this section, let us now investigate under which conditions (53) holds for a special class of shape-dependent integrands. For this, we first need a general-purpose chain rule for absolutely continuous functions:

Lemma 38. Let $f: \mathbb{R}^k \rightarrow \mathbb{R}$ be continuously differentiable and $g_1, \dots, g_k: \mathbb{R} \rightarrow \mathbb{R}$ be absolutely continuous. We consider

$$h: \mathbb{R} \rightarrow \mathbb{R}, \quad h(t) = f(g_1(t), \dots, g_k(t)).$$

Then h is also absolutely continuous and

$$h'(t) = \sum_{i=1}^k \partial_i f(g_1(t), \dots, g_k(t)) \cdot g'_i(t). \quad (56)$$

Proof. This follows from part (ii) of Theorem 4 on page 129 of [37]. \square

In applications such as the one discussed in Chapter 6, it is common that the shape dependence of the integrand f is due to some number of shape-dependent quantities. For instance, the integrand may depend on the volume $\text{vol}(\Omega)$ of the current domain or other, related values. For these integrands, we can use the results above to derive their shape derivatives as well. In particular, we are interested in integrands of the form

$$f(x, \Omega) = f(x, Q_1(\Omega), \dots, Q_k(\Omega)). \quad (57)$$

If the Q 's have shape derivatives themselves, Lemma 38 can be used together with Corollary 7. In this situation, J is again absolutely continuous with respect to t and we get

$$J(t) = J(0) + \int_0^t \left(\int_{\Gamma_s} F f \, d\sigma + \sum_{i=1}^k \int_{\Omega_s} \partial_i f \cdot Q'_i \, dx \right) ds. \quad (58)$$

Thus, if all the Q 's are domain functionals of the form (52), (57) themselves, we can recursively apply (58) to find shape derivatives. As long as there are no circular dependencies among the various shape-dependent quantities (i. e., the dependency graph is a *tree*), this process will work fine.

4.3 Lipschitz Continuity with Optimal Constants

It is a well-known fact that viscosity solutions of an initial-value problem (like the level-set equation (2)) often preserve Lipschitz continuity of the initial function ϕ_0 . Usually, this property is deduced from the comparison principle. See, for instance, Theorem 3.5.1 on page 139 of [41] or the related result in [50] for bounded domains. Following a slightly different route, we can also use our representation formula (33) to show Lipschitz continuity of ϕ both in time (see Theorem 11) and spatially (in Theorem 13). Based on the construction given in Example 8, we can even demonstrate that our results are sharp. Let us specifically emphasise that the results of this section are *only* based on the explicit representation formula (33) for ϕ and do not rely on the fact that ϕ is a viscosity solution of the level-set equation. This closes the gap we left open so far in Section 3.3, where we did not yet show continuity of the value function $V = \phi$.

Before we can show Lipschitz continuity of ϕ in time, we have to consider how admissible points in the minimum of (33) change if the upper bound t is modified.

Lemma 39. Let $F(x) \geq 0$ for some $x \in \mathbb{R}^n$. Assume that $|F| \leq \bar{F}$, $x^t \in \mathbb{R}^n$ and $s, t \geq 0$ with $d(x, x^t) \leq t$. Then there exists $x^s \in \mathbb{R}^n$ with $d(x, x^s) \leq s$ and $|x^s - x^t| \leq \bar{F}|t - s|$.

Proof. Consider first the trivial case $s = 0$: We can pick $x^s = x$ and know by Lemma 20 that

$$|x^s - x^t| = |x - x^t| \leq \bar{F} \cdot d(x, x^t) \leq \bar{F}t = \bar{F}|t - 0|.$$

Thus, assume now $s > 0$. Similarly, also the case $s \geq d(x, x^t)$ is trivial, as one can choose $x^s = x^t$. Consequently, we assume further $s < d(x, x^t) \leq t$ from now on. Choose a minimising path $\xi \in X_{\text{ad}}(x, x^t)$ with $l(\xi) = d(x, x^t)$. Since ξ and d are continuous, we know that $\tau \mapsto d(x, \xi(\tau))$ is continuous as well and ranges from zero at $\tau = 0$ to $d(x, x^t) > s$ at $\tau = 1$. Thus, the intermediate-value theorem implies the existence of $\tau_0 \in (0, 1)$ and $x^s = \xi(\tau_0)$ with $d(x, x^s) = s$. Denote by $\tilde{\xi}$ the part of ξ between x^s and x^t , i. e., for times in $[\tau_0, 1]$. Then we get

$$d(x, x^s) + l(\tilde{\xi}) = s + l(\tilde{\xi}) \leq l(\xi) \leq t$$

since $d(x, x^s)$ is the *shortest* distance between x and x^s , while the initial part of ξ is just a *particular* path. Hence we get also

$$l(\tilde{\xi}) \leq t - s = |t - s|,$$

which further implies that

$$|x^s - x^t| \leq \bar{F} \cdot l(\tilde{\xi}) \leq \bar{F} |t - s|.$$

□

Theorem 11. *Let $|F| \leq \bar{F}$ on \mathbb{R}^n . Then*

$$|\phi(x, s) - \phi(x, t)| \leq L_{\phi_0} \bar{F} \cdot |t - s|$$

for all $x \in \mathbb{R}^n$ and $s, t \geq 0$.

Proof. Let $x \in \mathbb{R}^n$ and $s, t \geq 0$. If $F(x) = 0$, then $\phi(x, t) = \phi(x, s) = \phi_0(x)$, thus this case is trivial. If $F(x) < 0$, we can use Lemma 14 to reduce the situation to the case of $F(x) > 0$. Thus, assume $F(x) > 0$ without loss of generality now. Pick x^t as minimiser of (33), such that $\phi(x, t) = \phi_0(x^t)$ and $d(x, x^t) \leq t$. Using Lemma 39, we can define x^s corresponding to s . Then, using again (33) and the Lipschitz continuity of ϕ_0 , we get

$$\phi(x, s) \leq \phi_0(x^s) \leq \phi_0(x^t) + L_{\phi_0} |x^s - x^t| \leq \phi(x, t) + L_{\phi_0} \bar{F} \cdot |s - t|.$$

Using a symmetric argument with s and t exchanged completes the proof. □

Next, we can show spatial Lipschitz continuity *in terms of the distance d* . This is a consequence of (33) and Lipschitz continuity in time. Note that d is itself Lipschitz continuous where F is bounded away from zero (recall Lemma 23). Consequently, Theorem 12 below actually gives a Lipschitz constant that is *uniform for all times* in these cases. However, where F may become zero or change its sign, this result makes no statement and the subsequent Theorem 13 must be applied instead.

Theorem 12. *Let $x, y \in \mathbb{R}^n$, $t \geq 0$ and $|F| \leq \bar{F}$. Denote by $L = L_{\phi_0} \bar{F}$ the temporal Lipschitz constant of ϕ according to Theorem 11. Then*

$$|\phi(x, t) - \phi(y, t)| \leq L \cdot d(x, y).$$

Proof. The claim is trivial if $x = y$, so assume $x \neq y$. Moreover, if $F(x) = 0$, $F(y) = 0$ or they have different signs, then $d(x, y) = \infty$ and nothing is to be shown. The case $F(x), F(y) < 0$ can be reduced to $F(x), F(y) > 0$ with the help of Lemma 14, so assume $F(x), F(y) > 0$ from now on. For the trivial case of $t = 0$, we get

$$|\phi(x, 0) - \phi(y, 0)| = |\phi_0(x) - \phi_0(y)| \leq L_{\phi_0} |x - y| \leq L_{\phi_0} \bar{F} \cdot d(x, y),$$

where the last estimate is due to Lemma 20.

Consider now $t > 0$ and note that ϕ is given by (33). If we choose x^t and y^t as minimisers for $\phi(x, t)$ and $\phi(y, t)$, respectively, we get

$$\phi(x, t) = \phi_0(x^t), \quad \phi(y, t) = \phi_0(y^t) \quad \text{and} \quad \max(d(x, x^t), d(y, y^t)) \leq t.$$

Define $s = d(x, y^t)$ and note that our assumption of Lipschitz continuity of ϕ in time gives

$$\phi(x, t) - L |t - s| \leq \phi(x, s) \leq \phi_0(y^t) = \phi(y, t),$$

so that further

$$\phi(x, t) \leq \phi(y, t) + L |t - d(x, y^t)|.$$

Consider first the case $d(x, y^t) \geq t$. Then

$$|t - d(x, y^t)| = d(x, y^t) - t \leq d(x, y) + d(y, y^t) - t \leq d(x, y),$$

which gives

$$\phi(x, t) \leq \phi(y, t) + L \cdot d(x, y).$$

In the second case of $d(x, y^t) < t$, we get

$$\phi(x, t) \leq \phi_0(y^t) = \phi(y, t) \leq \phi(y, t) + L \cdot d(x, y)$$

since y^t is admissible also for x in (33). If we repeat this argument now with x and y exchanged, the claimed Lipschitz continuity follows. \square

Let us continue with the final goal of deriving a spatial Lipschitz constant with respect to the usual Euclidean distance $|x - y|$. As a first step towards this result, we can show it in the case that $F(x) = 0$ holds at least for one of the two points involved. This is a very important piece of information, as it complements the earlier result in Theorem 12, which handles the situation within the support of F .

Lemma 40. *Let $x, y \in \mathbb{R}^n$, $t \geq 0$ and assume that $F(x) = 0$. If $y^t \in \mathbb{R}^n$ realises the minimum in (33) for $\phi(y, t)$, then*

$$|y^t - y| \leq (e^{L_F t} - 1) |x - y|$$

and, furthermore,

$$|\phi(x, t) - \phi(y, t)| \leq L_{\phi_0} e^{L_F t} \cdot |x - y|.$$

Proof. If $F(y) = 0$, then $y^t = y$ is the minimiser of (33), which makes the first estimate trivial. The same is true if $t = 0$. For $F(y) < 0$, we can use Lemma 14 to convert the situation to the remaining case of $F(y) > 0$ as before. Note that $F(y) \leq F(x) + L_F |x - y| = L_F |x - y|$. Combining this with the first estimate of Lemma 21 yields

$$|y - y^t| \leq \frac{F(y)}{L_F} (e^{L_F t} - 1) \leq (e^{L_F t} - 1) |x - y|.$$

For the second part, we use this result in combination with (33) to get

$$\begin{aligned} |\phi(x, t) - \phi(y, t)| &= |\phi_0(x) - \phi_0(y^t)| \leq L_{\phi_0} (|x - y| + |y - y^t|) \\ &\leq L_{\phi_0} (|x - y| + (e^{L_F t} - 1) |x - y|) = L_{\phi_0} e^{L_F t} \cdot |x - y|. \end{aligned}$$

\square

Lemma 41. *Let $x, y \in \Omega^+$ and $t > 0$. Assume that $\phi(y, t) = \phi_0(y^t)$ with $d(y, y^t) \leq t$. Then there exists $x' \in \mathbb{R}^n$ with $d(x, x') \leq t$ and $|x' - y^t| \leq e^{L_F t} |x - y|$.*

Proof. If $d(x, y^t) \leq t$, we can choose $x' = y^t$. Also, if $F(y) \leq L_F |x - y|$, we can use $x' = x$. In this situation, the first estimate in Lemma 21 gives

$$|x' - y^t| \leq |x - y| + |y - y^t| \leq |x - y| + \frac{F(y)}{L_F} (e^{L_F t} - 1) \leq |x - y| \cdot (1 + e^{L_F t} - 1) = e^{L_F t} |x - y|.$$

Thus consider now the case $d(x, y^t) > t$ and $F(y) > L_F |x - y|$. Let $s = l(S_{xy})$ denote the path length of the straight line S_{xy} from x to y . The third estimate in Lemma 21 implies

$$|x - y| \geq \frac{F(y)}{L_F} (1 - e^{-s L_F}),$$

which is equivalent to

$$(1 - e^{-s L_F}) \leq \frac{L_F |x - y|}{F(y)}. \quad (59)$$

Apply Lemma 19 to choose $\xi_y \in X_{\text{ad}}(y, y^t)$ with $l(\xi_y) = d(y, y^t) \leq t$. We will construct x' on the path ξ that is formed by first following S_{xy} from x to y and then moving along ξ_y from y to y^t . Note that S_{xy} is entirely inside of Ω^+ since $F(y) > L_F |x - y|$ and

$$F(S_{xy}(\tau)) = F(x + \tau(y - x)) \geq F(y) - L_F(1 - \tau) |x - y| > 0$$

for arbitrary $\tau \in [0, 1]$. The path ξ can be expressed explicitly as

$$\xi(\tau) = \begin{cases} S_{xy}(2\tau) & \text{for } \tau \in [0, 1/2], \\ \xi_y(2\tau - 1) & \text{for } \tau \in [1/2, 1]. \end{cases}$$

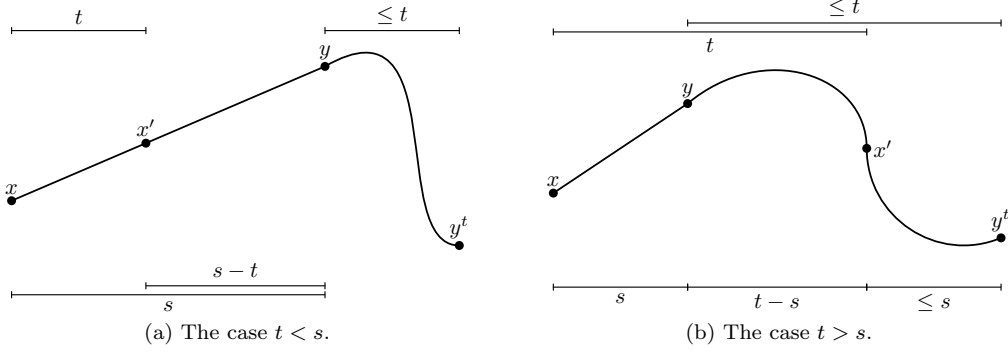


Figure 17: Sketches for the situations in the proof of Lemma 41. Indicated is always the path length according to l in Definition 6.

Denote for a moment the length of ξ restricted to $[0, \tau]$ by $\lambda(\tau)$ and note that λ is continuous. Since $\lambda(1) = l(\xi) \geq d(x, y^t) > t$ and $\lambda(0) = 0 < t$, we can find $\tau_0 \in (0, 1)$ with $\lambda(\tau_0) = t$. Choose $x' = \xi(\tau_0)$, so that $d(x, x') \leq \lambda(\tau_0) = t$. It remains to show $|x' - y^t| \leq e^{L_F t} |x - y|$. For this, we have to consider two cases depending on which segment of ξ the point x' comes to lie on. The path ξ is sketched for both situations in Figure 17.

If $\tau_0 \leq 1/2$, then x' is still part of the straight initial piece of ξ as shown in Figure 17a. This means that $t \leq s = l(S_{xy})$ as well as $|x - y| = |x - x'| + |x' - y|$. Equality holds here because x, x' and y are collinear. Since the path length from x' to y on S_{xy} is the remaining $s - t$ and thus also, in particular, $d(x', y) \leq s - t$, we can again employ Lemma 21 to find

$$|x' - y| \leq \frac{F(x')}{L_F} \left(e^{L_F d(x', y)} - 1 \right) \leq \frac{F(x')}{L_F} \left(e^{(s-t)L_F} - 1 \right).$$

Together with Lipschitz continuity, this yields

$$F(y) \leq F(x') + L_F |x' - y| \leq F(x') \left(1 + e^{(s-t)L_F} - 1 \right) = F(x') e^{(s-t)L_F} \quad (60)$$

and, consequently, $F(x') \geq F(y) e^{(t-s)L_F}$. Furthermore, since

$$F(x') \geq F(y) - L_F |x' - y| > L_F (|x - y| - |x' - y|) = L_F |x' - x|,$$

the third estimate of Lemma 21 is applicable again and gives

$$|x' - x| \geq \frac{F(x')}{L_F} (1 - e^{-tL_F}) \geq \frac{F(y)}{L_F} \left(e^{(t-s)L_F} - e^{-sL_F} \right) = \frac{F(y)}{L_F} (e^{L_F t} - 1) e^{-sL_F}.$$

All together, we have

$$\begin{aligned} |x' - y^t| &\leq |x' - y| + |y - y^t| = |x - y| + |y - y^t| - |x - x'| \\ &\leq |x - y| + \frac{F(y)}{L_F} (e^{L_F t} - 1) - \frac{F(y)}{L_F} (e^{L_F t} - 1) e^{-sL_F} \\ &= |x - y| + \frac{F(y)}{L_F} (e^{L_F t} - 1) (1 - e^{-sL_F}) \\ &\leq |x - y| + \frac{F(y)}{L_F} (e^{L_F t} - 1) \frac{L_F |x - y|}{F(y)} = e^{L_F t} |x - y|, \end{aligned}$$

which finishes the proof for this case. The last estimate is due to (59).

Now consider $\tau_0 \geq 1/2$, which means that $t \geq s$ and that x' lies on ξ_y between y and y^t . Take a look at Figure 17b. Consequently, if we consider the piece of ξ_y between y and x' (for times in $[1/2, \tau_0]$), its

path length is $t - s \geq 0$. Since $y^t = \xi_y(1)$ and $l(\xi_y) \leq t$, we know that the length of the remaining piece of ξ_y between x' and y^t is at most s . Thus

$$|x' - y^t| \leq \frac{F(x')}{L_F} (e^{L_F s} - 1) = \frac{F(x')}{L_F} e^{s L_F} (1 - e^{-s L_F})$$

by Lemma 21. Using (59), this yields

$$|x' - y^t| \leq \frac{F(x')}{L_F} e^{s L_F} \frac{L_F |x - y|}{F(y)} = \frac{F(x')}{F(y)} e^{s L_F} |x - y|. \quad (61)$$

Similarly to the last case and (60), we can combine Lemma 21 and the Lipschitz continuity of F to obtain

$$F(x') \leq F(y) + L_F |x' - y| \leq F(y) e^{(t-s)L_F},$$

which allows us to rewrite (61) to

$$|x' - y^t| \leq e^{t L_F} |x - y|.$$

□

Now we have everything together to show spatial Lipschitz continuity:

Theorem 13. *For all $x, y \in \mathbb{R}^n$ and $t \geq 0$, we have the Lipschitz estimate*

$$|\phi(x, t) - \phi(y, t)| \leq L_{\phi_0} e^{L_F t} \cdot |x - y|.$$

Proof. If $F(x) = 0$ or $F(y) = 0$, the result follows from Lemma 40. If $F(x)$ and $F(y)$ have different signs, we can split the straight line S_{xy} between x and y at some point z that has $F(z) = 0$, use Theorem 5 and apply Lemma 40 twice to get the claimed Lipschitz continuity. Also, if $t = 0$, the result follows since $\phi(\cdot, 0) = \phi_0$ is Lipschitz continuous. Thus it remains to consider, without loss of generality, the case $F(x), F(y) > 0$ and $t > 0$. Let $y^t \in \mathbb{R}^n$ with $d(y, y^t) \leq t$ and $\phi(y, t) = \phi_0(y^t)$ be a minimiser of (33). Using Lemma 41, we get $x' \in \mathbb{R}^n$ with $d(x, x') \leq t$ and $|x' - y^t| \leq e^{L_F t} |x - y|$. It follows that

$$\phi(x, t) \leq \phi_0(x') \leq \phi_0(y^t) + L_{\phi_0} |x' - y^t| \leq \phi(y, t) + L_{\phi_0} e^{L_F t} \cdot |x - y|,$$

which gives the claimed result when the same argument is applied again with x and y exchanged. □

We will now conclude this section with an example that demonstrates that the constants given in Theorem 11 and Theorem 13 are sharp:

Example 8. Let $L_{\phi_0}, L_F, a > 0$ be given. We define $\phi_0: \mathbb{R} \rightarrow \mathbb{R}$ by

$$\phi_0(x) = \begin{cases} 0 & \text{if } x \leq 0, \\ -L_{\phi_0} x & \text{for } x \in [0, 2a], \\ -2a L_{\phi_0} & \text{if } x \geq 2a \end{cases}$$

as well as $F: \mathbb{R} \rightarrow \mathbb{R}$ by

$$F(x) = \begin{cases} L_F x & \text{for } x \in [0, a], \\ L_F(2a - x) & \text{for } x \in [a, 2a], \\ 0 & \text{else.} \end{cases}$$

These functions are sketched in Figure 18. Note that ϕ_0 and F are Lipschitz continuous with Lipschitz constants L_{ϕ_0} and L_F , respectively, F has compact support on $[0, 2a]$ and that $F \geq 0$. Furthermore,

$$|F(x)| \leq \bar{F} = a L_F$$

for all $x \in \mathbb{R}$. This means that the parameter a can be used to choose the maximal value \bar{F} of F independently of the Lipschitz constants. Thus all quantities that appear in the proven Lipschitz constants can be influenced by the parameters in this example. This situation fulfils all assumptions we have made for the theoretical considerations above, so that our results apply here. If we denote the solution of (2) by ϕ as usual, Corollary 4 holds and thus ϕ is given by (33).

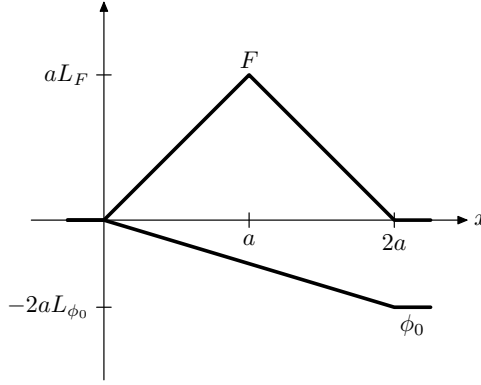


Figure 18: The situation of Example 8.

If x or y are not in $(0, 2a)$, then clearly $d(x, y) = \infty$ if $x \neq y$ and $d(x, y) = 0$ for $x = y$. In the case $x, y \in (0, 2a)$, we have

$$d(x, y) = \left| \int_x^y \frac{1}{F(\xi)} d\xi \right|.$$

Note that there is no real choice for different paths in one dimension. The absolute value ensures that the expression is correct even for $y < x$, when the integral itself is negative. Also note that $d(x, y) \rightarrow \infty$ for $y \rightarrow 2a^-$ and that ϕ_0 is strictly decreasing on $[0, 2a]$. This implies that for $x \in (0, 2a)$ and $t \geq 0$, the minimiser of (33) is always the unique $x^t \in [x, 2a)$ with $d(x, x^t) = t$. Assume $x \in (0, a]$ and $x' \in [x, a]$. Then $F(\xi) = L_F \xi$ for $\xi \in [x, x']$ and we can solve the integral to get

$$d(x, x') = \int_x^{x'} \frac{1}{L_F \xi} d\xi = \frac{\log x' - \log x}{L_F}. \quad (62)$$

Thus, if $t \leq d(x, a)$, we know that $x^t \in [x, a]$ can be found by solving $d(x, x^t) = t$ together with (62) for the unknown x^t . It is trivial to see that the result is $x^t = x e^{L_F t}$. Therefore, we have shown that for every $x \in (0, a)$ and $t \geq 0$ small enough, the evolved level-set function is given by

$$\phi(x, t) = \phi_0(x^t) = \phi_0(x e^{L_F t}) = -L_{\phi_0} x e^{L_F t}. \quad (63)$$

We will now take derivatives of (63) in order to verify that this solution does, indeed, realise the Lipschitz constants we have shown. Note that for arbitrarily large t , there always exists $x \in (0, a)$ with $t < d(x, a)$ so that (63) can be applied. Taking the derivative with respect to x shows that the maximum Lipschitz constant according to Theorem 13 is, indeed, tested with this example. For the time derivative, we get

$$\left| \frac{\partial \phi}{\partial t}(x, t) \right| = L_{\phi_0} L_F x e^{L_F t}$$

as lower bound on the Lipschitz constant, which is valid at least for every $x \in (0, a)$ and $0 \leq t \leq d(x, a)$. Clearly the largest bound is achieved if x is as large as possible, which means just so large that $t = d(x, a)$. By taking (62) into account, this is at $x = a e^{-L_F t}$. Consequently, the temporal Lipschitz constant must be at least

$$L_{\phi_0} L_F a e^{-L_F t} e^{L_F t} = a L_F L_{\phi_0} = \bar{F} L_{\phi_0}.$$

This matches the result from Theorem 11.

4.4 Propagation Speed of Perturbations

Since F in the level-set equation (2) describes a speed of movement, it is intuitive to assume that the maximal speed \bar{F} is also the maximal speed with which perturbations in the initial geometry and/or the speed field itself can propagate. With the help of the representation formula (33), this result can

be proven easily. We will assume here that a perturbation happens on some set $A \subset \mathbb{R}^n$ and that we consider a point $x \notin A$ with Euclidean distance $\delta > 0$ to A , i. e.,

$$\delta = \text{dist}(x, A) = \inf_{y \in A} |x - y| > 0. \quad (64)$$

The first result concerns perturbations in the initial geometry:

Lemma 42. *Assume $0 \leq F \leq \bar{F}$. Let ϕ_0 and $\tilde{\phi}_0$ be two initial level-set functions and $\phi, \tilde{\phi}$ be the corresponding solutions of (2) for the same F in both cases. Assume that $\phi_0(x) = \tilde{\phi}_0(x)$ for all $x \notin A$, and that $x \in \mathbb{R}^n \setminus \bar{A}$ is given with $\delta > 0$ defined according to (64). Then $\phi(x, t) = \tilde{\phi}(x, t)$ for all $t < \delta/\bar{F}$.*

Proof. We may assume that $F(x) > 0$ because $\phi(x, t) = \phi_0(x) = \tilde{\phi}_0(x) = \tilde{\phi}(x, t)$ otherwise, which makes the statement trivial. From Lemma 20 we know that $|x - y| \leq \bar{F} \cdot d(x, y)$ for all $y \in \mathbb{R}^n$. In particular, this implies for all $y \in A$:

$$\delta \leq |x - y| \leq \bar{F} \cdot d(x, y) \Rightarrow d(x, y) \geq \frac{\delta}{\bar{F}}$$

Choose now $t < \delta/\bar{F}$ and z with $d(x, z) \leq t$. It follows that $z \notin A$ and thus $\phi_0(z) = \tilde{\phi}_0(z)$. The claim follows now using the form (33) for the solutions as implied by Corollary 4. \square

Next, we consider what happens when the same initial geometry propagates with two different speed fields F and \tilde{F} :

Lemma 43. *Let $0 \leq F, \tilde{F} \leq \bar{F}$ be two different speed fields. Assume, furthermore, that $F(x) = \tilde{F}(x)$ for all $x \notin A$ and let ϕ_0 describe some initial geometry. We denote by d and \tilde{d} the distances induced by F and \tilde{F} , respectively, and by ϕ and $\tilde{\phi}$ the solutions of (2) for both speed fields with the same initial function ϕ_0 . For $x \in \mathbb{R}^n \setminus \bar{A}$, let $\delta > 0$ be as in (64). Then $\phi(x, t) = \tilde{\phi}(x, t)$ for all $t < \delta/\bar{F}$.*

Proof. The claim is clear if $F(x) = 0$, so assume $F(x) > 0$. Let $t < \delta/\bar{F}$ be given. Since $x \notin A$, this also implies $\tilde{F}(x) = F(x) > 0$. We want to show that

$$\{y \in \mathbb{R}^n \mid d(x, y) \leq t\} = \{y \in \mathbb{R}^n \mid \tilde{d}(x, y) \leq t\}, \quad (65)$$

which then implies the claim via (33) and Corollary 4. Choose $y \in \mathbb{R}^n$ with $d(x, y) \leq t < \delta/\bar{F}$. Let $\xi \in X_{\text{ad}}(x, y)$ be some admissible path with $l(\xi) < \delta/\bar{F}$. Assume there exists $t_0 \in [0, 1]$ with $z = \xi(t_0) \in A$. But then $l(\xi) \geq d(x, z) + d(z, y)$ and

$$d(x, z) \geq \frac{|x - z|}{\bar{F}} \geq \frac{\delta}{\bar{F}}$$

by Lemma 20, which is a contradiction. Thus ξ never touches A and, consequently, $l(\xi) = \tilde{l}(\xi)$. This implies that every (short enough) path contributing to the infimum for $d(x, y)$ is also admissible for $\tilde{d}(x, y)$ with the same length. Hence $\tilde{d}(x, y) \leq d(x, y)$, showing inclusion from left to right in (65). The inclusion from right to left works just the same. \square

As a final result, let us combine Lemma 42 and Lemma 43 into a single theorem:

Theorem 14. *Let $|F|, |\tilde{F}| \leq \bar{F}$ and $\phi_0, \tilde{\phi}_0$ be two initial level-set functions. Denote the corresponding solutions of (2) by ϕ and $\tilde{\phi}$, respectively. Assume that $F(x) = \tilde{F}(x)$ and $\phi_0(x) = \tilde{\phi}_0(x)$ for all $x \notin A$. Then for each $x \in \mathbb{R}^n \setminus A$ with $\delta > 0$ defined as per (64), we have $\phi(x, t) = \tilde{\phi}(x, t)$ for all $t \leq \delta/\bar{F}$.*

Proof. It is enough to consider $x \in \mathbb{R}^n \setminus \bar{A}$ and $t < \delta/\bar{F}$ since ϕ and $\tilde{\phi}$ are continuous. Thus, let $x \in \mathbb{R}^n \setminus \bar{A}$ and $t < \delta/\bar{F}$. Note that $F(x) = \tilde{F}(x)$ and that we can reduce the general case to that of $F, \tilde{F} \geq 0$ by using Theorem 5. We introduce an “intermediate solution” $\hat{\phi}$ as the solution of (2) with F and $\tilde{\phi}_0$. Lemma 42 implies that $\hat{\phi}(x, t) = \phi(x, t)$. Furthermore, Lemma 43 implies also $\hat{\phi}(x, t) = \tilde{\phi}(x, t)$, so that the claim is shown. \square

Note also that the upper bound δ/\bar{F} can be further improved if necessary: Instead of estimating F and \bar{F} very roughly by \bar{F} , we can define

$$d(x, A) = \inf_{y \in A} d(x, y) = \inf_{y \in A} \tilde{d}(x, y).$$

Equality between the definition with d and that with \tilde{d} is due to Lemma 26, which implies that the shortest paths must be outside of A . Following the proof of Theorem 14 closely, one can see that it remains true for all $t \leq d(x, A)$. Since $d(x, A) > \delta/\bar{F}$ in general, this leads to a stronger statement.

4.5 Distances between the Evolving Surfaces

It is, of course, intuitive that Ω_t and Γ_t should converge to Ω_0 and Γ_0 , respectively, for $t \rightarrow 0^+$. Let us now consider this question. Before we can do so, we have to actually define an appropriate notion of distance between these sets. There exist various concepts that define such a distance in the literature. See, specifically, [30]. Let us first consider the *Hausdorff distance*:

Definition 12. For $A, B \subset \mathbb{R}^n$, we define the *one-sided distance* as

$$d_H(A \rightarrow B) = \sup_{x \in A} \text{dist}(x, B) = \sup_{x \in A} \inf_{y \in B} |x - y|. \quad (66)$$

With it, the *Hausdorff distance* is the symmetrised expression

$$d_H(A, B) = \max(d_H(A \rightarrow B), d_H(B \rightarrow A)). \quad (67)$$

There exists a vast literature about the Hausdorff distance. See, for instance, Subsection 6.2.2 of [30] for a basic introduction. The Hausdorff distance can also be directly related to level-set and distance functions on a grid, as we have done in [57]. Note that, in general, $d_H(A \rightarrow B) \neq d_H(B \rightarrow A)$. (See Figure 19 and (68) below for such a situation.) Thus, the symmetrisation step in (67) is necessary. Also note that *both* distances $d_H(\Omega_0, \Omega_t)$ and $d_H(\Gamma_0, \Gamma_t)$ may be interesting depending on the situation. There is no clear relation among them: Consider the situation shown in Figure 19. For these sets A and B , it holds that

$$d_H(\partial B \rightarrow \partial A) > d_H(A \rightarrow B) > d_H(\partial A \rightarrow \partial B) > d_H(B \rightarrow A) = 0. \quad (68)$$

It is possible to define a speed field such that $B = \Omega_0$ and $A = \Omega_t$ is an evolved shape. The other way round, however, is also possible: At least if we introduce a small enough and smooth cut at the dashed line (which does not change the Hausdorff distances and (68) qualitatively), we can also define a speed field such that $A = \Omega_0$ and $B = \Omega_t$ for some $t > 0$. Choosing the negative distance function of B , i. e., $F = -\text{dist}(\cdot, B)$, leads (approximately) to this behaviour. This shows that all relative orders are possible for the distances between Ω_0 , Ω_t and the boundaries Γ_0 , Γ_t .

Thus, we have to consider both the distances between the open domains and the boundaries in the following. It turns out that the results we are interested in hold for both, and can be shown with similar arguments. For simplicity, we assume $\Omega_0 = \Gamma_0 \cup \Omega_0$ throughout this section.

4.5.1 Continuity of the Hausdorff Distance

Our first goal is to discuss under which conditions we can expect convergence of $d_H(\Omega_0, \Omega_t)$ and $d_H(\Gamma_0, \Gamma_t)$ to zero as $t \rightarrow 0^+$. It is relatively straight-forward to consider continuity of the distance *from* the evolved set *to* the original shape:

Lemma 44. *Let $t \geq 0$ and $|F| \leq \bar{F}$. Then*

$$\max(d_H(\Omega_t \rightarrow \Omega_0), d_H(\Gamma_t \rightarrow \Gamma_0)) \leq \bar{F}t.$$

Proof. Recall $|x - y| \leq \bar{F} \cdot d(x, y)$ from Lemma 20. We use this in the following to estimate the Euclidean distance in (66) by the F -induced distance. Let first $x \in \Omega_t$. If $x \in \Omega_0$ as well, then $\inf_{y \in \Omega_0} |x - y| = 0$ and nothing remains to be shown. So assume $x \notin \Omega_0$. By Corollary 5, this can only be the case if $x \in \Omega^+$ with $D(x) < t$. Then,

$$\bar{F}t > \bar{F} \cdot D(x) = \bar{F} \cdot \inf_{y \in \Gamma_0 \cup \Omega_0} d(x, y) = \bar{F} \cdot \inf_{y \in \Omega_0} d(x, y) \geq \inf_{y \in \Omega_0} |x - y|.$$

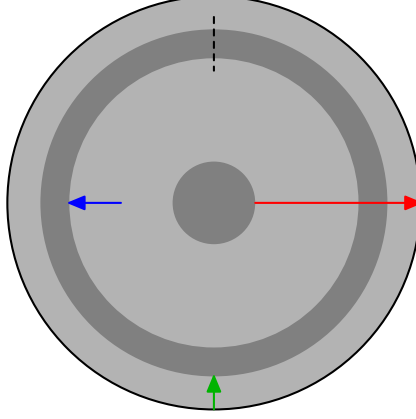


Figure 19: Possible situations for the (one-sided) Hausdorff distances between open sets A , B and their boundaries ∂A , ∂B . Here, A is the large circle and $B \subset A$ is the dark part. The set $A \setminus B$ is light grey. The outer line is ∂A , while ∂B is given by the interfaces between light and dark regions. Arrows indicate the various one-sided distances as per (68). The colours of the arrows correspond to the coloured expressions in (68).

Taking the supremum over all $x \in \Omega_t$ implies the claim.

Let us consider the case $x \in \Gamma_t$ now. If $x \in \Omega^z$, then the situation is trivial. So assume first $x \in \Omega^+$. Then $x \notin \Omega_0$, which implies

$$\inf_{y \in \Gamma_0 \cup \Omega_0} d(x, y) = \inf_{y \in \Gamma_0} d(x, y)$$

with an argument based on Lemma 26. Thus,

$$\overline{F}t = \overline{F} \cdot D(x) = \overline{F} \cdot \inf_{y \in \Gamma_0 \cup \Omega_0} d(x, y) = \overline{F} \cdot \inf_{y \in \Gamma_0} d(x, y) \geq \inf_{y \in \Gamma_0} |x - y|.$$

Similarly for $x \in \Omega^-$: If we write $\Omega'_0 = \mathbb{R}^n \setminus (\Gamma_0 \cup \Omega_0)$ as above, we can conclude $x \notin \Omega'_0$ and

$$\overline{F}t = -\overline{F} \cdot D(x) = \overline{F} \cdot \inf_{y \in \Gamma_0 \cup \Omega'_0} d(x, y) = \overline{F} \cdot \inf_{y \in \Gamma_0} d(x, y) \geq \inf_{y \in \Gamma_0} |x - y|.$$

This finishes the proof if we take again the supremum over all $x \in \Gamma_t$. \square

Lemma 44 can be understood intuitively by considering that each point $x \in \Gamma_t$ must be connected to some $x_0 \in \Gamma_0$ by a continuous path. For the distance *from* the original domain *to* the evolved shape, no such condition is automatically fulfilled. In this case, points on Γ_0 can vanish instantaneously for $t > 0$ when, for instance, holes disappear or lower-dimensional structures collapse. To avoid these situations, we need an additional condition:

$$\Gamma_0 \cap \Omega^+ = \partial\{x \in \Omega^+ \mid D(x) > 0\} \cap \Omega^+ \quad (69)$$

This roughly resembles (4.4) in [8]. It ensures that each point in Γ_0 is actually propagated to somewhere and cannot simply disappear immediately. Note that inclusion from right to left is always true in (69). The interesting direction is from left to right. Furthermore, we do not need to require the analogous condition for $\Gamma_0 \cap \Omega^-$, since it is automatically satisfied due to $\overline{\Omega}_0 = \Gamma_0 \cup \Omega_0$: Let $x \in \Gamma_0 \cap \Omega^-$, which also implies $x \in \overline{\Omega}_0$. It follows that there exists a sequence $(x_k)_{k \in \mathbb{N}} \subset \Omega_0 \cap \Omega^-$ with $x_k \rightarrow x$ as $k \rightarrow \infty$. For this sequence, $D(x_k) < 0$ is true for all $k \in \mathbb{N}$, while $D(x) = 0$. This implies $x \in \partial\{x \in \Omega^- \mid D(x) < 0\}$. A sufficient condition for (69) can be formulated in terms of the *density* of Ω_0 :

Definition 13. Let $x \in \Gamma_0$. We say that Ω_0 has *density* $\rho \in [0, 1]$ at x_0 if

$$\lim_{r \rightarrow 0^+} \frac{\text{vol}(B_r(x) \cap \Omega_0)}{\text{vol}(B_r(x))} = \rho.$$

The density is a well-studied quantity in geometric measure theory. See, for instance, page 158 of [4]. Points with density zero and one are called the *measure-theoretic exterior* and *interior* of Ω_0 , respectively. Points with density inbetween form, thus, the measure-theoretic boundary of Ω_0 . This yields:

Lemma 45. *Assume that $\text{vol}(\Gamma_0) = 0$ holds. If the density of Ω_0 is strictly smaller than one at each point of Γ_0 , then the condition (69) is satisfied.*

Proof. Choose $x_0 \in \Gamma_0 \cap \Omega^+$ and $r > 0$ arbitrarily. We have to show that there exists some $x \in \Omega^+$ with $D(x) > 0$ and $|x_0 - x| < r$. Since the density of Ω_0 at x_0 is strictly less than one and $\text{vol}(\Gamma_0) = 0$, there exists $x \in B_r(x_0)$ with $x \in \mathbb{R}^n \setminus (\Gamma_0 \cup \Omega_0)$. Hence, $D(x) > 0$ by definition in (40). \square

Note that the converse of Lemma 45 does not hold. It is very well possible to have points with density one that are still evolving properly and do not vanish immediately. See, for instance, Example 14. With the additional condition (69), we can now analyse convergence of the Hausdorff distances $d_H(\Omega_0 \rightarrow \Omega_t)$ and $d_H(\Gamma_0 \rightarrow \Gamma_t)$:

Lemma 46. *Let Ω_0 be bounded. Then $d_H(\Omega_0 \rightarrow \Omega_t) \rightarrow 0$ as $t \rightarrow 0^+$.*

Furthermore, condition (69) is equivalent to

$$\lim_{t \rightarrow 0^+} d_H(\Gamma_0 \rightarrow \Gamma_t) = 0.$$

Proof. Fix $\epsilon > 0$ and note that the open balls $B_\epsilon(x)$, $x \in \Omega_0$, define a cover of the compact set $\overline{\Omega_0}$. Thus, there exists a finite subset $X \subset \Omega_0$ such that $\overline{\Omega_0} \subset \bigcup_{x \in X} B_\epsilon(x)$. Furthermore, for each $x \in \Omega_0$, there exists $t_x > 0$ such that $x \in \Omega_t$ for all $t \in [0, t_x]$. This is clear for $x \in \Omega^+ \cup \Omega^z$. It follows for $x \in \Omega^-$ since $D(x) < 0$ in this case. Thus,

$$\text{dist}(y, \Omega_t) = \inf_{y' \in \Omega_t} |y - y'| \leq |y - x| < \epsilon \quad (70)$$

for all $x \in \Omega_0$, $y \in B_\epsilon(x)$ and $t \in [0, t_x]$. Let us now define $t_0 = \min_{x \in X} t_x > 0$ and choose $y \in \Omega_0$ arbitrarily. Since we have a cover of $\overline{\Omega_0}$, there exists $x_0 \in X$ such that $y \in B_\epsilon(x_0)$. Thus, (70) holds for all $t \in [0, t_0]$. As $y \in \Omega_0$ was arbitrary, this shows $d_H(\Omega_0 \rightarrow \Omega_t) < \epsilon$ if t is small enough.

If (69) holds, we can repeat this argument also for $d_H(\Gamma_0 \rightarrow \Gamma_t)$: As before, let $\epsilon > 0$ be given and consider some $x \in \Gamma_0$. If $F(x) > 0$, we can use (69) to conclude that there exist $x' \in B_\epsilon(x)$ and $t_x > 0$ such that $D(x') = t_x$. By the intermediate-value theorem, this also means that there exists $x^t \in B_\epsilon(x)$ with $D(x^t) = t$ for each $t \in [0, t_x]$. Hence, $B_\epsilon(x) \cap \Gamma_t \neq \emptyset$ for all $t \in [0, t_x]$. In the case $F(x) < 0$, we can use an argument similar to the one above to come to the same conclusion. For $F(x) = 0$, the situation is even easier; then, $x \in \Gamma_t$ for all $t \geq 0$. Proceeding with compactness as before, there is a finite set $X \subset \Gamma_0$ with $\Gamma_0 \subset \bigcup_{x \in X} B_\epsilon(x)$ and $t_0 = \min_{x \in X} t_x > 0$. If we now pick $x \in \Gamma_0$, there exists $x' \in X$ with $|x - x'| < \epsilon$. Furthermore, if $t \in [0, t_0]$, then there is also $y \in B_\epsilon(x') \cap \Gamma_t$. Thus,

$$\text{dist}(x, \Gamma_t) \leq |x - x'| + \text{dist}(x', \Gamma_t) \leq |x - x'| + |x' - y| < 2\epsilon.$$

This shows $d_H(\Gamma_0 \rightarrow \Gamma_t) \rightarrow 0$ in the limit $t \rightarrow 0^+$.

Let, finally, $d_H(\Gamma_0 \rightarrow \Gamma_t) \rightarrow 0$ as $t \rightarrow 0^+$. Pick $x_0 \in \Gamma_0 \cap \Omega^+$ and $r > 0$ small. Reducing r as necessary, we may assume that $B_r(x_0) \subset \Omega^+$. Choose $t > 0$ small enough, such that $d_H(\Gamma_0 \rightarrow \Gamma_t) < r$. This means, in particular, that there exists $x \in \Gamma_t$ with $|x_0 - x| < r$. Since $D(x) = t > 0$, this is all that we need in order to show (69). \square

Summarising the previous results, we have shown the following continuity of the Hausdorff distance:

Corollary 8. *Let Ω_0 be bounded, $\overline{\Omega_0} = \Gamma_0 \cup \Omega_0$ and (69) hold. Then*

$$\lim_{t \rightarrow 0^+} \max(d_H(\Omega_0, \Omega_t), d_H(\Gamma_0, \Gamma_t)) = 0.$$

4.5.2 Monotonicity of the Hausdorff Distance

Another interesting consideration is that of *monotonicity* of the Hausdorff distances $t \mapsto d_H(\Omega_0, \Omega_t)$, $t \mapsto d_H(\Gamma_0, \Gamma_t)$ and the corresponding one-sided distances. It can be easily seen from Corollary 5 that Ω_t evolves monotonically in time. Depending on the sign of F in some region, it either grows or shrinks there. It can never change the direction of evolution. This allows us to conclude:

Lemma 47. *The function $t \mapsto d_H(\Omega_t \rightarrow \Omega_0)$ is increasing in t .*

If $F \geq 0$ or $F \leq 0$ throughout \mathbb{R}^n , then also $t \mapsto d_H(\Omega_0 \rightarrow \Omega_t)$ is increasing.

Proof. Let us start with an auxiliary observation: Assume $t > 0$ and $x \in \Omega_t$. According to Corollary 5, we know that $x \in \Omega_0$ and thus $\text{dist}(x, \Omega_0) = 0$ if $F(x) \leq 0$. Hence,

$$d_H(\Omega_t \rightarrow \Omega_0) = \sup_{x \in \Omega_t} \text{dist}(x, \Omega_0) = \sup_{x \in \Omega_t \cap \Omega^+} \text{dist}(x, \Omega_0).$$

Now, let $0 \leq s \leq t$. This implies $\Omega_s \cap \Omega^+ \subset \Omega_t \cap \Omega^+$ and thus

$$d_H(\Omega_s \rightarrow \Omega_0) = \sup_{x \in \Omega_s \cap \Omega^+} \text{dist}(x, \Omega_0) \leq \sup_{x \in \Omega_t \cap \Omega^+} \text{dist}(x, \Omega_0) = d_H(\Omega_t \rightarrow \Omega_0).$$

If $F \geq 0$, then $\Omega_0 \subset \Omega_t$ for all $t \geq 0$ and $d_H(\Omega_0 \rightarrow \Omega_t) = 0$. This case is trivial. So assume $F \leq 0$, let $0 \leq s \leq t$ and $x \in \Omega_0$. Note that $\Omega_t \subset \Omega_s \subset \Omega_0$. Furthermore,

$$\text{dist}(x, \Omega_s) = \inf_{y \in \Omega_s} |x - y| \leq \inf_{y \in \Omega_t} |x - y| = \text{dist}(x, \Omega_t).$$

Thus also $d_H(\Omega_0 \rightarrow \Omega_s) \leq d_H(\Omega_0 \rightarrow \Omega_t)$. □

Unfortunately, the requirement that F must have a fixed sign throughout the domain is necessary for the second part of Lemma 47. As with continuity, the situation *from* the original *to* the evolved shape is more difficult. If we drop the assumption of a unique sign for the speed field, monotonicity of $d_H(\Omega_0 \rightarrow \Omega_t)$ is no longer given:

Example 9. Consider a situation as shown in Figure 20a. In this case, $d_H(\Omega_0 \rightarrow \Omega_t)$ increases initially with t , since the part of Ω_0 inside Ω^- shrinks. However, over time the ring “closes”. This has the effect that the bottom part of $\Omega_0 \cap \Omega^-$ is, again, close to Ω_t and the distance *decreases*. The time evolution of the one-sided distance $d_H(\Omega_0 \rightarrow \Omega_t)$ is shown in Figure 20b. It is even possible to modify the initial geometry slightly to see that also $d_H(\Omega_0, \Omega_t)$ may exhibit the same, non-monotonic behaviour.

The fundamental “problem” that makes this possible is the following: The sets themselves behave in a monotone way. However, the *minimiser* for some distance $\text{dist}(x, \Omega_t)$ with $x \in \Omega_0$ can jump around as the sets evolve. This is precisely what happens in the example.

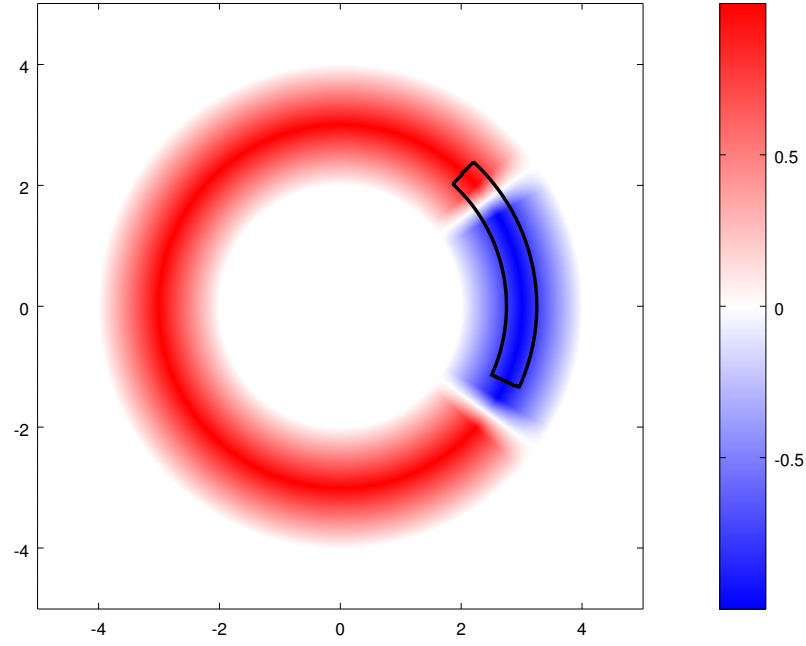
Let us now consider the distance between the *boundaries* Γ_0 and Γ_t . Here again, no monotone behaviour can be guaranteed: With a closer look at Example 9, one can see that the extremising points are actually on the boundary. Thus, the same example shows that $d_H(\Gamma_0 \rightarrow \Gamma_t)$ is not monotone either. For $d_H(\Gamma_t \rightarrow \Gamma_0)$, let us give two counterexamples that do not even need a sign change in the speed field. The first is based on the same underlying issue as Example 9, namely that the closest point of the target set can jump:

Example 10. Consider a one-dimensional situation such as $\Omega_0 = \mathbb{R}^n \setminus [0, 1]$. (We may also introduce a suitable cut off in the distance to get a bounded set, of course.) Then $\Gamma_0 = \{0, 1\}$ is the initial boundary. Set $F(x) = x$ on $[0, 1]$, with some appropriate continuation and cut off on the outside. This situation is depicted in Figure 21. Since $F(x_1) = F(0) = 0$, this part of the boundary is fixed during the time evolution. The other boundary point $x_2 = 1$, on the other hand, moves towards the origin over time. The time t to reach some point $x(t) \in (0, 1)$ can be computed similarly to (62), which gives $t = -\log x(t)$. Thus, $x(t) = e^{-t}$ and $\Gamma_t = \{0, e^{-t}\}$.

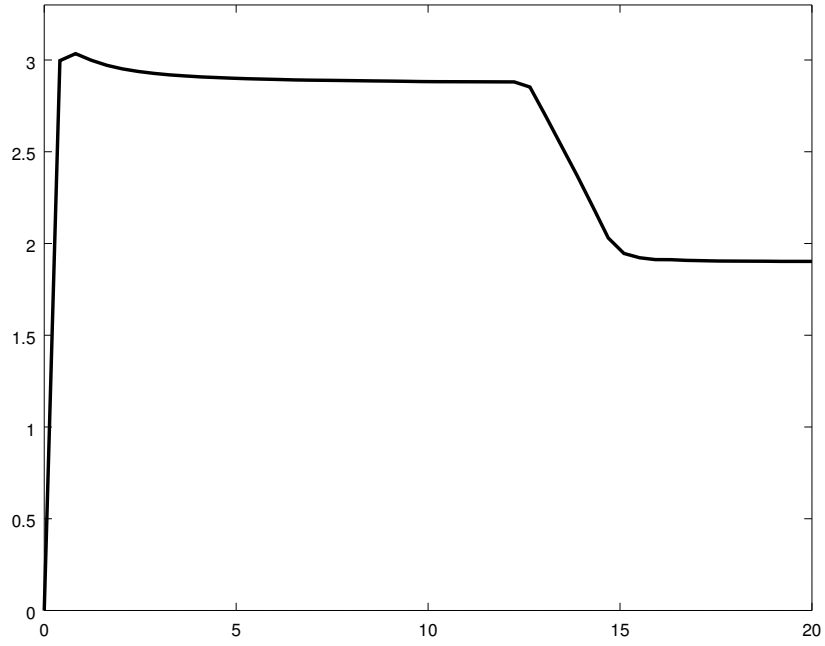
Considering $t \mapsto d_H(\Gamma_t \rightarrow \Gamma_0)$, we see the same effect as in Example 9: For small t , the evolved boundary point $x(t)$ is still closer to x_2 than to x_1 . As t grows, however, it gets closer to x_1 at one point. Thus the one-sided distance

$$t \mapsto d_H(\Gamma_t \rightarrow \Gamma_0) = \min(1 - e^{-t}, e^{-t})$$

is not monotone.



(a) The speed field F and initial geometry Ω_0 .



(b) Time evolution of $d_H(\Omega_0 \rightarrow \Omega_t)$.

Figure 20: Non-monotone behaviour of $t \mapsto d_H(\Omega_0 \rightarrow \Omega_t)$ if F is allowed to change sign. See Example 9.

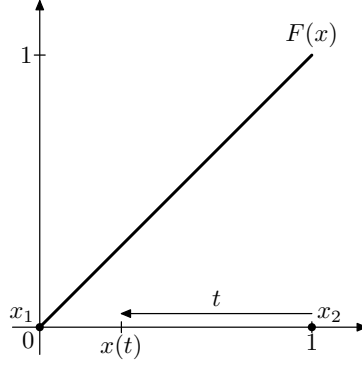


Figure 21: The situation of Example 10. The boundary point $x_1 = 0$ is stationary, while the right boundary $x(t)$ is initially at x_2 and moves towards the origin over time.

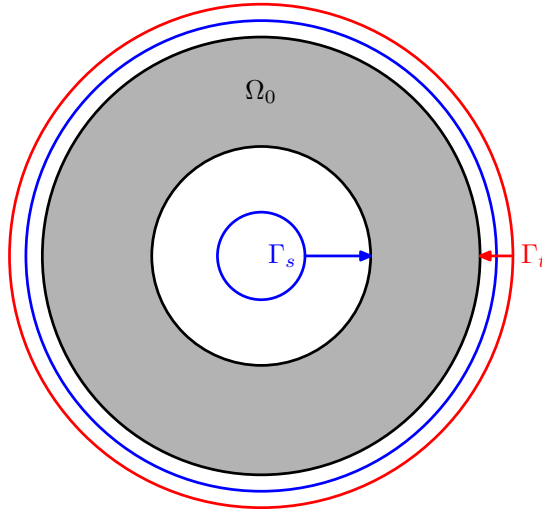


Figure 22: Non-monotonicity of $\tau \mapsto d_H(\Gamma_\tau \rightarrow \Gamma_0)$ due to topology changes as described in Example 11. The evolved contours Γ_s and Γ_t at times $0 < s < t$ are shown together with the corresponding longest distances $d_H(\Gamma_s \rightarrow \Gamma_0)$ and $d_H(\Gamma_t \rightarrow \Gamma_0)$.

Another example is the following, which is based on a change in topology where one part of the boundary vanishes at a certain time:

Example 11. Let Ω_0 be a ring-shaped initial geometry and define $F > 0$ to be large around the hole of the ring and small at its outer boundary. In this situation, the hole shrinks rapidly while the outer boundary grows only slowly. If we choose $0 < s < t$ in such a way that the hole vanishes between the times s and t , we get a downward jump in $\tau \mapsto d_H(\Gamma_\tau \rightarrow \Gamma_0)$ when this happens. This is shown in Figure 22. (Note that in this situation, the condition (69) is not fulfilled at the instant in time when the hole vanishes. Thus, the jump is not in contradiction to Corollary 8.)

4.5.3 The Distance in Measure

Another possibility to define a distance between sets is via the volume of their symmetric set difference:

Definition 14. Let $A, B \subset \mathbb{R}^n$ be open. We define the *symmetric set difference* as

$$A \Delta B = (A \setminus B) \cup (B \setminus A)$$

and the *distance in measure* between A and B as $\text{vol}(A \Delta B)$.

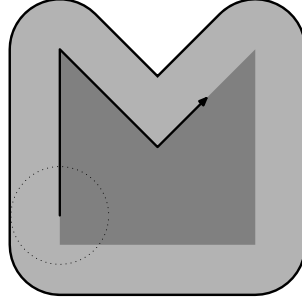


Figure 23: The smoothing effect of an evolution with $F = 1$. The initial set Ω_0 is dark, the added part $\Omega_t \setminus \Omega_0$ is light grey. The black line shows the resulting boundary Γ_t .

This concept is equivalent to the L^1 -distance between the characteristic functions of A and B . See also Section 5.3 of [30]. It is much simpler than the Hausdorff measure, since it is a-priori symmetric and it is inherently useful only for the domains and not the boundaries (as the latter usually have measure zero anyway). Thus, there are a lot less cases and technical difficulties to consider than before:

Corollary 9. *The function $t \mapsto \text{vol}(\Omega_0 \Delta \Omega_t)$ is absolutely continuous and increasing on $[0, \infty)$.*

Proof. This is a direct consequence of Theorem 10 and, in particular, (49). We simply use $f = 1$. \square

4.6 Reachable Shapes

When we use the level-set method to evolve geometries as part of an optimisation procedure, the following question is of interest: *Which kind of shapes can actually be reached by propagating some given initial geometry along any speed field?* This is important, because it determines the class of shapes among which an optimum can be found. In the current section, we will address this question in two steps: First, in Subsection 4.6.1 we will see that all evolved shapes with a Lipschitz continuous speed field possess a certain type of regularity. This, in turn, implies that not all open sets can be evolved shapes. Second, we will discuss possible relaxations of our situation in Subsection 4.6.2. It is possible to reach every open set in the limit $t \rightarrow \infty$, and it is also possible to *rescale* the speed field to get the same effect with a finite end time. The rescaling, however, may result in a speed field that is no longer Lipschitz continuous. Its regularity will be discussed in Subsection 4.6.3, where it turns out that one can reach a wide class of additional shapes with speed fields that are not Lipschitz but at least *Hölder continuous*.

Note that we will always concentrate on *local regularity* of the desired shape. There are also certain restrictions on which shapes are reachable based on global properties (in particular, the topology). These are, however, an entirely different matter. Thus, let us, for simplicity, assume that $F \geq 0$ is non-negative and that the initial geometry Ω_0 is a subset of the desired shape throughout this section. We can also assume that both shapes are connected. It is possible to use Theorem 5 and other techniques to extend the results below to more general situations. Finally, let us assume $\overline{\Omega_0} = \Gamma_0 \cup \Omega_0$ throughout this section.

4.6.1 Density Regularity

Let us, for a moment, assume $F = 1$. This situation was already discussed in Section 3.1. A possible interpretation of the solution formula (25) is the following: The evolved set Ω_t for some $t > 0$ is formed from Ω_0 by drawing with a blunt, circular pen of radius t along the initial boundary Γ_0 . This obviously implies that Ω_t has a “smoothed” boundary as shown in Figure 23. Even if F is not constantly one, Lipschitz continuity has the effect that this picture is still correct at least qualitatively. Note, in particular, that outward-pointing corners are not possible. (If the speed field is positive; for negative speed fields, everything is turned around and outward-pointing corners *are* possible, while inward-pointing ones cannot occur.) This is our main result of the current subsection, which will be proven below:

Theorem 15. *Let the speed field F be Lipschitz continuous, $t > 0$, $x \in \Gamma_t$ and $F(x) > 0$. Then Ω_t has density at least $1/2$ at x .*

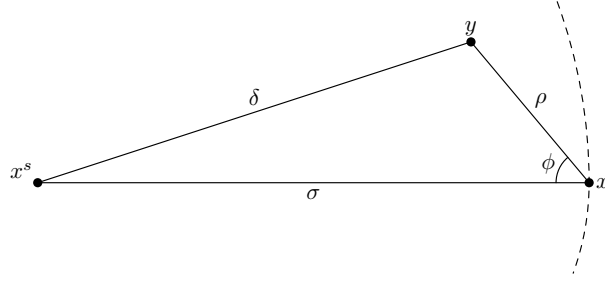


Figure 24: The notation and geometric situation of Lemma 49.

To prove Theorem 15, we need some auxiliary results first. Let us start with an extension of Lemma 19 and Lemma 33. It can also be interpreted as a variant of superoptimality as shown in Lemma 30 above.

Lemma 48. *Let $t > 0$ and $x \in \Gamma_t \cap \Omega^+$. Then there exists $x_0 \in \Gamma_0$ with $t = d_0(x) = d(x_0, x)$. Furthermore, for each $s \in (0, t)$, there is $x^s \in \Gamma_s$ such that $d_0(x^s) = d(x_0, x^s) = t - s$ and $d(x^s, x) = s$.*

Proof. Existence of x_0 follows from Lemma 33. (Recall that we assume $\overline{\Omega_0} = \Gamma_0 \cup \Omega_0$.) According to Lemma 19, we can find $\xi \in X_{\text{ad}}(x_0, x)$ such that $l(\xi) = d(x_0, x) = t$. Let now $s \in (0, t)$ be given. By the intermediate-value theorem, there exists $t_s \in (0, 1)$ such that the restriction ξ_1 of ξ to times in $[0, t_s]$ has $l(\xi_1) = t - s$, while the remaining part ξ_2 has $l(\xi_2) = s$. Set $x^s = \xi(t_s)$. This implies $\xi_1 \in X_{\text{ad}}(x_0, x^s)$ and $\xi_2 \in X_{\text{ad}}(x^s, x)$. Clearly also

$$d_0(x^s) \leq d(x_0, x^s) \leq l(\xi_1) = t - s \quad \text{and} \quad d(x^s, x) \leq l(\xi_2) = s.$$

Since $d_0(x) \leq d_0(x^s) + d(x^s, x)$, we find

$$t = d_0(x) \leq d_0(x^s) + d(x^s, x) \leq (t - s) + s = t.$$

Thus, equality holds throughout. This implies the claim. \square

Next we present an argument based on geometry and the estimates of Lemma 21. For this, let $x^s, y \in \mathbb{R}^n$ and $x \in \Omega^+$ be given. Assume $d(x^s, x) = s$ and let us introduce the notation

$$\sigma = |x^s - x|, \quad \delta = |x^s - y| \quad \text{and} \quad \rho = |x - y|.$$

Denote the angle x^s - x - y by ϕ . This situation is depicted in Figure 24. The dashed line corresponds to $B_\sigma(x^s)$. This can, roughly, also be seen as $\{x' \in \mathbb{R}^n \mid d(x^s, x') < s\}$. Hence, it seems plausible that $d(x^s, y) < s$ if $\rho \ll \sigma$ and $\phi < \pi/2$. A rigorous estimate is the following:

Lemma 49. *Consider the situation described above. Assume $\phi \in [0, \pi/2)$ and $L\sigma < F(x^s)$, where L is the Lipschitz constant of F . Then*

$$\cos \phi > \frac{\rho L}{2F(x^s)} (1 - e^{-Ls})^{-1} + \frac{F(x^s)}{2L\rho} (1 - e^{-Ls}) (e^{2Ls} - 1) \quad (71)$$

is a sufficient condition for $d(x^s, y) < s$.

Proof. With the third estimate of Lemma 21, we get $\sigma \geq F(x^s)/L \cdot (1 - e^{-Ls})$. Thus, (71) implies

$$2\sigma \cdot \cos \phi > \rho + \frac{F(x^s)^2}{L^2 \rho} (1 - e^{-Ls})^2 (e^{2Ls} - 1),$$

which can be written equivalently as

$$\rho^2 - 2\sigma\rho \cdot \cos \phi < \frac{F(x^s)^2}{L^2} (1 - e^{-Ls})^2 (1 - e^{2Ls}).$$

According to the first estimate of Lemma 21,

$$\sigma^2 = |x^s - x|^2 \leq \frac{F(x^s)^2}{L^2} (e^{Ls} - 1)^2 = \frac{F(x^s)^2}{L^2} e^{2Ls} (1 - e^{-Ls})^2.$$

Adding the last two inequalities and using the law of cosines yields:

$$\delta^2 = \sigma^2 + \rho^2 - 2\sigma\rho \cdot \cos \phi < \frac{F(x^s)^2}{L^2} (1 - e^{-Ls})^2 \Leftrightarrow |x^s - y| < \frac{F(x^s)}{L} (1 - e^{-Ls})$$

This is equivalent to

$$\frac{1}{L} \log \frac{F(x^s)}{F(x^s) - L|x^s - y|} < s,$$

so that the second statement of Lemma 21 finally yields the desired

$$d(x^s, y) \leq \frac{1}{L} \log \frac{F(x^s)}{F(x^s) - L|x^s - y|} < s.$$

□

We have now everything together to provide the actual proof of Theorem 15. So let $t > 0$ and $x \in \Gamma_t \cap \Omega^+$ be given. For $s \in (0, t)$, choose x^s according to Lemma 48, i. e., $d_0(x^s) = t - s$ and $d(x^s, x) = s$. If s is small enough, we can achieve

$$0 < \frac{F(x)}{2} \leq F(x^s) \leq 2F(x).$$

This implies an upper bound for the right-hand side of (71), so that also

$$\cos \phi > \frac{\rho L}{F(x)} (1 - e^{-Ls})^{-1} + \frac{F(x)}{L\rho} (1 - e^{-Ls}) (e^{2Ls} - 1) \quad (72)$$

is sufficient for $d(x^s, y) < s$. Since

$$d_0(y) \leq d_0(x^s) + d(x^s, y) < t - s + s = t,$$

this implies, in particular, also $y \in \Omega_t$.

For any given $\rho > 0$, set $s = \rho^{3/4}$. Note that the right-hand side of (72) goes to zero with this substitution if we let $\rho \rightarrow 0^+$. In other words, we have shown: For any $\epsilon > 0$, there exists $\rho_0 > 0$ such that $y \in \Omega_t$ for all $\rho \in (0, \rho_0)$ and $y \in \partial B_\rho(x)$ on a spherical sector with aperture $\pi/2 - \epsilon$. It remains to estimate the volume of all those y 's. For this, let us state a basic geometric fact that will be shown later in Lemma 54: There exists a continuous mapping r with $r(\pi/2) = 1/2$ and such that $r(\phi) \cdot \text{vol}(B_\rho(x))$ is the volume of the spherical sector with aperture ϕ and radius ρ . Thus,

$$\text{vol}(B_\rho(x) \cap \Omega_t) \geq r\left(\frac{\pi}{2} - \epsilon\right) \cdot \text{vol}(B_\rho(x))$$

for all $\rho \in (0, \rho_0)$. Since ϵ was arbitrary and r is continuous, this implies

$$\lim_{\rho \rightarrow 0^+} \frac{\text{vol}(B_\rho(x) \cap \Omega_t)}{\text{vol}(B_\rho(x))} \geq r\left(\frac{\pi}{2}\right) = \frac{1}{2}.$$

Thus, Theorem 15 is shown.

We will now also see that Theorem 15 can be “turned around”: At least for certain $x \in \Gamma_0$, we can use it to conclude that the density of Ω_0 can be at most $1/2$ at x_0 . This part of the boundary will be characterised later on as the *backwards reachable set* (see Definition 20). A similar result will be derived in Lemma 59. The bound there is actually weaker, but it holds uniformly in a certain sense.

Corollary 10. *Let $F \geq 0$ be Lipschitz continuous and $x_0 \in \Gamma_0 \cap \Omega^+$ such that there exists $x \in \mathbb{R}^n$ with $0 < d_0(x) = d(x_0, x)$. Then Ω_0 has density at most $1/2$ at x_0 .*

Proof. Let such x_0 and x be given and set $t = d(x_0, x)$. With $\Omega'_0 = \mathbb{R}^n \setminus (\Gamma_t \cup \Omega_t)$, we define

$$\Omega'_t = \{y \in \mathbb{R}^n \mid d(y_0, y) < t \text{ for some } y_0 \in \Omega'_0\}.$$

Roughly speaking, we use the evolved set at time t as new initial geometry and let it evolve “backwards” according to the same speed field (compare also Lemma 14). Define $\Gamma'_0 = \partial\Omega'_0 = \partial(\mathbb{R}^n \setminus \Omega_t) = \Gamma_t$ and $\Gamma'_t = \partial\Omega'_t$. Since $x \in \Gamma_t$, we know that $x \in \Gamma'_0$ as well. This, in turn, implies $x_0 \in \Gamma'_t$. Note that Theorem 15 applies to Ω'_t , so that Ω'_t has density at least $1/2$ at x_0 . If we can show that Ω_0 and Ω'_t are disjoint, this implies the claim. Thus, assume $y \in \Omega_0 \cap \Omega'_t$. Since $y \in \Omega'_t$, there exists $y_0 \in \Omega'_0$ with $d(y_0, y) < t$. By $y \in \Omega_0$, this implies $y_0 \in \Omega_t$, which is a contradiction to the definition of Ω'_0 . \square

4.6.2 Speed Rescaling

We have just seen in Theorem 15 that time evolution along a Lipschitz continuous speed field necessarily produces a certain regularity of the resulting domain. This also means that it is not possible to achieve an arbitrary open set as the result of such an evolution. In this subsection, we will discuss possible relaxations of the assumptions that allow more shapes to be reached. Note that it is trivially possible to reach an arbitrary open shape Ω_d from an initial domain $\Omega_0 \subset \Omega_d$ if the speed field is not required to be continuous. One can, for instance, simply use the characteristic function of Ω_d . Discontinuous speed fields are, however, quite an extreme situation. In the following, we will assume that the speed field remains continuous but may no longer be Lipschitz continuous. In this case, some parts of our theory about viscosity solutions for the level-set equation (2) break down. It is, however, still possible to use the Hopf-Lax formula (in particular, Theorem 7) directly to *define* evolved shapes.

Before we can start with the actual discussion of reachable shapes, we need a technical lemma. It allows us to approximate bounded, open sets by compact subsets in the Hausdorff distance:

Lemma 50. *Let $\Omega \subset \mathbb{R}^n$ be open and bounded. Then, for arbitrary $\epsilon > 0$, there exists a compact subset $K \subset \Omega$ with $d_H(\Omega, K) = d_H(\Omega \rightarrow K) < \epsilon$.*

Proof. Since we will construct K as subset of Ω , it is clear that $d_H(\Omega, K) = d_H(\Omega \rightarrow K)$ and we only have to consider $d_H(\Omega \rightarrow K)$ in the following. Let $\epsilon > 0$ be given arbitrarily. Since $\partial\Omega$ is compact, there exists a finite subset $X \subset \partial\Omega$ such that we get $\partial\Omega \subset \bigcup_{x \in X} B_{\epsilon/3}(x)$. For each $x \in X$, there further exists $c_x \in \Omega$ with $|x - c_x| < \epsilon/3$. Since Ω is open, we can, in turn, find $r_x > 0$ with $B_{r_x}(c_x) \subset \Omega$. We now define $\rho' = \min_{x \in X} r_x > 0$, $\rho = \min(\rho'/2, \epsilon/3)$ and

$$K = \overline{\Omega} \setminus \bigcup_{z \in \partial\Omega} B_\rho(z).$$

Then $K \subset \Omega$ is clearly compact. Consider $y \in \Omega \setminus K$ arbitrarily. For it, there are $z \in \partial\Omega$ with $|y - z| < \rho$ and $x \in X$ with $|z - x| < \epsilon/3$. Let $c_x \in \Omega$ denote the point constructed above for this x . Note that $B_{r_x}(c_x) \subset \Omega$ implies that c_x has distance at least ρ' to the boundary of Ω and, consequently, $c_x \in K$. This yields the estimate

$$\text{dist}(y, K) \leq |y - c_x| \leq |y - z| + |z - x| + |x - c_x| < \rho + \epsilon/3 + \epsilon/3 \leq \epsilon.$$

Since y was arbitrary, the claim follows. \square

We are now ready to prove our first result about reachable shapes. It shows that arbitrary shapes can be reached in the limit $t \rightarrow \infty$:

Lemma 51. *Let $\Omega_d \subset \mathbb{R}^n$ be open, bounded and connected. Furthermore, assume that $\Omega_0 \subset \Omega_d$ and that $F: \mathbb{R}^n \rightarrow \mathbb{R}$ is continuous. If $F > 0$ on Ω_d and $F = 0$ else, then*

$$\Omega_d = \bigcup_{t > 0} \Omega_t. \tag{73}$$

In particular, $\Omega_t \rightarrow \Omega_d$ for $t \rightarrow \infty$ both in the Hausdorff distance and in measure.

Proof. Note that the structure of F implies $\Omega_0 \subset \Omega_s \subset \Omega_t \subset \Omega_d$ for any $0 \leq s \leq t$. Let $x \in \Omega_d$. Since Ω_d is open and connected, it is, in particular, path-connected. Since $\Omega_0 \subset \Omega_d$, there definitely exist $x_0 \in \Omega_0$ and a path $\xi \in X_{\text{ad}}(x_0, x)$ connecting x to Ω_0 . Thus, $d_0(x) \leq l(\xi) < \infty$. This implies that $x \in \Omega_t$ for all $t \geq l(\xi)$. Hence, (73) is shown.

Convergence in measure follows directly from Lebesgue's dominated convergence theorem. For convergence in the Hausdorff distance, observe the following: If $K \subset \Omega_d$ is compact, there exists some $t_0 \geq 0$ such that $K \subset \Omega_t$ for all $t \geq t_0$. This yields

$$d_H(\Omega_t, \Omega_d) = d_H(\Omega_d \rightarrow \Omega_t) \leq d_H(\Omega_d \rightarrow K).$$

The claim now follows, since the last distance can be made arbitrarily small according to Lemma 50. \square

A particular speed field F that can be used in Lemma 51 is the distance function of $\mathbb{R}^n \setminus \Omega_d$. It has precisely the right properties. In fact, as long as the topology of Ω_0 matches that of Ω_d close enough, one can also use the negative signed distance function of Ω_d even without requiring $\Omega_0 \subset \Omega_d$. If the set $\Omega_0 \setminus \Omega_d$ is not empty, this speed field $F = -\text{sd}_{\Omega_d}$ is negative there. Therefore, $\Omega_0 \setminus \Omega_d$ vanishes for $t \rightarrow \infty$ in the same way as $\Omega_d \setminus \Omega_0$ vanishes according to Lemma 51.

The main “feature” of Lemma 51, however, is that the statement holds in the limit of large times. It is far more interesting to reach a target shape at a precise, *finite* end time. To achieve this, let us try to *rescale the time*. A similar approach is also described on page 20 of [41], although it is based on a level-set equation. Our scheme directly utilises the Hopf-Lax formula. The basic idea is the following: Let ξ be some optimal path as per Lemma 19. Assume, without loss of generality, that ξ is parametrised by arc length, i. e., $|\xi'| = 1$. This path then defines d_0 for all of its points, which yields

$$\frac{d}{dt}d_0(\xi(t)) = \frac{1}{F(\xi(t))}$$

for all $t \in (0, 1)$ and points $\xi(t)$ on the path. If we now multiply the speed field F by some factor, this corresponds to scaling the *derivative* of d_0 . When the rescaling factor is constructed in the right way, this allows us to rescale d_0 itself (and thus the evolution time). Note that the rescaling factor must not depend explicitly on x , since the scaling must be uniform across *all* minimising paths. It can, however, depend on the arrival times (i. e., $d_0(x)$).

This process creates, of course, technical difficulties. Let us now address them and execute the rescaling rigorously. As a first step, we need a variant of Lemma 36 that gives us also information about the *directional derivative* of d_0 along a minimising path. A further difficulty when considering ∇d_0 along a path is that the image of the path has measure zero, so that the almost-everywhere derivative we get from Lipschitz continuity and Rademacher's theorem does not help us. For *optimal* paths, however, we can still show the result using an idea similar to superoptimality:

Lemma 52. *Let $x \in \Omega^+$ be given such that $d_0(x) < \infty$. Assume $x_0 \in \Gamma_0$ and that $\xi \in X_{\text{ad}}(x_0, x)$ is an optimal path with $d_0(x) = d(x_0, x) = l(\xi)$ as per Lemma 19 and Lemma 33. Assume that the path is parametrised by arc length. Then $d_0 \circ \xi$ is continuously differentiable on $(0, 1)$ with*

$$(d_0 \circ \xi)'(t) = \frac{|\xi|}{F(\xi(t))}.$$

Proof. Take a close look at the proof of Lemma 48. This argument actually proves that we can pick a single optimal path ξ and then choose x^s for every $s \in (0, t)$ on the same path. In other words, we get for arbitrary $t \in [0, 1]$:

$$d_0(x) \leq d_0(\xi(t)) + d(\xi(t), x) \leq d(x_0, \xi(t)) + d(\xi(t), x) = l(\xi) = d_0(x)$$

Thus, equality holds throughout and we find that $d_0(\xi(t)) = d(x_0, \xi(t))$ for all $t \in [0, 1]$. Furthermore, this distance equals the path length of ξ restricted to times in $[0, t]$. With this reasoning, we can also show the following: For $t \in (0, 1)$ and $h \in (0, 1 - t)$, denote the part of ξ restricted to $[t, t + h]$ by $\tilde{\xi}$. Then

$$d_0(\xi(t + h)) - d_0(\xi(t)) = l(\tilde{\xi}) = \int_t^{t+h} \frac{|\xi|}{F(\xi(s))} ds.$$

The same holds also if $h \in (-t, 0)$ is negative. Note that the integrand is continuous. Dividing by h and letting $h \rightarrow 0$, this implies the claim. \square

We can now state and prove the main rescaling theorem:

Theorem 16. *Let $\psi: [0, S) \rightarrow [0, T)$ be continuously differentiable with $\psi' > 0$ and thus strictly increasing and bijective. Let F be some continuous speed field. For $x \in \Omega^+$, we denote the arrival time based on this speed field by $t(x) = d_0(x)$. If we define the rescaled speed field*

$$\tilde{F}(x) = \psi'(\psi^{-1}(t(x))) \cdot F(x), \quad (74)$$

then $\psi(s(x)) \leq t(x)$ holds for the arrival time $s(x)$ based on the speed field \tilde{F} and all x with $d_0(x) < T$.

Proof. Let us define the rescaled function σ by $\sigma = \psi^{-1} \circ t$. Note that (a variant of) Lemma 38 applies to this function. Choose x arbitrarily with $d_0(x) < T$. If $d_0(x) = 0$, then $x \in \overline{\Omega}_0$ and the statement is trivial. So assume $0 < t(x) < T$ from now on. There exist $x_0 \in \Gamma_0$ and $\xi \in X_{\text{ad}}(x_0, x)$ such that $l(\xi) = d(x_0, x) = t(x)$. For this path, Lemma 52 yields

$$(\sigma \circ \xi)'(\tau) = (\psi^{-1})'(t(\xi(\tau))) \cdot (t \circ \xi)' = \frac{1}{\psi'(\psi^{-1}(t(\xi(\tau))))} \frac{|\xi|}{F(\xi(\tau))} = \frac{|\xi|}{\tilde{F}(\xi(\tau))}$$

for all $\tau \in (0, 1)$. Let us denote the path length of ξ based on \tilde{F} by $\tilde{l}(\xi)$. Then, using the fundamental theorem of calculus,

$$s(x) \leq \tilde{l}(\xi) = \int_0^1 \frac{|\xi'(\tau)|}{\tilde{F}(\xi(\tau))} d\tau = \int_0^1 (\sigma \circ \xi)'(\tau) d\tau = \sigma(\xi(1)) - \sigma(\xi(0)) = \sigma(x).$$

This finishes the proof, since ψ is increasing and thus $\psi(s(x)) \leq \psi(\sigma(x)) = t(x)$. \square

We only get the inequality $\psi(s) \leq t$ since it is not a-priori clear whether the path ξ which is optimal for F is also optimal for the rescaled speed field \tilde{F} . In the proof of Theorem 16, we have only analysed how the scaling affects the length of this particular path. Note, though, that the rescaling is, in principle, symmetric. We can apply it again in the other direction to show equality. The only difficulty is the fact that the original arrival time is part of the scaling factor in (74).

Corollary 11. *Consider the situation of Theorem 16 and assume, in addition, that ψ is twice differentiable and either convex or concave. Then $\psi(s) = t$ holds. Consequently also $\tilde{\Omega}_\sigma = \Omega_{\psi(\sigma)}$ for all $\sigma \in [0, S)$, where $\tilde{\Omega}_\sigma$ denotes the evolved shape according to \tilde{F} .*

Proof. Let us assume, without loss of generality, that ψ is concave. If it is convex, we can apply everything to ψ^{-1} instead. Define another rescaled speed

$$\hat{F}(x) = (\psi^{-1})'(\psi(s(x))) \cdot \tilde{F}(x) = \frac{\tilde{F}(x)}{\psi'(s(x))}.$$

Since ψ is concave, ψ' is decreasing. Hence, $\psi'(s) \geq \psi'(\psi^{-1}(t))$. This implies $\hat{F} \leq \tilde{F}$. Let us denote the arrival time for the speed field \hat{F} by \hat{t} . Then, due to $\hat{F} \leq \tilde{F}$, we know that $t \leq \hat{t}$. Furthermore, if we apply Theorem 16 again for \hat{F} , we find $\psi^{-1}(\hat{t}) \leq s$. Taking both inequalities together, we have $t \leq \hat{t} \leq \psi(s)$. This shows $\psi(s) = t$. For the evolved shapes, consider Theorem 7:

$$x \in \tilde{\Omega}_\sigma \Leftrightarrow s(x) < \sigma \Leftrightarrow t(x) = \psi(s(x)) < \psi(\sigma) \Leftrightarrow x \in \Omega_{\psi(\sigma)}$$

\square

Let us finally make use of Theorem 16 to address the question of reachable shapes. Take note that we only need Theorem 16 for this, not the sharper statement of Corollary 11.

Corollary 12. *Let Ω_d and F be as in Lemma 51 and consider the situation of Theorem 16. Assume, furthermore, that $T = \infty$, i. e., $\lim_{\tau \rightarrow S^-} \psi(\tau) = \infty$. Then $\tilde{\Omega}_\sigma = \Omega_d$ for all $\sigma \geq S$.*

Proof. Note first that $F = 0$ on $\mathbb{R}^n \setminus \Omega_d$, which carries over to \tilde{F} and ensures that $\tilde{\Omega}_\sigma \subset \Omega_d$ for all σ . We have to show the reverse inclusion in case of $\sigma \geq S$. Choose $x \in \Omega_d$. As in Theorem 16, let us denote the corresponding arrival times for F and \tilde{F} by $t(x)$ and $s(x)$, respectively. Due to Theorem 16, we know that $s(x) \leq \psi^{-1}(t(x)) < S$. Hence, $x \in \tilde{\Omega}_\sigma$ for all $\sigma \geq S$. This finishes the proof. \square

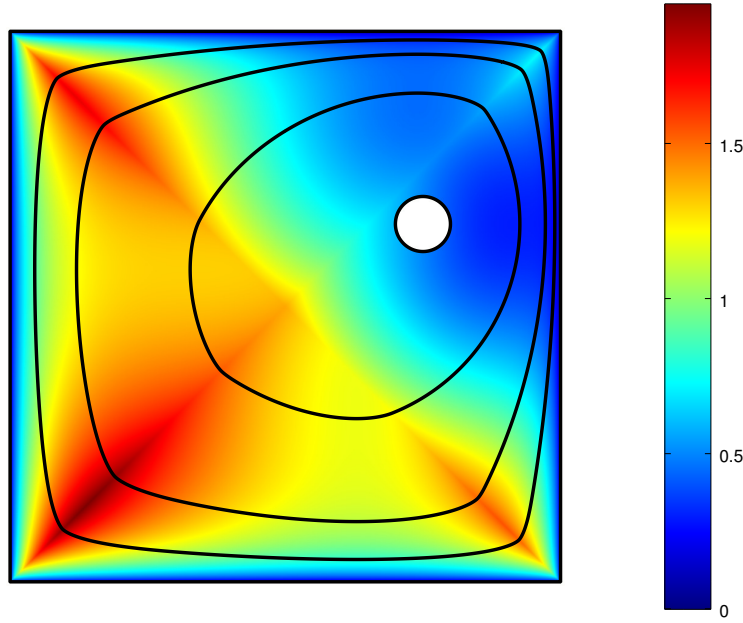


Figure 25: Example of a speed field rescaled according to (75). The initial geometry is the small circle, the target shape Ω_d the square. Some intermediate evolution steps are shown as well.

4.6.3 Hölder Continuous Speed Fields

To conclude the discussion about reachability, let us check what regularity we can expect from a speed field rescaled according to Theorem 16. Throughout this subsection, let us assume that the original speed field F is the distance function of $\mathbb{R}^n \setminus \Omega_d$ and choose $\psi(t) = \tan t$. This choice fulfils all requirements of Theorem 16, Corollary 11 and Corollary 12. In particular, it gives $\hat{\Omega}_{\pi/2} = \Omega_d$. The rescaled speed from (74) is in this case:

$$\tilde{F}(x) = \tan'(\arctan(t(x))) \cdot F(x) = (1 + t(x)^2) \cdot F(x) = (1 + d_0(x)^2) \cdot F(x) \quad (75)$$

Note that this is easily accessible also in a numerical setting. The arrival times d_0 can be calculated with the Fast Marching Method described in Subsection 3.5.2 (as can F , which is a distance function itself). The effect of this rescaling is illustrated in Figure 25: The plot shows a speed field constructed by (75) with the goal to transform a circle into a square. Take note that Theorem 15 forbids such a “squaring the circle” for Lipschitz continuous speed fields, since the square has density $1/4$ at the corners. It is, nevertheless, possible by the rescaled speed shown in the plot. The black contours indicate also some intermediate evolution steps. One can numerically verify the statement of Corollary 11 for them.

Let us now go back to the question of regularity of a speed field \tilde{F} rescaled according to (75). Of course, the interesting situation here is behaviour near the boundary. According to Lemma 34, the functions d_0 and thus also \tilde{F} are *locally* Lipschitz continuous in the interior of Ω_d anyway. Thus, we have to consider \tilde{F} near $\partial\Omega_d$. We want the rescaled speed to go continuously to zero there. Furthermore, recall that the possibility to produce (outward-pointing) corners is precisely what sets a rescaled speed field apart from a Lipschitz continuous one. Thus, considering the decay of \tilde{F} at corners is the most critical thing to do. In fact, one can even see in Figure 25 that \tilde{F} vanishes most slowly towards the corners. Unfortunately, continuity at a corner is not true in general. If we are looking at a cusp, then a rescaled speed field according to (75) fails to be continuous:

Example 12. Consider a cusp formed by two touching circles as shown in Figure 26. Assume that this is part of the boundary of Ω_d . The global structure of Ω_d and the initial geometry Ω_0 are not important

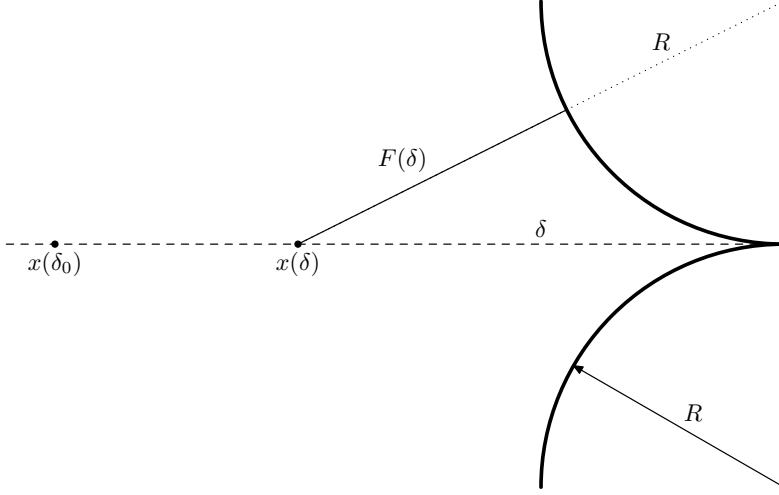


Figure 26: The situation and notation of Example 12.

here. Let us consider, in particular, F , d_0 and \tilde{F} along the dashed line. We characterise points on this line by their distance δ from the cusp, as shown in the figure. The initial speed field (as distance function to the boundary of Ω_d) is then

$$F(\delta) = F(x(\delta)) = \sqrt{R^2 + \delta^2} - R.$$

(Compare also Figure 28b.) Since the speed F is largest on the dashed line, we may assume that Ω_0 is such that all shortest paths to points $x(\delta)$ go along the dashed line. In this case,

$$d_0(\delta) = d_0(x(\delta)) = d_0(x(\delta_0)) + d(x(\delta_0), x(\delta)) = d_0(x_0) + \int_{\delta}^{\delta_0} \frac{1}{F(\delta')} d\delta'.$$

This integral, however, diverges so strongly for $\delta \rightarrow 0^+$ that $\tilde{F}(\delta) = (1 + d_0(\delta)^2) \cdot F(\delta)$ does not vanish in the limit $\delta \rightarrow 0^+$. A numerical evaluation of this rescaled speed field is shown (for some values of the parameters) in Figure 27. While the function is continuous on $(0, \delta_0)$, it *does not vanish* for $\delta \rightarrow 0^+$ and is thus not continuous across the boundary of Ω_d .

The problem in the situation of Example 12 is this: Due to the cusp, there is no guaranteed *minimal increase* of the original speed field F . Even if F is not required to be a distance function, this situation can still not be avoided: As long as F is assumed to be Lipschitz continuous, it can always be bounded from above by the distance function to $\mathbb{R}^n \setminus \Omega_d$ since $F = 0$ on this set. This leads to the same conclusion as in the example. Thus, we have to make an additional assumption on Ω_d to avoid a discontinuity in the rescaled speed field:

Assumption 1. Let Ω_d be bounded. We assume that there exists a compact set $K \subset \Omega_d$ and a constant $c > 0$ such that: For each $x \in \Omega_d$, there must be $x_k \in K$ and a path $\xi \in X_{\text{ad}}(x, x_k)$ such that

$$\nabla F(\xi(t)) \cdot \xi'(t) \geq c |\xi'(t)| \quad (76)$$

for almost all times $t \in [0, 1]$.

This assumption ensures that each point of Ω_d can be connected to some compact set (on with d_0 is uniformly bounded) with a path that ensures a certain minimal gradient of F . This is the case for a wide range of shapes. In particular, it allows non-cusp outward-pointing corners as in Figure 25, while it excludes the situation of Example 12. This is illustrated for the square $\Omega_d = [-1, 1]^2 \subset \mathbb{R}^2$ in Figure 28a: We can choose $K = \{0\}$ to be the singleton containing only the square's centre. For some other point in Ω_d , we can use a path as indicated in the figure. Since it follows the gradient of the distance function until it reaches a diagonal of the square, the directional derivative is one along this initial part of the

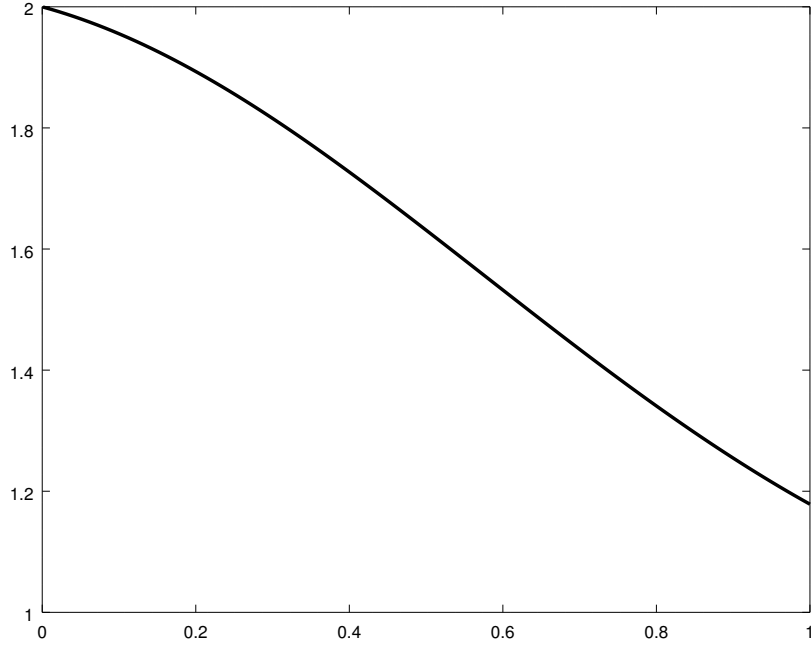


Figure 27: Evaluation of the rescaled speed field $\tilde{F}(\delta)$ in Example 12 with numerical quadrature. Clearly $\tilde{F}(\delta) \not\rightarrow 0$ for $\delta \rightarrow 0^+$.

path. But also afterwards, following the diagonal, the derivative is still uniformly positive as well. This is unlike a cusp, where the gradient along the “ridge” has no uniform lower bound as depicted in Figure 28b.

Based Assumption 1, we can now immediately show:

Lemma 53. *Let Assumption 1 hold. Then there exist constants $\bar{d}, M > 0$ such that*

$$d_0(x) \leq \bar{d} + \frac{1}{c} \log \left(1 + \frac{M}{F(x)} \right) \quad (77)$$

for all $x \in \Omega_d$.

This implies, in particular, also the following Hölder estimate: Let $\alpha \in (0, 1)$ be given and consider the rescaled speed field \tilde{F} from (75). Then there exists $C > 0$ such that

$$|\tilde{F}(x)| \leq C \cdot \text{sd}_{\mathbb{R}^n \setminus \Omega_d}(x)^\alpha = C \cdot F(x)^\alpha \quad (78)$$

for all $x \in \Omega_d$.

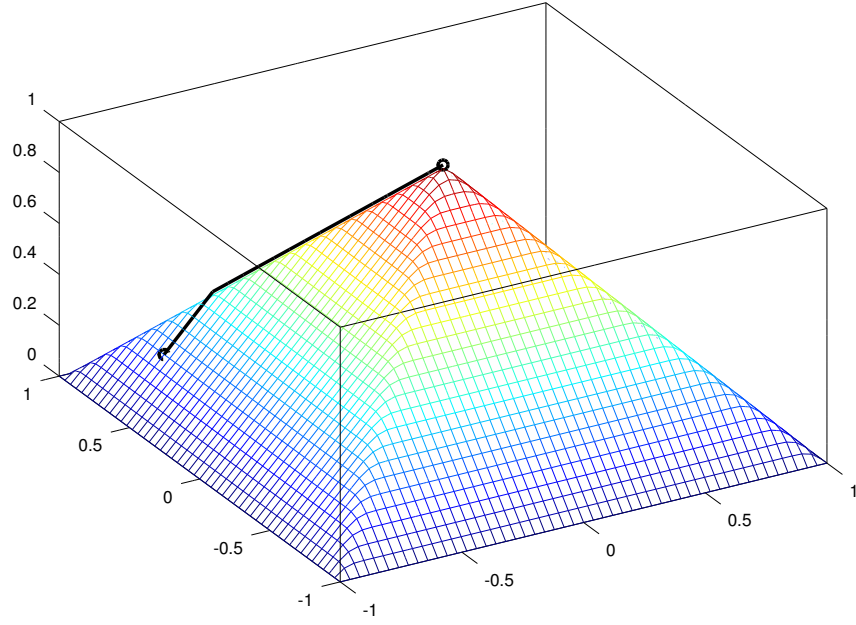
Proof. Let $x \in \Omega_d$ be given. Choose $x_k \in K$ and $\xi \in X_{\text{ad}}(x, x_k)$ according to Assumption 1. Without loss of generality, we can assume that ξ is parametrised such that $|\xi'(t)| = |\xi|$ for all $t \in [0, 1]$. Furthermore, due to (76), this also implies

$$F(\xi(t)) = F(x) + \int_0^t \nabla F(\xi(\tau)) \cdot \xi'(\tau) d\tau \geq F(x) + ct |\xi|. \quad (79)$$

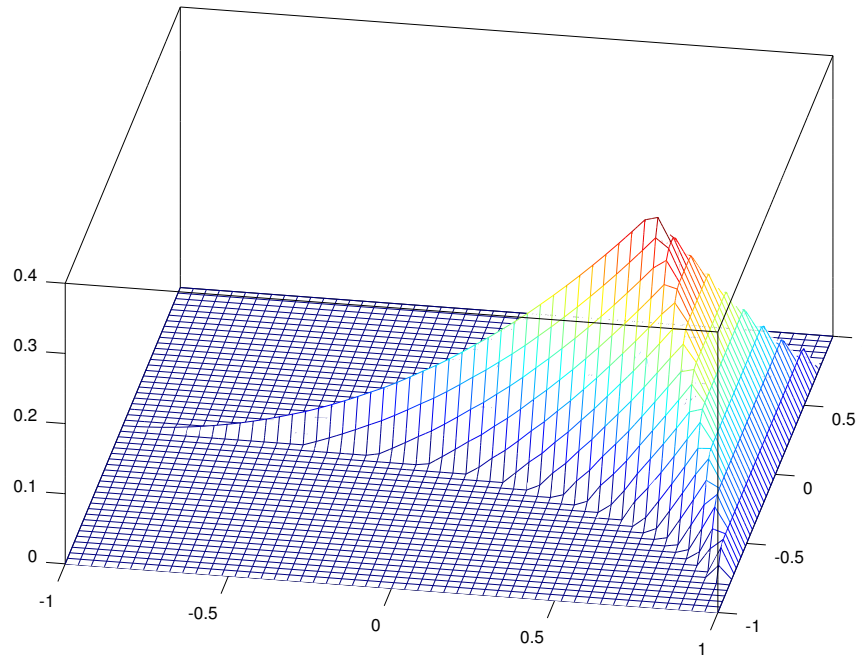
Hence, if we set $\bar{d} = \sup_{y \in K} d_0(y)$, it follows that

$$d_0(x) \leq d_0(x_k) + d(x_k, x) \leq \bar{d} + \int_0^1 \frac{|\xi|}{F(\xi(t))} dt \leq \bar{d} + \int_0^1 \frac{|\xi|}{F(x) + ct |\xi|} dt = \bar{d} + \frac{1}{c} \log \left(1 + \frac{c |\xi|}{F(x)} \right).$$

Since F is bounded on the compact set $\overline{\Omega_d}$, the relation (79) also implies that $|\xi|$ can be uniformly bounded. If we define M accordingly, (77) follows. For (78), just note that the right-hand side of (77) vanishes in the limit $x \rightarrow \partial\Omega_d$ if multiplied by any power $F(x)^{1-\alpha}$. \square



(a) For a square as Ω_d , the indicated path ensures (76).



(b) No uniform lower bound exists for the gradient along the ridge in case of a cusp.

Figure 28: Illustration of Assumption 1 for the case of a square (where the assumption is satisfied) and a cusp (where it does not hold).

The estimate (78) means, roughly speaking, that \tilde{F} is *Hölder continuous* (with arbitrary exponent less than one) towards the boundary. To see this, recall that $F(x) = |x - x_0|$ for some $x_0 \in \partial\Omega_d$ and that $\tilde{F}(x_0) = 0$. To conclude our analysis, let us finally extend this result and show that the rescaled speed field \tilde{F} is, indeed, Hölder continuous:

Theorem 17. *Let Assumption 1 hold. Then the rescaled speed field \tilde{F} from (75) is Hölder- α continuous for any $\alpha < 1/2$.*

Proof. Let $x, y \in \Omega_d$ be fixed, $\beta \in (0, 1)$ and consider the straight line S_{xy} connecting both points to each other. Without loss of generality, let us assume that $|x - y| < 1$. This is the interesting case. Assume first that $F(S_{xy}(\tau_0)) \leq |x - y|^\beta$ for some $\tau_0 \in [0, 1]$. This implies that there exists $x_0 \in \partial\Omega_d$ such that $F(S_{xy}(\tau_0)) = |x_0 - S_{xy}(\tau_0)|$ and

$$\max(F(x), F(y)) \leq \max(|x - x_0|, |y - x_0|) \leq |x - y| + |x_0 - S_{xy}(\tau_0)| \leq 2|x - y|^\beta.$$

Using Lemma 53, this yields

$$\left| \tilde{F}(x) - \tilde{F}(y) \right| \leq \left| \tilde{F}(x) - \tilde{F}(x_0) \right| + \left| \tilde{F}(x_0) - \tilde{F}(y) \right| = \left| \tilde{F}(x) \right| + \left| \tilde{F}(y) \right| \leq 2^{1+\alpha} C \cdot |x - y|^{\alpha\beta} \quad (80)$$

for any $\alpha < 1$ and some corresponding constant C .

Now, assume that $F(S_{xy}(\tau)) \geq |x - y|^\beta$ for all $\tau \in [0, 1]$. This implies

$$d_0(y) \leq d_0(x) + \frac{|S_{xy}|}{|x - y|^\beta} = d_0(x) + |x - y|^{1-\beta}.$$

Doing the same calculation the other way round, we get the Hölder estimate $|d_0(x) - d_0(y)| \leq |x - y|^{1-\beta}$. This implies for (75):

$$\begin{aligned} \tilde{F}(y) &= (1 + d_0(y)^2) \cdot F(y) \leq \left(1 + \left(d_0(x) + |x - y|^{1-\beta} \right)^2 \right) \cdot (F(x) + |x - y|) \\ &= \tilde{F}(x) + \left(1 + \left(d_0(x) + |x - y|^{1-\beta} \right)^2 \right) \cdot |x - y| + \left(|x - y|^{1-\beta} + 2d_0(x) \right) F(x) \cdot |x - y|^{1-\beta} \end{aligned} \quad (81)$$

Recall (77), which implies that $d_0(x)$ and with it the corresponding terms on the right-hand side of (81) are bounded when multiplied with any power of $F(x)$. Since

$$|x - y|^\alpha \leq |x - y|^{\alpha\beta} \leq F(x)^\alpha,$$

this is also true for any power of $|x - y|$. Again using this argument also the other way round, this implies a Hölder estimate of \tilde{F} .

Let us now summarise the results we have: In the first case, (80) implies that \tilde{F} is Hölder continuous with any exponent less than β . In the second, (81) gives Hölder continuity with exponents up to $1 - \beta$. Thus, if we choose $\beta = 1/2$, we have shown the claim. \square

5 Perimeter of the Evolving Sets for Constant Speed

Unfortunately, the shape calculus presented in Section 4.2 still has a small gap: We have only derived *weak* shape derivatives in the sense of absolutely continuous functions. Based on Lebesgue's differentiation theorem, this allows us to conclude the existence of a classical derivative for *almost all* times in the shape evolution as in the proof of Corollary 6. While this may be a good justification in practice, it is still very interesting to investigate whether or not the derivative actually exists everywhere. This is the case if the weak shape derivative (51) can be extended continuously to all times t . If we assume that the integrand Ff in this expression is continuous, the crucial question is *whether or not the* surface measure of Γ_t *depends continuously on t* . We believe that this is true under reasonable assumptions, but are, unfortunately, not able to give a full proof.

More generally, the regularity of level sets is a classical research topic. This can be seen already in the context of Sard's theorem and the co-area formula (see page 112 of [37]). For recent work in this direction, let us refer to [1]. Our situation is similar: By Corollary 5, the evolving boundary Γ_t can be written precisely in terms of the level sets of the distance function D . There already exists literature about the measure of level sets of distance functions, see, for instance, [18]. Research of this subject can be motivated directly by the famous paper [3] of Almgren, Taylor and Wang. Note carefully, though, that all of these results share the property that they are, more or less, based on the co-area formula. Consequently, they hold only for *almost all* level sets. This is of no use in our case, since we need statements about all times t of the shape evolution in order to derive continuity.

Our own paper [60] discusses an alternative approach in this direction, which is directly based on fundamental geometric and measure-theoretic arguments. The resulting statements are true *for all* level sets. In this chapter, we present these results. For this, let us concentrate on the effect of the initial geometry and not the speed field. Thus, we assume constant outward motion (i. e., $F = 1$) throughout most of this chapter. For simplicity, let us also study only the case of a non-fat initial boundary, which means $\overline{\Omega_0} = \Gamma_0 \cup \Omega_0$. This situation was already discussed in Section 3.1. Recall that the evolved sets Ω_t and Γ_t are given by the level sets of the distance function sd_{Ω_0} to the initial geometry as per (25). While this was not fully proven in Section 3.1 itself, it follows easily from the general Hopf-Lax theory presented later on and, in particular, Theorem 7.

To motivate the following considerations, we start with an example in Section 5.1. It shows that blow-up of the perimeter of Ω_t can happen for $t \rightarrow 0^+$ even if Ω_0 is a smooth Caccioppoli set. After investigating some auxiliary properties of spherical sectors in Section 5.2, we are able to show that all evolved sets Ω_t have *finite perimeter* if Ω_0 is bounded. This will be done in Subsection 5.3.1 with the help of an *inverse isoperimetric inequality* that we can prove for a special situation. The upper bound for the perimeter, however, diverges like $1/t$ for $t \rightarrow 0^+$. This matches our observations from the motivating example formulated in Theorem 18. Under an additional uniform-density assumption, we will improve the result in Subsection 5.3.2 to arrive at a *uniform bound* for $t \rightarrow 0^+$. Note, however, that these results do not yet yield a full proof for continuity of the perimeter. We develop, however, useful tools for further steps in this direction. At the end of this chapter, we will briefly discuss in Section 5.4 how these tools may be used in the future to prove continuity of $t \mapsto P(\Omega_t)$. We also give some ideas on how to generalise the results to the case of non-constant speed fields.

5.1 Motivating Example for Perimeter Blow-Up

Before we start working towards the main results of this chapter, let us give a motivating example. It shows why it is necessary to introduce the notion of uniform lower density in Subsection 5.3.2 together with the complexities it creates.

There is a classical textbook example for elementary geometry: Let a rope be put tightly around the Earth's equator. If the rope is now prolonged by a single metre, how far will it be above the surface? With a trivial calculation, one arrives at the surprising result that the distance is not negligible. In fact, the relationship between the changes in a circle's radius and its perimeter is *independent of the circle's size*. We can exploit this fact not just for huge but also for tiny circles. This allows us to show that the perimeter of Ω_t can blow up for $t \rightarrow 0^+$ even if Ω_0 has finite perimeter and is bounded:

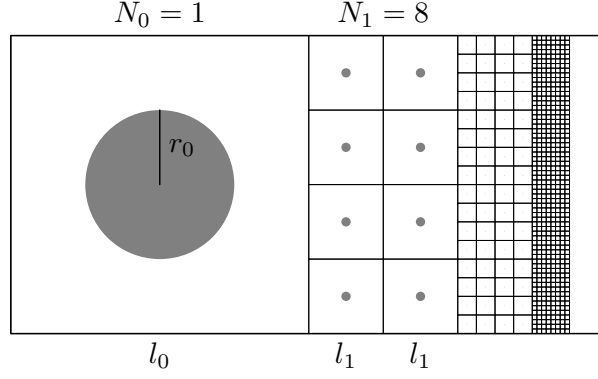


Figure 29: The notation and initial set Ω_0 used in Example 13. Ω_0 consists of the union of all grey balls.

Example 13. Consider $D = [0, 2] \times [0, 1] \subset \mathbb{R}^2$ as hold-all domain. For $k = 0, 1, \dots$, define

$$l_k = 4^{-k}, \quad r_k = \frac{(l_k)^2}{4} = \frac{1}{4} \cdot 16^{-k} \quad \text{and} \quad N_k = \frac{2^{-k}}{(l_k)^2} = 8^k.$$

Based on these definitions, we choose Ω_0 as an infinite union of balls as depicted in Figure 29. Specifically, Ω_0 is constructed by splitting D first into a sequence of vertical strips with widths 2^{-k} . Each strip is then further divided into squares of size $l_k \times l_k$. Into each such square, we put a ball with radius r_k . For each k , there is a total of N_k such squares and balls.

Each ball at level k has perimeter $2\pi r_k$, so that the total perimeter of Ω_0 is given as

$$P(\Omega_0) = \sum_{k=0}^{\infty} N_k \cdot 2\pi r_k = \frac{\pi}{2} \sum_{k=0}^{\infty} \left(\frac{8}{16} \right)^k = \pi.$$

Thus, Ω_0 is a bounded set of finite perimeter. It is also clear that it has a smooth boundary, since it consists entirely of balls. However, since the radii of the balls become arbitrarily small, the curvature of Γ_0 is not bounded. For the time evolution of Ω_0 , note that each circle grows outwards and is a circle of radius $r_k + t$ at time t . This works as long as t is small enough, so that the circle does not yet hit another growing circle. If we let t_k be the time at which the circles of level k hit their enclosing squares, we find that

$$t_k = \frac{l_k}{2} - r_k = \frac{1}{2} \cdot 4^{-k} - \frac{1}{4} \cdot 16^{-k} = \frac{1}{2} \cdot 4^{-k} \left(1 - \frac{1}{2} \cdot 4^{-k} \right) \geq \frac{1}{4} \cdot 4^{-k}. \quad (82)$$

The other way round, this means that for times $t < t_k$, all circles up to (and including) level k have certainly not touched any others. Let $t > 0$ be given and m such that $t_{m+1} \leq t < t_m$. If we use only circles up to level m to estimate the perimeter of Ω_t , this yields

$$P(\Omega_t) \geq \sum_{k=0}^m N_k \cdot 2\pi(r_k + t) \geq 2\pi \sum_{k=0}^m N_k t \geq 2\pi t_{m+1} \sum_{k=0}^m 8^k \geq \frac{\pi}{2} \frac{1}{4^{m+1}} \frac{8^{m+1} - 1}{7} \geq \frac{\pi}{14} (2^{m+1} - 1). \quad (83)$$

Note that we can see already here that this expression is unbounded for $t \rightarrow 0^+$, since this limit corresponds to $m \rightarrow \infty$. To get a more precise estimate, we can rewrite (82) to get

$$4^m \geq \frac{1}{4t_m} \Leftrightarrow 2^m \geq \frac{1}{2\sqrt{t_m}} \Rightarrow 2^{m+1} \geq \frac{1}{2\sqrt{t_{m+1}}} \geq \frac{1}{2\sqrt{t}}.$$

Combining this result with (83) finally gives

$$P(\Omega_t) \geq \frac{\pi}{14} \left(\frac{1}{2\sqrt{t}} - 1 \right),$$

which diverges like $1/\sqrt{t}$ as $t \rightarrow 0^+$ and certainly becomes unbounded.

If one considers the calculations in Example 13 carefully, one can see that the base number in the definition of l_k (four in the example) influences only the constant in front of the final estimate as long as it is larger than two. The exponent $1/2$ determining the rate to be $1/\sqrt{t}$ comes from the fact that each level of balls gets assigned only *half* the area that was assigned to the previous level. We can increase this fraction as long as it is *less than one* if we still want to get a bounded set as result. This line of thought can be extended to the following result:

Theorem 18. *Let $n \geq 2$ and $0 < s < 1$ be given. Then there exists a Caccioppoli set $\Omega_0 \subset \mathbb{R}^n$ bounded and with smooth boundary, such that*

$$P(\Omega_t) \geq \frac{C}{t^s}$$

for some constant C and $t > 0$ small enough. This gives, in particular, a rate of divergence for $t \rightarrow 0^+$.

Proof. We replicate the construction of Example 13: For the desired result, choose some $\alpha > 1$ and set

$$f = \alpha^{s-1} \in (0, 1).$$

Note that $f\alpha^n > f\alpha = \alpha^s > 1$. We define

$$l_k = \alpha^{-k}, \quad r_k = \frac{(l_k)^n}{4} = \frac{\alpha^{-kn}}{4} \quad \text{and} \quad N_k = \lceil f^k \alpha^{nk} \rceil.$$

This leads to a total volume of all $(l_k)^n$ -cubes of

$$\sum_{k=0}^{\infty} N_k (l_k)^n \leq \sum_{k=0}^{\infty} (f^k \alpha^{nk} + 1) \alpha^{-kn} = \sum_{k=0}^{\infty} f^k + \sum_{k=0}^{\infty} (\alpha^{-n})^k = \frac{1}{1-f} + \frac{1}{1-\alpha^{-n}} < \infty.$$

Hence, since $f < 1$, we can fit everything into a bounded set as before. Clearly, Ω_0 has again a smooth boundary. Its perimeter is also finite since

$$\begin{aligned} P(\Omega_0) &= C \sum_{k=0}^{\infty} N_k (r_k)^{n-1} \leq C \sum_{k=0}^{\infty} (f^k \alpha^{nk} + 1) r_k \\ &= \frac{C}{4} \left(\sum_{k=0}^{\infty} f^k + \sum_{k=0}^{\infty} (\alpha^{-n})^k \right) = \frac{C}{4} \left(\frac{1}{1-f} + \frac{1}{1-\alpha^{-n}} \right). \end{aligned}$$

On the other hand, we still find that balls at level k have not yet hit anything else until time

$$t_k = \frac{l_k}{2} - r_k = \frac{\alpha^{-k}}{2} - \frac{\alpha^{-kn}}{4} \geq \frac{\alpha^{-k}}{2} - \frac{\alpha^{-k}}{4} = \frac{\alpha^{-k}}{4}. \quad (84)$$

Thus, for $t > 0$ with $t_{m+1} \leq t < t_m$, we know that

$$\begin{aligned} P(\Omega_t) &\geq C \sum_{k=0}^m N_k (r_k + t)^{n-1} \geq C (t_{m+1})^{n-1} \cdot \sum_{k=0}^m N_k \geq C \left(\frac{\alpha^{-(m+1)}}{4} \right)^{n-1} \cdot \sum_{k=0}^m (f\alpha^n)^k \\ &= \frac{C}{4^{n-1}} (\alpha^{n-1})^{-(m+1)} \frac{f^{m+1} (\alpha^n)^{m+1} - 1}{f\alpha^n - 1} \geq \frac{C}{4^{n-1} (f\alpha^n - 1)} ((f\alpha)^{m+1} - 1) = C' ((\alpha^s)^{m+1} - 1), \end{aligned}$$

where we have defined the constant C' suitably. From (84), it follows that

$$\alpha^{m+1} \geq \frac{1}{4t_{m+1}} \geq \frac{1}{4t} \Leftrightarrow (\alpha^s)^{m+1} \geq \frac{4^{-s}}{t^s}.$$

Combining this with the estimate for $P(\Omega_t)$ above shows the claim. \square

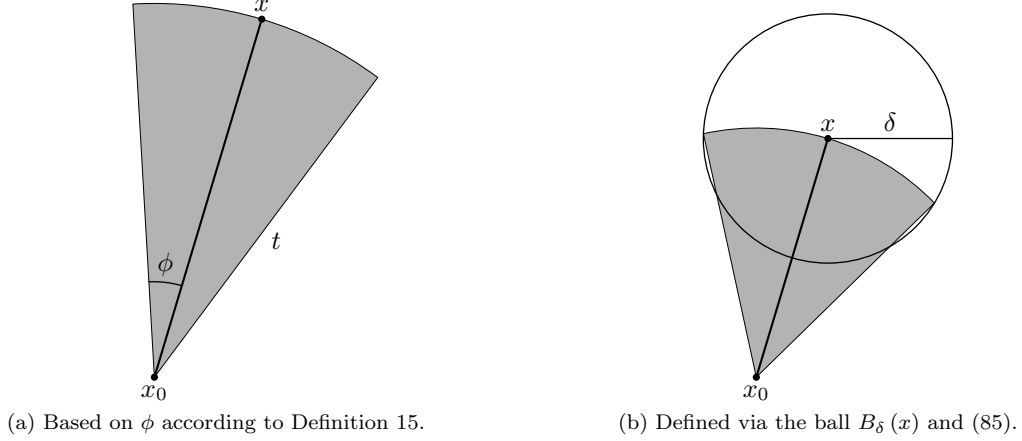


Figure 30: Definitions of the sector $S_\phi(x_0, x)$.

5.2 Auxiliary Geometric Results

In order to show our main results in Section 5.3 (in particular, Theorem 20), we need some auxiliary results. They are only based on elementary geometry and will be prepared in this section. The basic object studied is what we will call a *sector* below:

Definition 15. Let $x_0, x \in \mathbb{R}^n$, $x_0 \neq x$ and $\phi \in [0, \pi/2]$. We define

$$S_\phi(x_0, x) = \{y \in \mathbb{R}^n \mid 0 < |x_0 - y| < |x_0 - x| \text{ and } (y - x_0) \cdot (x - x_0) > |x_0 - y| |x_0 - x| \cdot \cos \phi\}.$$

We will often set $t = |x_0 - x|$ to be the sector's radius. The set $S_\phi(x_0, x)$ is an open sector of the ball with centre x_0 and radius t . The value of ϕ , which corresponds to the maximum allowed angle $x-x_0-y$, defines the sector's aperture.

Besides using the angle ϕ directly, we will also need to define such a sector via an auxiliary ball $B_\delta(x)$ for $\delta < t$. The idea is depicted in Figure 30b: In this case, the sector's aperture is defined *indirectly* via δ . It is chosen as the angle at which the ball around x intersects the larger sphere with centre x_0 . With basic trigonometry, one can derive

$$\phi(\delta) = \arccos\left(1 - \frac{\delta^2}{2t^2}\right) \quad (85)$$

for the corresponding aperture angle. In the following, we will only need two basic properties of this explicit function: $\delta < t\phi(\delta)$ holds for all δ and $t\phi(\delta)/\delta \rightarrow 1$ in the limit $\delta \rightarrow 0^+$. In other words, $t\phi(\delta) \approx \delta$ asymptotically for small δ .

The first part of our geometric analysis of sectors is concerned with determining their volume, i. e., n -dimensional Lebesgue measure. For this, let us state the following fundamental geometric facts:

Lemma 54. Let $n \geq 2$. The volume of a ball with radius $\rho > 0$ is given by

$$\text{vol}(B_\rho(x)) = \omega_n \rho^n, \text{ where } \omega_n = \frac{\pi^{n/2}}{\Gamma(n/2 + 1)}.$$

This holds obviously for arbitrary $x \in \mathbb{R}^n$.

Furthermore, there exists a mapping $r: [0, \pi/2] \rightarrow [0, 1/2]$ which is continuous, bijective, strictly increasing and satisfies

$$\text{vol}(S_\phi(x_0, x)) = r(\phi) \cdot \text{vol}(B_t(0)) = r(\phi) \cdot \omega_n t^n \quad (86)$$

for all $x_0, x \in \mathbb{R}^n$ and $\phi \in [0, \pi/2]$. Here, we have set $t = |x_0 - x|$ as before. In addition,

$$\lim_{\phi \rightarrow 0^+} \frac{r(\phi)}{\phi^{n-1}} > 0 \quad (87)$$

exists and is strictly positive.

Proof. The volume of n -dimensional balls is a well-known result. See, for instance, Theorem 26.13 on page 666 of [85]. In order to compute the volume of $S_\phi(x_0, x)$, we use spherical coordinates:

$$\begin{aligned} y_1 &= r \cdot \cos \phi_1, \\ y_k &= r \cdot \prod_{i=1}^{k-1} \sin \phi_i \cdot \cos \phi_k \text{ for } k = 2, \dots, n-2, \\ y_{n-1} &= r \cdot \prod_{i=1}^{n-2} \sin \phi_i \cdot \sin \phi_{n-1}, \\ y_n &= r \cdot \prod_{i=1}^{n-2} \sin \phi_i \cdot \cos \phi_{n-1} \end{aligned}$$

For a derivation of spherical coordinates particularly suited to our purposes, see [12]. Based on the derivation given there, it is easy to see that

$$S_\phi(x_0, x) = \{x_0 + y \in \mathbb{R}^n \mid y = y(r, \phi_1, \dots, \phi_{n-1}), r \in (0, t), \phi_1 \in [0, \phi]\}.$$

The other angles are drawn from their full range, i. e., $\phi_k \in [0, \pi]$ for $k = 2, \dots, n-2$ and $\phi_{n-1} \in [0, 2\pi]$. Since the Jacobian determinant of this transformation to spherical coordinates is

$$\det J(r, \phi_1, \dots, \phi_{n-1}) = r^{n-1} \cdot \prod_{i=1}^{n-2} (\sin \phi_i)^{n-i-1},$$

we find by simple integration that

$$\text{vol}(S_\phi(x_0, x)) = \int_0^t r^{n-1} dr \cdot \int_0^\phi (\sin \phi_1)^{n-2} d\phi_1 \cdot \prod_{i=2}^{n-2} \int_0^\pi (\sin \phi_i)^{n-i-1} d\phi_i \cdot \int_0^{2\pi} d\phi_{n-1}.$$

Note that the integral over r is trivial to compute. The integrals over $\phi_2, \dots, \phi_{n-1}$ result in a dimensional constant. If ϕ is chosen as π , we recover the full volume of $B_t(x_0)$. Thus,

$$r(\phi) = \frac{\int_0^\phi (\sin \phi')^{n-2} d\phi'}{\int_0^\pi (\sin \phi')^{n-2} d\phi'}$$

fulfils (86). All other claimed properties of the function r follow from this expression. \square

We can also relate the surface area of a sector's base to its volume. This result will be used later when we prove Theorem 20. It follows immediately from Lemma 54 and, in particular, (87):

Lemma 55. *For fixed $t > 0$, there exist $\delta_0 > 0$ and a dimensional constant C such that*

$$\delta^{n-1} \omega_{n-1} \leq C \frac{\text{vol}(S_{\phi(\delta)}(x_0, x))}{t}$$

for all $\delta \in (0, \delta_0)$ and arbitrary $x_0, x \in \mathbb{R}^n$ with $|x_0 - x| = t$.

Proof. By (87), there exist $\phi_0 > 0$ and C' such that $\phi^{n-1} \leq C' r(\phi)$ holds for all $\phi \in (0, \phi_0)$. Since $\delta < t\phi(\delta)$ according to (85), it follows that

$$\delta^{n-1} \omega_{n-1} < t^{n-1} \phi(\delta)^{n-1} \omega_{n-1} \leq C' \frac{\omega_{n-1}}{\omega_n} \cdot r(\phi(\delta)) \cdot \omega_n t^{n-1} = C' \frac{\omega_{n-1}}{\omega_n} \cdot \frac{\text{vol}(S_{\phi(\delta)}(x_0, x))}{t}.$$

This estimate holds as long as $\phi(\delta) \in (0, \phi_0)$. Since t is fixed and $t\phi(\delta)/\delta \rightarrow 1$, we can choose $\delta_0 > 0$ suitably such that this condition is satisfied for all $\delta \in (0, \delta_0)$. \square

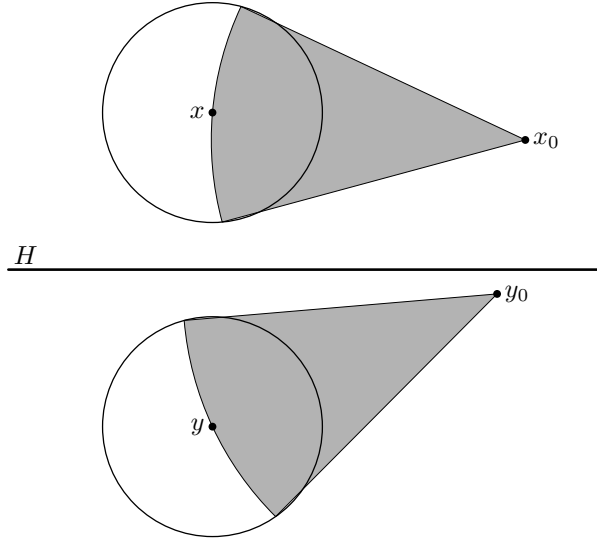


Figure 31: The hyperplane H separates both the balls and the full sectors from each other when (88) holds. This is the main idea in the proof of Lemma 56.

Finally, let us consider *two* sectors $S_\phi(x_0, x)$ and $S_\phi(y_0, y)$. The angle is the same for both, and we assume that $\phi = \phi(\delta)$ for some $\delta > 0$. Let also $t = |x_0 - x| = |y_0 - y|$. We are particularly interested in the situation

$$\overline{B_\delta(x)} \cap \overline{B_\delta(y)} = \emptyset \text{ and } t \leq \min(|x_0 - y|, |y_0 - x|). \quad (88)$$

A main ingredient for the proof of Theorem 20 is the fact that this condition is sufficient for both sectors to be disjoint. This is illustrated in Figure 31: If the balls are disjoint, we can construct the hyperplane H that divides the line x - y at its midpoint and is perpendicular to it. This plane has the property that all points “above” it are closer to x than to y , and vice-versa for points on the other side. Thus, (88) implies that x_0 is on the same side as x , while y_0 must be on the other side together with y . Hence, the plane separates the convex sets $S_\phi(x_0, x)$ and $S_\phi(y_0, y)$ from each other, which means that the sectors must be disjoint. This is the main idea behind the following result:

Lemma 56. *Let $\delta > 0$ and $x_0, y_0, x, y \in \mathbb{R}^n$ with $t = |x_0 - x| = |y_0 - y|$ such that (88) holds. Then*

$$S_{\phi(\delta)}(x_0, x) \cap S_{\phi(\delta)}(y_0, y) = \emptyset.$$

Proof. With a proper translation, we can assume, without loss of generality, that $y = -x$. Because $\overline{B_\delta(x)}$ and $\overline{B_\delta(y)}$ are disjoint, the hyperplane

$$H = \{p \in \mathbb{R}^n \mid x \cdot p = 0\}$$

separates both balls (see Figure 31). Furthermore, by (88) we know

$$|x_0 - x|^2 = t^2 \leq |x_0 - y|^2 = |x_0 + x|^2.$$

Multiplying this inequality out, we find $0 \leq x \cdot x_0$. This means that x and x_0 are on the same side of H . Similarly, we also find that y and y_0 are on one side of H . Since $y = -x$, this means

$$0 \leq y \cdot y_0 \Leftrightarrow x \cdot y_0 \leq 0.$$

Hence, x_0 and y_0 are *on different sides* of the hyperplane H . Thus, H separates also the convex hulls of $\overline{B_\delta(x)} \cup \{x_0\}$ and $\overline{B_\delta(y)} \cup \{y_0\}$, which contain $S_\phi(x_0, x)$ and $S_\phi(y_0, y)$, respectively. This shows that the sectors are, indeed, disjoint. \square

5.3 Estimates of the Perimeter

With all the preparations of Section 5.2 in place, we can now proceed to show the main estimates. As before, let us assume that $\Omega_0 \subset \mathbb{R}^n$ is an open set. We denote its boundary by $\Gamma_0 = \partial\Omega_0$ and introduce $d_0 = \text{sd}_{\Omega_0}$ as the distance function of Ω_0 . Recall also the definitions of Ω_t and Γ_t from (25). An immediate consequence of the definition of the signed distance function in (1) is the following property of d_0 :

Lemma 57. *For each $x \in \mathbb{R}^n \setminus \Omega_0$,*

$$d_0(x) = \inf_{y \in \Gamma_0} |x - y|. \quad (89)$$

Furthermore, there exists $x_0 \in \Gamma_0$ with $d_0(x) = |x - x_0|$.

In the following, we are interested in estimating the “surface area” of Ω_t for $t > 0$. Before we can do that, let us briefly recall the applicable concepts for defining such a surface area in the first place:

Definition 16. Let $\Omega \subset \mathbb{R}^n$ be open. We define its *perimeter* as the quantity

$$P(\Omega) = \sup \left\{ \int_{\mathbb{R}^n} \text{div}(\psi) \, dx \mid \psi \in C^1(\Omega) \text{ has compact support and } \|\psi\|_\infty \leq 1 \right\}.$$

The set Ω is said to have finite perimeter or to be a *Caccioppoli set* if $P(\Omega) < \infty$.

See, for instance, Definition 3.35 on page 143 of [4] and Section 3.3 of this book in general for more details about sets of finite perimeter. Furthermore, let us also introduce the *Hausdorff measure* following Definition 2.46 on page 72 of [4]:

Definition 17. Let $k \in \mathbb{N}$ and $\Omega \subset \mathbb{R}^n$. For $\delta > 0$, we define

$$\mathcal{H}_\delta^k(\Omega) = \inf \left\{ \sum_{i=1}^{\infty} \left(\frac{d_i}{2} \right)^k \omega_k \mid \Omega \subset \bigcup_{i=1}^{\infty} U_i, d_i = \sup_{x, y \in U_i} |x - y|, d_i \leq 2\delta \right\}.$$

Here, ω_k denotes the volume of the k -dimensional unit ball as in Lemma 54. The value d_i is the *diameter* of the set U_i , and it is allowed to be at most 2δ in order for $(U_i)_{i \in \mathbb{N}}$ to be an admissible δ -covering of Ω .

Furthermore, the *k-dimensional Hausdorff measure* of Ω is then given by

$$\mathcal{H}^k(\Omega) = \sup_{\delta > 0} \mathcal{H}_\delta^k(\Omega) = \lim_{\delta \rightarrow 0^+} \mathcal{H}_\delta^k(\Omega).$$

Note that we define the Hausdorff measure in such a way that \mathcal{H}^n corresponds to the n -dimensional Lebesgue measure. (For a proof, see Theorem 2.53 on page 76 of [4].) This is the reason for including ω_k in the definition. Other authors (e. g., [85]) do not add this normalisation constant, which results in a notion of \mathcal{H}^k that is different from Definition 17 by a constant.

For the case of only one dimension, the situation is simple since sets of finite perimeter in one dimension can be represented (up to a set of measure zero) as the union of a finite number of intervals:

Theorem 19. *Let $n = 1$ and $\Omega_0 \subset \mathbb{R}$ be open and bounded. Then Γ_t is a finite set for each $t > 0$ and its cardinality is non-increasing with respect to t . Furthermore,*

$$\mathcal{H}^0(\Gamma_t) \leq P(\Omega_0). \quad (90)$$

If Ω_0 has finite perimeter and t is sufficiently small, then both values are actually equal.

Proof. Let $t > 0$ and $x \in \Gamma_t$. Lemma 57 implies that there exists $x_0 \in \Gamma_0$ with $|x - x_0| = t$. Assume, without loss of generality, that $x_0 < x$. It follows that $I_x = (x_0, x) \subset d_0^{-1}((0, t))$. Furthermore, if $y \in \Gamma_t$ and $x \neq y$, then $I_x \cap I_y = \emptyset$. Since $\text{vol}(I_x) = t > 0$ for each $x \in \Gamma_t$ and Ω_t is bounded, the cardinality of Γ_t is bounded as $\mathcal{H}^0(\Gamma_t) \leq \text{vol}(\Omega_t)/t$ and thus finite. If we have $0 < s < t$, the estimate (90) implies

$$\mathcal{H}^0(\Gamma_t) \leq P(\Omega_s) \leq \mathcal{H}^0(\Gamma_s).$$

Hence it follows that the cardinality is non-increasing when we have established (90).

For (90), assume that Ω_0 has finite perimeter (the situation is trivial otherwise). According to Proposition 3.52 on page 153 of [4], there exist $p \in \mathbb{N}$ and p disjoint intervals $J_i = [a_i, b_i]$ such that $\Omega_0 \subset \bigcup_{i=1}^p J_i$. The two sets can only differ by a set of measure zero. Furthermore, $P(\Omega_0) = 2p$. As before, we can associate an interval $I_x \subset d_0^{-1}((0, t))$ to each $x \in \Gamma_t$ and all I_x are disjoint. If we assume that $I_x = (x_0, x)$, then $x_0 = b_i$ for some $1 \leq i \leq p$. Similarly, $x_0 = a_i$ if $I_x = (x, x_0)$. Because of

$$\mathcal{H}^0(\Gamma_t) \leq 2p = P(\Omega_0),$$

the relation (90) follows. If we assume an ordering such as

$$a_1 < b_1 < a_2 < b_2 < \dots < a_p < b_p$$

and denote by

$$L = \inf_{i=1, \dots, p-1} (a_{i+1} - b_i) > 0$$

the minimal distance between the intervals J_i , then equality holds with $\mathcal{H}^0(\Gamma_t) = 2p$ for $t < L/2$. \square

5.3.1 A Bound on the Hausdorff Measure

Intuitively, Ω_t is constructed from Ω_0 by adding a “layer” of thickness t onto Γ_0 . Following this picture, one can imagine that the volume of this layer should roughly equal t times the surface area (i. e., perimeter) of either Ω_0 or Ω_t . This argument can be made rigorous by estimating the volume in terms of $P(\Omega_0)$ and then $\mathcal{H}^{n-1}(\Gamma_t)$ in terms of the volume. The former will be done in Subsection 5.3.2. We will show the latter as our first main result in this subsection. This is, somehow, an *inverse isoperimetric inequality*. Of course, in the general situation no inverse to the classical isoperimetric inequality (see Subsection 5.6.2 of [37]) holds. In our case, however, it works because the considered volume is not allowed to be “arbitrarily thin”.

Definition 18. For a fixed initial set Ω_0 and $t > 0$, we define the *newly created volume* to be

$$U_t = \left(\bigcup_{x_0 \in \Gamma_0} B_t(x_0) \right) \setminus \overline{\Omega_0} = \{x \in \mathbb{R}^n \mid 0 < d_0(x) < t\}.$$

We can now state and prove the first main result of this chapter:

Theorem 20. *There exists a dimensional constant C such that*

$$P(\Omega_t) \leq \mathcal{H}^{n-1}(\Gamma_t) \leq C \cdot \frac{\text{vol}(U_t)}{t}$$

holds for all $t > 0$.

Proof. The first inequality is a well-known fact about the relation between perimeter and the Hausdorff measure. See, for instance, Proposition 3.62 on page 159 of [4]. We will now show the second inequality. For this, let $\delta > 0$ be given. Then clearly $\Gamma_t \subset \bigcup_{x \in \Gamma_t} \overline{B_\delta(x)}$. According to Vitali’s covering theorem (see Theorem 1 on page 27 of [37]), there exists a countable subset $X \subset \Gamma_t$ such that

$$\Gamma_t \subset \bigcup_{x \in X} \overline{B_{5\delta}(x)} \tag{91}$$

and all $\overline{B_\delta(x)}$ are disjoint for $x \in X$. Note that X is, in fact, finite if Ω_0 and thus also Γ_t are bounded.

For each $x \in \Gamma_t$, there exists a corresponding point $x_0 \in \Gamma_0$ with $|x - x_0| = t$ according to Lemma 57. Furthermore, note that $t \leq |y - y_0|$ for all $y \in \Gamma_t$ and $y_0 \in \Gamma_0$. For $x \in X$ and its associated point $x_0 \in \Gamma_0$, let us define

$$S_x = S_{\phi(\delta)}(x_0, x).$$

Note that the condition (88) is satisfied for each pair (S_x, S_y) with $x, y \in X$, so that all S_x and S_y with $x \neq y$ are disjoint by Lemma 56. Also note that a basic geometric argument implies $S_x \cap \overline{\Omega_0} = \emptyset$ for small enough δ . Thus, we find that each S_x is contained in the newly created volume and get

$$\sum_{x \in X} \text{vol}(S_x) = \text{vol} \left(\bigcup_{x \in X} S_x \right) \leq \text{vol}(U_t). \tag{92}$$

Since the enlarged balls in (91) provide a particular 5δ -covering of Γ_t , we know that

$$\mathcal{H}_{5\delta}^{n-1}(\Gamma_t) \leq \sum_{x \in X} (5\delta)^{n-1} \omega_{n-1} \leq 5^{n-1} \frac{C'}{t} \sum_{x \in X} \text{vol}(S_x).$$

The last estimate and the constant C' come from Lemma 55. Together with (92), this yields

$$\mathcal{H}_{5\delta}^{n-1}(\Gamma_t) \leq 5^{n-1} C' \cdot \frac{\text{vol}(U_t)}{t}.$$

The bound on the right-hand side does not depend on δ any more, so that we can take the limit $\delta \rightarrow 0^+$ to finish the proof. \square

Having this first result, we can already show that all evolved sets Ω_t must be Caccioppoli sets:

Corollary 13. *Let Ω_0 be bounded. Then Ω_t has finite perimeter for all $t > 0$.*

Proof. From the boundedness of Ω_0 , we can directly conclude that also Ω_t and U_t are bounded sets for any fixed t . Thus, $\text{vol}(U_t) < \infty$ and Theorem 20 implies that $\mathcal{H}^{n-1}(\Gamma_t)$ is finite for each t . It follows now again from Proposition 3.62 on page 159 of [4] that Ω_t is a set of finite perimeter. \square

Take note that the actual bound we get from Corollary 13 diverges like $1/t$ for $t \rightarrow 0^+$. It will be the focus of the next subsection (in particular, Corollary 14) to show a *uniform* bound in the limit $t \rightarrow 0^+$ under additional assumptions. Without these assumptions, however, we can not hope for any strong improvement of Corollary 13: As we have seen in Theorem 18, the optimal upper bound must diverge stronger than $1/t^s$ for any $s \in (0, 1)$.

5.3.2 Uniform Bounds

As we have seen above in Theorem 20, the quantity $\text{vol}(U_t)/t$ is crucial as it gives an upper bound on the evolved sets' perimeters. Particularly interesting is the limit $t \rightarrow 0^+$. As our second main result of this chapter, we show in this subsection that there exists a uniform upper bound for $t \rightarrow 0^+$ as long as a *uniform-density condition* holds for the initial set Ω_0 . This condition prevents arbitrarily sharp corners and cusps. To be precise:

Definition 19. Let $A \subset \Gamma_0$, $c \in (0, 1)$ and $t_0 > 0$. We say that Ω_0 has (t_0, c) -uniform lower density on A if the estimate

$$0 < c \leq \frac{\text{vol}(B_t(x) \cap \Omega_0)}{\text{vol}(B_t(x))} \quad (93)$$

holds for all $t \in (0, t_0)$ and $x \in A$. Similarly, Ω_0 is said to have (t_0, c) -uniform upper density on A if

$$\frac{\text{vol}(B_t(x) \cap \Omega_0)}{\text{vol}(B_t(x))} \leq 1 - c < 1. \quad (94)$$

When both conditions are satisfied together, Ω_0 simply has (t_0, c) -uniform density on A .

For fixed x and in the limit $t \rightarrow 0^+$, the quotient in (93) and (94) gives the density of Ω_0 at x that was introduced in Definition 13. A related concept that is important for us is the so-called *reduced boundary* $\mathcal{F}\Omega$ of an open set Ω . (Roughly speaking, this is the set of all boundary points where a measure-theoretic variant of the normal vector to the boundary can be defined. See Definition 3.54 on page 154 of [4].) This set has the property that Ω has density $1/2$ at all points in $\mathcal{F}\Omega$, as shown in Theorem 3.61 on page 158 of [4]. Note, however, that this is also true in the example constructed in Section 5.1. Hence, *uniformity* of the estimates is really crucial for our purposes in the following. Note that we are not the first to introduce the concept of uniform lower density. It has been used already by others in a similar context. See, for instance, Proposition 4.2 in [3] and Theorem 6 in [18]. The relation between uniform density and other, more established geometric properties will be discussed in more detail in Subsection 5.3.3.

For our estimate of $\text{vol}(U_t)$, we need to somehow get an upper bound on t in terms of the perimeter of Ω_0 . For a classical result in this direction, see (3.54) on page 156 of [4]. Unfortunately, this estimate

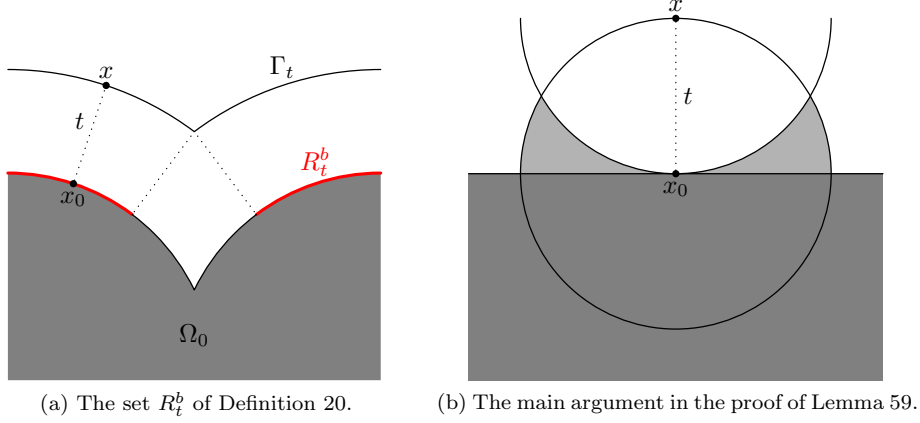


Figure 32: The backwards reachable set and its regularity with respect to uniform upper density. The dark grey region is Ω_0 . The point x_0 is on $R_t^b \subset \Gamma_0$, with $x \in \Gamma_t$ such that (96) holds.

is local in nature and not uniform over the whole boundary of Ω_0 . Note, however, that (93) and (94) together are equivalent to

$$c \leq \frac{\min(\text{vol}(B_t(x) \cap \Omega_0), \text{vol}(B_t(x) \setminus \Omega_0))}{\text{vol}(B_t(x))}. \quad (95)$$

This relation can be combined with the *relative isoperimetric inequality* (see, for instance, Theorem 2 on page 190 of [37]) to get the uniform estimate that we need:

Lemma 58. *Let Ω_0 have (t_0, c) -uniform density on A . Then there exists a dimensional constant C with*

$$t^{n-1} \leq C \left(\frac{1}{c} \right)^{\frac{n-1}{n}} \mathcal{H}^{n-1}(B_t(x) \cap \mathcal{F}\Omega_0)$$

for all $x \in A$ and $t \in (0, t_0)$.

Proof. Since we assume uniform density, (95) implies that

$$c \cdot \text{vol}(B_t(x)) = c \cdot \omega_n t^n \leq \min(\text{vol}(B_t(x) \cap \Omega_0), \text{vol}(B_t(x) \setminus \Omega_0))$$

for all $t \in (0, t_0)$. If we also apply the relative isoperimetric inequality, we get

$$t^{n-1} \leq C \left(\frac{1}{c} \right)^{\frac{n-1}{n}} P(\Omega_0; B_t(x))$$

for some dimensional constant C . This implies the result together with the well-known relation between perimeter and \mathcal{H}^{n-1} that can be found in Theorem 3.59 on page 157 of [4]. \square

So far, we have assumed uniform density of Ω_0 . It will turn out, however, that it is enough to require only uniform *lower* density. Uniform upper density is provided automatically if we choose the subset $A \subset \Gamma_0$ in the right way:

Definition 20. We say that $x_0 \in \Gamma_0$ is *backwards reachable* for time $t > 0$ if there exists $x \in \mathbb{R}^n$ with

$$t \leq |x_0 - x| = d_0(x). \quad (96)$$

The set of all backwards reachable points for time t is denoted by R_t^b .

See Figure 32a for an illustration of the set R_t^b : The point $x_0 \in R_t^b$ is shown together with a possible $x \in \Gamma_t$ that fulfils (96). Note that only the red part of Γ_0 is backwards reachable. Thus, we see that R_t^b is actually more regular than Γ_0 itself. In particular, Ω_0 has always uniform upper density on R_t^b . To understand why this must be the case, take a look at Figure 32b: Whenever x_0 and x are as indicated, the ball $B_t(x)$ must be disjoint to $\overline{\Omega_0}$ since otherwise $d_0(x) < t$ would be the case. Thus, the volume of $B_t(x) \cap B_t(x_0)$ can never be part of Ω_0 , which implies an upper bound for the density of Ω_0 at x_0 . (For the shown situation, the density is actually $1/2$. The maximal possible density would be achieved if also the light grey area were part of Ω_0 .) Let us formalise this argument now:

Lemma 59. *Let $t > 0$ and R_t^b be the backwards reachable set for time t . Then Ω_0 has (t, c) -uniform upper density on R_t^b , where c is a dimensional constant.*

Proof. Let $e \in \mathbb{R}^n$ be arbitrary with $|e| = 1$. We define

$$0 < c = \frac{\text{vol}(B_1(0) \cap B_1(e))}{\text{vol}(B_1(0))} < 1.$$

Now choose $x_0 \in R_t^b$ and $\tau \leq t$. We have to show that (94) holds for $B_\tau(x_0)$ with the defined c . By Definition 20, there exists $x \in \mathbb{R}^n$ such that $\tau \leq t \leq |x_0 - x| = d_0(x)$. We can assume, without loss of generality, that $|x_0 - x| = \tau$. Considering Figure 32b, this implies $B_\tau(x) \cap \Omega_0 = \emptyset$. Hence:

$$\frac{\text{vol}(B_\tau(x_0) \cap \Omega_0)}{\text{vol}(B_\tau(x_0))} = 1 - \frac{\text{vol}(B_\tau(x_0) \setminus \Omega_0)}{\text{vol}(B_\tau(x_0))} \leq 1 - \frac{\text{vol}(B_\tau(x_0) \cap B_\tau(x))}{\text{vol}(B_\tau(x_0))} = 1 - c$$

□

Another important observation is that the backwards reachable set is already sufficient for the construction of the newly created volume U_t . This allows us to restrict our considerations to the more regular R_t^b instead of Γ_0 itself later on.

Lemma 60. *For $0 < s < t$, $R_t^b \subset R_s^b$. Furthermore,*

$$U_t \setminus U_s \subset \bigcup_{x_0 \in R_s^b} B_t(x_0).$$

Proof. The inclusion $R_t^b \subset R_s^b$ is immediately clear from Definition 20. Pick $x \in U_t \setminus U_s$ arbitrarily. By Lemma 57 we can find $x_0 \in \Gamma_0$ with $d_0(x) = |x_0 - x|$. Moreover, $x \notin U_s$ implies that $d_0(x) \geq s$, so that $x_0 \in R_s^b$. Similarly, $x \in U_t$ yields $d_0(x) < t$ and thus $x \in B_t(x_0)$. □

With this result, all preparations are in place and we can proceed to the actual estimate of $\text{vol}(U_t)$. This is done in two steps: First, we estimate $\text{vol}(U_{2t} \setminus U_t)$. The regularity of the backwards reachable set with respect to uniform upper density of Ω_0 can be used for this situation. Afterwards, we build the union of a sequence of such strips in order to get $\text{vol}(U_t)$ itself.

Lemma 61. *Assume that Ω_0 has (t_0, c) -uniform lower density on Γ_0 . Then there exists a dimensional constant C such that*

$$\text{vol}(U_{2t} \setminus U_t) \leq C \left(1 + \frac{1}{c}\right)^{\frac{n-1}{n}} t \cdot P(\Omega_0)$$

holds for all $t \in (0, t_0)$.

Proof. According to Lemma 59, we know that Ω_0 has (t, c') -uniform upper density on R_t^b with some dimensional c' . Since it has uniform lower density per assumption, it has (t, c'') -uniform density (both upper and lower) with $c'' = \min(c, c')$. Furthermore, note that

$$\frac{1}{c''} = \frac{1}{\min(c, c')} \leq \frac{1}{c} + \frac{1}{c'}.$$

Thus Lemma 58 implies that

$$t^n \leq C' \left(\frac{1}{c} + \frac{1}{c'}\right)^{\frac{n-1}{n}} t \cdot \mathcal{H}^{n-1}(B_t(x_0) \cap \mathcal{F}\Omega_0)$$

for all $x_0 \in R_t^b$ with some dimensional C' . Taking it even further, this yields also

$$\text{vol} \left(\overline{B_{10t}(x_0)} \right) = 10^n \cdot \text{vol} \left(B_t(x_0) \right) \leq C \left(1 + \frac{1}{c} \right)^{\frac{n-1}{n}} t \cdot \mathcal{H}^{n-1}(B_t(x_0) \cap \mathcal{F}\Omega_0) \quad (97)$$

for yet another dimensional constant C .

Making use of Lemma 60, we know that

$$U_{2t} \setminus U_t \subset \bigcup_{x_0 \in R_t^b} B_{2t}(x_0).$$

With Vitali's covering theorem (see, again, Theorem 1 on page 27 of [37]), we can construct $X \subset R_t^b$ at most countable such that the sets $B_{2t}(x_0)$ are disjoint for $x_0 \in X$, but still

$$U_{2t} \setminus U_t \subset \bigcup_{x_0 \in X} \overline{B_{10t}(x_0)}.$$

Taking the measure on both sides of this inclusion and using (97), we finally find

$$\begin{aligned} \text{vol}(U_{2t} \setminus U_t) &\leq \sum_{x_0 \in X} \text{vol} \left(\overline{B_{10t}(x_0)} \right) \leq C \left(1 + \frac{1}{c} \right)^{\frac{n-1}{n}} t \cdot \sum_{x_0 \in X} \mathcal{H}^{n-1}(B_t(x_0) \cap \mathcal{F}\Omega_0) \\ &\leq C \left(1 + \frac{1}{c} \right)^{\frac{n-1}{n}} t \cdot \mathcal{H}^{n-1}(\mathcal{F}\Omega_0) = C \left(1 + \frac{1}{c} \right)^{\frac{n-1}{n}} t \cdot P(\Omega_0). \end{aligned}$$

The simplification of the sum is justified because all sets $B_t(x_0)$ are disjoint. \square

Theorem 21. *Let Ω_0 have (t_0, c) -uniform lower density on Γ_0 . Then*

$$\frac{\text{vol}(U_t)}{t} \leq C \left(1 + \frac{1}{c} \right)^{\frac{n-1}{n}} P(\Omega_0)$$

for all $t \in (0, t_0)$ and a dimensional constant C .

Proof. Let $t \in (0, t_0)$ be given. Then the disjoint telescopic decomposition

$$U_t = (U_t \setminus U_{t/2}) \cup (U_{t/2} \setminus U_{t/4}) \cup \dots = \bigcup_{k=1}^{\infty} (U_{2t/2^k} \setminus U_{t/2^k})$$

holds. Together with Lemma 61 this yields

$$\text{vol}(U_t) = \sum_{k=1}^{\infty} \text{vol}(U_{2t/2^k} \setminus U_{t/2^k}) \leq C \left(1 + \frac{1}{c} \right)^{\frac{n-1}{n}} P(\Omega_0) \cdot \sum_{k=1}^{\infty} \frac{t}{2^k} = C \left(1 + \frac{1}{c} \right)^{\frac{n-1}{n}} t \cdot P(\Omega_0).$$

This finishes the proof. \square

When we combine Theorem 21 with Theorem 20, we finally get a uniform bound for $\mathcal{H}^{n-1}(\Gamma_t)$. This result is very similar to Theorem 6 in [18], but note that it holds for all $t \geq 0$ and not just for almost all:

Corollary 14. *Assume that Ω_0 has (t_0, c) -uniform lower density on Γ_0 and that Ω_0 is bounded. In particular, let $\Omega_0 \subset B_R(0)$ for some $R > 0$. Then*

$$\mathcal{H}^{n-1}(\Gamma_t) \leq C \cdot (1 + P(\Omega_0) + t^{n-1}) \quad (98)$$

for all $t \geq 0$. The constant C depends only on n, t_0, c and R but no other properties of Ω_0 .

Proof. Note that the situation is clear for $t = 0$ as long as we choose $C \geq 1$. From Theorem 21, we know that $\text{vol}(U_t)/t \leq C'P(\Omega_0)$ for all $t \in (0, t_0)$. Furthermore, since $\Omega_0 \subset B_R(0)$, note that $\Omega_t \subset B_{R+t}(0)$. Thus, for $t \geq t_0$,

$$\text{vol}(U_t) \leq \omega_n(R+t)^n \leq C''(1+t^n) \Rightarrow \frac{\text{vol}(U_t)}{t} \leq C'' \left(\frac{1}{t} + t^{n-1} \right) \leq C'''(1+t^{n-1}).$$

The claim now follows from Theorem 20, if we combine both estimates for $\text{vol}(U_t)/t$. \square

5.3.3 Geometric Regularity Properties in the Literature

The main ingredient for the results in the previous Subsection 5.3.2 is a particular geometric property of the initial set Ω_0 , namely uniform density from Definition 19. As pointed out above, this notion has been used already by others to achieve similar results (see [3] and [18]). We are not aware of any applications in a broader context, though. Thus, it makes sense to put it into perspective with similar geometric properties that are more established in the literature and more widely used. In particular, a variety of so-called (*uniform*) *segment* and *cone properties* is often used to characterise geometric regularity of sets. For a thorough introduction, see Section 2.6 of [30].

Since uniformity plays an important role for the results of Subsection 5.3.2, it makes only sense to consider the *uniform* variants of those segment properties. (All non-uniform properties are fulfilled by the example developed in Section 5.1, since it is constructed only from circles.) Furthermore, the uniform (fat) segment property alone also provides very little regularity. For instance, a cusp satisfies it while it clearly does not have uniform lower density. Thus, let us focus on the *uniform cone property*. For convenience, we recall Definition 6.3 on page 115 of [30]:

Definition 21. For $x_0, x \in \mathbb{R}^n$ and $\phi \in [0, \pi/2]$, define the open cone

$$C_\phi(x_0, x) = \left\{ y \in \mathbb{R}^n \mid |x_0 - y| |x_0 - x| \cdot \cos \phi < (y - x_0) \cdot (x - x_0) < |x_0 - x|^2 \right\}.$$

This is similar to the sector $S_\phi(x_0, x)$ of Definition 15 studied above, but it describes a cone with flat base, i. e., without a spherical cap.

Now, let $\Omega \subset \mathbb{R}^n$ be open. We say that Ω satisfies the *uniform cone property* if there exist $t > 0$, $\phi \in (0, \pi/2)$ and $\rho > 0$ such that for all $x_0 \in \partial\Omega$ there is $x \in \mathbb{R}^n$ with $|x_0 - x| = t$ and

$$x + d \in \overline{\Omega} \Rightarrow C_\phi(x_0 + d, x + d) \subset \Omega$$

for all $d \in B_\rho(0)$.

Since the uniform cone property ensures for each boundary point the existence of a cone that is entirely contained in Ω , we can use this cone's volume as a lower bound on the density of Ω . Thus, the uniform cone property is a stronger condition than uniform lower density:

Theorem 22. Let $\Omega \subset \mathbb{R}^n$ satisfy the uniform cone property with t and ϕ as in Definition 21. Then Ω has $(t, r(\phi))$ -uniform lower density on $\partial\Omega$. Similarly, if $\mathbb{R}^n \setminus \overline{\Omega}$ has the uniform cone property with these constants, then Ω has $(t, r(\phi))$ -uniform upper density.

Proof. Let $x_0 \in \partial\Omega$ be given. According to Definition 21, there exists $x \in \mathbb{R}^n$ with $|x_0 - x| = t$ such that $C_\phi(x_0, x) \subset \Omega$. Note that $S_\phi(x_0, x) \subset C_\phi(x_0, x)$ since

$$|x_0 - y| < |x_0 - x| \Rightarrow (y - x_0) \cdot (x - x_0) \leq |y - x_0| \cdot |x - x_0| < |x_0 - x|^2.$$

Thus, for each $\tau \in (0, t)$, clearly

$$B_\tau(x_0) \cap S_\phi(x_0, x) \subset B_\tau(x_0) \cap C_\phi(x_0, x) \subset B_\tau(x_0) \cap \Omega.$$

Hence, we can estimate

$$\text{vol}(B_\tau(x_0) \cap \Omega) \geq \text{vol}(B_\tau(x_0) \cap S_\phi(x_0, x)) = r(\phi) \cdot \text{vol}(B_\tau(x_0))$$

based on (86). This shows the claim. The proof for uniform upper density works analogously. \square

Another concept related to our definition of uniform lower density are sets with *finite density perimeter* as defined in [13] and Subsection 3.1 of [29]:

Definition 22. Let $\Omega \subset \mathbb{R}^n$ be open and $h > 0$. The *h-density perimeter* of Ω is defined as

$$P_h(\Omega) = \sup_{0 < \epsilon < h} \frac{\text{vol}(V_\epsilon(\partial\Omega))}{2\epsilon}, \quad (99)$$

where $V_\epsilon(\partial\Omega)$ is the ϵ -envelope of $\partial\Omega$:

$$V_\epsilon(\partial\Omega) = \bigcup_{x \in \partial\Omega} B_\epsilon(x) = \{x \in \mathbb{R}^n \mid \text{sd}_{\partial\Omega}(x) < \epsilon\} \quad (100)$$

If $P_h(\Omega)$ is finite, we call Ω a set of *finite h-density perimeter*.

This can be interpreted as a relaxation of the $(n-1)$ -dimensional Minkowski content (see, for instance, 3.2.37 on page 273 of [40]). To be precise, the Minkowski content results if the supremum in (99) is replaced by the limit $\epsilon \rightarrow 0^+$. It is easy to see that $V_\epsilon(\Omega_0)$ is related to the newly created volume U_ϵ of Definition 18: The set U_ϵ is the part of $V_\epsilon(\Omega_0)$ which is outside of $\overline{\Omega_0}$. Hence, an argument similar to the proof of Theorem 21 can be applied to show that *uniform density implies finite density perimeter*.

5.4 Outlook

In the end of this chapter, let us give a brief outlook. In particular, recall what we have shown above: For $F = 1$, we were able to derive upper bounds for the perimeters $P(\Omega_t)$ of evolved sets. This is definitely a new and interesting result, but it does not fully solve the motivating problem. For this, two more steps are necessary: First, we need to completely rule out jumps to get *continuity* of the perimeter; upper bounds as we have shown so far are not enough. Second, the ultimate goal is to have this result not just for $F = 1$ but for arbitrary (Lipschitz continuous) speed fields. While we do not yet have any conclusive answers to these questions, we believe that it should be possible to resolve them positively (at least under suitable additional assumptions). There are some preliminary arguments supporting this claim, which we want to give below.

5.4.1 Showing Continuity

For the question of *continuity* of the evolved perimeters, note that we only have to deal with *upper semi-continuity*. Lower semi-continuity is a direct consequence of the corresponding well-known property of the variation measure. See, for instance, Remark 3.5 on page 119 of [4] and our later discussion in Lemma 63. Furthermore, it is also well-known that the perimeter is even *differentiable* for a sufficiently smooth initial set Ω_0 . In this case, the derivative can be expressed in terms of the mean curvature κ :

$$p(t) = P(\Omega_t) \Rightarrow p'(t) = \int_{\Gamma_t} \kappa d\sigma \quad (101)$$

See Section 2.33 of [78] and the discussion in Section 8.1 (focused on the case of a general speed field).

Let us now consider what happens in 2D if the boundary is only piecewise smooth with corners between the smooth parts. Depending on the direction of the corner (outward- or inward-pointing), there are two possible situations to consider. They are illustrated in Figure 33. With elementary geometry, one can deduce that the change in perimeter (highlighted in red in the figure) is given by

$$\Delta P = \begin{cases} \Delta\omega \cdot t & \text{for outward-pointing corners,} \\ 2(1 - \cos \Delta\omega) / \sin \Delta\omega \cdot t & \text{in the inward-pointing case.} \end{cases}$$

(We use the convention that $\Delta\omega > 0$ for an outward-pointing corner and $\Delta\omega < 0$ otherwise. Note that $\Delta P < 0$ in the latter case.) This formula can also be used to define an *extended curvature* such that (101) still holds for $p'(0)$. In addition to κ for smooth parts of Γ_t as in (101), this extended curvature is a measure that also has Dirac-delta components concentrated on the corners.

To see why the perimeter of such a domain with piecewise smooth boundary should behave continuously during the shape evolution, it remains to make two important observations: First, let us assume that Ω_0 is convex. In this case, Γ_0 is a single closed curve and the integral in (101) always results in $p'(0) = 2\pi$. This works both for smooth parts and outward-pointing corners. As long as there are only finitely many components of Ω_0 , this implies continuity of the perimeter. (For Example 13, this is not the case. The individual components, however, actually *are* convex and have a smooth boundary.) Second, note that ΔP is always negative for inward-pointing corners; furthermore, *it is larger in magnitude than the corresponding positive change for an outward-pointing corner with the same $|\Delta\omega|$* . Hence, even if the boundary curve is non-convex, the total derivative cannot exceed 2π . This implies upper semi-continuity.

On the other hand, note that $\Delta P/t$ can get arbitrarily negative if $\omega \rightarrow \pi^-$. The perimeter is still lower semi-continuous, of course, but the derivative $p'(0)$ is not bounded from below. This can be seen with a simple example that exhibits a cusp:

Example 14. Let Ω_0 be formed by two touching circles, such that a double cusp is produced. For instance, let us choose

$$\Omega_0 = B_1(-1, 0) \cup B_1(1, 0).$$

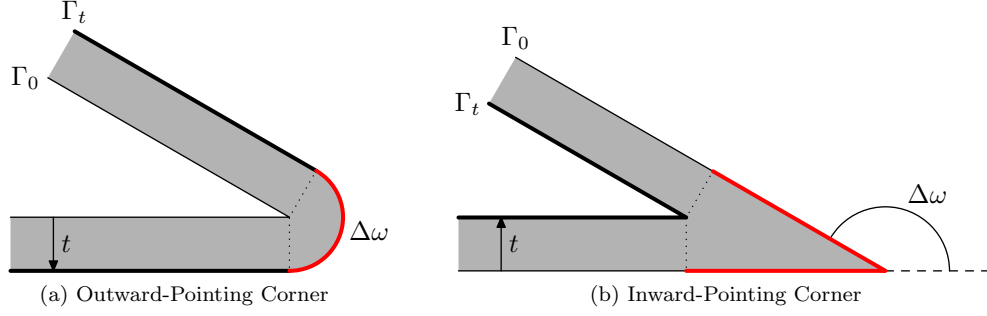


Figure 33: Evolution of the perimeter at a corner. The change in angle at the corner is (in magnitude) $\Delta\omega$. The grey area is the newly created volume due to the time evolution, the change in perimeter is indicated in red.

If we evolve this initial geometry along $F = 1$, the circles grow uniformly in time. At $t \geq 0$, their radii are $r(t) = 1 + t$. The intersection points of both circles lie on the y -axis (due to symmetry reasons) and can easily be computed as $(0, \pm y(t))^T$ with

$$y(t) = \sqrt{r(t)^2 - 1} = \sqrt{t(2+t)}.$$

It remains to compute the perimeter of Ω_t . For this, note that Γ_t consists of four symmetric circular arcs. Each one of them was initially a half circle. Over time, it grows in radius but only covers the angle $\pi - \omega(t)$, where $\omega(t)$ is the angle of the point $y(t)$ seen from the centres of the circles. Basic trigonometry gives $\omega(t) = \arctan y(t)$ and thus

$$P(\Omega_t) = 4 \cdot r(t) \cdot (\pi - \omega(t)) = 4(1+t) \left(\pi - \arctan \left(\sqrt{t(2+t)} \right) \right).$$

This function is clearly not Lipschitz continuous and has, in particular, derivative $-\infty$ at $t = 0$.

5.4.2 General Speed Fields

Finally, let us discuss the modifications required to extend the results of this chapter to more general speed fields. Since one can always employ Theorem 5, it is enough to consider $F \geq 0$. Lipschitz continuity is, in general, a quite strong requirement that allows us to treat the speed field as “almost constant” in neighbourhoods that are small enough. Such an argument is used successfully, for instance, to prove Theorem 15 and to derive the results in Subsection 7.2.2. Thus, there is hope that a general (Lipschitz continuous) speed field does not introduce too many additional difficulties. It is plausible that the most difficult situations when analysing the evolution of $P(\Omega_t)$ are caused by an irregular *initial geometry* and not a non-constant speed field. Difficulties related to the initial geometry, however, are already handled above. Of course, it is still by no means guaranteed that one can really carry through the proofs above for more general speed fields. We were not yet able to do so. Nevertheless, let us, at least, give a potential substitute for Theorem 21:

Lemma 62. *Let Ω_0 have (t_0, c) -uniform density on Γ_0 . Assume that F has Lipschitz constant L and that $0 \leq F \leq \bar{F}$. Then there exists a dimensional constant C such that*

$$\frac{\text{vol}(U_t)}{t} \leq C \left(\frac{1}{c} \right)^{\frac{n-1}{n}} \cdot \frac{e^{Lt}}{1 - Lt \cdot e^{Lt}} \int_{\Gamma_0} F d\sigma$$

for all $t > 0$ with $Lt \cdot e^{Lt} < 1$ and $t\bar{F} \cdot e^{Lt} < t_0$.

Proof. The proof follows, for the most part, Lemma 61. For simplicity, we do not bother with the strips used there. Since we assume *full* uniform density of Ω_0 here, this is not necessary. Let us start by analysing the newly created volume U_t for the considered situation. Based on the first estimate in Lemma 21, we can deduce the inclusion

$$\{y \in \mathbb{R}^n \mid d(x, y) < t\} \subset B_{r_x(t)}(x), \text{ where } r_x(t) = \frac{F(x)}{L} (e^{Lt} - 1) \leq tF(x) \cdot e^{Lt}.$$

The last inequality can be proven with a series expansion. Furthermore, note that $U_t = \Omega_t \setminus \overline{\Omega_0}$ can be covered by

$$U_t \subset \bigcup_{x \in \Gamma_0} B_{r_x(t)}(x) \subset \bigcup_{x \in X} \overline{B_{5r_x(t)}(x)}.$$

Here, we have used Vitali's covering theorem again to find a countable subset $X \subset \Gamma_0$. This allows us, in particular, to make $B_{r_x(t)}(x)$ and $B_{r_y(t)}(y)$ disjoint for all $x, y \in X$.

By assumption, $r_x(t) < t_0$ for all $x \in \Gamma_0$. Thus, Lemma 58 can be used to conclude

$$\text{vol} \left(\overline{B_{5r_x(t)}(x)} \right) \leq C \left(\frac{1}{c} \right)^{\frac{n-1}{n}} r_x(t) \cdot \mathcal{H}^{n-1} (B_{r_x(t)}(x) \cap \mathcal{F}\Omega_0).$$

Lipschitz continuity of F implies that

$$|y - x| < r_x(t) \leq tF(x) \cdot e^{Lt} \Rightarrow F(y) \geq F(x) (1 - Lt \cdot e^{Lt})$$

for all $x \in \Gamma_0$ and $y \in B_{r_x(t)}(x)$. Both estimates together yield

$$\begin{aligned} \text{vol}(U_t) &\leq \sum_{x \in X} \text{vol} \left(\overline{B_{5r_x(t)}(x)} \right) \leq C \left(\frac{1}{c} \right)^{\frac{n-1}{n}} \sum_{x \in X} r_x(t) \cdot \mathcal{H}^{n-1} (B_{r_x(t)}(x) \cap \mathcal{F}\Omega_0) \\ &\leq C \left(\frac{1}{c} \right)^{\frac{n-1}{n}} e^{Lt} \cdot t \sum_{x \in X} F(x) \int_{B_{r_x(t)}(x) \cap \Gamma_0} d\sigma \leq C \left(\frac{1}{c} \right)^{\frac{n-1}{n}} e^{Lt} \cdot t \int_{\Gamma_0} \frac{F(y)}{1 - Lt \cdot e^{Lt}} d\sigma. \end{aligned}$$

This implies the claim. □

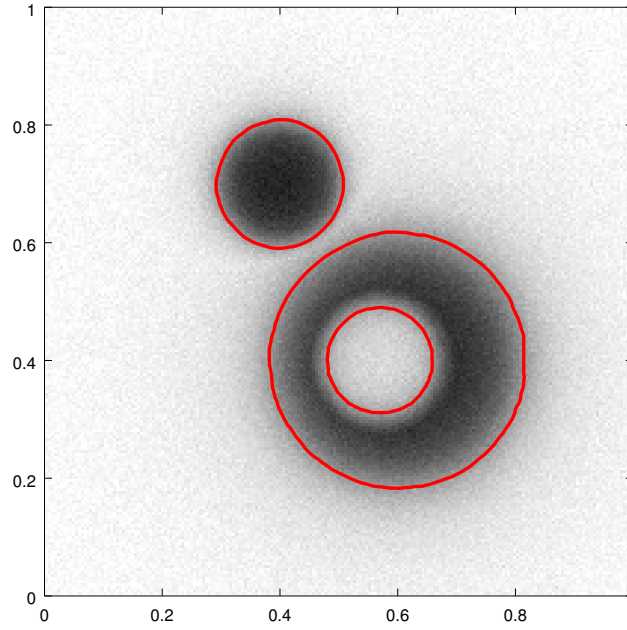


Figure 34: Our goal of the example optimisation problem considered throughout Chapter 6 is to find a shape matching one segment of a given grey-scale image. Here, the solution is shown with the red contour. It consists of the dark ring and disc.

6 Gradient Descent for Shape Optimisation

In the previous chapters, we have discussed how to describe and also modify shapes in the level-set framework. Furthermore, we have seen in Section 4.2 that these results can, in particular, be used to develop a shape calculus. We now finally turn our attention to actual *shape optimisation* based on this foundation. See also [14] for a more general framework for shape optimisation with level sets and [75] for an early work that captures already the basic ideas (although in a non-rigorous fashion). Throughout this chapter, we will discuss and develop a gradient-descent method based on a model for image segmentation. Our goal with this optimisation problem is shown in Figure 34: Given a grey-scale image, we want to identify the shape of a *segment*, i. e., a region with approximately homogeneous intensity, of the image. We do this by minimising the following shape functional:

$$J(\Omega) = \int_{\Omega} (u(x) - \bar{u})^2 dx - 2\gamma \cdot \sigma \cdot \text{vol}(\Omega) \quad (102)$$

Here, $u: D \rightarrow I \subset \mathbb{R}$ is the grey-scale image. Typically, we consider $D = [0, 1]^2$ and $I = [0, 1]$. The set $\Omega \subset D$ is the shape we are looking for, which should be a part of the domain D on which the image u attains an approximately constant intensity. The quantities \bar{u} and σ in (102) are the mean intensity and the standard deviation of the image over Ω ,

$$\bar{u} = \frac{1}{\text{vol}(\Omega)} \int_{\Omega} u(x) dx \quad \text{and} \quad \sigma^2 = \frac{1}{\text{vol}(\Omega)} \int_{\Omega} (u(x) - \bar{u})^2 dx.$$

The variable $\gamma > 0$ is a constant parameter. Thus, our goal is to minimise (102) over all possible open sets $\Omega \subset D$. We call D the *hold-all domain* and assume it to be bounded.

Note that this approach is slightly different from the usual meaning of *image segmentation*. We are only trying to identify a single segment's shape, which is a problem suited very well for demonstrating our general optimisation framework. In the literature, image segmentation usually means to find *all* segments

of the image. In other words, one looks not just for $\Omega \subset D$, but instead for a disjoint decomposition of D into $\Omega_1 \cup \Omega_2 \cup \dots \cup \Omega_N$. One can, however, extend the model in (102) to include corresponding terms for $D \setminus \Omega$ as well. This leads to a so-called *two-phase image segmentation*. It is straight-forward to adapt the techniques developed below to this situation. We have, in fact, implemented it as well. Furthermore, using *two* sets Ω_1 and Ω_2 as optimisation variables, we can even characterise *four* different phases. With the Four-Colour Theorem, this is enough to describe all possible (regular) image segmentations. Again, our theory and methods can be extended to this case as well. Such *multi-phase* image-segmentation approaches were introduced in [81].

We would also like to point out that our model (102) is not meant to be a state-of-the-art method for image segmentation. Instead, it is just a convenient example problem for the discussion of the general optimisation framework we want to present. Let us now briefly interpret the chosen cost functional J : The first term in (102) is a data-fitting term that penalises segments which do not have a nearly uniform intensity. This term is already present in the classical Chan-Vese model for image segmentation described in [21]. Instead of approximating the segment with a constant intensity \bar{u} , one can also use higher-order polynomials. See, for instance, [22]. This is, again, a straight-forward extension of the method discussed in the following. Probably more interesting (and non-standard), however, is the second term in (102): Since it prefers Ω to become larger due to the negative sign, it creates a *balloon force* that prevents Ω from collapsing to the empty set. The weight of this force is given by the parameter γ and, more importantly, by the standard deviation σ of the image over the segment. In other words, if the constant intensity \bar{u} is a poor fit for the actual image over Ω , we increase the force. This may happen, for instance, if the image is very noisy. In these cases, the stronger balloon force is needed to overcome the penalisation imposed by the data-fitting term. When we have derived the shape derivative of J , we will see much better how these two competing forces interact.

6.1 Shape Derivatives for the Example Problem

Our model (102) is covered completely by the general shape calculus derived above in Section 4.2. Thus, we can calculate the shape derivatives (in the weak sense of absolutely continuous functions as before) according to these rules. Let F be some fixed speed field. For simplicity, we denote the weak shape derivative in direction F just by a prime. Recall our shape-dependent quantities:

$$\text{vol}(\Omega) = \int_{\Omega} dx, \quad \bar{u} = \frac{1}{\text{vol}(\Omega)} \int_{\Omega} u dx, \quad \text{Var}(u) = \frac{1}{\text{vol}(\Omega)} \int_{\Omega} (u - \bar{u})^2 dx \quad \text{and} \quad \sigma = \sqrt{\text{Var}(u)}$$

Thus, the shape derivatives are:

$$\begin{aligned} \text{vol}(\Omega)' &= \int_{\Gamma} F d\sigma, \\ \bar{u}' &= \frac{1}{\text{vol}(\Omega)} \int_{\Gamma} u F d\sigma - \frac{\text{vol}(\Omega)'}{\text{vol}(\Omega)^2} \int_{\Omega} u dx = \frac{1}{\text{vol}(\Omega)} \int_{\Gamma} (u - \bar{u}) F d\sigma, \\ \left(\int_{\Omega} (u - \bar{u})^2 dx \right)' &= \int_{\Gamma} (u - \bar{u})^2 F d\sigma + 2\bar{u}' \int_{\Omega} (\bar{u} - u) dx = \int_{\Gamma} (u - \bar{u})^2 F d\sigma, \\ \text{Var}(u)' &= \frac{1}{\text{vol}(\Omega)} \int_{\Gamma} (u - \bar{u})^2 F d\sigma - \frac{\text{vol}(\Omega)'}{\text{vol}(\Omega)^2} \int_{\Omega} (u - \bar{u})^2 dx \\ &= \frac{1}{\text{vol}(\Omega)} \int_{\Gamma} ((u - \bar{u})^2 - \text{Var}(u)) F d\sigma, \\ \sigma' &= \frac{\text{Var}(u)'}{2\sqrt{\text{Var}(u)}} = \frac{\text{Var}(u)'}{2\sigma} = \frac{1}{2 \cdot \text{vol}(\Omega)} \int_{\Gamma} \left(\frac{(u - \bar{u})^2}{\sigma} - \sigma \right) F d\sigma \end{aligned}$$

Using these results, we can now finally also compute the shape derivative of J in direction F :

$$\begin{aligned} dJ(\Omega; F) &= \int_{\Gamma} (u - \bar{u})^2 F d\sigma - 2\gamma\sigma \int_{\Gamma} F d\sigma - \gamma \int_{\Gamma} \left(\frac{(u - \bar{u})^2}{\sigma} - \sigma \right) F d\sigma \\ &= \int_{\Gamma} \left((u - \bar{u})^2 \left(1 - \frac{\gamma}{\sigma} \right) - \gamma\sigma \right) F d\sigma \end{aligned} \tag{103}$$

Note that $dJ(\Omega; \cdot)$, interpreted as functional operating on the speed field F , is supported on the *boundary* Γ of our domain Ω . This corresponds to the well-known *Hadamard-Zolésio structure theorem*, see Theorem 3.6 on page 479 of [30]. We will soon discuss this interpretation of the shape derivative as a functional on speed fields in Section 6.2.

Let us give a rough interpretation of this result: Assume that $x \in \Gamma$ and that $F(x) > 0$. This means that propagation of Ω in direction F adds x to the domain. For this situation, the integrand's value at x tells us how J changes when a neighbourhood of x is included into the image segment. (This concept is related to *topological derivatives*, which appear naturally for our example in the shape differential (103). See the discussion later on in Section 7.5.) In particular, the *sign* of the integrand at x tells us whether or not x “should” be included in the segment. This leads to the *inclusion criterion*

$$(u(x) - \bar{u})^2 \left(1 - \frac{\gamma}{\sigma}\right) < \gamma\sigma. \quad (104)$$

In the case $\gamma < \sigma$, this condition is fulfilled if and only if $u(x)$ is “close enough” to the current segment intensity \bar{u} . The right-hand side (proportional to σ) defines the threshold that tells us *how close* that actually is. The larger the variance of pixels in the segment already is, the higher is also the tolerance for adding new pixels. This corresponds to our earlier interpretation of the balloon force generated by the second term in (102). If $\gamma \geq \sigma$, the inclusion criterion (104) is always satisfied. In this case, the balloon force is so strong that the tracking term in (102) can never counterbalance it, no matter in how bad a way the pixel $u(x)$ fits to the current segment.

Note that the criterion (104) really compares the *standard deviation* to the *quadratic* error term $(u(x) - \bar{u})^2$. Intuitively, it would make much more sense to compare the quadratic error to, say, the *variance*. One can also construct cost functionals whose derivatives produce such a criterion. They are, however, less interesting to consider as example models. Furthermore, the draft paper [51] also proposes a pixelwise condition similar to (104) in an ad-hoc way to define a post-processing step. It was found there empirically that the standard deviation gives, indeed, much better results than using the variance in the threshold condition.

6.2 Shape Gradients as Steepest-Descent Directions

As we have just seen, the expression $dJ(\Omega; F)$ from (103) above can be used to compute the directional shape derivative of J in some direction characterised by the speed field F . Taking a closer look, we see that it is actually a *linear* expression in F . If we choose the speed field from a suitable function space \mathcal{H} such that its trace on Γ can be defined, then $dJ(\Omega; \cdot)$ defines a *continuous linear functional* on \mathcal{H} . In other words, it is an element of the *dual space* of \mathcal{H} . This corresponds to the *Jacobian matrix* in a finite-dimensional setting. For a scalar function J , the Jacobian is a *row vector*. The gradient, on the other hand, is a *column vector*. It lives in the *same* space from which also directions are chosen, not the dual space. (Note that some authors do not make this distinction and interpret gradient and Jacobian as the same thing. In contrast, for our discussion both of these objects will be seen as related but not equal. We believe that this makes the underlying structure clearer. See also part (iv) of Remark 2.34 in [52].) However, if \mathcal{H} is a *Hilbert space*, we can use the Riesz representation theorem to associate $dJ(\Omega; \cdot) \in \mathcal{H}'$ to some element $G \in \mathcal{H}$. The Riesz representative G is characterised by the variational equality

$$\langle F, G \rangle = dJ(\Omega; F) \quad (105)$$

which must be satisfied for all $F \in \mathcal{H}$. In the following, we will call this G the *shape gradient*.

Since G is an element of \mathcal{H} itself, we can interpret it as a speed field. This allows us to define a *steepest-descent direction*, namely $-G$. In other words, the conversion from $dJ(\Omega; \cdot)$ to its Riesz representative G provides a natural extension of the derivative functional that is concentrated on Γ onto the full domain Ω . Of course, it is also possible to extend the derivative from the boundary onto the domain in a more ad-hoc fashion. For instance, one can use the integrand in (103) and transfer it onto Ω such that the extension is constant along normal directions. This, roughly, means that we fix the speed field on Γ itself and then move each point on the original boundary with a constant speed for the entire time propagation. (Actually, the movement of boundary points depends on the speed field itself. If it is not constant throughout D , the movement will deviate from the normal direction over time. One could try to apply a self-consistency idea similar to Section 7.1, but this makes the situation even

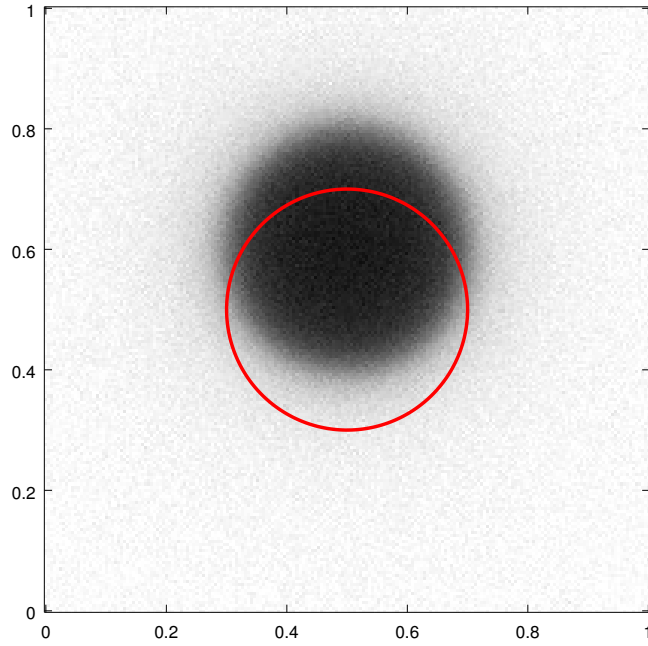


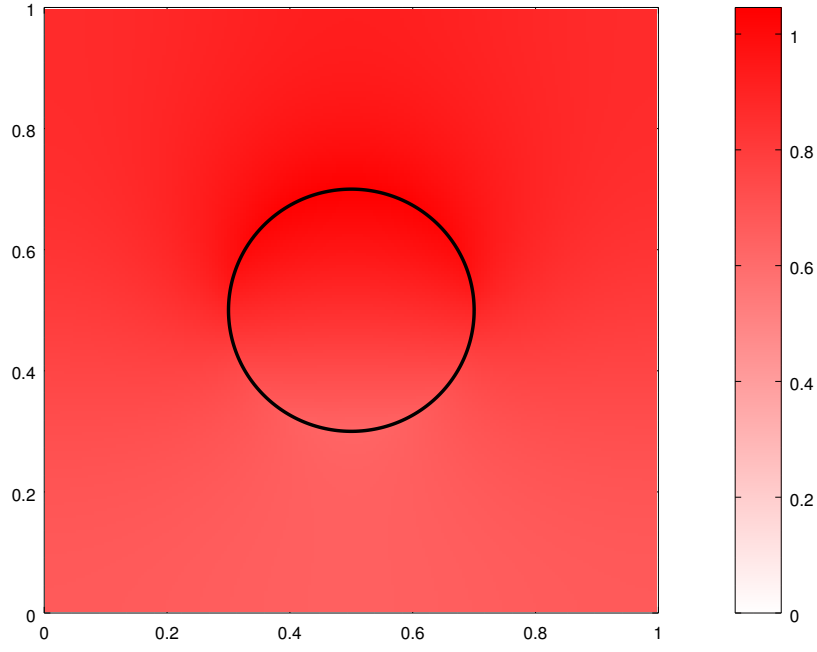
Figure 35: The input image u and current shape Ω_0 used for Figure 36 and Figure 37.

worse.) Our experiments, however, show that an extension like this produces very irregular speed fields (see Figure 37 below). It is much better and more stable to use an appropriate shape gradient to define a descent direction. If \mathcal{H} is a space with high regularity, this has the additional effect that solving (105) for G is strongly smoothing and regularising. This is often beneficial, although a too smooth speed field also carries the risk of not being flexible enough for the required shape changes. Compare Figure 39a and Figure 57a to see the effect of this smoothing property in a practical situation.

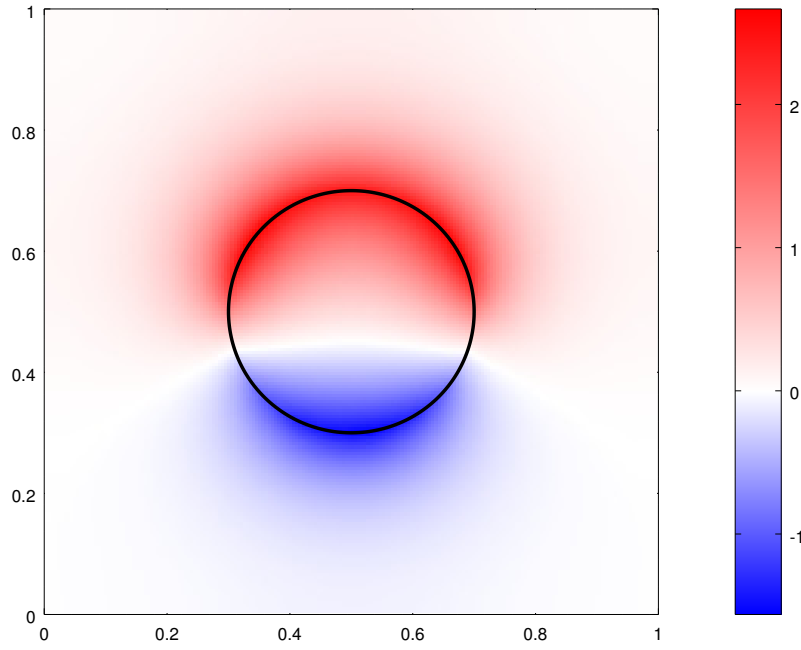
So far, we have not specified what space \mathcal{H} actually is. This choice is important, as it has a large influence on the resulting speed fields. They, in turn, determine the performance of our descent method. Canonical candidates for \mathcal{H} are, of course, the Sobolev spaces $H^k(D) = W^{k,2}(D)$. (See, for instance, Chapter 5 of [36] for a broad introduction into this classical topic of functional analysis.) If $k \geq 2 + \lfloor n/2 \rfloor$, the Sobolev embedding theorem (see Theorem 6 on page 270 of [36]) implies that \mathcal{H} is continuously embedded into $C^1(D)$. Thus, every $F \in \mathcal{H}$ is, in particular, Lipschitz continuous and fits to our theory developed in the previous chapters. Furthermore, since those speeds are then also continuous, the trace on Γ can clearly be defined. This works even without requiring any more regularity of Γ , in contrast to the trace theorem for Sobolev functions. Unfortunately, choosing such a large k usually turns out to be not very practical. It requires higher-order approximations in the numerics and, in particular, smooths the speed fields often too strongly. (See [53] for a comparison of different spaces for the shape gradient in a related setting.) We have seen good numerical results with $\mathcal{H} = H_0^1(D)$, even though this choice is not justified in theory. Choosing $H_0^1(D)$ instead of $H^1(D)$ has the advantage that all speed fields get drawn to zero near the boundary of the hold-all domain. This has the desirable effect that all shape evolutions stay well inside D . Furthermore, one can also introduce an additional weighting factor $\beta > 0$ and use

$$\langle F, G \rangle_\beta = \int_D (FG + \beta \langle \nabla F, \nabla G \rangle) dx \quad (106)$$

instead of the standard inner product on $H_0^1(D)$. By choosing $\beta \ll 1$, one can achieve some smoothing but also allow more variations in the speed field than for $\beta = 1$. This turns out to be beneficial in practice, as we have demonstrated in [58]. We will also discuss the choice of β for practical computations in Section 8.3 later on.



(a) $\beta = 1$



(b) $\beta = 10^{-2}$

Figure 36: The shape gradient G for the situation of Figure 35 computed for $\mathcal{H} = H^1(D)$. We use $\langle \cdot, \cdot \rangle_\beta$ from (106) with different values of β as the inner product.

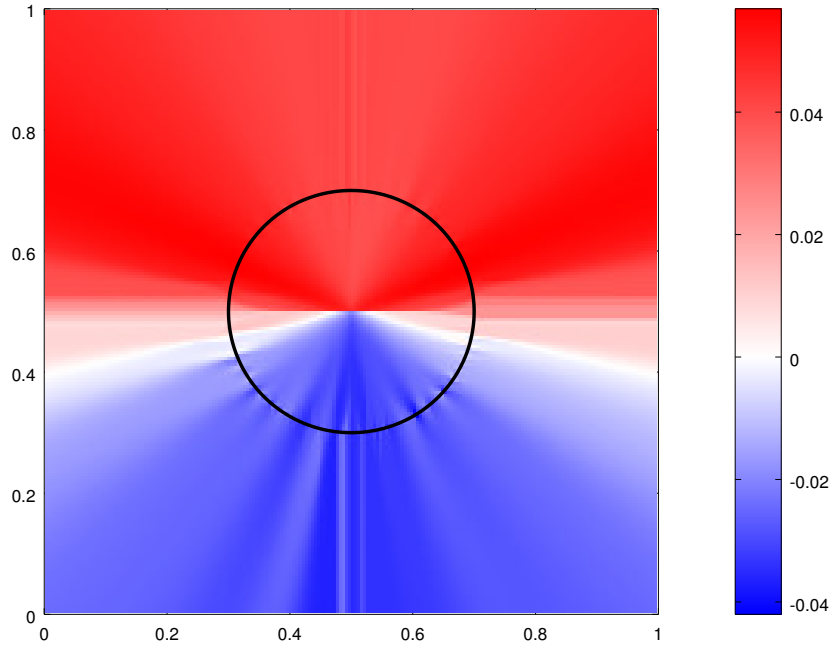


Figure 37: The speed field for the situation of Figure 35 resulting from an extension of the trace functional into the domain along normal directions.

Let us now briefly discuss the effect of various methods to construct a descent speed field with an example. We use our image-segmentation model (102) and look for a descent direction for the situation shown in Figure 35. Since we expect the optimal shape to roughly correspond to the dark circle, the boundary should be pushed outwards (positive speed) on the upper half and inwards (negative speed) on the lower half. Figure 36 shows how the shape gradient G looks like if we use $\mathcal{H} = H^1(D)$ with the inner product defined according to (106). The upper Figure 36a uses $\beta = 1$, i. e., the standard inner product of H^1 . As a result, G is smoothed very strongly. Instead of a negative speed in the lower half, it is only slightly “less positive” there. This is clearly not an optimal direction. In the lower plot Figure 36b, we have used $\beta = 10^{-2}$. This gives enough smoothing to remove any effect of the noise in the original image, but it also allows enough variation to cover the expected sign change in G . This speed field looks like what one expects intuitively. Figure 37, finally, shows the result of extending the functional from the boundary onto the domain along normal directions. This allows for very rapid changes along Γ , which also capture the expected sign change nicely. The resulting speed looks reasonable in the upper half. There, the main contribution of the trace functional is the balloon force and not the actual image data. Since this is smooth and also the normal directions behave nicely (as Ω_0 is just a circle), we get a nice extension. However, in the lower half, where the trace functional is determined mostly by the noisy image data, the extended speed field is quite irregular. If the original shape would be something less smooth than a circle, this would exaggerate the irregularities even more.

6.3 The Gradient-Descent Method

With the steepest-descent directions discussed above in Section 6.2, we can now turn our attention to an actual optimisation method. By evolving the geometry at each step into the corresponding direction and adding a simple line-search procedure, we arrive at a basic *gradient-descent method* for our shape-optimisation problem:

1. Given a current shape Ω_0 , calculate the corresponding shape-dependent quantities. In our case, they are \bar{u} , σ and $\text{vol}(\Omega)$. With these, compute $dJ(\Omega_0; \cdot)$.

2. Solve the variational problem (105) for the shape gradient G . We suggest $\mathcal{H} = H^1(D)$ or alternatively $\mathcal{H} = H_0^1(D)$ with the inner product $\langle \cdot, \cdot \rangle_\beta$ from (106).
3. Evolve Ω_t according to the speed $F = -G$ for some time $t > 0$. This can be done using the methods developed in Chapter 3. The step length t can be chosen with a suitable line-search procedure.
4. Repeat with the new shape Ω_t as Ω_0 until the descent converges.

Methods like this are, of course, classical. See, for instance, Chapter 3 of [65] for a general discussion in the finite-dimensional setting. For our situation, there are some subtle issues to consider: The image u is only given on grid points (the pixels). The level-set function of the current shape Ω_0 , on the other hand, usually allows us to construct the boundary Γ_0 as a polygon *between* the grid points. Thus, one needs to define a suitable interpolation procedure in order to evaluate the shape derivative (103) on Γ_0 . For the computation of the shape gradient with (105), one has to solve the PDE that corresponds to the variational problem. Let us defer a description of our numerical methods to Section 8.2.

For determining the step length t , we employ the well-known Armijo rule (see also Section 3.1 of [65]). In particular, we look for $t > 0$ satisfying

$$J(\Omega_t) \leq J(\Omega_0) + \tau t \cdot dJ(\Omega_0; F) = J(\Omega_0) - \tau t \cdot |dJ(\Omega_0; F)|. \quad (107)$$

Roughly speaking, this condition guarantees *sufficient decrease* of the cost with the current step. The number $\tau \in (0, 1)$ is a parameter that is usually chosen small, e. g., $\tau = 10^{-1}$. With $\tau = 1$, the right-hand side of (107) corresponds to the linearisation of $t \mapsto J(\Omega_t)$. Thus, since $\tau < 1$ is a relaxation of the steepest descent, the condition is fulfilled for small enough t . See also Figure 38a and the discussion in Section 6.4. In order to find a suitable t , usually a *backtracking strategy* is employed: One starts with some initial guess $t_0 > 0$, which can be just a constant or some multiple of the last successful step length. Then, t_0 is repeatedly decreased by a factor $\sigma \in (0, 1)$ until (107) is satisfied. In other words, one sets $t = \sigma^k \cdot t_0$ for the smallest $k \in \mathbb{N}$ that fulfils the condition. If the shape evolution is computed with our Hopf-Lax formula introduced in Chapter 3, note that the Eikonal equations for D only need to be solved *once*. When this is done, it is very easy (and cheap) to compute Ω_t for multiple trial step lengths according to (47). Furthermore, also the computation of $J(\Omega_t)$ can be carried out independently for different values of t . This allows us to try out multiple values of t in parallel for a further speed-up and, hence, take advantage of the multiple processing cores that are readily available with modern computers.

6.4 Line Search with Wolfe Conditions

Let us now take a closer look at the line search that is employed in a typical gradient-descent method similar to the one described above in Section 6.3. In particular, it is, of course, interesting to consider two questions: First, whether it can be guaranteed that a step length that satisfies the imposed conditions can be found. Second, whether the line search provably leads to convergence of the gradient descent to a critical point. It turns out that while it is easy to find step lengths that satisfy the Armijo rule (107) with a backtracking strategy, this may lead to steps that are too short and do not guarantee convergence to a critical point. Thus, we have to introduce an additional condition: For $\sigma \in (\tau, 1)$, look for a step length t that satisfies

$$|dJ(\Omega_t; F)| \leq \sigma |dJ(\Omega_0; F)| \quad (108)$$

in addition to the Armijo rule (107). The condition (108) is called *strong curvature condition*. Both conditions together are the (strong) *Wolfe conditions*. They are well-known and widely studied in optimisation theory, starting with the seminal paper [84] by Wolfe. The Armijo rule (107) guarantees sufficient decrease of the cost, while the curvature condition (108) ensures decrease in the directional derivative. If the derivative is uniformly continuous, this implies also a certain minimum decrease of the *full gradient* and leads to convergence to a critical point.

Our goal for the current section is to analyse the Wolfe conditions in the context of our shape-optimisation framework. This creates, of course, many additional difficulties. Motivated by our shape calculus of Section 4.2 and the image-segmentation example, let us consider a problem of the form

$$dJ(\Omega_t; F) = \int_{\Gamma_t} F f(x, \Omega_t) d\sigma, \quad J(\Omega_t) = J(\Omega_0) + \int_0^t dJ(\Omega_s; F) ds. \quad (109)$$

The integrand f is allowed to depend on the current shape Ω_t . Note, however, that the line search is applied only after a descent direction has been constructed. Thus, we can assume that a speed field F corresponding to the considered direction is fixed. Consequently, we can write $f(x, t) = f(x, \Omega_t)$ to make the integrand *time dependent instead of shape dependent*. We also need the following property:

Assumption 2. Let Ω_0 be bounded and $P(\Omega_0) < \infty$. We assume, furthermore, that $(x, t) \mapsto F(x)f(x, t)$ is continuous and strictly negative on $\Gamma_0 \times \{0\}$.

Note that this assumption (particularly continuity of f) is usually not satisfied for the image-segmentation problem because the image u is not required to be continuous. Furthermore, a speed field constructed as a negative shape gradient needs not necessarily satisfy $Ff < 0$ *everywhere* on Γ . This can be seen, for instance, in Figure 36. Nevertheless, this assumption usually seems to be satisfied at least approximately in practice. Especially if the speed field is constructed based on the idea in Chapter 7, this is not a problem at all; a self-consistent gradient flow as per Definition 24 has $Ff < 0$ automatically by (119). In this situation, the arguments of Subsection 7.2.3 can be used to also show continuity, so that Assumption 2 holds.

Unfortunately, we do not know whether $t \mapsto dJ(\Omega_t; F)$ is continuous. (This was discussed thoroughly in Chapter 5.) The standard proof for the existence of step lengths that satisfy the Armijo rule relies on *continuous* differentiability. On a closer look, however, it turns out that *semi-continuity* is enough. This is something that we can show relatively easily for our shape derivative:

Lemma 63. *Let Assumption 2 hold. Then $t \mapsto dJ(\Omega_t; F)$ is upper semi-continuous in zero, i. e.,*

$$dJ(\Omega_0; F) \geq \limsup_{t \rightarrow 0^+} dJ(\Omega_t; F).$$

Proof. For ease of notation, let us write $g(x, t) = F(x)f(x, t)$. Then g is continuous and $g(x, 0) < 0$ for all $x \in \Gamma_0$. Let us first consider $t \mapsto P(\Omega_t) = \int_{\Gamma_t} d\sigma$. Since Corollary 9 implies that $\Omega_t \rightarrow \Omega_0$ in measure as $t \rightarrow 0^+$, standard results imply lower semi-continuity of this function. See, for instance, Remark 3.5 on page 119 of [4]. We will now exploit continuity of g to generalise this result to $t \mapsto dJ(\Omega_t; F) = \int_{\Gamma_t} g d\sigma$.

For this, let $\epsilon > 0$ be arbitrary and define

$$U_\epsilon = V_\epsilon(\Gamma_0) = \{x \in \mathbb{R}^n \mid \text{sd}_{\Gamma_0}(x) < \epsilon\}$$

as the ϵ -envelope of Γ_0 (recall (100)). Note that Γ_0 and thus also $\overline{U_\epsilon}$ are compact. This implies that g is *uniformly* continuous on $U_\epsilon \times [0, T]$ for all fixed $T > 0$. Hence, we can choose $\delta > 0$ such that $|g(x, t) - g(y, s)| < \epsilon$ for all $x, y \in U_\epsilon$ with $|x - y| < \delta$ and $s, t \in [0, \delta]$. By compactness of $\overline{U_\epsilon}$, there exists a finite set $X \subset U_\epsilon$ such that

$$U_\epsilon \subset \bigcup_{x \in X} B_{\delta/2}(x).$$

Let us assume, furthermore, that this finite cover is made disjoint. This means that there are $N \in \mathbb{N}$ and $A_k \subset U_\epsilon$, $k = 1, \dots, N$, such that all A_k are pairwise disjoint and still $U_\epsilon = \bigcup_{k=1}^N A_k$ holds. If we construct the A_k in such a way that their diameter remains smaller than δ , we know $|g(x, t) - g(y, s)| < \epsilon$ for all $x, y \in A_k$, $k = 1, \dots, N$, and $s, t \in [0, \delta]$. Note also that $\Gamma_t \subset U_\epsilon$ if t is small enough, which follows from Lemma 44.

Define now $g_k = \sup\{g(x, t) \mid x \in A_k, t \in [0, \delta]\}$ and note that $g_k - \epsilon \leq g(x, t) \leq g_k$ holds for all $x \in A_k$, $k = 1, \dots, N$, and for all $t \in [0, \delta]$. Since $g(\cdot, 0) < 0$ on the compact set Γ_0 , we can assume that ϵ is small enough to give $0 < \epsilon < \inf_{x \in \Gamma_0} |g(x, 0)|$ and, consequently, $g_k < 0$. Thus, we can apply lower semi-continuity of the variation measure to derive

$$\begin{aligned} \int_{\Gamma_0 \cap A_k} g d\sigma &= \int_{\Gamma_0 \cap A_k} (g - g_k) d\sigma + g_k \int_{\Gamma_0 \cap A_k} d\sigma \geq \int_{\Gamma_0 \cap A_k} (g - g_k) d\sigma + g_k \cdot \liminf_{t \rightarrow 0^+} \int_{\Gamma_t \cap A_k} d\sigma \\ &= \int_{\Gamma_0 \cap A_k} (g - g_k) d\sigma + \limsup_{t \rightarrow 0^+} \int_{\Gamma_t \cap A_k} g_k d\sigma \geq -\epsilon \int_{\Gamma_0 \cap A_k} d\sigma + \limsup_{t \rightarrow 0^+} \int_{\Gamma_t \cap A_k} g d\sigma \end{aligned}$$

for all $k = 1, \dots, N$. Summing up over all disjoint A_k , this means

$$\int_{\Gamma_0} g d\sigma \geq \limsup_{t \rightarrow 0^+} \int_{\Gamma_t} g d\sigma - \epsilon \cdot P(\Omega_0).$$

Since $P(\Omega_0)$ is finite by assumption and ϵ arbitrary, this implies the claim. \square

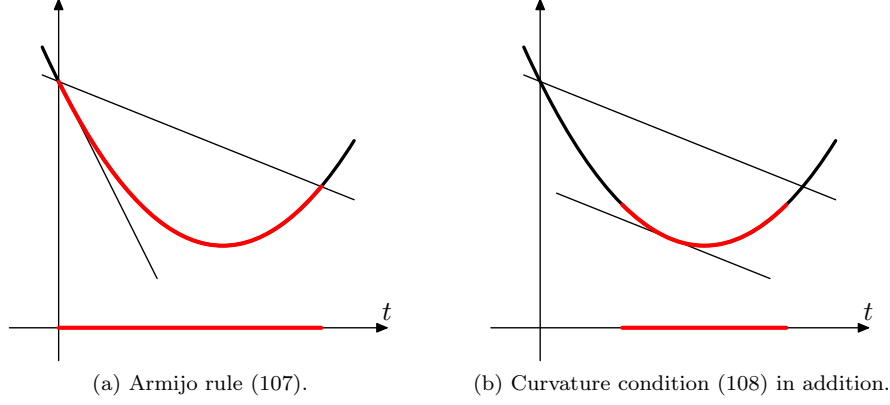


Figure 38: Existence of steps that satisfy the Wolfe conditions. The slope relaxed by τ is shown. Steps that satisfy the conditions are highlighted. See Theorem 23.

Based on this continuity result, we can now show that there are, indeed, always admissible step lengths that satisfy the Wolfe conditions. Our argument follows the standard one, as it is outlined already in the proof of Lemma 2 in [84]. The main idea is depicted in Figure 38: Due to the parameter $\tau \in (0, 1)$, the slope of $J(\Omega_t)$ at $t = 0$ gets relaxed as shown in Figure 38a. Assuming continuity of the derivative for a moment, this implies that all sufficiently small step lengths fulfil (107) as shown in red. Let us now require the curvature condition (108) in addition. If J is bounded from below, we can use the mean-value theorem to find a tangent to $J(\Omega_t)$ with the *relaxed* slope $\tau \cdot dJ(\Omega_0; F)$. This is illustrated in Figure 38b. Since $\sigma > \tau$ is a weaker relaxation, we can conclude that (108) holds at least in a neighbourhood around this point. With the help of Lemma 63, we can now carry out this argument rigorously for our situation:

Theorem 23. *Let Assumption 2 hold. There exists $t_0 > 0$ such that (107) is fulfilled for all $t \in (0, t_0)$. If J is, furthermore, bounded from below, then there exists $t \in (0, t_0)$ such that (108) holds in addition.*

Proof. Since $Ff < 0$ on Γ_0 by assumption, we know, in particular, $dJ(\Omega_0; F) < 0$. Let us define

$$\epsilon = (1 - \tau) |dJ(\Omega_0; F)| = -(1 - \tau) \cdot dJ(\Omega_0; F) > 0.$$

Due to Lemma 63, there exists $t_0 > 0$ such that

$$dJ(\Omega_0; F) \geq \limsup_{s \rightarrow 0^+} dJ(\Omega_s; F) \geq dJ(\Omega_t; F) - \epsilon$$

for all $t \in (0, t_0)$. Integrating this inequality over the interval $(0, t)$ yields

$$t \cdot dJ(\Omega_0; F) \geq \int_0^t dJ(\Omega_s; F) ds - \epsilon t = J(\Omega_t) - J(\Omega_0) - \epsilon t.$$

This, in turn, implies (107) since

$$J(\Omega_t) \leq J(\Omega_0) + t(dJ(\Omega_0; F) + \epsilon) = J(\Omega_0) + \tau t \cdot dJ(\Omega_0; F).$$

Assume now that J is bounded. Together with $dJ(\Omega_0; F) < 0$, this implies that there exists $T > 0$ such that the Armijo rule (107) does *not* hold for T . Also note that $t \mapsto J(\Omega_t)$ is absolutely continuous. By the intermediate-value theorem, there must be some $t \in [t_0, T]$ such that equality holds in (107), i. e.,

$$J(\Omega_t) = J(\Omega_0) + \tau t \cdot dJ(\Omega_0; F).$$

Without loss of generality, we can choose the *smallest* such value. This ensures that the Armijo rule holds for all $s \in (0, t)$. Using (109) again, we can conclude

$$0 > \frac{1}{t} \int_0^t dJ(\Omega_s; F) ds = \tau \cdot dJ(\Omega_0; F) > \sigma \cdot dJ(\Omega_0; F).$$

Thus, there are at least some $s \in (0, t)$ with $dJ(\Omega_s; F) \geq \sigma \cdot dJ(\Omega_0; F)$. This finishes the proof. \square

Let us now come back to the question about convergence to a critical point. As we have seen in Theorem 23, there are always steps that satisfy the Wolfe conditions. If we assume, as before, that J is bounded from below, the Armijo rule implies that at least one of the step length and the gradient have to go to zero during the descent iteration. Since the gradient vanishing is exactly what we want, let us assume, instead, that the step length t becomes small. At this point, let us recall two important facts: First, the curvature condition (108) implies that the *directional derivative* in the fixed descent direction is reduced at least by a constant factor during each step. Second, if we use the negative gradient as direction, the directional derivative $dJ(\Omega_0; F)$ at the initial geometry corresponds directly to the norm of the gradient. The standard argument (see, for instance, Theorem 1 in [84]) continues like this: *Assume uniform continuity of the derivative, which implies*

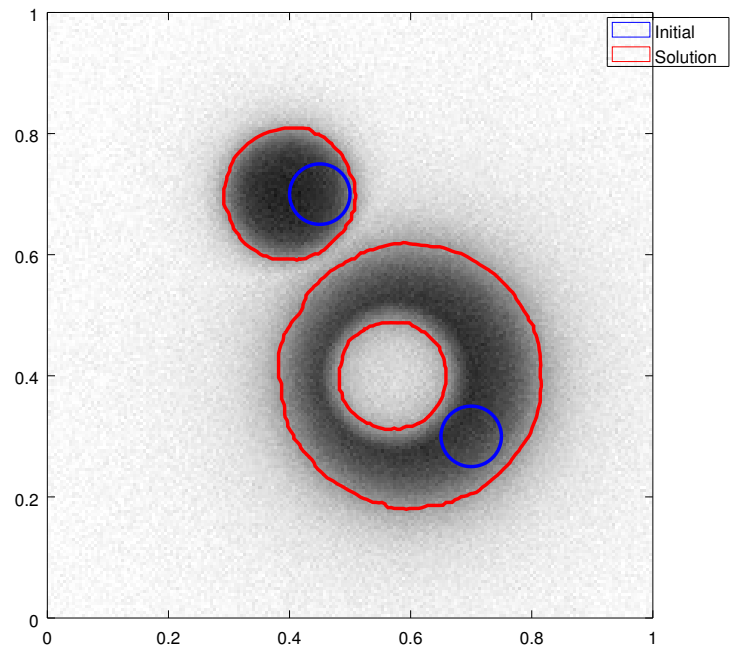
$$t \rightarrow 0^+ \Rightarrow dJ(\Omega_t; F) \rightarrow dJ(\Omega_0; F). \quad (110)$$

Then, since $dJ(\Omega_t; F) \approx dJ(\Omega_0; F)$ and $|dJ(\Omega_t; F)| \leq \sigma |dJ(\Omega_0; F)|$, we get convergence of $dJ(\Omega_0; F)$ to zero as $t \rightarrow 0^+$ during the iteration. This, in turn, implies convergence to a critical point. Unfortunately, it is not clear whether this approach can be applied in our situation. In principle, upper semi-continuity of the derivative as per Lemma 63 is all that we need to apply this argument. Full continuity per (110) is not necessary. However, we need semi-continuity to be *uniform for all steps*. This is not guaranteed by our proof for Lemma 63, which assumes a fixed geometry and speed field. Later on in Section 7.4, we will discuss an alternative approach that may allow us to circumvent this issue.

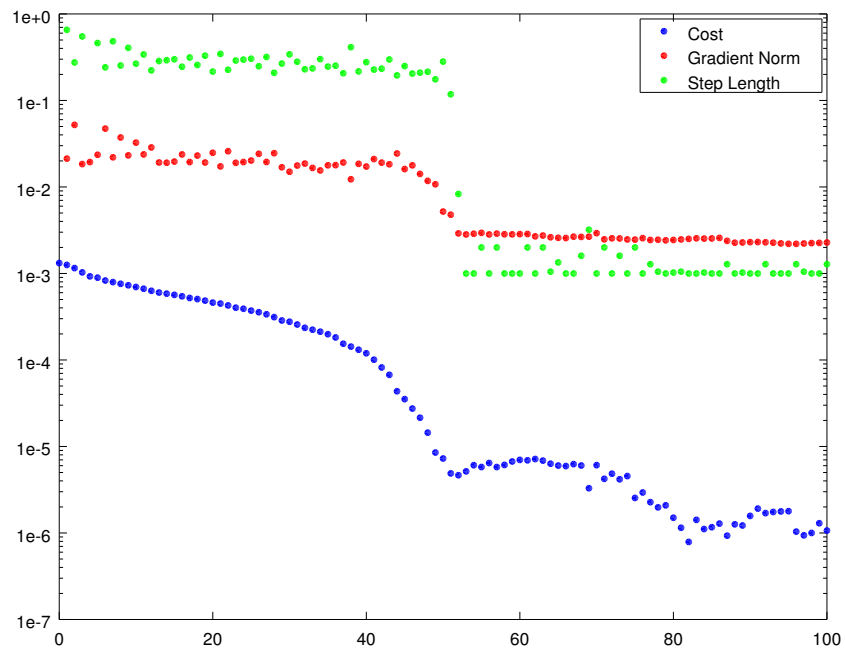
6.5 Numerical Examples for the Gradient-Descent Method

A numerical example of the gradient-descent method applied to our image-segmentation model is shown in Figure 39. Note that we use only the Armijo rule for the line search as described in Section 6.3, not the Wolfe conditions discussed above in Section 6.4. This works well in practice. The input image is artificially created and has noise added. It is plotted together with the initial (blue curve) and final (red) shapes in Figure 39a. Note that a change in topology happens when the segment forms the ring. This does not disturb the method at all. Figure 39b shows how the cost and gradient norm (blue and red) decrease with the descent iterations. The cost is relative to an “exact” value that was computed for the same noisy image by using the gradient descent starting from an “informed guess” for the initial shape. In particular, the initial segment was chosen as the shape used when generating the image itself. The gradient norm is the H^1 -norm of the shape gradient as discussed in Section 6.2. The green dots show the accepted step length t satisfying the Armijo rule (107) at each iteration. We enforce a minimum step length of $t_{\min} = 10^{-3}$. Around iteration 50, this limit becomes active since the final shape is already attained and the cost and gradient norm no longer decrease significantly. A very similar result can also be seen in Figure 40, where a different image is segmented. Here again, the topology is changed and a hole forms. Note, though, that this usually does not happen when the dark centre is part of the initial shape. In the latter situation, the full disc is returned as the segment. This, however, is mostly a characteristic of the underlying model and the concrete problem at hand. Both configurations are local minima, with the one found in Figure 40a having a lower cost. It is also the more plausible segmentation considering that our model tries to identify a segment with constant intensity.

However, the same gradient-descent method does not work very well for images with *sharp edges*. See, for instance, the situation shown in Figure 41. Even though many more steps have been performed than for the previous examples, the descent gets stuck very quickly and hits the step-size limit at $t = t_{\min}$ without actually reaching the final solution. The lower line of green dots in Figure 41b is t_{\min} , as before. The second line above it is at $2t_{\min}$, which is the first step size tried after a step with t_{\min} has been taken. In many iterations, the enforced step length makes the situation worse, so that the following step is immediately accepted and “corrects” this again. This leads to these distinct *two* lines of green dots. In order to understand why the gradient descent performs so poorly with sharp edges, it is useful to consider the shape gradients that occur when the descent is stuck. The speed fields computed for two consecutive iterations are shown in Figure 42. If one looks at even more consecutive steps, one finds that the whole iteration sequence is a back-and-forth between situations similar to these two. In particular, where the current shape is already at the image’s edge, the shape is repeatedly moved over the edge and back. This can be seen clearly in the figure: The speed is negative (blue) in all these regions in Figure 42a and positive (red) in Figure 42b. The front is only moved consistently forward where it is

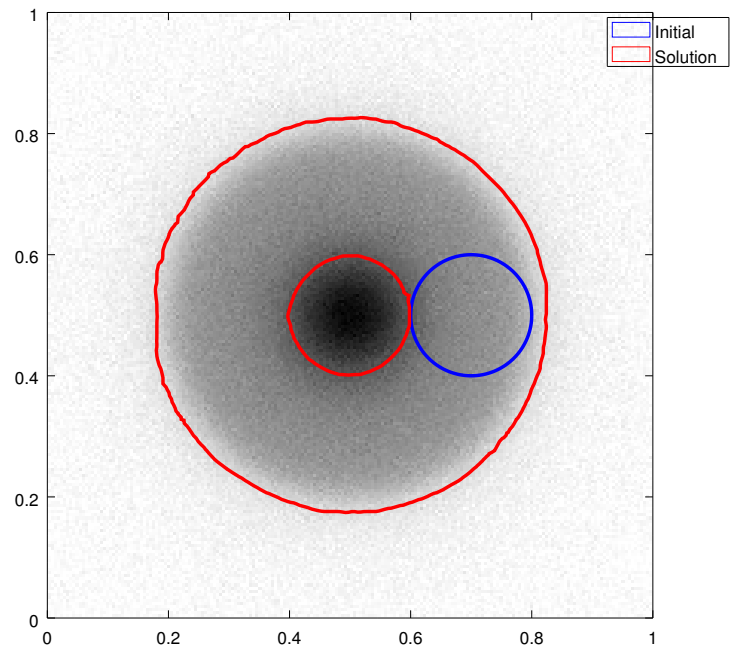


(a) Initial (blue) and resulting (red) shapes on top of the segmented image.

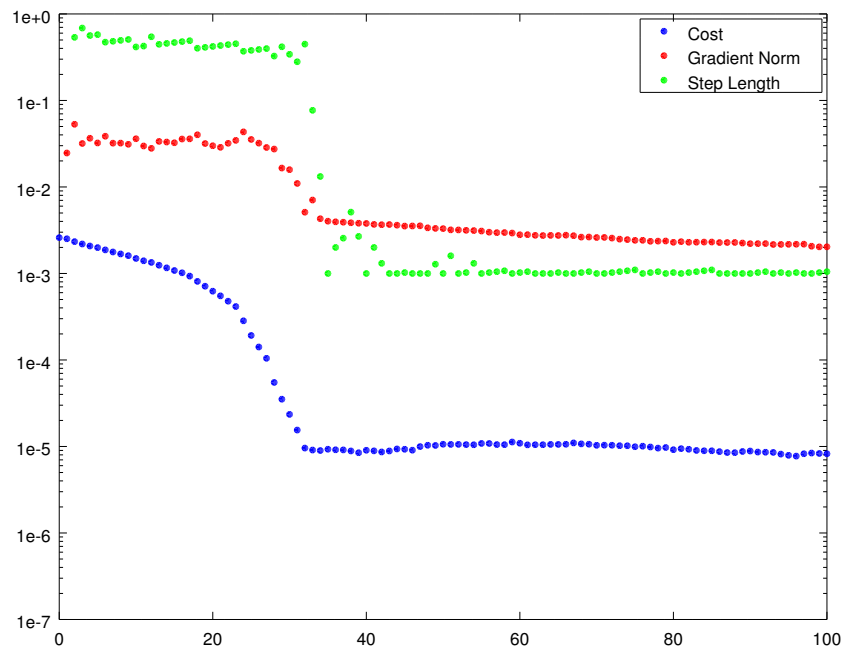


(b) Evolution of the cost (blue), gradient norm (red) and line-search step length (green).

Figure 39: Gradient descent for image segmentation.



(a)



(b)

Figure 40: Continuation of Figure 39 with a different image.

still in the process of closing around the hole. A consequence of this behaviour is that each step is forced to be very short by the line search, so that the descent is not able to progress any further.

In fact, this kind of *zig-zag movement* is a general “feature” of gradient-descent methods. A possible solution for this problem is the use of *second-order methods*. In our particular situation, we would like to weight the speed such that it is decreased accordingly at image edges. This is precisely what a Newton-type method would do, since the Hessian would, roughly speaking, consist of the normal derivatives of the image data. This means that the gradient would be divided by a large value where the shape is close to an edge and by a small value elsewhere. The drawback of such a method, however, is that derivatives of the image data are required. For a noisy image, they are not easy to evaluate in a robust way. Because of this, we propose an alternative idea to improve the gradient descent in Chapter 7.

6.6 Geometric Constraints

Many applications for shape optimisation are based on a practical problem where the desired shape cannot be chosen entirely freely. In such situations, it may be necessary to impose *geometric constraints* on the admissible shapes. A problem with this characteristic has been tackled recently with the help of penalisation in [54]. Our discussion of regularisation with the boundary length in Chapter 8 is related as well, since it enforces a certain smoothness of the boundary. In this section, we want to discuss ways to enforce constraints directly, resulting in *feasible* gradient-descent methods. For this, let us consider *forbidden regions*, i. e., for some $B \subset D$, we require that $\Omega \cap B = \emptyset$. It is straight-forward to modify our results to constraints of the form $B \subset \Omega$ instead. See [53] for a practical problem that gives rise to both types of constraints in a natural way. Section 5 of the paper also briefly discusses methods to deal with the constraints, as does Section 2.13 of [52]. Below, we want to expand this discussion and give more details, particularly about the underlying theoretical considerations.

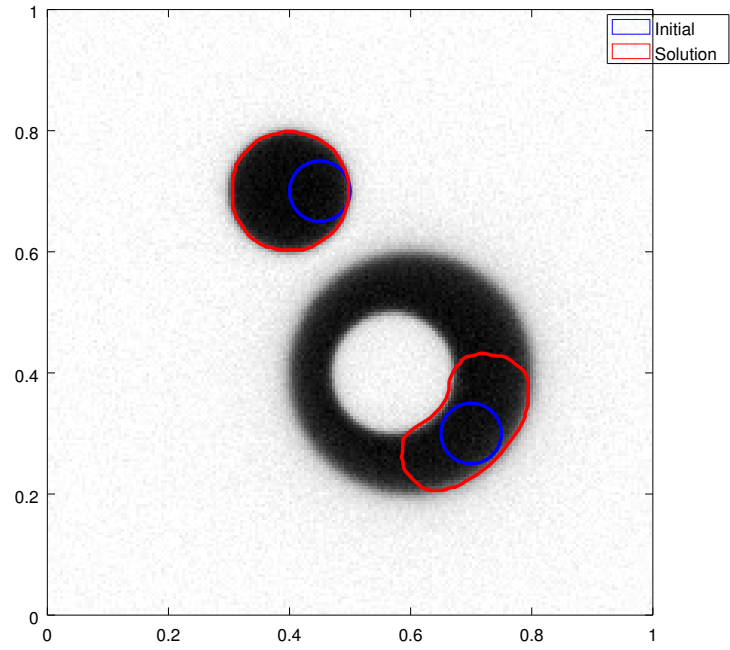
When dealing with constrained shape-optimisation problems, there are, in general, two basic strategies to ensure that the gradient descent stays feasible: One can either modify the shape after each step to satisfy the constraints, or one can adapt the speed field before a step to ensure that it only leads to feasible evolved shapes. The former approach is usually called *projected-gradient method* (see, for instance, Algorithm 2.3 on page 105 of [47]). In the context of shapes, however, there is no canonical way to “project” them to ensure feasibility. (It is, nevertheless, possible to define a “reasonable” shape projection. This will be done in Subsection 6.6.1.) Thus, it also makes sense to consider the second idea: Based on Corollary 5, it is clear that requiring $F = 0$ on B ensures that $B \cap \Omega_t$ is stationary throughout the time evolution. In other words, feasible initial shapes always lead to evolved shapes that also satisfy the constraints. A similar idea of projecting the speed field was already used in [66], although for different types of shape constraints and without any deeper analysis. In our case, we want to ensure that the speed field vanishes on the forbidden region. To do so, there are, again, two possible strategies we want to discuss: The most natural way is to project the speed field in the same Hilbert space \mathcal{H} that is also used for the computation of the shape gradient with (105). This is done in [53], based, in particular, on Theorem 3 there. Projection in \mathcal{H} ensures that the constraints are incorporated into the descent method in a consistent way. It also has the feature that the speed field *gets drawn to zero continuously* towards the forbidden region. While this leads to better regularity properties, it also has a potential drawback: Due to Lemma 17, it enforces small movements of the boundary close to the forbidden region. In particular, the boundary will never fully reach B , leading to a kind of “interior-point method”. Once the boundary gets close to B , it also takes a relatively long time to get away again. Thus, let us also consider cutting off the speed in a way that avoids these potential issues:

$$F^p(x) = \begin{cases} 0 & \text{if } x \in B \text{ and } F(x) > 0, \\ F(x) & \text{else} \end{cases} \quad (111)$$

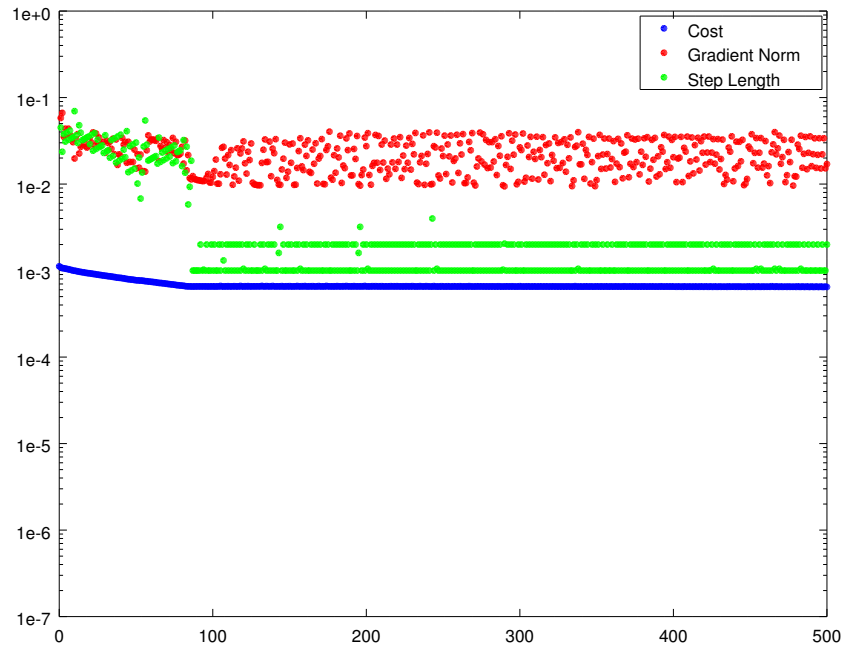
The speed field F^p can be seen as projection in L^2 instead of the Hilbert space \mathcal{H} with higher regularity. The particular form of (111), however, also ensures that we force the speed to zero *only when growing towards B* . On the other hand, a negative speed is allowed inside of B . This ensures that the evolving boundary of Ω is able to get away again after touching B . This projection is implemented (for more general shape constraints) as `ls_enforce_speed` in [59].

To summarise, we have identified three methods to handle shape constraints in our descent method:

- Projection of the speed in \mathcal{H} , resulting in a continuous speed field,

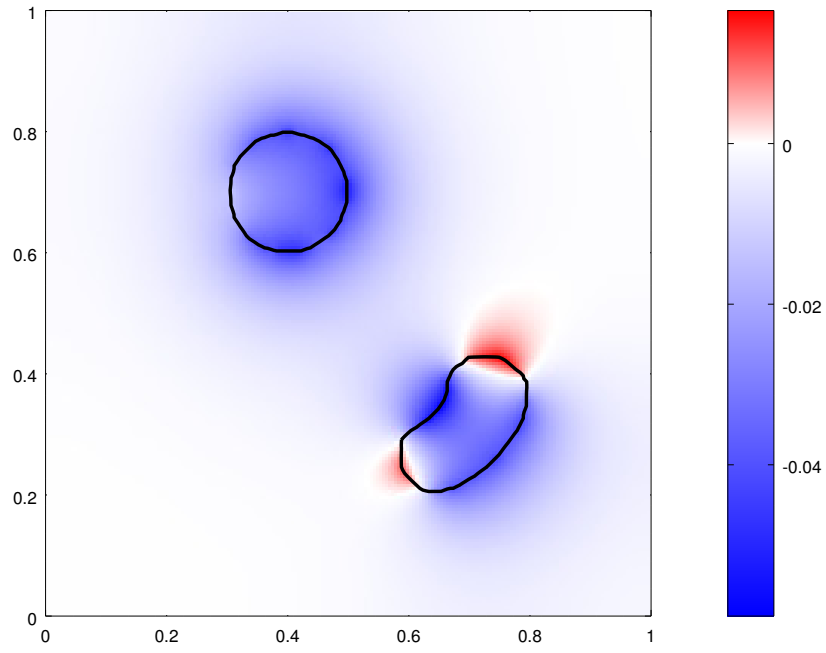


(a)

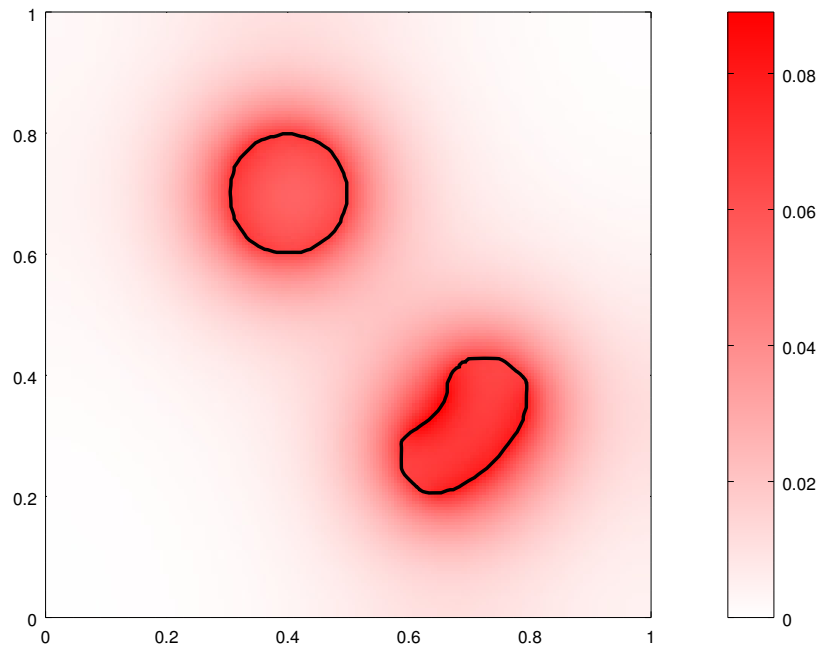


(b)

Figure 41: Continuation of Figure 39 for an image with sharper edges. Here, much more steps would be required to find the actual solution. Note that the number of steps shown is already five times the number used in Figure 39 and Figure 40.



(a) Iteration 400



(b) Iteration 401

Figure 42: Speed fields at two consecutive iteration steps in the stuck descent of Figure 41. The current shape is plotted with the black line.

- projection of the speed in L^2 according to (111), resulting in a *discontinuous* speed field F^p , and
- projection of the shape after evolving it.

We will see in Subsection 6.6.2 and, in particular, Theorem 24, that the last two strategies lead to very similar results under certain regularity assumptions on B . Subsection 6.6.3 compares all three methods to each other in numerical experiments. Let us, however, stress once again that the most consistent method with respect to the gradient descent is the speed projection in \mathcal{H} . It is the only strategy that ensures that we end up with a descent in every step. The other methods tamper with the speed field and geometry in a way that invalidates the directional derivative computed from (105), which may lead to problems with the line search and descent in general. This effect will be seen in the numerics, but we will also see that the other two methods have their justification as well in certain circumstances.

6.6.1 Shape Projections

Assume now that $\Omega \subset D$ is some open domain, but that the constraint $\Omega \cap B = \emptyset$ is not fulfilled. The straight-forward way to fix this is, of course, to define the *shape projection*

$$\pi(\Omega) = \Omega \setminus B. \quad (112)$$

If we assume B to be closed, then $\pi(\Omega)$ is again an open domain. However, the usual, more systematic approach to define projections (in general) is to consider a minimisation of the form

$$\min_{\Omega'} d^s(\Omega, \Omega'), \quad (113)$$

where $d^s(\cdot, \cdot)$ is some kind of distance measure and Ω' runs through all admissible shapes, i. e., all open sets $\Omega' \subset D$ with $\Omega' \cap B = \emptyset$. Let us consider (113) now with respect to both metrics for shapes introduced in Section 4.5. The distance in measure (recall Definition 14) is easy to do:

Lemma 64. *The set $\pi(\Omega)$ from (112) is, up to changes of measure zero, the unique minimiser of (113) if $d^s(\cdot, \cdot)$ is the distance in measure. Consequently, it is also the unique minimiser among open sets.*

Proof. Let Ω' be feasible, i. e., $\Omega' \cap B = \emptyset$. Then necessarily

$$\Omega \cap B \subset \Omega \Delta \Omega',$$

so that also

$$\text{vol}(\Omega \Delta \Omega') \geq \text{vol}(\Omega \cap B) = \text{vol}(\Omega \Delta \pi(\Omega)).$$

Hence, $\pi(\Omega)$ is indeed a minimiser of (113).

To show uniqueness, assume now that Ω' is also a minimiser of (113), which means

$$\text{vol}(\Omega \Delta \Omega') = \text{vol}(\Omega \cap B) = \text{vol}(\Omega \Delta \pi(\Omega)). \quad (114)$$

Note that the disjoint decomposition

$$\Omega \Delta \Omega' = (\Omega \cap B) \cup (\Omega' \setminus \Omega) \cup (\Omega \setminus (\Omega' \cup B))$$

holds. Taking the measure and observing (114) implies

$$\text{vol}(\Omega' \setminus \Omega) = \text{vol}(\Omega \setminus (\Omega' \cup B)) = 0.$$

Since by (112) also

$$\text{vol}(\Omega' \Delta \pi(\Omega)) = \text{vol}(\Omega' \setminus (\Omega \setminus B)) + \text{vol}((\Omega \setminus B) \setminus \Omega') = \text{vol}(\Omega' \setminus \Omega) + \text{vol}(\Omega \setminus (\Omega' \cup B))$$

holds, this implies $\text{vol}(\Omega' \Delta \pi(\Omega)) = 0$ and thus we get uniqueness up to changes of measure zero. \square

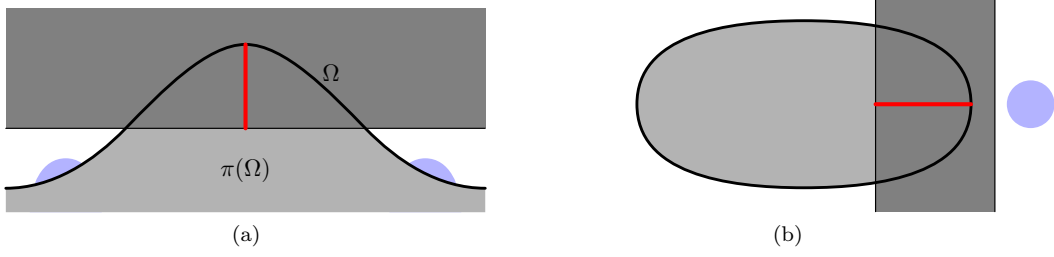


Figure 43: Shape projection according to (113) with $d^s(\cdot, \cdot)$ chosen as the Hausdorff distance. The dark strip is the forbidden region B , the light grey area the projected shape $\pi(\Omega)$ of (112). The red line indicates $d_H(\Omega \rightarrow \pi(\Omega))$.

Let us now consider the Hausdorff distance (see Definition 12) in (113) instead. This makes things more complicated. First, we can immediately observe that uniqueness does not hold in general for a minimiser of (113) with respect to the Hausdorff distance. It is possible to add arbitrary disturbances to any minimiser, as long as they are smaller in amplitude than the Hausdorff distance to Ω . This is illustrated with the blue parts in Figure 43a. Second, the minimiser of (113) may not be a subset of Ω . Adding the blue part in Figure 43b actually *reduces* the Hausdorff distance with respect to using $\pi(\Omega)$ alone (the light grey area). However, it makes, of course, sense to require that the projected shape should be a subset of Ω if we only want to *forbid* certain regions. Thus, let us make the following assumption:

Assumption 3. Let B be bounded. Since ∂B is compact, for arbitrary $x \in \Omega \cap B$ there exists $y_x \in \partial B$ as minimiser of the distance, i. e., such that

$$|x - y_x| = \text{dist}(x, \partial B) = \inf_{y \in \partial B} |x - y|. \quad (115)$$

We assume that $y_x \in \Omega^\circ$ for all $x \in \Omega \cap B$.

This assumption excludes a situation like Figure 43b. On the other hand, it is usually satisfied if Ω is produced from some feasible initial shape Ω_0 by slightly moving its boundary. It allows us to show that $\pi(\Omega)$ is also a minimiser of (113) for the Hausdorff distance:

Lemma 65. *Let Assumption 3 hold or restrict the considered Ω' in (113) to subsets of Ω . Assume that $\Omega \setminus B$ is not empty. Then $\pi(\Omega)$ is a minimiser of (113) with respect to the Hausdorff distance $d_H(\cdot, \cdot)$.*

Proof. If $\Omega \cap B = \emptyset$ already, then $\pi(\Omega) = \Omega$ and $d_H(\Omega, \pi(\Omega)) = 0$. In this case, the result is clear. Thus assume $\Omega \cap B \neq \emptyset$. Since $\pi(\Omega) \subset \Omega$, we know that $d_H(\pi(\Omega) \rightarrow \Omega) = 0$. On the other hand,

$$d_H(\Omega, \pi(\Omega)) = d_H(\Omega \rightarrow \pi(\Omega)) = \sup_{x \in \Omega} \inf_{y \in \pi(\Omega)} |x - y| = \sup_{x \in \Omega \cap B} \inf_{y \in \Omega \setminus B} |x - y|.$$

Now assume that Ω' is admissible in (113), i. e., $\Omega' \cap B = \emptyset$. Again, we get

$$d_H(\Omega, \Omega') \geq d_H(\Omega \rightarrow \Omega') = \sup_{x \in \Omega} \inf_{y \in \Omega'} |x - y| \geq \sup_{x \in \Omega \cap B} \inf_{y \in \Omega'} |x - y|.$$

If now $\Omega' \subset \Omega$, then also $\Omega' \subset \Omega \setminus B$. Thus

$$d_H(\Omega, \Omega') \geq \sup_{x \in \Omega \cap B} \inf_{y \in \Omega'} |x - y| \geq \sup_{x \in \Omega \cap B} \inf_{y \in \Omega \setminus B} |x - y| = d_H(\Omega, \pi(\Omega)).$$

This finishes the proof for this case. So let Assumption 3 hold and note that

$$\sup_{x \in \Omega \cap B} \inf_{y \in \Omega'} |x - y| \geq \sup_{x \in \Omega \cap B} \min_{y \in \partial B} |x - y|$$

must be true since $\Omega' \subset \mathbb{R}^n \setminus B$. Let $x \in \Omega \cap B$ be arbitrary. By the assumption, there exists $y_x \in \partial B$ such that (115) holds. Since $y_x \in \Omega^\circ$, there exists a sequence $(y_k)_{k \in \mathbb{N}} \subset \Omega \setminus B$ converging to y_x as $k \rightarrow \infty$. This sequence also realises the minimum in the limit since the Euclidean distance is continuous. Hence

$$\min_{y \in \partial B} |x - y| = |x - y_x| = \lim_{k \rightarrow \infty} |x - y_k| \geq \inf_{y \in \Omega \setminus B} |x - y|.$$

This inequality remains intact if we take the supremum over all $x \in \Omega \cap B$, yielding the desired

$$d_H(\Omega, \Omega') \geq \sup_{x \in \Omega \cap B} \min_{y \in \partial B} |x - y| \geq \sup_{x \in \Omega \cap B} \inf_{y \in \Omega \setminus B} |x - y| = d_H(\Omega, \pi(\Omega)).$$

□

Initially, we defined the projection (112) mainly based on intuition. With Lemma 64 and Lemma 65, we are now able to justify it based on the abstract shape projection (113):

Corollary 15. *Let Assumption 3 hold and let $\Omega \setminus B \neq \emptyset$. Then the shape projection $\pi(\Omega)$ from (112) is the unique open set that minimises (113) for the distance in measure. It is, at the same time, a minimiser for the Hausdorff distance.*

6.6.2 The Relation between Shape and Speed Projections

Following up on Subsection 6.6.1, let us now compare the result of a shape projection with (112) to a projection of the speed field in L^2 according to (111). Both methods are in contrast to a speed projection in \mathcal{H} , since they allow (and somewhat “encourage”) the constraint to become fully active. For simplicity, let us assume $F \geq 0$ here. This is the interesting case for forbidden regions. Let us denote the evolved shape according to the projected speed F^p by Ω_t^p , where $t \geq 0$ is, as usual, the propagation time. Since $F^p \leq F$, it is clear by Lemma 12 that the inclusion $\Omega_t^p \subset \Omega_t$ holds. Noting that $\pi(\Omega_t)$ is the largest admissible subset of Ω_t , we can also conclude $\Omega_t^p \subset \pi(\Omega_t)$. This inclusion is, in general, strict: With a projected speed, the forbidden region creates a kind of “shadow” for the shape evolution. This effect is not present if the shape is allowed to propagate unhindered at first and only projected later according to (112). See Figure 44 for an illustration.

The worst-case situation for this shadowing effect is a sharp corner, as shown in Figure 45. The Hausdorff distance between Ω_t^p and $\pi(\Omega_t)$ for this situation is indicated with the red line in Figure 45b. A basic geometric argument quickly reveals that it is proportional to the evolution time t . If we exclude this case, however, and assume that the boundary of B is smooth, it turns out that both approaches yield approximately the same shapes for small step sizes, meaning that $d_H(\Omega_t^p, \pi(\Omega_t)) = o(t)$. This will be our main result of the current subsection, formulated and shown below in Theorem 24. The kind of smoothness required is a well-known geometric condition, which we recall briefly for convenience (see also, for instance, Definition 3.1 on page 68 of [30]):

Definition 23. Let $\Omega \subset \mathbb{R}^n$ be open. Assume that for every point $p \in \partial\Omega$ there exist $r > 0$ and a bijection $h: Q \rightarrow B_r(p)$ such that both h and h^{-1} are in C^1 . Furthermore, we require that

$$h(Q_0) = \partial\Omega \cap B_r(p) \quad \text{and} \quad h(Q_-) = \Omega \cap B_r(p).$$

Here, $Q = B_1(0)$ is the open unit ball and

$$Q_0 = \{x \in Q \mid x_n = 0\}, \quad Q_- = \{x \in Q \mid x_n < 0\}.$$

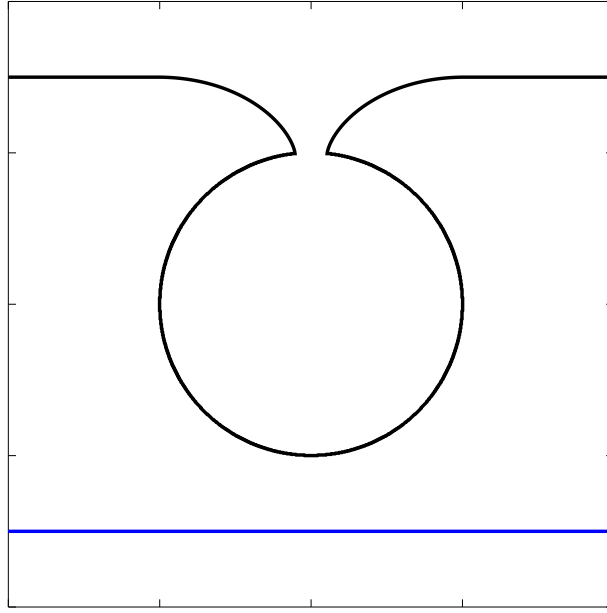
If this is the case, then Ω is said to be a C^1 -domain.

The main ingredient for the estimation of $d_H(\Omega_t^p, \pi(\Omega_t))$ is the ability to construct paths between points $x, y \notin B$ that do not cross the forbidden region B and are not too long. This can be achieved with a C^1 -domain as illustrated in Figure 46: If we “zoom in” far enough towards a piece of the boundary, it becomes almost flat due to the required smoothness. This makes it easy to construct a path $\xi \in X_{\text{ad}}(x, y)$ that avoids B entirely. This idea can be formalised, which yields the main technical construction for the proof of Theorem 24:

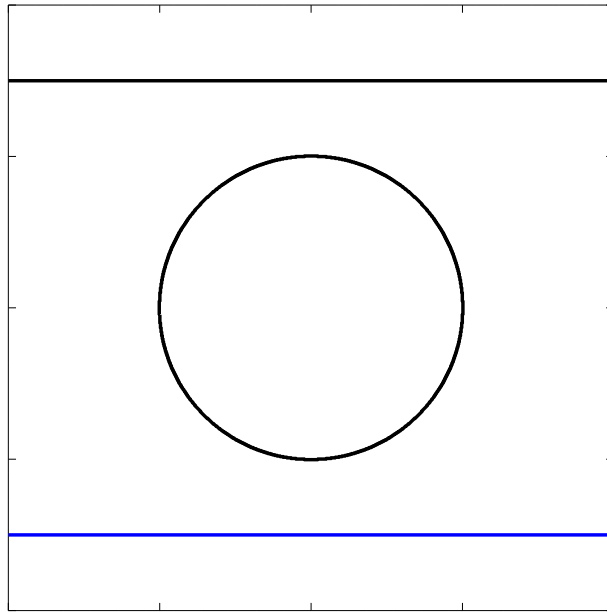
Lemma 66. *Let B be compact and such that B° is a C^1 -domain. Then for every $\epsilon > 0$ there exists a neighbourhood U of ∂B and a $\delta > 0$ such that for every $x, y \in U$ with $|x - y| < \delta$ there is a path $\xi \in X_{\text{ad}}(x, y)$ with*

$$|\xi| \leq (1 + \epsilon) |x - y|.$$

If $x, y \notin B$, then also ξ is entirely outside of B .



(a) Ω_t^p corresponding to a speed projection in L^2 .



(b) Projected shape $\pi(\Omega_t)$.

Figure 44: Comparison of the evolved domains Ω_t^p and $\pi(\Omega_t)$ (in black). The initial geometry is the front shown in blue, which evolves with $F = 1$ around a circular forbidden region.

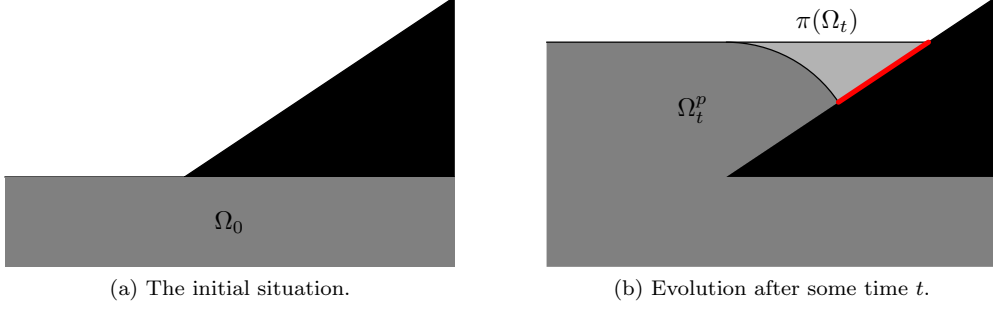


Figure 45: The shadowing effect for a corner. The forbidden region is black, the evolved shape Ω_t^p is dark and the additional set part of $\pi(\Omega_t)$ is light grey. The red line indicates the Hausdorff distance between the two evolved sets.

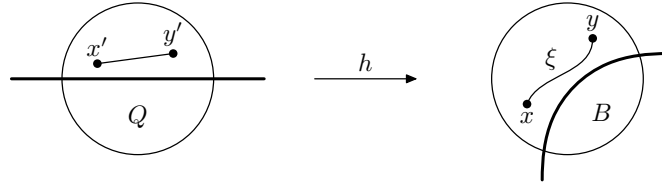


Figure 46: Sketch of the transformation h from Definition 23 mapping the reference domain Q (left) to a neighbourhood of the boundary of B (right). We also show a possible path connecting x and y without going through B .

Proof. Let us start with a standard compactness argument applied to ∂B : For every $x \in \partial B$, let r_x denote the radius of the neighbourhood $B_{r_x}(x)$ given by Definition 23. Then we can choose a finite subset $Z \subset \partial B$ such that

$$\partial B \subset \bigcup_{z \in Z} B_{r_z/3}(z) = U.$$

Choose $\delta_1 = \min_{z \in Z} r_z/3$. Now let $x, y \in U$ and $|x - y| < \delta_1$. Then there is some $z \in Z$ with $x \in B_{r_z/3}(z)$. Since $|z - y| \leq |z - x| + |x - y| < 2/3 \cdot r_z$, it follows that $x, y \in B_{2/3 r_z}(z)$. Also note the following: If we denote the bijection of Definition 23 for each $x \in \partial B$ by h_x , then all functions h_z , h_z^{-1} , Dh_z and Dh_z^{-1} are uniformly bounded and uniformly continuous on their respective domains for $z \in Z$. We can, furthermore, find bounds that are actually independent of z .

Consider now some fixed $z \in Z$ and $x, y \in B_{r_z}(z)$. Let us write $h = h_z$ for the bijection on $B_{r_z}(z)$. We define the path $\xi \in X_{\text{ad}}(x, y)$ by

$$\xi(t) = (h \circ S_{x'y'})(t) = h(x' + t(y' - x')) = h(h^{-1}(x) + t(h^{-1}(y) - h^{-1}(x))).$$

I. e., we use a straight line in the transformed picture (on Q), as shown also in Figure 46. Obviously, if $x, y \notin B$, then also ξ will never be inside B . The fundamental theorem of calculus states that

$$y' - x' = h^{-1}(y) - h^{-1}(x) = \int_0^1 Dh^{-1}(x + s(y - x)) ds.$$

(Note that $B_{r_z}(z)$ is convex, so that all intermediate values are in the domain of h^{-1} .) This implies also

the following estimate for the derivative of ξ :

$$\begin{aligned}
|\xi'(t)| &= |Dh(x' + t(y' - x'))(y' - x')| = \left| \int_0^1 Dh(x' + t(y' - x')) Dh^{-1}(x + s(y - x))(y - x) ds \right| \\
&\leq |y - x| \int_0^1 \|Dh(x' + t(y' - x')) Dh^{-1}(x + s(y - x))\| ds \\
&= |y - x| \int_0^1 \|1 + Dh(x' + t(y' - x')) (Dh^{-1}(x + s(y - x)) - Dh^{-1}(h(x' + t(y' - x'))))\| ds
\end{aligned}$$

Here we have used the well-known relation between the derivatives of a function and its inverse,

$$(Dh(x' + t(y' - x')))^{-1} = Dh^{-1}(h(x' + t(y' - x'))).$$

Further estimation yields

$$|\xi'(t)| \leq |y - x| \left(1 + \|Dh\|_\infty \int_0^1 \|Dh^{-1}(x + s(y - x)) - Dh^{-1}(h(x' + t(y' - x')))\| ds \right). \quad (116)$$

Also note that $|\xi|$ can be bounded by the same quantity, since $|\xi| = \int_0^1 |\xi'(t)| dt$ by definition.

Thus, it remains to find a uniform bound for the norms in the right-hand side of (116). The term $\|Dh_z\|_\infty$ can be bounded uniformly in z by compactness as discussed above. Furthermore, note that for every $\delta' > 0$ there is $\delta_2 > 0$ such that $|x - y| < \delta_2$ implies

$$|x + s(y - x) - h_z(x' + t(y' - x'))| < \delta'$$

for all $t, s \in [0, 1]$, $z \in Z$ and $x, y \in B_{r_z}(z)$. To see this, note $h_z(x') = x$ and that h_z and h_z^{-1} are uniformly continuous. Thus, uniform continuity of Dh_z^{-1} implies that we can have

$$\|Dh_z\|_\infty \int_0^1 \|Dh_z^{-1}(x + s(y - x)) - Dh_z^{-1}(h_z(x' + t(y' - x')))\| ds \leq \epsilon$$

if only $|x - y| < \delta = \min(\delta_1, \delta_2)$. This finishes the proof. \square

We can even get rid of the neighbourhood U in Lemma 66 with a simple further construction:

Lemma 67. *Lemma 66 holds also for all $x, y \in \mathbb{R}^n$ with $|x - y| < \delta$, dropping the condition $x, y \in U$.*

Proof. Choose δ for ϵ according to Lemma 66 and let $x, y \in \mathbb{R}^n$ be given with $|x - y| < \delta$. We consider the straight line S_{xy} . If it does not intersect B , then we can simply use $\xi = S_{xy}$ with $|\xi| = |x - y|$. So assume that $x, y \notin B$ but that S_{xy} intersects B at some point. Then there exist times $0 \leq t_1 < t_2 \leq 1$ such that $x_1, x_2 \in U \setminus B$, where we have introduced the notation $x_1 = S_{xy}(t_1)$ and $x_2 = S_{xy}(t_2)$. We can, in addition, choose t_1 and t_2 such that S_{xy} does neither intersect B on $[0, t_1]$ nor on $[t_2, 1]$. Apply now Lemma 66 to get a path $\xi \in X_{\text{ad}}(x_1, x_2)$ that connects the two points without intersecting B . It is clear that this is possible since we have $|x_1 - x_2| \leq |x - y| < \delta$. Then set ξ_c to be the concatenation of S_{xy} on $[0, t_1]$, ξ and S_{xy} on $[t_2, 1]$. This yields

$$|\xi_c| = |x_1 - x| + |\xi| + |y - x_2| \leq |x_1 - x| + (1 + \epsilon) |x_2 - x_1| + |y - x_2| \leq (1 + \epsilon) |y - x|,$$

where we have used that the points x, x_1, x_2 and y are collinear. \square

Based on Lemma 67, we can now show the main estimate of $d_H(\Omega_t^p, \pi(\Omega_t))$. For this, it mostly remains to handle the speed field F . Due to Lipschitz continuity, this is not a big problem.

Theorem 24. *Let Ω_0 be bounded and assume that B is compact and such that B° is a C^1 -domain. Let F be Lipschitz continuous, $F \geq 0$ and $\inf_{x \in B} F(x) > 0$. Then $d_H(\Omega_t^p, \pi(\Omega_t)) = o(t)$ as $t \rightarrow 0^+$.*

Proof. Note that our assumptions imply that there exists an open neighbourhood $U \supset B$ and $\underline{F} > 0$ such that $F \geq \underline{F}$ on U . Furthermore, since Ω_0 is bounded and F continuous, we may assume, without loss of generality, that $F \leq \bar{F}$. Since $\Omega_t^p \subset \pi(\Omega_t)$, we only have to consider $d_H(\pi(\Omega_t) \rightarrow \Omega_t^p)$. Let $t > 0$ be small and $y \in \pi(\Omega_t) \setminus \Omega_t^p$. Since $y \in \Omega_t$, there exist $x \in \Omega_0$ and $\xi_0 \in X_{\text{ad}}(x, y)$ with $l(\xi_0) < t$. Note that $|x - y| \leq \bar{F} \cdot l(\xi_0) < \bar{F}t$ by Lemma 20, so that $|x - y|$ gets arbitrarily small in the limit $t \rightarrow 0^+$. Because $y \notin \Omega_t^p$, we can conclude that the path ξ_0 must intersect B . By making t and thus $|x - y|$ small enough, we can assume that $x, y \in U$.

For any given $\epsilon > 0$, we can now apply Lemma 67 to get a corresponding δ . Assume that t is chosen small enough to yield $|x - y| < \delta$. By reducing δ further, we can also guarantee $(1 + \epsilon)L|x - y| < \underline{F}$, where L denotes the Lipschitz constant of F . For our x and y , Lemma 67 gives a path $\xi \in X_{\text{ad}}(x, y)$ with $|\xi| \leq (1 + \epsilon)|x - y|$ and such that $\xi(\tau) \notin B$ for all $\tau \in [0, 1]$. Following the proof of Lemma 21 for ξ instead of S_{xy} , we can derive the following estimates:

$$l(\xi) \leq \frac{1}{L} \log \left(\frac{F(y)}{F(y) - (1 + \epsilon)L|x - y|} \right), \quad t > d(x, y) \geq \frac{1}{L} \log \left(\frac{F(y) + L|x - y|}{F(y)} \right)$$

Setting $\tilde{d} = l(\xi) - t$ and $\lambda = L|x - y|/F(y)$, these estimates imply further

$$e^{L\tilde{d}} - 1 \leq \frac{F(y)}{F(y) - (1 + \epsilon)L|x - y|} \cdot \frac{F(y)}{F(y) + L|x - y|} - 1 = \frac{\epsilon\lambda + (1 + \epsilon)\lambda^2}{1 - \epsilon\lambda - (1 + \epsilon)\lambda^2}.$$

Because $y \notin \Omega_t^p$, we know that $l(\xi) \geq t$ must hold. Hence, the intermediate-value theorem implies that there exists some $\tau \in (0, 1]$ such that ξ split into ξ_1 on $[0, \tau]$ and ξ_2 on $[\tau, 1]$ implies $l(\xi_1) = t$. Set $\tilde{x} = \xi_1(1) = \xi_2(0) = \xi(\tau)$. It is clear that $\tilde{x} \in \Omega_t^p$ since $l(\xi_1) = t$. Because x is in the *interior* of the open set Ω_0 , we actually also get $\tilde{x} \in \Omega_t^p$. Since $\xi_2 \in X_{\text{ad}}(\tilde{x}, y)$ and $l(\xi_2) = l(\xi) - t = \tilde{d}$, Lemma 21 yields

$$|\tilde{x} - y| \leq \frac{F(y)}{L} (e^{L\tilde{d}} - 1) \leq \frac{F(y)}{L} \cdot \frac{\epsilon\lambda + (1 + \epsilon)\lambda^2}{1 - \epsilon\lambda - (1 + \epsilon)\lambda^2}. \quad (117)$$

By the same lemma, we also know

$$|x - y| \leq \frac{F(y)}{L} (e^{Lt} - 1) \Leftrightarrow \lambda \leq e^{Lt} - 1.$$

Note that the right-hand side of (117) is increasing in λ if $|x - y|$ and thus λ are small enough. Thus, we can combine everything and use a series expansion to finally find

$$|\tilde{x} - y| \leq \frac{F(y)}{L} (L\epsilon t + O(t^2)) \leq \bar{F}\epsilon \cdot t + O(t^2).$$

Taking the supremum over y in this inequality yields an estimate for $d_H(\pi(\Omega_t) \rightarrow \Omega_t^p)$. Since ϵ can be chosen arbitrarily small for the limit $t \rightarrow 0^+$, this implies the claim. \square

We require that $\inf_{x \in B} F(x)$ must be strictly positive to avoid a situation like Figure 47. If a line with $F = 0$ touches B , then we may get a qualitative difference between the time evolution of Ω_t^p and that of $\pi(\Omega_t)$: In the shown situation, $\Omega_t^p = \Omega_0$ for all $t \geq 0$ since there is no possibility for the initial region to grow anywhere with speed F^p . On the other hand, Ω_t will grow inside B and, at some point, also reach the upper area outside of B . When this happens, $\pi(\Omega_t)$ contains parts of the quarter plane in the north west. Let us briefly analyse this effect also more explicitly. For this, choose the speed field as

$$F(x, y) = \begin{cases} |y| & \text{if } x \leq 0, \\ \sqrt{x^2 + y^2} & \text{if } x \geq 0. \end{cases}$$

The forbidden region is the half-plane $B = \{(x, y) \in \mathbb{R}^2 \mid x \geq 0\}$. This matches the schematic illustration of Figure 47. For Ω_0 to reach the north-west region, we have to consider paths like $\xi \in X_{\text{ad}}(p, q)$ shown in the sketch. Note that F is constant along such a path, so that

$$l(\xi) = \frac{\pi r}{F} = \pi,$$

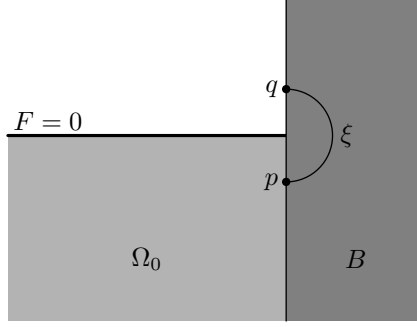


Figure 47: Sketch of a possible situation where Ω_t^p and $\pi(\Omega_t)$ do not match qualitatively in their time evolution. The dark grey area is the forbidden region B . We choose $F = 0$ on the horizontal line and $F > 0$ everywhere else.

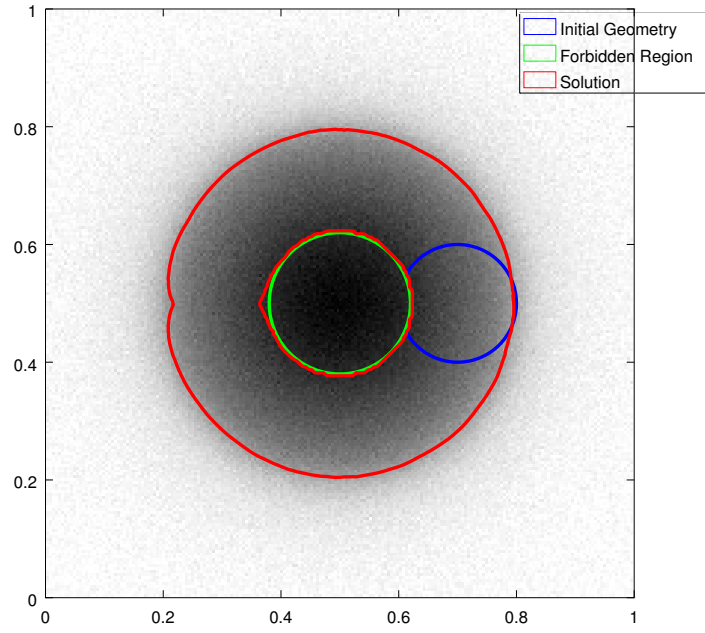
where r is the radius of the circular arc. In particular, *the path length is independent of r* . This implies that it is not possible to reach the north west after arbitrarily small times, even though p and q can be as close together as we wish. Hence, the statement of Theorem 24 is actually still true for this situation (since we take the limit $t \rightarrow 0^+$). We believe that it is possible to exploit Lipschitz continuity of F to show that this must always be the case and that Theorem 24 holds generally without the strict positivity requirement. This is, however, only a minor detail. The qualitative difference between Ω_t^p and $\pi(\Omega_t)$ that arises in a situation like Figure 47 is more important in practice than the fact that this can only happen after some (possibly very small) time interval.

6.6.3 Numerical Experiments

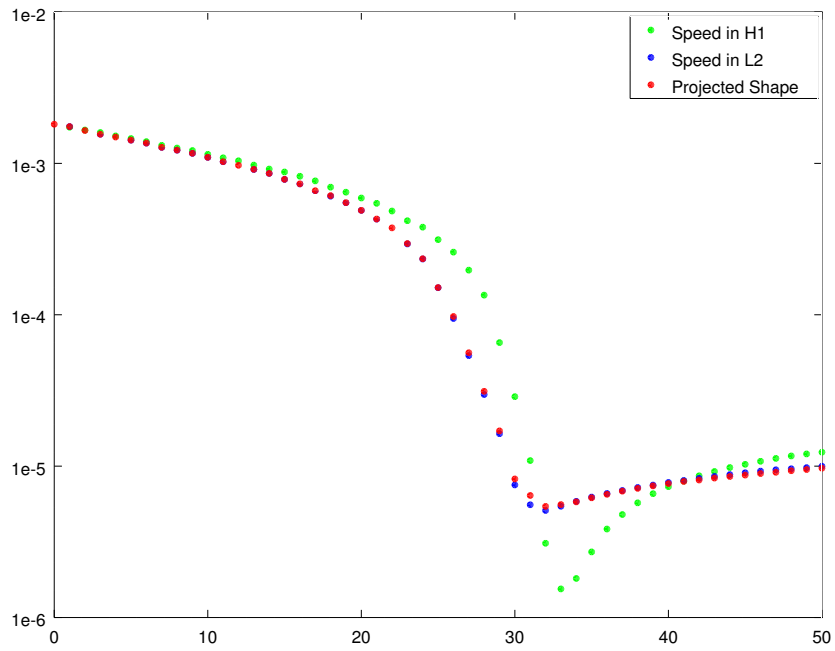
To conclude this discussion, let us consider some numerical results. We have implemented all three strategies for handling shape constraints discussed above. They are applied to the image-segmentation problem (102) with various kinds of forbidden regions. Note that we are neither aware of any other work about image segmentation with geometric constraints nor of an actual application of such a problem. It is, however, a very instructive model problem for an analysis of the behaviour of the descent methods. Furthermore, we believe that geometric constraints in a segmentation model could be used to incorporate “outside information” into the segmentation process. This additional information could either be provided by a human operator in a semi-automatic method or it could come from a second channel of measurement data.

All computations are done with 2% of Gaussian noise added. We perform the descent run for 50 different random configurations in each problem setting to make the qualitative result more representative. The cost evolutions are averaged over all runs, for which we employ the *geometric mean* since it fits better to the logarithmic scaling of the y -axis. We chose a small minimum step length of $t_{\min} = 10^{-6}$ to ensure that no effects of the constraints (which are our main object of interest) are obscured by time-stepping artefacts. Since we do not know the true optimal cost, we use the smallest achieved value for a particular configuration (over all iteration steps and with all three methods) as base value.

Figure 48, Figure 49 and Figure 50 show the results for three different configurations of the forbidden region. For each case, the top plot shows the basic situation (initial geometry Ω_0 , forbidden region B and the approximate final solution). The bottom plot compares the averaged decrease of the cost value for the three methods we consider. The first situation in Figure 48 has the “easiest” constraint. The region B in this case is, in particular, smooth. Consequently, Theorem 24 tells us that the results of using the speed projection in L^2 and projecting the shape should be very similar. This statement is, indeed, confirmed by Figure 48b: The blue and red dots match quite well. The green dots, corresponding to a speed projection in H^1 instead, show a different behaviour: The decrease is more slowly here in the beginning, which can be explained by the fact that the speed field gets drawn to zero where the constraint is almost active and thus the whole descent is done in a more cautious fashion. This, however, also leads to a (slightly) better minimal cost in the end. In Figure 49, the forbidden region is a triangle with sharp corners. This set B *does not* fulfil the requirements of Theorem 24, and we can see that also

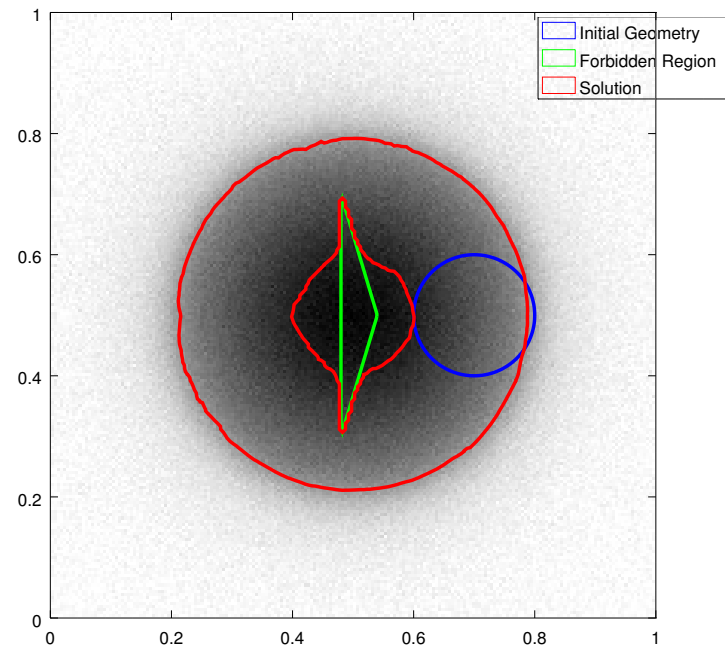


(a) The basic configuration in this example.

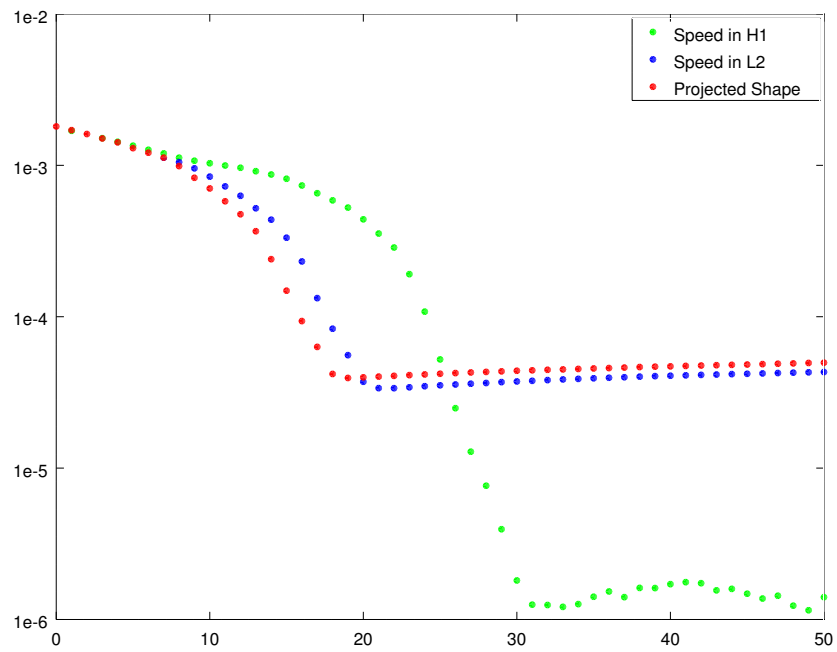


(b) Average decrease of the cost during the iteration for all methods.

Figure 48: Comparison of the three methods for handling constraints. These are projection of the speed in H^1 , in L^2 with (111) and projection of the shape with (112).

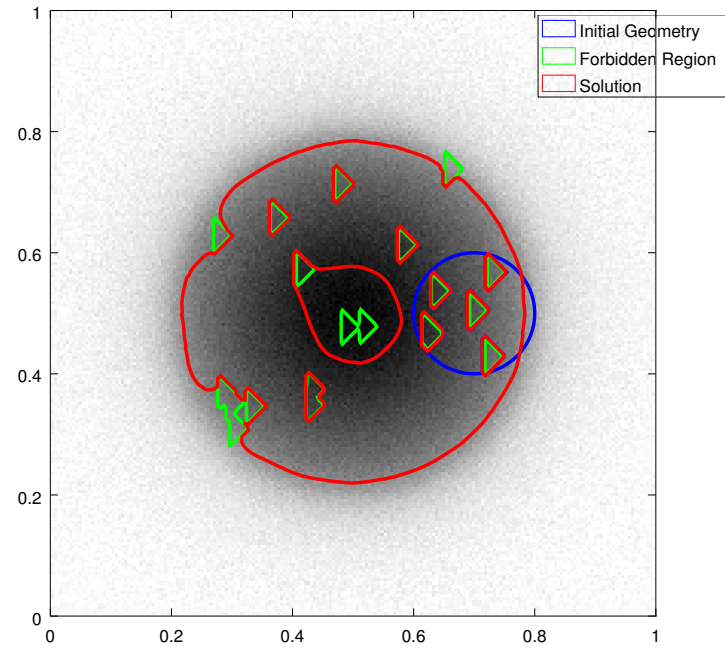


(a)

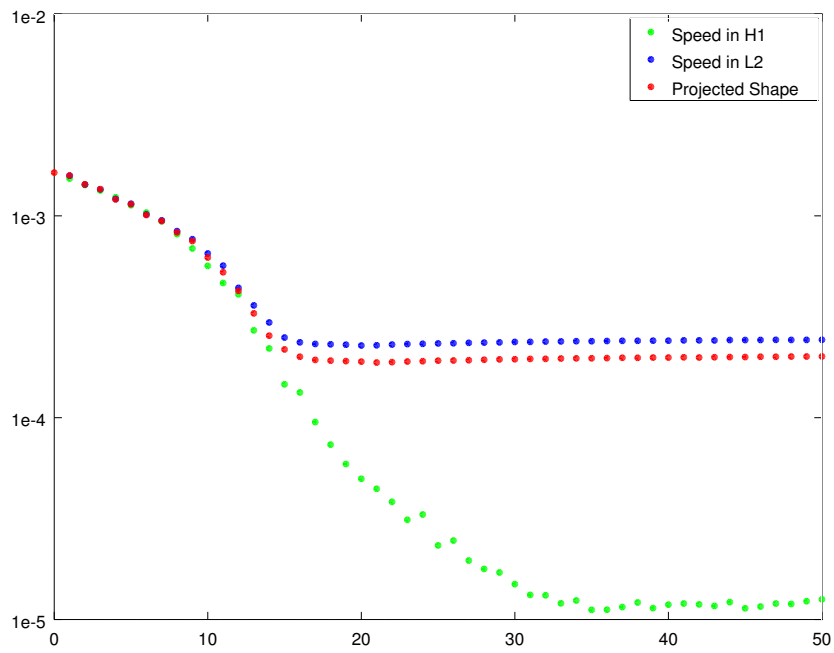


(b)

Figure 49: Continuation of Figure 48 for a different configuration of the forbidden region.



(a)

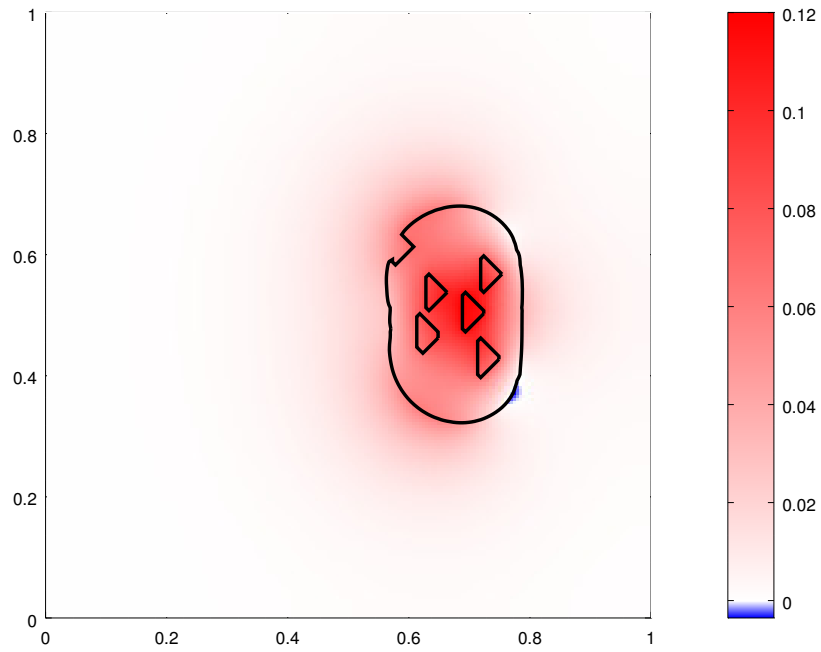


(b)

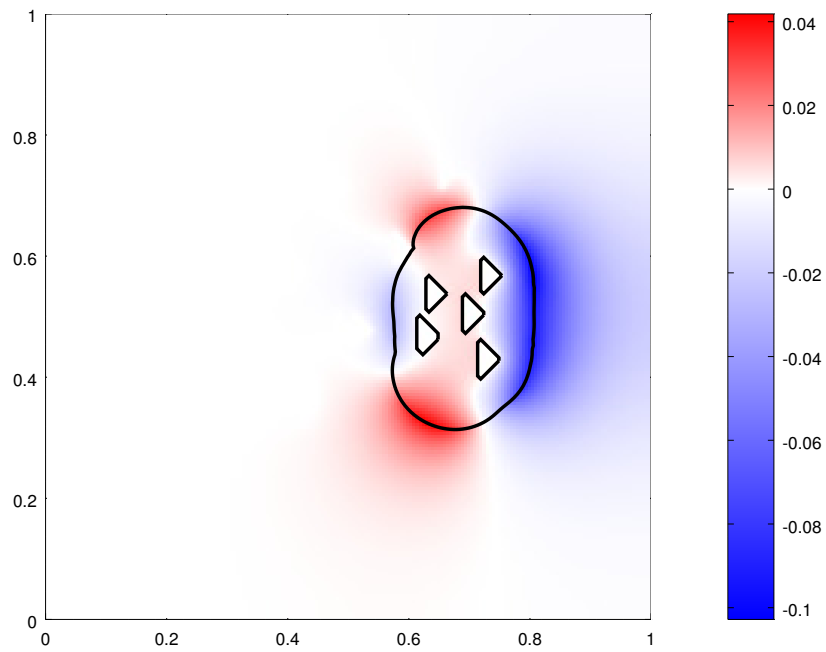
Figure 50: Continuation of Figure 48 with a forbidden region that consists of multiple, randomly placed triangles. Each run has not only different noise, but also a different arrangement of the triangles.

the corresponding cost descents in Figure 49b are not as similar as before. The blue and red dots clearly diverge from each other around iteration eight, which is when the growing domain starts to wrap around the corners of the triangle. This is in nice correspondence to our theory discussed in Subsection 6.6.2. The green curve shows the same behaviour as before, but much more pronounced this time. The decrease is more slowly at the beginning, but the descent is more robust and leads to a much better result.

This effect can be seen and interpreted even better with the setting of Figure 50: Here, the forbidden region is even more complex and difficult than before. Figure 51 shows typical speed fields as they occur in the descent with shape projection (Figure 51a) and the speed projected in H^1 (Figure 51b). In the former case, we get very large speed values around the parts of B that are already surrounded by the growing domain. This is the case since it would be good for decreasing the cost to include them in Ω , and the speed field does not know anything about the constraints that forbid this. With a projection in H^1 , on the other hand, the speed field *does* include information about the constraints. Consequently, the speed is small (and continuous) around those regions. Note that our descent algorithm computes the directional shape derivative according to (105) and uses it for the Armijo rule (107) as the expected cost decrease. This, however, only works when the constraints are correctly accounted for in the shape gradient. Consequently, the Armijo rule expects a much larger cost decrease than we can actually achieve for the situation of Figure 51a. This leads to the effect that only the minimal step length is accepted from this iteration onward, and the final shape looks almost the same as the black shape indicated in Figure 51a. This is clearly suboptimal. With the speed projection in H^1 , on the other hand, the shape from Figure 51b continues to evolve and results in the correct geometry shown also in Figure 50a. One can confirm this interpretation by lowering the relaxation parameter τ in the Armijo rule (107) sharply. This improves the performance of the shape-projection method in relation to speed projection in H^1 considerably, and avoids a stuck situation as in Figure 51a. Let us, however, remark that the opposite effect is possible as well: If the forbidden triangles are placed such that they obstruct the growth of the domain severely, it can happen that the speed projection in H^1 gets stuck (due to drawing down the speed field) while using a shape projection converges to the optimal shape. Based on our experience with these numerical tests, however, this seems to be a less common situation. Thus, the interpretation given above is what causes the effect seen in the averaged plot Figure 50b.



(a) Projection of the shape with (112).



(b) Projection of the speed field in H^1 .

Figure 51: Typical speed fields during the descent for the problem from Figure 50.

7 Self-Consistent Gradient Flow

In the previous Chapter 6, we have seen how a basic gradient-descent method for shape optimisation can be developed. We have also seen that it is prone to inefficient zig-zag movement in certain situations. Now, we want to mention a new and different approach to shape optimisation within our level-set framework. The proposed method can be interpreted as a *gradient flow*. Particularly for images with sharp edges (like Figure 41), this method is more efficient than a plain gradient descent. Unlike Newton-type methods, our approach does not need derivatives of the image data. This makes it potentially more stable for noisy images.

7.1 Self-Consistent Speed Fields

The basic idea of our method relies on two crucial observations about the shape evolution of some initial geometry Ω_0 along a given speed field F :

- Recall that the value $F(x)$ of the speed field at some position $x \in \mathbb{R}^n$ defines the normal speed of movement of the boundary Γ at this point x . This, however, means that the value of $F(x)$ is only significant at the instant t in time when $x \in \Gamma_t$.
- If $F > 0$, then the evolution of Ω is monotone. In particular, our domain always grows. This implies that each point $x \notin \Omega_0$ is reached by the advancing front at a precisely defined, *unique arrival time*. In other words, for each such point there is a unique $t \geq 0$ such that $x \in \Gamma_t$. For all $\tau < t$, it follows that $x \notin \Gamma_\tau \cup \Omega_\tau$. If, on the other hand, $\tau > t$, then $x \in \Omega_\tau$. This t is, in fact, given by the distance $d_0(x)$ of Definition 11.

Particularly interesting is the following conclusion, which can be drawn by combining both observations: *If we are given some monotone shape evolution, then a single speed field is enough to encode the propagation for all times.* This is even true if the shape evolution is defined in terms of multiple speed fields (e. g., descent steps) or with a time-dependent speed. (The latter situation has not been treated rigorously above. This is, however, not important for our discussion.)

As above in Section 6.4, let us assume now that we have an optimisation problem whose shape derivative has the form

$$dJ(\Omega; F) = \int_{\Gamma} F f(x, \Omega) d\sigma \quad (118)$$

for some *shape-dependent* function f . We have already seen in (103) that our image-segmentation problem is of this type. Note, however, that we will have to make some assumptions on f later on in Section 7.2 before we can derive theoretical results. These assumptions are usually not fulfilled for the image-segmentation problem. Nevertheless, the method still works very well in practice. This will be demonstrated in Section 7.4. We will, though, at least assume $f < 0$ already now. This ensures that the resulting shape evolution is always monotonically growing. The idea can be adapted in a straightforward way for $f > 0$ and a monotonically shrinking domain as well. If the sign of f is not fixed (which is usually the case in optimisation since we are looking for a zero of the gradient), the approach still works in practice (see Section 7.4). Now, in order to solve the optimisation problem, we are interested in a speed field that has the following property:

Definition 24. The speed field F is called a *self-consistent gradient flow* if

$$F(x) = -f(x, \Omega_t) \quad (119)$$

for all $t \geq 0$ and $x \in \Gamma_t$. Here, Ω_t is the time evolution of Ω_0 with respect to the speed field F itself.

Clearly, F defined in this way is a descent direction not only at $\Omega = \Omega_0$ but all along the time evolution, i. e., for all $\Omega = \Omega_t$ with $t \geq 0$, as the shape derivative (118) is negative by definition. In fact, we have (in some sense) chosen F to be the negative shape derivative. This is the same idea that was already used in [75]. It motivates the claim that this speed field corresponds, somehow, to a gradient flow. It has to be noted, however, that it does, in general, *not* correspond to the shape gradient introduced in Section 6.2 as the *Riesz representative* of the shape derivative. For instance, the smoothing effect due to computation of the shape gradient by solving (105) is not present in F defined according to (119).

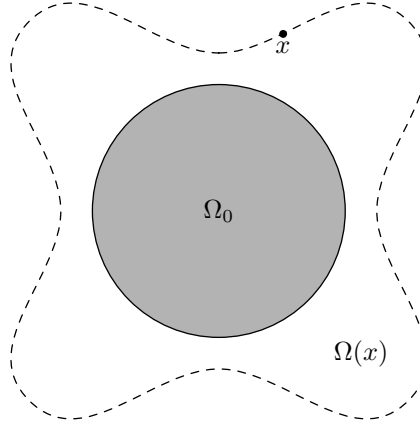


Figure 52: Computation of $F = \psi(F_0)$ at some point x . The shape $\Omega(x)$, on which the shape-dependent quantities are based, is indicated with the dashed outline.

Another important issue is the following: In order to make sense of the condition (119), we already have to know some shape evolution on which Ω_t and Γ_t can be based. In other words, one *already needs a speed field* in order to apply (119)! In fact, for Definition 24 to be fulfilled, this condition needs to hold assuming the shape evolution induced by the speed field F itself. This is the reason for calling it “self-consistent”. Thus, (119) can not be used directly to compute such a self-consistent gradient flow. What we can do, however, is to define an *iteration*: Given an initial speed field F_0 , we can, indeed, use (119) to define another speed field $F = \psi(F_0)$. The self-consistent gradient flow that we are looking for is then a *fixed point* of ψ . With certain assumptions, we will see in Section 7.2 that such a fixed point exists, the iteration converges to it and that all speed fields produced on the way are Lipschitz continuous. The computation of $F = \psi(F_0)$ is depicted in Figure 52: For some fixed $x \notin \Omega_0$, we compute $t = d_0(x)$. Next, the evolved shape $\Omega(x) = \Omega_t$ at this time is found. It corresponds to the snapshot in the shape evolution when x lies precisely on the advancing front Γ_t . As discussed above, the speed field F_0 is used to compute d_0 and the shape evolution. When this is done, we set

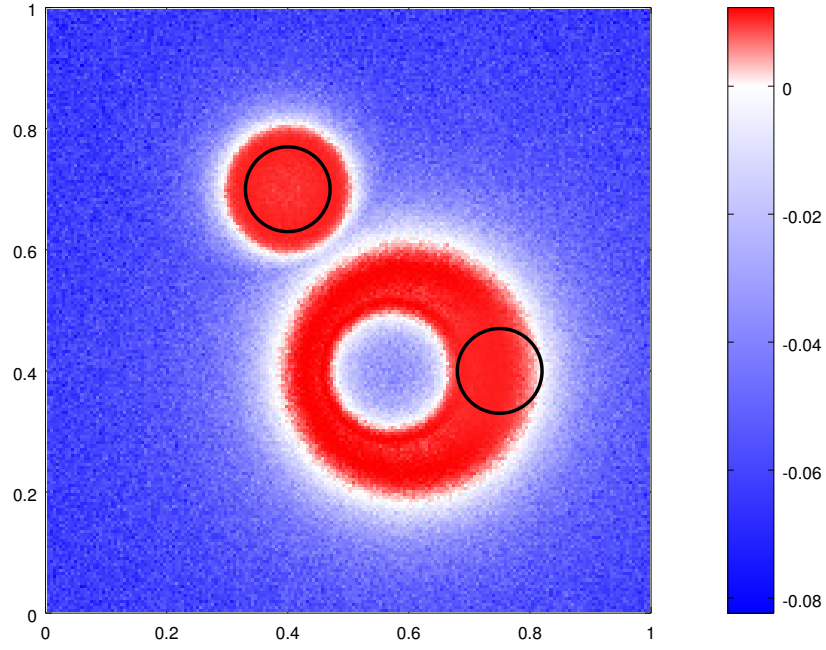
$$\psi(F_0)(x) = F(x) = -f(x, \Omega(x)) \quad (120)$$

according to (119). This means that we evaluate the shape dependence of f for the domain $\Omega(x)$. (Note that the value of F does not matter for $x \in \Omega_0$. Since we assumed a monotonically growing shape, changes to the speed field in Ω_0 will not influence the shape evolution at all.)

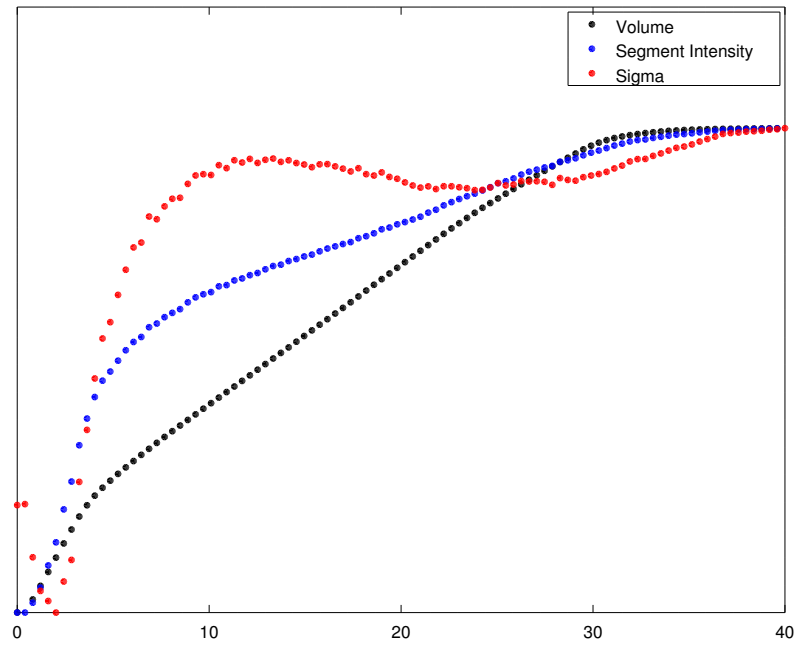
Of course, it is not possible in practice to compute all of the evolved shapes $\Omega(x)$ for $x \in \mathbb{R}^n$. Doing so would, roughly speaking, correspond to performing a gradient descent with infinitesimally small time steps. Even the computation for all points of a discrete grid has a prohibitive computational cost and cannot be done practically. One can, however, compute just a handful of snapshots together with the corresponding shape-dependent quantities. The shape dependence at some point x can then be found by interpolating these values for the desired time $d_0(x)$. The qualitative behaviour of the important shape-dependent quantities in our case is plotted in Figure 53b for a sample time evolution. This shows that they behave “nicely”, which means that it is, indeed, justified to apply some suitable interpolation method in practice. Note that this is the case even though neither the speed field nor the image are actually continuous for the example (due to the added noise). Later on, we will also see in Lemma 72 and Lemma 73 that certain assumptions ensure that the shape-dependent quantities are actually Lipschitz continuous with respect to the evolution time t . Thus, there exists also a theoretical justification for the suggested interpolation approach. Hence, we are perfectly able not only to *define* $\psi(F_0)$, but also to *compute* it without too much difficulty.

7.2 Local Existence of a Fixed Point

We continue now with a theoretical analysis of the mapping ψ introduced above. In particular, we are interested in the following two questions:



(a) The speed field and initial configuration used.



(b) Values of the quantities for the evolved shapes.

Figure 53: Behaviour of the shape-dependent quantities that appear in $dJ(\Omega; F)$ of the image-segmentation model (see (103)) during a sample time evolution. An affine transformation has been applied to make the values comparable to each other.

- Will $\psi(F)$ again be a *Lipschitz continuous* speed field if F is Lipschitz continuous?
- Is there a fixed point of ψ ? If we manage to find one, we have found a self-consistent gradient flow according to Definition 24.

It will turn out in Subsection 7.2.4 that the answer to both questions is “yes”. To show this, however, we need some additional assumptions. Throughout this section, we will require that $0 < \underline{F} \leq F, G \leq \overline{F}$, where $F, G: \mathbb{R}^n \rightarrow \mathbb{R}$ are speed fields. The strictly positive lower bound is, unfortunately, crucial. Example 15 shows that we can not hope for Lipschitz continuity of $\psi(F)$ if no lower bound is present. The initial domain Ω_0 is assumed to be fixed. We further require $\overline{\Omega}_0 = \Gamma_0 \cup \Omega_0$, i. e., assume that Γ_0 has empty interior.

In order to show existence of a fixed point (as well as convergence of the fixed-point iteration with ψ), we want to apply Banach’s fixed-point theorem. A natural Banach space for the speed fields is $C(\mathbb{R}^n)$. Thus, besides some further technical issues, we have to find a *contraction estimate* on $\|\psi(F) - \psi(G)\|_\infty$ in terms of $\|F - G\|_\infty$. Although the space $C^{0,1}(\mathbb{R}^n)$ of Lipschitz continuous functions may look like an even better choice at the first glance, it will be convenient to only require continuity in the underlying space. We show actual Lipschitz estimates for $\psi(F)$ in a separate step. Let us also introduce the set

$$E_t = \overline{V_{\underline{F}t}(\Omega_0)} \setminus \Omega_0 = \{x \notin \Omega_0 \mid \text{sd}_{\Omega_0}(x) \leq \underline{F}t\} = \{x \in \mathbb{R}^n \mid 0 \leq \text{sd}_{\Omega_0}(x) \leq \underline{F}t\}.$$

Here, $V_\epsilon(\Omega_0)$ is, as before, the ϵ -envelope of Ω_0 introduced in (100). The set E_t is a (closed) band around Ω_0 that contains all points that can be reached in time t , based on the minimal speed \underline{F} . In other words, $E_t \subset \Omega_t(F) \setminus \Omega_0$ for arbitrary speed fields F used in the evolution. Hence also $d_0(x) \leq t$ for all $t \geq 0$ and $x \in E_t$. In the following, we present some estimates that ultimately show *Lipschitz continuity* of ψ with respect to the speed field in the supremum norm. Furthermore, it will turn out that the Lipschitz constant tends to zero with $t \rightarrow 0^+$ if we restrict ourselves to such a band E_t . Consequently, we can, indeed, ensure the contraction property on E_t if only t is small enough. Thus, our results will be *local* in nature. We will, however, also discuss a possible strategy to globalise them in certain cases in the following Section 7.3.

7.2.1 Lipschitz Continuity of Arrival Times

The first step in the evaluation of $\psi(F)$ at some $x \in E_t$ is the computation of the arrival time $d_0(x)$. This motivates us to consider how this time behaves if we change the speed field. In order to denote arrival times for different speed fields unambiguously, we use $d_0(x; F)$ and $d_0(x; G)$ for the arrival times at x based on the speed fields F and G , respectively. Then, the following Lipschitz estimate holds:

Lemma 68. *Let $t \geq 0$ be fixed and $x \in E_t$. Then*

$$|d_0(x; F) - d_0(x; G)| \leq \frac{t}{\underline{F}} \|F - G\|_\infty.$$

Proof. For $x \in E_t$, we can choose $x_0 \in \Gamma_0$ and a path $\xi \in X_{\text{ad}}(x_0, x)$ with $l(\xi; F) = d_0(x; F)$. This works due to Lemma 19 and Lemma 33. Note that

$$\left| \frac{1}{F(y)} - \frac{1}{G(y)} \right| = \left| \frac{G(y) - F(y)}{F(y)G(y)} \right| \leq \frac{\|F - G\|_\infty}{\underline{F}^2}$$

for all y . Thus, using the path ξ also for the speed field G , we find

$$d_0(x; G) \leq l(\xi; G) = \int_0^1 \frac{|\xi|}{G(\xi(\tau))} d\tau \leq l(\xi; F) + |\xi| \int_0^1 \left| \frac{1}{F(\xi(\tau))} - \frac{1}{G(\xi(\tau))} \right| d\tau \leq d_0(x; F) + \frac{|\xi|}{\underline{F}} \|F - G\|_\infty.$$

It remains to estimate $|\xi|$. For this, consider the straight line $S_{x'_0 x}$ connecting x to some $x'_0 \in \Gamma_0$ with $\text{sd}_{\Omega_0}(x) = |x - x'_0|$. We know that $|S_{x'_0 x}| = |x - x'_0| \leq \underline{F}t$ by definition of E_t . Hence

$$\frac{1}{\underline{F}} |\xi| \leq \int_0^1 \frac{|\xi|}{F(\xi(\tau))} d\tau = l(\xi; F) = d_0(x; F) \leq l(S_{x'_0 x}; F) = \int_0^1 \frac{|S_{x'_0 x}|}{F(S_{x'_0 x}(\tau))} d\tau \leq \frac{\underline{F}t}{\underline{F}} = t.$$

Taking the estimates together, we have shown

$$d_0(x; G) \leq d_0(x; F) + \frac{t}{\underline{F}} \|F - G\|_\infty.$$

If we repeat this argument with the roles of F and G exchanged, the proof is finished. \square

One can easily see that a lower bound \underline{F} on the speed fields is necessary already for this result: Assume that there is $x_0 \in \Gamma_0$ with $F(x_0) = 0$ but $G(x_0) > 0$. Then, for a sequence $x_k \rightarrow x_0$, Lemma 17 implies that $d_0(x_k; F) \rightarrow \infty$ while $d_0(x_k; G) \rightarrow d_0(x_0; G) < \infty$. Thus, we can not hope for any Lipschitz constant that works uniformly for all x in some E_t . On the other hand, assume that F and G are strictly positive on Γ_0 . In this case, continuity implies that a lower bound $\underline{F} > 0$ exists also on some band E_t if t is chosen small enough, so that this requirement of Lemma 68 is no real restriction. See also Example 15.

7.2.2 Uniform-Density Estimates

In the next subsection, we show that the volume $\text{vol}(\Omega)$ as shape-dependent quantity is Lipschitz continuous with respect to the employed speed field (in the sense discussed in Section 7.1). Theorem 21 from Chapter 5 can be used for this estimate. In order to do so, we need a uniform-density property not only for Ω_0 (which we can assume) but also for the evolved sets Ω_t . Let us now investigate how uniform lower density is preserved by a shape evolution. This is related to our previous result Theorem 15, but here we focus on *uniform estimates* of the density.

For simplicity, we discuss the case $F = 1$ first in order to introduce the idea that will be used later to prove the general case. In this situation, (t_0, c) -uniform lower density of Ω_0 is completely preserved for all times of the shape propagation. This is illustrated in Figure 54a. In particular, let $x \in \Gamma_t$ be an arbitrary point of the evolved boundary and choose some radius $\rho > 0$. By Lemma 57, there exists $x_0 \in \Gamma_0$ with $t = |x - x_0|$. Whenever $y_0 \in B_\rho(x_0) \cap \Omega_0$, then the shifted $y = y_0 + (x - x_0)$ must be part of Ω_t : If this were not the case, then $d_0(y) \geq t$. However, this contradicts

$$d_0(y) < d(y, y_0) = |y - y_0| = |x - x_0| = t.$$

Intuitively speaking, y has definitely been reached by the propagating front at time t since it has, in particular, been reached already by the elementary wave originating at y_0 . Thus, we have shown that

$$(B_\rho(x_0) \cap \Omega_0) + (x - x_0) \subset B_\rho(x) \cap \Omega_t.$$

This, in turn, implies the claimed preservation of uniform lower density.

We can also apply the same idea if F is not constant. In this case, however, shifting a path slightly distorts its length. As a consequence, uniform lower density is not fully preserved. In particular, the constant c_0 is possibly reduced. This weaker result will be sufficient for our purposes, though. As a preparation for the proof, let us estimate how the length of a path changes when it is shifted:

Lemma 69. *Let F have Lipschitz constant L . Choose $d \in \mathbb{R}^n$ with $|d| < \underline{F}/L$, points $x_0, x \in \mathbb{R}^n$ and some path $\xi \in X_{\text{ad}}(x_0, x)$. Denote by $\tilde{\xi} \in X_{\text{ad}}(x_0 + d, x + d)$ the path shifted by d , i. e., $\tilde{\xi}(\tau) = \xi(\tau) + d$ for $\tau \in [0, 1]$. Then*

$$l(\tilde{\xi}) \leq \frac{l(\xi)}{1 - |d|L/\underline{F}}.$$

Proof. Assume that ξ is parametrised by arc length and that $|\xi| = v$. Then clearly also $|\tilde{\xi}| = v$. Note that by Lipschitz continuity

$$\begin{aligned} F(\tilde{\xi}(\tau)) &\geq F(\xi(\tau)) - L |\tilde{\xi}(\tau) - \xi(\tau)| = F(\xi(\tau)) - |d|L \\ &= F(\xi(\tau)) \left(1 - \frac{|d|L}{F(\xi(\tau))}\right) \geq F(\xi(\tau)) \left(1 - \frac{|d|L}{\underline{F}}\right) > 0 \end{aligned}$$

holds for arbitrary $\tau \in [0, 1]$. This now implies

$$l(\tilde{\xi}) = \int_0^1 \frac{v}{F(\tilde{\xi}(\tau))} d\tau \leq \int_0^1 \frac{v}{F(\xi(\tau))} \frac{1}{1 - |d|L/\underline{F}} d\tau = \frac{l(\xi)}{1 - |d|L/\underline{F}}.$$

\square

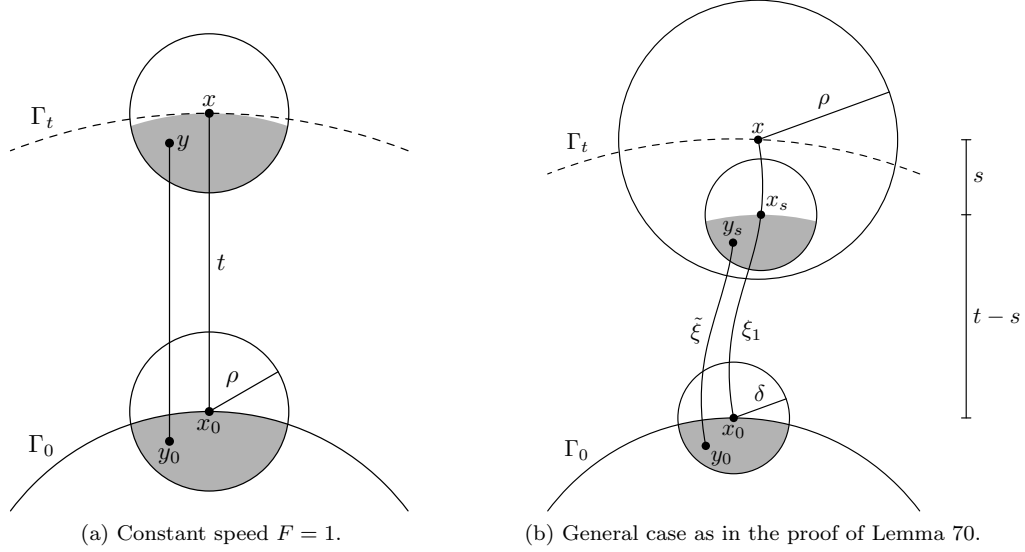


Figure 54: Preservation of uniform lower density during the shape propagation. The grey volume is part of Ω_0 and, after an appropriate shift, still part of Ω_t .

This allows us now to show that uniform lower density of Ω_0 carries, indeed, over to Ω_t :

Lemma 70. *Let F have Lipschitz constant L . Assume that Ω_0 has (ρ_0, c_0) -uniform lower density. Then, for $t \geq 0$, the evolved set Ω_t has (ρ_0, c_t) -uniform lower density. Here,*

$$c_t = c_0 \cdot \left(1 + tL \cdot \frac{\overline{F}}{\underline{F}}\right)^{-n}.$$

Proof. For $t = 0$, the statement is clear. Let thus $t > 0$, $x \in \Gamma_t$ and $\rho \in (0, \rho_0)$. According to Lemma 19 and Lemma 33, there are $x_0 \in \Gamma_0$ and $\xi \in X_{\text{ad}}(x_0, x)$ with $l(\xi) = d(x_0, x) = d_0(x) = t$. We set

$$\delta = \frac{\rho}{1 + tL\overline{F}/\underline{F}} < \rho \quad \text{and} \quad s = t \cdot \min\left(1, \frac{\delta L}{\underline{F}}\right) \leq t. \quad (121)$$

Furthermore, split ξ at some point x^s into $\xi_1 \in X_{\text{ad}}(x_0, x^s)$ and $\xi_2 \in X_{\text{ad}}(x^s, x)$ such that $l(\xi_1) = t - s$ and $l(\xi_2) = s$. See also the sketch in Figure 54b. Now, consider first the case $\delta < \underline{F}/L$. In this situation,

$$l(\xi_1) = t - s = t \left(1 - \delta \frac{L}{\underline{F}}\right).$$

For $y_0 \in B_\delta(x_0) \cap \Omega_0$ and $d = y_0 - x_0$, note that $|d| < \delta$. Thus, we know from Lemma 69 for $y^s = x^s + d = y_0 + (x^s - x_0)$ and $\tilde{\xi} = \xi_1 + d \in X_{\text{ad}}(y_0, y^s)$ that

$$l(\tilde{\xi}) \leq \frac{l(\xi_1)}{1 - |d|L/\underline{F}} < \frac{t(1 - \delta L/\underline{F})}{1 - \delta L/\underline{F}} = t.$$

Hence $y^s \in \Omega_t$, so that we have shown the inclusion

$$(B_\delta(x_0) \cap \Omega_0) + (x^s - x_0) \subset B_\delta(x^s) \cap \Omega_t. \quad (122)$$

In the case $\delta \geq \underline{F}/L$, we have $s = t$ and $x^s = x_0$. Since $F \geq 0$ and thus $\Omega_0 \subset \Omega_t$, the inclusion (122) holds also in this situation.

As the next step, take note that

$$|y^s - x| \leq |x - x^s| + |x^s - y^s| < \overline{F}s + \delta \leq t\delta L \frac{\overline{F}}{\underline{F}} + \delta = \rho$$

for all $y^s \in B_\delta(x^s)$. This implies $B_\delta(x^s) \subset B_\rho(x)$. Thus, since the shift is a rigid transformation and preserves volumes, we finally get

$$\text{vol}(B_\rho(x) \cap \Omega_t) \geq \text{vol}(B_\delta(x^s) \cap \Omega_t) \geq \text{vol}(B_\delta(x_0) \cap \Omega_0) \geq c_0 \cdot \text{vol}(B_\delta(x_0)) = c_0 \cdot \left(\frac{\delta}{\rho}\right)^n \cdot \text{vol}(B_\rho(x)).$$

The claim now follows by expressing δ/ρ with (121). \square

7.2.3 Shape-Dependent Quantities

Let us now try to understand better how f in (120) depends on the shape Ω . We are particularly interested in domain functionals. Hence, the most important step is to observe how the *volume* behaves as shape-dependent quantity when the underlying speed field is varied. As we will see in Lemma 72, it turns out that the volume is actually Lipschitz continuous with respect to F under certain assumptions. This result can also be generalised to more complicated shape-dependent quantities of the form analysed already in Section 4.2, i. e., (52), (57). We will do that in Lemma 73.

Our main tool in estimating volume differences is Theorem 21 combined with the uniform-density properties shown in Subsection 7.2.2. However, we also need to get a handle on the perimeter of evolved sets. This is the problem tackled, for the case $F = 1$, in Chapter 5. Unfortunately, the results there are not general enough for our purposes here. Thus, we have to *assume* the necessary properties for now. We believe that our assumption is likely true in general, but do not yet have a proof for it.

Assumption 4. Let $\Omega_0 \subset \mathbb{R}^n$ and L be given. We assume that there exist P and $t_p > 0$ such that

$$P(\Omega_t(F)) \leq P$$

holds for all $t \in [0, t_p]$ and speed fields F with Lipschitz constant L . Here, $\Omega_t(F)$ denotes the time evolution of Ω_0 at time t according to the speed field F .

Under this assumption, we can now apply Theorem 21 to estimate the volume of a band of width ρ around an evolved set Ω_t :

Lemma 71. *Let F have Lipschitz constant L and Ω_0 have (ρ_0, c) -uniform lower density. Furthermore, let Assumption 4 hold. Then*

$$\text{vol}(\Omega_{t+\rho} \setminus \Omega_t) \leq \rho \cdot \bar{F} \left(1 + \left(\frac{1}{c} \right)^{\frac{n-1}{n}} \left(1 + tL \frac{\bar{F}}{\underline{F}} \right)^{n-1} \right) PC$$

for all $t \in [0, t_p]$, $\rho \in (0, \rho_0)$ and with some dimensional constant C .

Proof. According to Lemma 70, the evolved set Ω_t has (ρ_0, c') -uniform lower density with

$$c' = c \left(1 + tL \frac{\bar{F}}{\underline{F}} \right)^{-n}. \quad (123)$$

Note that $0 \leq F \leq \bar{F}$ implies the inclusion

$$\Omega_{t+\rho} \setminus \overline{\Omega_t} \subset U_{\rho \bar{F}},$$

where $U_{\rho \bar{F}}$ is the newly created volume according to Definition 18 based on Ω_t as the initial geometry. Thus, Theorem 21 implies

$$\text{vol}(\Omega_{t+\rho} \setminus \Omega_t) \leq \rho \bar{F} \cdot \left(1 + \frac{1}{c'} \right)^{\frac{n-1}{n}} P(\Omega_t) C' \leq \rho \bar{F} \cdot \left(1 + \left(\frac{1}{c'} \right)^{\frac{n-1}{n}} \right) P(\Omega_t) C.$$

This finishes the proof if we use the explicit form of c' in (123) and Assumption 4 for $P(\Omega_t)$. \square

With this result, we can now show a general Lipschitz estimate for the volume of the evolved domain. This estimate allows both the times and the speed fields for the compared evolutions to be different:

Lemma 72. Let $\underline{F} \leq F, G \leq \overline{F}$ be two speed fields with Lipschitz constant L . Let Ω_0 have (ρ_0, c) -uniform lower density and let Assumption 4 hold. Then

$$|\text{vol}(\Omega_t(F)) - \text{vol}(\Omega_s(G))| \leq \text{vol}(\Omega_t(F) \Delta \Omega_s(G)) \leq K \left(\frac{\overline{F}}{\underline{F}^2} \cdot \max(s, t) \cdot \|F - G\|_\infty + |t - s| \right) \quad (124)$$

for all $s, t \in [0, t_0]$, where

$$t_0 = \min \left(t_p, \frac{\rho_0}{1 + (\overline{F}/\underline{F})^2} \right), \quad K = \overline{F} \left(1 + \left(\frac{1}{c} \right)^{\frac{n-1}{n}} \left(1 + t_0 L \frac{\overline{F}}{\underline{F}} \right)^{n-1} \right) PC \quad (125)$$

and C is a dimensional constant.

Proof. The first half of (124) is a general property of the symmetric set difference: If A and B are two arbitrary sets, then

$$\begin{aligned} |\text{vol}(A) - \text{vol}(B)| &= |\text{vol}(A \cap B) + \text{vol}(A \setminus B) - \text{vol}(B \cap A) - \text{vol}(B \setminus A)| \\ &\leq \text{vol}(A \setminus B) + \text{vol}(B \setminus A) = \text{vol}(A \Delta B). \end{aligned}$$

(This can be seen as a variant of the inverse triangle inequality.) Furthermore, set $\tilde{F} = \min(F, G)$, $\tilde{G} = \max(F, G)$, $\tilde{t} = \min(t, s)$ and $\tilde{s} = \max(t, s)$. Then

$$\Omega_{\tilde{t}}(\tilde{F}) \subset \Omega_t(F) \cap \Omega_s(G) \subset \Omega_t(F) \cup \Omega_s(G) \subset \Omega_{\tilde{s}}(\tilde{G}).$$

This yields, in particular, the relation

$$\Omega_t(F) \Delta \Omega_s(G) \subset \Omega_{\tilde{s}}(\tilde{G}) \setminus \Omega_{\tilde{t}}(\tilde{F}) = \Omega_{\tilde{s}}(\tilde{G}) \Delta \Omega_{\tilde{t}}(\tilde{F}).$$

Note that $\|F - G\|_\infty = \|\tilde{F} - \tilde{G}\|_\infty$ and $|t - s| = |\tilde{t} - \tilde{s}|$. This implies that the right-hand side of (124) is not changed if we formulate it using \tilde{F} , \tilde{G} instead of F , G and with \tilde{t} , \tilde{s} instead of t , s . Hence, we may assume, without loss of generality, that $F \leq G$ and $t \leq s$. It remains to estimate $\text{vol}(\Omega_s(G) \setminus \Omega_t(F))$.

For this, choose $x \in \Omega_s(G) \setminus \Omega_t(F)$ arbitrarily. Note that $x \in E_{s'}$ with $s' = \overline{F}/\underline{F} \cdot s$ and, per assumption, $s = \max(s, t)$. Thus, Lemma 68 gives

$$d_0(x; F) \leq d_0(x; G) + \frac{\overline{F}}{\underline{F}^2} s \|F - G\|_\infty < s + \frac{\overline{F}}{\underline{F}^2} s \|F - G\|_\infty = t + \frac{\overline{F}}{\underline{F}^2} \cdot \max(s, t) \cdot \|F - G\|_\infty + |t - s|.$$

If we set

$$\rho = \frac{\overline{F}}{\underline{F}^2} \cdot \max(s, t) \cdot \|F - G\|_\infty + |t - s|,$$

this implies $x \in \Omega_{t+\rho}(F)$. Hence, we have shown the inclusion

$$\Omega_s(G) \setminus \Omega_t(F) \subset \Omega_{t+\rho}(F) \setminus \Omega_t(F).$$

Also, since $\|F - G\|_\infty \leq \overline{F}$ and $|t - s| < t_0$, we know

$$\rho < t_0 \left(1 + \left(\frac{\overline{F}}{\underline{F}} \right)^2 \right) \leq \rho_0.$$

This means that we can apply Lemma 71 to finish the proof. \square

So far, we have considered, in particular, the *volume* as a simple shape-dependent quantity. However, note that Lemma 72 allows us to control the symmetric set difference $\Omega_t(F) \Delta \Omega_s(G)$ and not only the volume difference. Based on this, we can generalise the result to other, more complex *domain functionals*. Let us first define an abstract notion for the Lipschitz property (124):

Definition 25. Let Q be a shape-dependent quantity and $\Omega_0 \subset \mathbb{R}^n$ be an initial domain. We say that Q is *Lipschitz regular* at Ω_0 if there exists a constant C such that

$$|Q(\Omega_t(F)) - Q(\Omega_s(G))| \leq C (\max(s, t) \cdot \|F - G\|_\infty + |t - s|)$$

for all L , an upper bound $t_0 = t_0(L)$, all $s, t \in [0, t_0]$ and all speed fields F, G with Lipschitz constant L . In particular, note that C must be independent of L while t_0 may depend on the Lipschitz constant.

The volume $\text{vol}(\cdot)$ is Lipschitz regular according to Lemma 72: While the constant K in (125) depends on L , we can always choose t_0 smaller in order to ensure, for instance, $t_0 L \bar{F} / \underline{F} \leq 1$. With this trick,

$$K \leq \bar{F} \left(1 + 2^{n-1} \left(\frac{1}{c} \right)^{\frac{n-1}{n}} \right) PC \quad (126)$$

independently of L by making t_0 depend on L instead. Reducing t_0 a little also ensures that Lemma 72 holds for all $s, t \in [0, t_0]$ with the upper bound included. Similarly, also more general domain functionals are Lipschitz regular if the integrand depends on the shape only via other Lipschitz regular quantities:

Lemma 73. *Let Ω_0 be bounded, have uniform lower density and let Assumption 4 hold. Assume that Q_1, \dots, Q_k are Lipschitz regular at Ω_0 . Furthermore, let Q be a shape-dependent quantity according to (52) and (57), i. e.,*

$$Q(\Omega) = \int_{\Omega} g(x, Q_1(\Omega), \dots, Q_k(\Omega)) dx.$$

If the integrand $g: \mathbb{R}^n \times \mathbb{R}^k \rightarrow \mathbb{R}$ is Lipschitz continuous, then Q itself is Lipschitz regular at Ω_0 .

Proof. Let some Lipschitz constant L be fixed and choose t_0 as the minimum of all time intervals for Lipschitz regularity of the Q 's and small enough that Lemma 72 holds. Note that boundedness of Ω_0 ensures that all evolved sets $\Omega_t(F)$, with $t \in [0, t_0]$ and $\underline{F} \leq F \leq \bar{F}$, are bounded themselves. Hence, we may assume, without loss of generality, that g is bounded. For simplicity, we introduce the short-hand notation $g(x, \Omega) = g(x, Q_1(\Omega), \dots, Q_k(\Omega))$.

Let now $s, t \in [0, t_0]$ and F, G be given. By the triangle inequality, it follows that

$$\begin{aligned} |Q(\Omega_t(F)) - Q(\Omega_s(G))| &\leq \left| \int_{\Omega_t(F)} g(x, \Omega_t(F)) dx - \int_{\Omega_s(G)} g(x, \Omega_t(F)) dx \right| \\ &\quad + \int_{\Omega_s(G)} |g(x, \Omega_t(F)) - g(x, \Omega_s(G))| dx. \end{aligned}$$

The first term expresses the difference introduced by the explicit Ω -dependence of Q via the domain of integration, while the latter shows the difference due to the shape dependence of the integrand g itself. If we denote the Lipschitz constant of g by L_g , we can further estimate both terms to get

$$|Q(\Omega_t(F)) - Q(\Omega_s(G))| \leq \text{vol}(\Omega_t(F) \Delta \Omega_s(G)) \cdot \|g\|_\infty + \text{vol}(\Omega_s(G)) \cdot L_g \sum_{i=1}^k |Q_i(\Omega_t(F)) - Q_i(\Omega_s(G))|.$$

The claim now follows if we use Lemma 72 for the symmetric set difference and the assumed Lipschitz regularity of all Q 's. (Note that $\text{vol}(\Omega_s(G))$ is bounded independently of G and s .) \square

Recall that the primary goal of the analysis above is to find a contraction property of the iteration $F \mapsto \psi(F)$. For this, we are specifically interested in the case that the times t and s are not explicit but defined implicitly as the arrival times at some fixed $x \in \mathbb{R}^n \setminus \Omega_0$. Let us write $Q(x; F) = Q(\Omega_t(F))$ in this situation, where $t = d_0(x; F)$ and Q is some shape-dependent quantity. Using Lemma 68, we can easily arrive at the following conclusion:

Lemma 74. *Let Q be Lipschitz regular and fix the Lipschitz constant L . Choose $t \in [0, t_0]$. Then*

$$|Q(x; F) - Q(x; G)| \leq Ct \left(1 + \frac{1}{\underline{F}} \right) \|F - G\|_\infty$$

for all $x \in E_t$ and speed fields F, G that admit the Lipschitz constant L .

Proof. According to Lipschitz regularity, we have

$$|Q(x; F) - Q(x; G)| \leq C (\max(d_0(x; F), d_0(x; G)) \|F - G\|_\infty + |d_0(x; F) - d_0(x; G)|).$$

Since $x \in E_t$, clearly $\max(d_0(x; F), d_0(x; G)) \leq t$. Furthermore, Lemma 68 implies

$$|d_0(x; F) - d_0(x; G)| \leq \frac{t}{\underline{F}} \|F - G\|_\infty.$$

With this, the claim follows. \square

7.2.4 Convergence of the Fixed-Point Iteration

With all the technical preparations in place now, we can finally show the two important properties of ψ that we have claimed at the beginning of this section: Namely that iteration with ψ converges to a fixed point and that there exists a uniform Lipschitz constant for all iterated speed fields and for the limit. Let us recall (120) and assume that the shape dependence of f is only via Lipschitz regular quantities Q_1, \dots, Q_k , i. e.,

$$f: \mathbb{R}^n \times \mathbb{R}^k \rightarrow \mathbb{R}, \quad f(x, \Omega) = f(x, Q_1(\Omega), \dots, Q_k(\Omega)). \quad (127)$$

Denote by C a constant for Lipschitz regularity that works for all Q 's and by $t_0 = t_0(L)$ the minimum time interval. Furthermore, let $0 < \underline{F} \leq -f \leq \overline{F}$ and f have Lipschitz constant L_f . This ensures, first of all, that any speed field F defined via (120) is between \underline{F} and \overline{F} . Thus, all iterated speed fields are automatically bounded away from zero as we have assumed it above.

Note that this is a practically quite restricting requirement: Particularly for optimisation, we would much rather allow a convergence towards zero, which occurs at a critical point. If we do not impose this restriction, however, we can not guarantee that iterated speed fields are Lipschitz continuous and thus consistent with our theory developed in the previous chapters. This can be seen in Example 15. Nevertheless, the results of Section 7.4 show that the self-consistent gradient flow still works for optimisation purposes in practice.

Example 15. Consider the initial speed field

$$F(x) = \begin{cases} 0 & \text{if } x \leq 0, \\ 1 & \text{if } x \geq 1, \\ x & \text{else.} \end{cases}$$

Clearly, F is Lipschitz continuous, bounded and non-negative. It does not, however, have a strictly positive lower bound $\underline{F} > 0$. Choose now $\Omega_0 = (1, 2)$. Then $d_0(x) = x - 2$ for all $x \geq 2$, while

$$d_0(x) = \left| \int_1^x \frac{1}{F(\xi)} d\xi \right| = \int_x^1 \frac{1}{\xi} d\xi = -\log x$$

for $x \in (0, 1]$. When Ω_0 evolves in time according to F , the set grows with a constant rate to the right. In particular, note that $\text{vol}(\Omega_t) \geq 1 + t$. On the other hand, it takes the left boundary of the evolving Ω_t infinitely long to move from one to zero. Thus, $\text{vol}(\Omega; x)$ defined via the arrival time at x is *not* Lipschitz continuous in x : Define the sequence $x_k = 2^{-k}$ for $k \in \mathbb{N}$. Then clearly $|x_k - x_{k-1}| = 2^{-k} \rightarrow 0$ with $k \rightarrow \infty$. On the other hand, since

$$|d_0(x_k) - d_0(x_{k-1})| = \log \frac{x_{k-1}}{x_k} = \log 2,$$

we find that

$$\text{vol}(\Omega; x_k) - \text{vol}(\Omega; x_{k-1}) \geq \log 2 \not\rightarrow 0.$$

Thus, Lemma 72 is, indeed, not true in this situation. It is now easy to choose $f(\Omega) = f(\text{vol}(\Omega))$ in such a way that $\psi(F)$ defined by (120) will not be Lipschitz continuous as well.

As a first step, let us show a generic Lipschitz estimate for $\psi(F)$. This works similar to Lemma 74 by combining Lipschitz regularity with an estimate for the arrival times. However, note that this time the estimate is in space between x and y for a single speed field F , while Lemma 74 had x fixed and *two different* speed fields F and G .

Lemma 75. *Let F be a speed field with Lipschitz constant L and assume that f has the form described above. This then implies*

$$|\psi(F)(x) - \psi(F)(y)| \leq L_f \left(1 + k \frac{C}{\underline{F}}\right) \cdot |x - y|$$

for all $x, y \in E_{t_0}$.

Proof. Clearly $d_0(x)$ and $d_0(y)$ are both in $[0, t_0]$. Hence Lipschitz regularity of all Q 's implies

$$|Q_i(x; F) - Q_i(y; F)| \leq C |d_0(x) - d_0(y)|$$

for $i = 1, \dots, k$. Recall that we assume a strictly positive lower bound \underline{F} on the speed field F . With this additional information, the proof of Lemma 34 implies that d_0 has the (global) Lipschitz constant $1/\underline{F}$. Since f is Lipschitz continuous and ψ defined via (120), we get the claimed

$$\begin{aligned} |\psi(F)(x) - \psi(F)(y)| &\leq L_f |x - y| + L_f \sum_{i=1}^k |Q_i(x; F) - Q_i(y; F)| \\ &\leq L_f (|x - y| + kC |d_0(x) - d_0(y)|) \leq L_f \left(1 + k \frac{C}{\underline{F}}\right) \cdot |x - y|. \end{aligned}$$

□

For proving convergence of the fixed-point iteration with ψ , we want to apply Banach's fixed-point theorem. For that, we need two ingredients: A contraction property of the iteration mapping ψ and an invariant, closed subset of a Banach space. Let us define the latter now:

Definition 26. We denote the Lipschitz constant of Lemma 75 by L_0 , i. e.,

$$L_0 = L_f \left(1 + k \frac{C}{\underline{F}}\right).$$

For $t \geq 0$, we define

$$X(t) = \{ F: E_t \rightarrow [\underline{F}, \overline{F}] \mid F \text{ has Lipschitz constant } L_0 \} \subset C(E_t).$$

Furthermore, let us introduce

$$\|\psi\|_{X(t)} = \sup_{F, G \in X(t)} \frac{\|\psi(F) - \psi(G)\|_\infty}{\|F - G\|_\infty}$$

for the (a-priori possibly infinite) Lipschitz constant of the fixed-point operator ψ .

It is easy to see that $X(t)$ is a suitable set for our purposes:

Lemma 76. *Let $t \geq 0$. The set $X(t) \subset C(E_t)$ is closed. If $t \leq t_0$ with t_0 chosen according to L_0 , then $X(t)$ is, in addition, invariant under application of ψ and*

$$\|\psi\|_{X(t)} \leq t \cdot L_f C k \left(1 + \frac{1}{\underline{F}}\right).$$

Proof. It is clear that $X(t) \subset C(E_t)$ and that the latter is a Banach space. Let $(F_k)_{k \in \mathbb{N}} \subset X(t)$ be a sequence converging towards some $F \in C(E_t)$. To show that $F \in X(t)$, we have to show that the limit F is Lipschitz continuous itself with the same constant L_0 . To see this, let $x, y \in E_t$. Then

$$|F(x) - F(y)| \leq |F(x) - F_k(x)| + |F_k(x) - F_k(y)| + |F_k(y) - F(y)| \leq L_0 |x - y| + 2 \|F - F_k\|_\infty$$

for arbitrary $k \in \mathbb{N}$. This implies that $|F(x) - F(y)| \leq L_0 |x - y|$ and thus $F \in X(t)$. Invariance under ψ follows from Lemma 75. The lower and upper bounds \underline{F} and \overline{F} hold because they are true for $-f$.

It remains to estimate the Lipschitz constant of ψ . For this, let $x \in E_t$ be arbitrary. Then

$$|\psi(F)(x) - \psi(G)(x)| \leq L_f \sum_{i=1}^k |Q_i(x; F) - Q_i(x; G)| \leq t \cdot L_f C k \left(1 + \frac{1}{\underline{F}}\right) \cdot \|F - G\|_\infty$$

according to Lemma 74. This implies the claim. □

Note, specifically, that we can turn ψ into a contraction if we choose t so small that $\|\psi\|_{X(t)} < 1$. Taking all together, we have shown the following local existence of a fixed point:

Theorem 25. *Let f have the form (127) and let all shape-dependent quantities Q_i be domain functionals according to (52) and (57). The integrands may be shape dependent themselves if the shape dependence is, again, of this form. Furthermore, assume that*

- f is Lipschitz continuous and $0 < \underline{F} \leq -f \leq \overline{F}$,
- Ω_0 has uniform lower density, and
- Assumption 4 holds.

Then there exists a time $t > 0$ such that ψ has a unique fixed point F^ on E_t . Iteration with ψ converges towards F^* starting from any speed field in $X(t)$. All iterates and F^* itself are Lipschitz continuous. Any constant speed field with value in $[\underline{F}, \overline{F}]$ is a suitable starting point for the fixed-point iteration. The speed field F^* is a self-consistent gradient flow according to Definition 24 for times up to t .*

7.3 A Strategy for Globalisation

In the previous section, we discussed the existence of a self-consistent gradient flow *locally* around the initial geometry Ω_0 . Let us now consider a possible way to globalise the result of Theorem 25. The strategy that we have in mind is the following: Use Theorem 25 to construct a self-consistent speed field F^* in E_t , then propagate the initial geometry along F^* for a time short enough to remain in E_t . Afterwards, use the resulting geometry as new Ω_0 to construct another band, and so on. This idea is precisely what we will employ for numerical computations in Section 7.4. It is, however, also justified from a purely theoretical point of view. We will see in Theorem 26 that this idea can, indeed, be used to construct a fixed point of ψ on an extended area. Unfortunately, it is not guaranteed that even the repeated addition of new bands leads to a self-consistent gradient flow on the whole domain. It may happen that the widths of our bands shrink so fast that also the union of infinitely many of them is still just a bounded set. We will discuss this situation at the end of the current section.

The first important piece of information is the following *forward-in-time property*: If two speed fields are equal close to the initial geometry, this implies that d_0 is equal for both speed fields in that area as well. Consequently, also evolved sets (and thus all shape-dependent quantities) are equal for small enough times. This implies, in particular, that the property of F being a fixed point of ψ on E_t can never be destroyed by iterating with ψ , even if we consider an extended area larger than E_t .

Lemma 77. *Let $F, G \geq 0$ be two Lipschitz continuous speed fields and $\Omega_0 \subset \mathbb{R}^n$ an initial domain. Assume that $F = G$ holds on $(\Omega_t(F) \cap \Omega_t(G)) \setminus \overline{\Omega_0}$ for some $t > 0$. Then $d_0(x; F) = d_0(x; G)$ for all $x \in \Omega_t(F) \cup \Omega_t(G)$ and $\Omega_s(F) = \Omega_s(G)$ for all $s \in [0, t]$.*

Proof. Since d_0 is continuous, it suffices to show equality for $x \in \Omega_t(F) \cup \Omega_t(G)$. So let, without loss of generality, $x \in \Omega_t(F)$ be given. If $x \in \overline{\Omega_0}$, then clearly $d_0(x; F) = d_0(x; G) = 0$. So assume $x \in \Omega_t(F) \setminus \overline{\Omega_0}$. According to Lemma 19 and Lemma 33, there exist $x_0 \in \Gamma_0$ and $\xi \in X_{\text{ad}}(x_0, x)$ such that $d_0(x; F) = l(\xi; F) < t$. Consider the set

$$S = \{\tau \in [0, 1) \mid F(\xi(\tau)) \neq G(\xi(\tau))\}$$

and assume that it is not empty. In that case, set $\tau_0 = \inf S$ and note that $\tau_0 \in [0, 1)$. Furthermore, by definition of S and τ_0 , we know that $F(\xi(\tau)) = G(\xi(\tau))$ for all $\tau \in [0, \tau_0]$. Thus, if we denote by $\xi_0 \in X_{\text{ad}}(x_0, \xi(\tau_0))$ the restriction of ξ to the time interval $[0, \tau_0]$, we can conclude

$$d_0(\xi(\tau_0); G) \leq l(\xi_0; G) = l(\xi_0; F) < t.$$

By continuity of d_0 and ξ , there exists $\tau > \tau_0$ such that this inequality still holds. In other words, $\xi(\tau) \in (\Omega_t(F) \cap \Omega_t(G)) \setminus \overline{\Omega_0}$. The same is, in fact, true for all $\tau' \in (0, \tau]$. This by assumption also implies $F(\xi(\tau')) = G(\xi(\tau'))$, which is a contradiction to the definition of τ_0 . Thus, S must be empty. This means that $F = G$ along the path ξ . Hence,

$$d_0(x; G) \leq l(\xi; G) = l(\xi; F) = d_0(x; F).$$

Finally, with this result, we know that $x \in \Omega_t(G)$. Thus, we can apply the same argument again with the roles of F and G exchanged. This implies $d_0(x; G) \geq d_0(x; F)$ and thus equality.

It remains to show that the evolved sets are equal as well. So let $s \in [0, t]$ be given and choose $x \in \Omega_s(F)$. By the previous result, we know that $d_0(x; G) = d_0(x; F) < s$, and thus $x \in \Omega_s(G)$. Similarly, we can also show $\Omega_s(G) \subset \Omega_s(F)$. \square

For the next step, we consider the situation that the initial set is changed to an already evolved domain. This is what happens when we want to add a second band around the first. The first lemma in this direction concerns the distance d_0 :

Lemma 78. *Let $F \geq 0$ be a Lipschitz continuous speed field and Ω_0 be given. For $t > 0$, we denote the evolution of Ω_0 by Ω_t as usual. Then*

$$d_0(x; \Omega_0) = t + d_0(x; \Omega_t)$$

for all $x \in \mathbb{R}^n \setminus \Omega_t$ with $d_0(x; \Omega_0) < \infty$.

Proof. Let $x^t \in \Gamma_t$ and $\xi_2 \in X_{\text{ad}}(x^t, x)$ be given such that $d_0(x; \Omega_t) = l(\xi_2)$. Furthermore, there also exist $x_0 \in \Gamma_0$ and $\xi_1 \in X_{\text{ad}}(x_0, x^t)$ with $t = d_0(x^t; \Omega_0) = l(\xi_1)$. Thus, defining $\xi \in X_{\text{ad}}(x_0, x)$ as the concatenation of ξ_1 and ξ_2 , we find

$$d_0(x; \Omega_0) \leq l(\xi) = l(\xi_1) + l(\xi_2) = t + d_0(x; \Omega_t).$$

For the other way round, choose $x_0 \in \Gamma_0$ and $\xi \in X_{\text{ad}}(x_0, x)$ with $l(\xi) = d_0(x; \Omega_0)$. Since $x \notin \Omega_t$, we know $l(\xi) \geq t$. Hence, by the intermediate-value theorem, there exists $\tau \in (0, 1]$ such that ξ_1 as the restriction of ξ to $[0, \tau]$ has $l(\xi_1) = t$. Clearly $x^t = \xi(\tau) \in \Gamma_t \cup \Omega_t$. Let $\xi_2 \in X_{\text{ad}}(x^t, x)$ be the restriction of ξ to the remaining time interval $[\tau, 1]$. Then

$$t + d_0(x; \Omega_t) \leq t + d(x^t, x) \leq t + l(\xi_2) = l(\xi_1) + l(\xi_2) = l(\xi) = d_0(x; \Omega_0).$$

Thus, equality holds. \square

Based on Lemma 78, we can now show a general *semi-group property* for the time evolution of our shapes. The semi-group property, in turn, allows us to analyse the behaviour of the iteration mapping ψ when the initial set is varied:

Lemma 79. *Let $F \geq 0$ be a Lipschitz continuous speed field, $\Omega_0 \subset \mathbb{R}^n$ be an initial domain and $s, t \geq 0$. We denote the evolution of the already evolved set Ω_t for a further time of s by $(\Omega_t)_s$. Then*

$$(\Omega_t)_s = \Omega_{s+t}.$$

Assume further $F \geq \underline{F} > 0$ and consider the iteration mapping ψ as before. Then

$$\psi(F; \Omega_0)(x) = \psi(F; \Omega_t)(x) \tag{128}$$

for all $x \in \mathbb{R}^n \setminus \Omega_t$.

Proof. Let $x \in (\Omega_t)_s$. By Theorem 7, this means $d_0(x; \Omega_t) < s$. Hence Lemma 78 implies $d_0(x; \Omega_0) < s + t$ and thus $x \in \Omega_{s+t}$. For the other inclusion, let $x \in \Omega_{s+t}$ be given. Then $d_0(x; \Omega_0) < s + t$. Again by Lemma 78, we can now conclude that $d_0(x; \Omega_t) < s$ and thus $x \in (\Omega_t)_s$ must be true. This shows the claimed semi-group property.

Let now be $F \geq \underline{F} > 0$ and $x \in \mathbb{R}^n \setminus \Omega_t$. The lower bound on F ensures that $d_0(x)$ is finite. Set $s = d_0(x; \Omega_t)$. Then Lemma 78 implies

$$d_0(x; \Omega_0) = t + d_0(x; \Omega_t) = t + s,$$

so that $\Omega(x; \Omega_0) = \Omega_{s+t}$. On the other hand, $\Omega(x; \Omega_t) = (\Omega_t)_s$. The semi-group property ensures that both sets are equal. Consequently also (128) holds. \square

Based on the previous results, we can now conclude that it is, indeed, possible to first construct a self-consistent speed field on some band E_t , then evolve the domain according to this speed field, and finally look for another band starting from the evolved domain. The resulting combined speed field is then a fixed point of ψ on the extended band. In particular:

Theorem 26. *Let F_1 be a fixed point of ψ on $E_t(\Omega_0)$ according to Theorem 25. Let $\tau > 0$ and $\Omega_\tau \subset E_t(\Omega_0)$ be the evolved set according to F_1 . Furthermore, assume that F_2 is a fixed point of ψ on $E_s(\Omega_\tau)$. Denote the extended area by $E = E_s(\Omega_\tau) \cup (\Omega_\tau \setminus \Omega_0)$ and introduce $F: E \rightarrow \mathbb{R}$ by*

$$F(x) = \begin{cases} F_1(x) & \text{for } x \in \Omega_\tau, \\ F_2(x) & \text{else.} \end{cases}$$

Then F is Lipschitz continuous and $\psi(F) = F$ on E .

Proof. Consider $x \in \Gamma_\tau$. Since both F_1 and F_2 are self-consistent gradient flows according to Definition 24, note that

$$F_1(x) = -f(x, \Omega_\tau) = F_2(x).$$

This implies that F is continuous across the interface Γ_τ . Both F_1 and F_2 are Lipschitz continuous on $E_t(\Omega_0)$ and $E_s(\Omega_\tau)$, respectively. Thus F is Lipschitz continuous as well. For $\psi(F)$, let us write

$$\psi(F)(x) = \begin{cases} \tilde{F}_1(x) & \text{for } x \in \Omega_\tau, \\ \tilde{F}_2(x) & \text{else.} \end{cases}$$

It remains to show that $F_1 = \tilde{F}_1$ and $F_2 = \tilde{F}_2$ on the respective subsets of E .

Choose first $x \in \Omega_\tau$. Note that F_1 is defined on the whole of $\mathbb{R}^n \setminus \Omega_0$, even though we know $F_1 = \psi(F_1)$ only on $E_t(\Omega_0)$. By definition, $F_1 = F$ on Ω_τ . Thus Lemma 77 implies that $d_0(x; F_1) = d_0(x; F)$ and also $\Omega(x; F_1) = \Omega(x; F)$. Hence

$$F(x) = F_1(x) = \psi(F_1; \Omega_0)(x) = \psi(F; \Omega_0)(x),$$

which shows that $F_1 = \tilde{F}_1$ on Ω_τ . Let now $x \in E_s(\Omega_\tau)$. Then

$$\psi(F)(x) = \psi(F; \Omega_0)(x) = \psi(F; \Omega_\tau)(x) = \psi(F_2; \Omega_\tau)(x) = F_2(x)$$

according to Lemma 79 and thus $F_2 = \tilde{F}_2$ on $E_s(\Omega_\tau)$. This finishes the proof. \square

Thus, we have seen that we can, roughly speaking, always extend the local region of Theorem 25 by yet another band. This allows us to enlarge it in theory with an infinite number of steps. This, however, does not guarantee that the resulting region will be arbitrarily large. It may happen that the widths of the extension bands shrink so fast that their sum remains bounded. In fact, a rough estimation of the possible extension widths implies that this is a case we have to expect. Let us conclude this section now with a discussion of this effect.

For this, we have to understand which quantities restrict the band width t in Theorem 25. Some of the constants that appear in the calculations throughout Section 7.2 describe only the properties of the problem at hand. They are neither influenced by the fixed-point iteration nor the fact that our initial geometry evolves from step to step in the extension process. Consequently, these constants are not of special interest for our purposes here. In particular, the values of \underline{F} , \overline{F} , L_f , n and k fall in this category. Furthermore, let us include Assumption 4 here as well. This is, of course, a very optimistic assumption: In general, we should actually expect that the estimate on the perimeter of Ω_t depends both on Ω_0 and the speed field F . However, we have no information about how this dependence may look like besides the statements for the case $F = 1$ in Chapter 5. We believe that it is, nevertheless, a good idea to make an *optimistic* assumption here since our final result for the extension area is still negative. All of these quantities will be included in a generic constant M in the following.

The remaining property that is important for our considerations below is uniform lower density of Ω_0 . It is definitely conceivable that the domain gets more irregular with every extension step. In particular, recall Lemma 70: The evolved set Ω_t has (ρ_0, c_t) -uniform lower density where ρ_0 matches the uniform lower density of the initial Ω_0 but c_t gets reduced from the initial c_0 according to

$$c_t = c_0 \cdot \left(1 + tL \cdot \frac{\overline{F}}{\underline{F}}\right)^{-n}. \quad (129)$$

This constant c , in turn, appears in the estimates of Subsection 7.2.3 and Subsection 7.2.4. Particularly important is also K estimated in (126):

$$K \leq M \cdot \left(\frac{1}{c}\right)^{\frac{n-1}{n}} \quad (130)$$

According to Lemma 72, this constant determines Lipschitz regularity of the volume functional. Via Lemma 73, it also influences Lipschitz regularity for more general domain functionals. Thus, let us use (130) for Lipschitz regularity in the estimates of Subsection 7.2.4. From Lemma 75, we know that the Lipschitz constant of the self-consistent speed field in a particular step can be bounded by

$$L \leq M \cdot \left(\frac{1}{c}\right)^{\frac{n-1}{n}}. \quad (131)$$

Finally, we get estimates on the possible band width t : For t to be admissible, the two main conditions are the following: First, we have required that $t_0 L \bar{F} / \underline{F} \leq 1$ to derive (126) and thus (130). Second, we need $\|\psi\|_{X(t)}$ in Lemma 76 to be small enough to get a contraction. Thus, the resulting length is, roughly, allowed to be

$$t = \frac{1}{M} \cdot \min\left(\frac{1}{L}, \frac{1}{K}\right) = \frac{1}{M} \cdot c^{\frac{n-1}{n}} \quad (132)$$

if M is suitably large (but independent of the extension step as discussed above).

With all these estimates in place, let us now consider what a potential sum of all band widths can be. For this, we have to combine (132) with (129). Recall that we require $t L \bar{F} / \underline{F} \leq 1$. With this additional information, (129) becomes

$$c_t \geq c_0 (1 + 1)^{-n} = \frac{c_0}{2^n}.$$

Thus, the constant c at the m -th extension step is $c_m = c_0 \cdot (2^{-n})^m$. Consequently,

$$t_m = \frac{1}{M} \cdot c_m^{\frac{n-1}{n}} = \frac{1}{M} c_0^{\frac{n-1}{n}} \cdot \left(\frac{1}{2^{n-1}}\right)^m$$

is an allowed band width at this step. As a geometric series, we finally see that

$$\sum_{m=0}^{\infty} t_m = \frac{1}{M} c_0^{\frac{n-1}{n}} \cdot \sum_{m=0}^{\infty} \left(\frac{1}{2^{n-1}}\right)^m = \frac{1}{M} c_0^{\frac{n-1}{n}} \frac{2^n}{2^n - 2} < \infty.$$

(Under the assumption $n \geq 2$. For $n = 1$, the situation is not interesting. In that case, the evolving domain has no chance to become “more irregular”, so that an infinite extension actually works.)

Another approach to the same conclusion is the following: If we introduce $\lambda(t) = \log c_t$, the relation (129) can be turned into

$$\lambda(t) - \lambda(0) = -n \log\left(1 + tL \cdot \frac{\bar{F}}{\underline{F}}\right) \Rightarrow \dot{\lambda}(t) = - \lim_{t \rightarrow 0^+} \frac{n}{t} \log\left(1 + tL \cdot \frac{\bar{F}}{\underline{F}}\right) = -n \frac{\bar{F}}{\underline{F}} \cdot L.$$

Since the expected behaviour of the extension steps is to have a band width that tends to zero, it makes sense to consider t as a continuous variable and, furthermore, the limit $t \rightarrow 0^+$ above. The quantity L on the right-hand side of the differential equation depends on $c(t)$ according to (131). Note that $c \in (0, 1)$ and thus $\lambda < 0$. Let us introduce $\mu = -\lambda > 0$ instead. If we also redefine the generic constant M accordingly, this yields

$$-\dot{\lambda}(t) = \dot{\mu}(t) = M \left(\frac{1}{c}\right)^{\frac{n-1}{n}} = M \exp\left(-\frac{n-1}{n} \lambda(t)\right) = M \alpha^{\mu(t)}. \quad (133)$$

Here, $\alpha = \exp((n-1)/n)$. If $n \geq 2$, we have $\alpha > 1$. In this situation, (133) blows up in finite time. This corresponds to $c \rightarrow 0^+$, such that the extension process gets stuck and the self-consistent gradient flow exists only on a bounded region. For the situation $n = 1$, on the other hand, $\alpha = 1$ and the equation has a solution for all times.

Let us now briefly summarise what we have seen in this section: First, it is possible to perform multiple extension steps according to Theorem 25 after each other and to combine them to get an extended self-consistent gradient flow. Second, however, it is not necessarily the case that this procedure allows to define such a gradient flow on an arbitrarily large region. The crucial issue is how uniform lower density of the geometry degenerates with each extension step. Thus, if we know for some reason (or simply assume) that all iterated domains have a *uniform* constant c , then we can, indeed, generate a globalised version of the gradient flow.

7.4 Numerical Results

Following up on the theoretical analysis in Section 7.2, let us now discuss numerical computations based on the idea of self-consistent gradient flows. The numerical evaluation of ψ for a single fixed-point iteration follows the description given already in Section 7.1. In order to build a complete optimisation procedure out of it, let us recall two important difficulties that arose in the theoretical analysis: First, the result of Theorem 25 is only local in nature. To work around this issue, we employ the strategy described above in Section 7.3 and, in particular, Theorem 26. Instead of trying to really find *a single* self-consistent speed field for the whole descent, we perform multiple steps:

1. Choose a *step length* t_0 that is small enough. For our purposes, it was always enough to consider t_0 simply as a fixed parameter in the algorithm. It could, however, also be chosen based on some convergence criteria if necessary.
2. Choose some initial speed field F_0 . A possible choice is the steepest-descent speed under the assumption that all shape-dependent quantities are constant, i. e.,

$$F_0(x) = -f(x, \Omega_0).$$

3. Evaluate $\psi(F_0)$ numerically on a suitable neighbourhood of Ω_0 . Iterate ψ a few times until a fixed point F^* is found approximately.
4. Propagate Ω_0 along F^* up to time t_0 . Repeat the procedure with the new set as Ω_0 .

The second difficulty to keep in mind is that all analysis above assumed $0 < \underline{F} \leq F \leq \overline{F}$. In the context of an optimisation algorithm, we actually expect the speed field to converge to zero when the shape approaches a critical point. Furthermore, it is very restrictive to assume that the shape only grows throughout the optimisation descent. This assumption can be violated even if the initial domain is a subset of the final optimal shape. We will demonstrate this situation on a simple example in Subsection 7.4.1. In this example, the real gradient flow is such that certain points $x \notin \Omega_0$ come to lie *twice* on the boundary of the evolving domain during the whole propagation: Once when they are temporarily added to the current shape and once when they are removed from it again later on. It will turn out, however, that these situations pose no problem to the *multi-step optimisation strategy* described above. Each step is, of course, limited to monotone behaviour in the sense that each point can, at most, either be added to or removed from Ω_0 at a single instant in time. During the course of multiple steps, however, the “direction of monotonicity” may change. This is another reason in favour of a multi-step approach with a finite step length t_0 for each iteration. We will see below that it does, indeed, work very well for practical shape optimisation.

Let us also briefly revisit the analysis of the Wolfe conditions (see Section 6.4) in light of this multi-step algorithm: If t_0 at a particular iteration can be chosen to fulfil the Wolfe conditions (see Theorem 23), then the directional derivative $dJ(\Omega_{t_0}; F)$ corresponds, by definition of the self-consistent speed field F , to the gradient norm *of the next iterate*. In this case, no uniform continuity is needed. Instead, the curvature condition (108) implies directly that the gradient norm decreases geometrically with each iteration. Note, however, that there is no guarantee that the step length t_0 for which the fixed-point iteration produces a self-consistent speed field is long enough to satisfy the Wolfe conditions. Furthermore, as mentioned already, our assumption $F \geq \underline{F} > 0$ for the speed field breaks down if we try to analyse convergence to a critical point. Thus, this is an interesting idea, but it needs further research.

7.4.1 Demonstration in 1D

Before we turn our attention back to the image-segmentation problem of Chapter 6, let us first consider a modified version in only one dimension. This simplified problem allows us to demonstrate some basic properties of our multi-step gradient-flow algorithm. In particular, we want to minimise the cost function

$$J(\Omega) = \int_{\Omega} (u(x) - u_0)^2 dx + \frac{\gamma}{\text{vol}(\Omega)}. \quad (134)$$

This is similar to (102) of our image-segmentation model, but note that u_0 is assumed to be independent of the shape Ω here. Also the form of the balloon force with $\text{vol}(\Omega)$ is changed. Based on the results of Section 6.1, we can easily compute the shape derivative of (134) to be

$$dJ(\Omega; F) = \int_{\Gamma} \left((u - u_0)^2 - \frac{\gamma}{\text{vol}(\Omega)^2} \right) F d\sigma. \quad (135)$$

In other words, moving Γ across some point x is beneficial if and only if

$$|u(x) - u_0|^2 < \frac{\gamma}{\text{vol}(\Omega)^2}.$$

From this equation, we can clearly see that this tolerance for adding points to the domain decreases if the volume of Ω grows. This is a main feature of the new balloon force in comparison to the one used in the original image-segmentation model (102).

Shape optimisation itself simplifies a lot if only one space dimension is used. If, in particular, the initial domain $\Omega_0 = (a_0, b_0)$ is an interval, it is enough to track the movement of the interval's boundary points in time to describe the shape evolution. In other words, we only have to solve a two-dimensional ODE instead of the level-set equation to compute the domain's time propagation:

$$\begin{aligned} \dot{a}(t) &= -F(a(t), \Omega_t) = -F(a(t), a(t), b(t)), \\ \dot{b}(t) &= F(b(t), \Omega_t) = F(b(t), a(t), b(t)) \end{aligned}$$

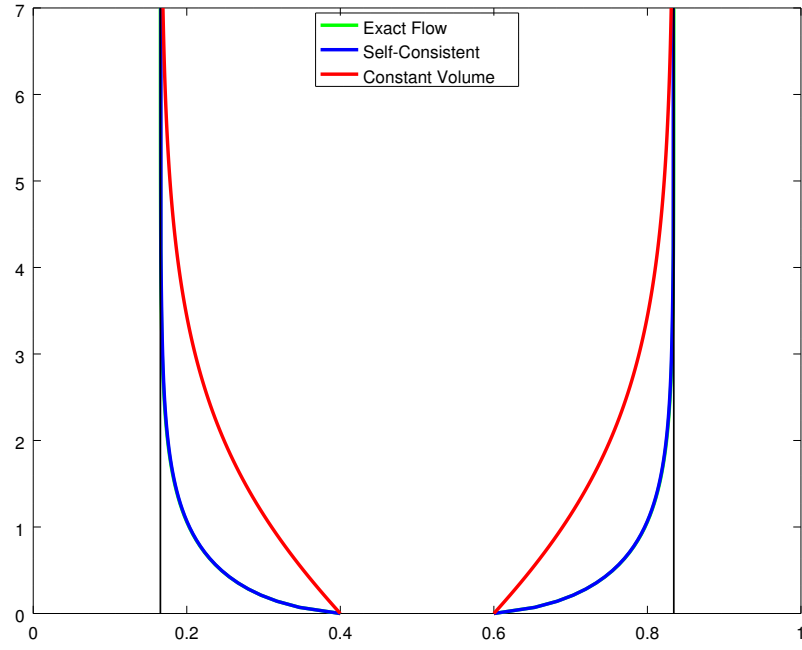
with initial values $a(0) = a_0$ and $b(0) = b_0$. This is, of course, much easier. It even allows us to compute the *exact gradient flow* just by using an ODE solver. The speed field corresponding to the steepest descent depends only on the current shape's volume $\text{vol}(\Omega_t) = b(t) - a(t)$ and follows from (135). In particular, we have

$$F(x, a, b) = \frac{\gamma}{(b - a)^2} - (u(x) - u_0)^2. \quad (136)$$

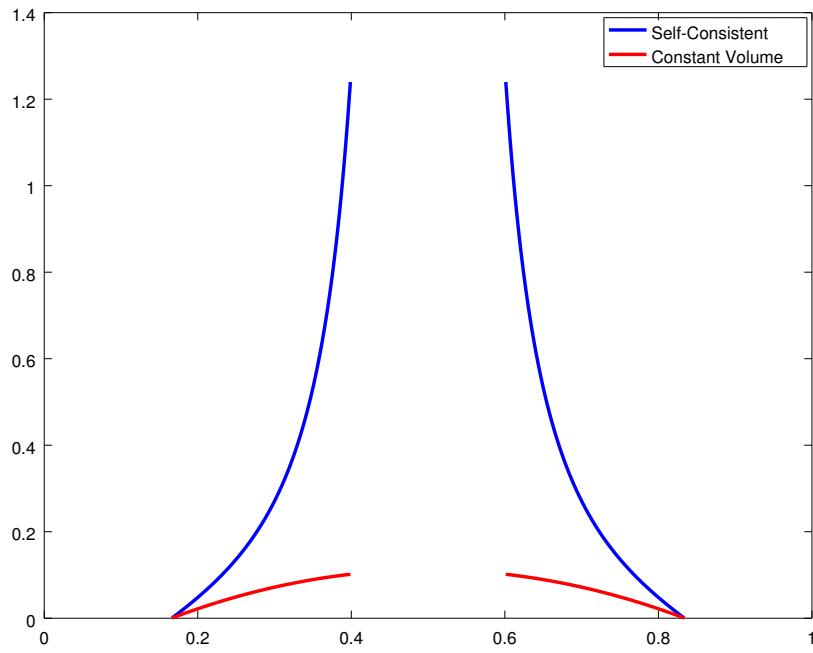
Let us simplify the problem even further: We assume that the “image” u is fixed as $u(x) = x$. For this situation, we expect that the optimal shape is given by an interval $(a^*, b^*) = (u_0 - \delta, u_0 + \delta)$ symmetric around u_0 . The width 2δ depends on the parameter γ and arises when the error term $(u - u_0)^2 = \delta^2$ and the balloon force $\gamma/(b - a)^2 = \gamma/(2\delta)^2$ are in equilibrium. This is the case for

$$\delta = \sqrt[4]{\frac{\gamma}{4}} \Rightarrow a^* = u_0 - \delta, b^* = u_0 + \delta.$$

The numerical results for $\gamma = 5 \cdot 10^{-2}$ and the symmetric initial shape $(a_0, b_0) = (0.4, 0.6)$ are shown in Figure 55. In this situation, the shape grows monotonically until it reaches the optimal interval indicated by the vertical lines in Figure 55a. The blue line shows the shape evolution according to the self-consistent gradient flow. It matches the exact gradient flow (green line) almost perfectly. For this situation with monotonic growth, only a single step of the procedure outlined above is necessary. The speed field itself is shown in Figure 55b. It vanishes at a^* and b^* . This corresponds to the behaviour that the evolving shape converges to the optimal interval for $t \rightarrow \infty$. Let us also show that self-consistency really makes a difference: The red line in both plots corresponds to the speed field chosen as the steepest descent (136), but with the shape dependence (i. e., the volume $b - a$) *fixed* at the optimal shape. In this case, we still see convergence towards the optimal shape, but in a clear contrast to the desired gradient flow. Also note that convergence to the optimal shape itself stems only from the fact that we have



(a) Evolution of the interval boundaries (x -axis) in time (on the y -axis). Note that the blue and green curves are very close to each other and mostly overlap.



(b) The speed fields for the shape evolutions in Figure 55a.

Figure 55: Shape evolution for the 1D problem (134) according to the exact gradient flow (green), the self-consistent speed field (blue) and the steepest-descent speed under the assumption of a constant volume $b^* - a^*$ (red). The vertical lines indicate the boundaries a^* and b^* of the optimal shape.

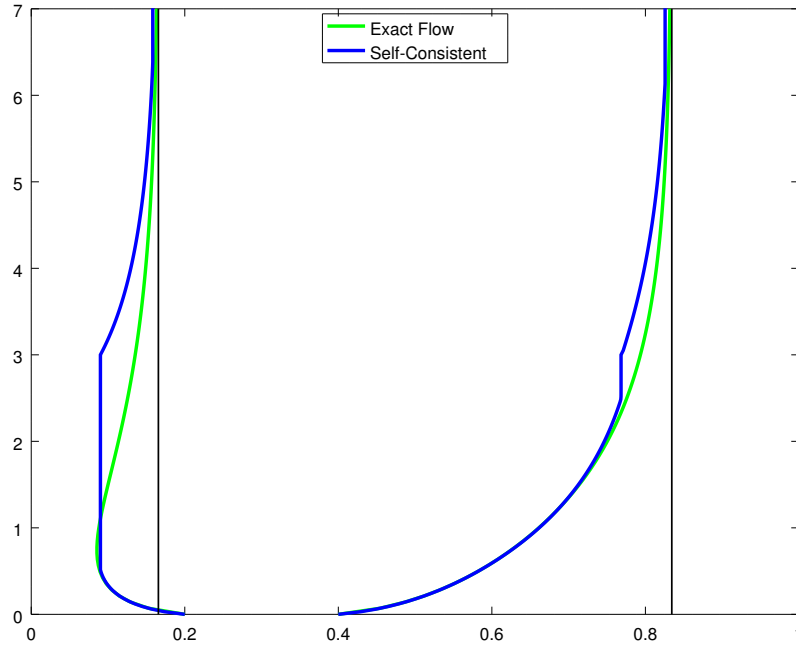


Figure 56: The exact gradient flow (green) and the result of two steps with self-consistent speed field (blue) for the 1D example problem in a non-monotone situation. Compare Figure 55a.

used precisely the *optimal shape's* volume. This is something that can, of course, not be done in a real computation when the solution is not already known a-priori.

It is also interesting to consider the same example with an initial interval that is not symmetric around u_0 . The result for the choice $(a_0, b_0) = (0.2, 0.4)$ is shown in Figure 56. As before, the exact gradient flow is depicted in green. One can clearly see that the lower bound $a(t)$ behaves *non-monotonically* in this situation: When Ω_t is small at the beginning, the balloon force is strong enough to grow the interval at both boundaries. This is even true after the lower boundary crosses over the equilibrium value a^* . However, at some point, the expansion due to the upper boundary decreases the force until the lower boundary starts to *increase* again. For $t \rightarrow \infty$, both boundaries converge towards their equilibrium values from below. Note that this phenomenon occurs even though the initial interval is a strict subset of the optimal shape. From a naive point of view, one might have expected a monotonic growth towards the optimal shape. To handle this situation with our method, we need at least two steps. The blue curve shows the result with a length of $t_0 = 3$ for the first step. One can nicely see that the evolution according to the self-consistent speed field matches the exact gradient flow initially as before. However, as soon as the lower boundary would have to turn around, it gets stuck instead. With the second step, the direction of the lower boundary is reversed and it converges, as expected, to a^* from below. This shows that the multi-step procedure does, indeed, work well also for difficult situations with non-monotonic behaviour.

7.4.2 The Image-Segmentation Problem

Next, we apply the multi-step self-consistent gradient-flow method to the full image-segmentation problem of Chapter 6. For the examples in this subsection, we always use a fixed step length of $t_0 = 10$. The result for an image without sharp edges (see also Figure 39) is illustrated in Figure 57. The first five steps of the evolution are shown in Figure 57a. The result is already very close to the final shape. Compare also the cost decrease in Figure 57b to Figure 39b: For the gradient descent, roughly 50 steps are required to bring the cost down to 10^{-5} . The same decrease is realised by the gradient-flow method in only a tenth of this number of steps! Of course, each step for the gradient flow is more expensive as it involves multiple fixed-point iterations with ψ . For this example, however, four iterations per step are

enough to reach a point where an increase in the number of fixed-point iterations does not cause any noticeable difference in the result anymore. Thus, even if we take the fixed-point iterations themselves into account as well, it still requires only 20 “operations” to converge to the final shape. The gradient flow is also clearly more efficient in terms of computation time.

If one compares the resulting shapes between Figure 39a and Figure 57a, a striking difference lies in the regularity of the boundary. The gradient descent produces a much smoother boundary than the gradient flow. To understand this effect, note that the problem itself (i. e., the cost function in (102)) does not include any regularisation for the boundary at all. Since our input images contain noise, the natural result of the optimisation procedure is thus an irregular boundary as seen in Figure 57a. The smoother boundary of Figure 39a, on the other hand, is a result of the computation of the shape gradient as discussed in Section 6.2.

Let us now do the same comparison for the image of Figure 41, which has sharper edges. The gradient-descent method does not work on this image, and the desire to find an alternative method was our main motivation for the work on the gradient-flow idea after all. This, of course, leads to the question whether the gradient-flow method performs better for this image. The answer can be seen in Figure 58: It does. It requires more descent steps (the first six are shown in Figure 58a), but it still shows convergence to the desired shape. The situation is also slightly more delicate with respect to the fixed-point steps, since the sharp edges lead to larger Lipschitz constants for the shape-dependent quantities. For the shown result, we used ten fixed-point iterations for each descent step. Nevertheless, it is clear that the method works quite well, while we have seen in Figure 41b that gradient descent simply fails for this image due to excessive “zig-zaging”.

7.5 Topological Derivatives

One of the major advantages that level-set methods have over other strategies is their flexibility with respect to topological changes. This was already discussed above and demonstrated in Figure 2. However, even though our speed method is, in theory, able to change the topology, there are often situations where these changes are not actually performed in practice. Often, the gradient descent of Chapter 6 or the gradient flow discussed in this chapter avoid topology changes and converge instead to a local minimum with the same topology as the initial geometry. A main issue here is that the speed method is based on transforming the *boundary* of the current domain. Thus, it is neither able to create holes in the interior of Ω nor new components of the domain in $\mathbb{R}^n \setminus \overline{\Omega}$. A common method to overcome this difficulty is to use an initial geometry with lots of components and holes. During the optimisation process, unnecessary holes and components can then disappear or join together. See, for instance, [21] and [83].

For more systematic approaches, a concept called the *topological derivative* can be used. See, for instance, the methods described in [15] and [69]. In particular, this quantity characterises how the cost changes when new components of the domain are created. (It is also often defined as the change of the cost when holes are punched into Ω , but the basic idea is the same. For our discussion, we will for simplicity concentrate on the situation of new components.) This is in contrast to the shape derivative discussed so far, which describes the change of the cost when the boundary of Ω is moved. For some $x \in \mathbb{R}^n \setminus \overline{\Omega}$, a simple version of the topological derivative can be formally defined as

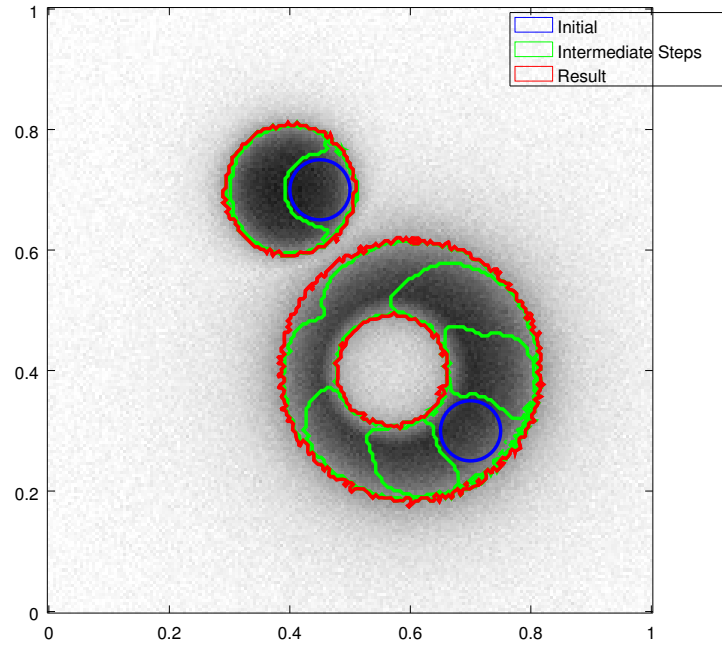
$$d_T J(\Omega; x) = \lim_{\rho \rightarrow 0^+} \frac{J(\Omega \cup B_\rho(x)) - J(\Omega)}{\text{vol}(B_\rho(x))}.$$

The definition for $x \in \Omega$ and the creation of holes can be done in a similar way. While we do not want to discuss technical details here, let us still describe, at least in an informal way, how topological derivatives can be incorporated into our gradient flow. This results quite naturally in a hybrid method that performs much better for some problems.

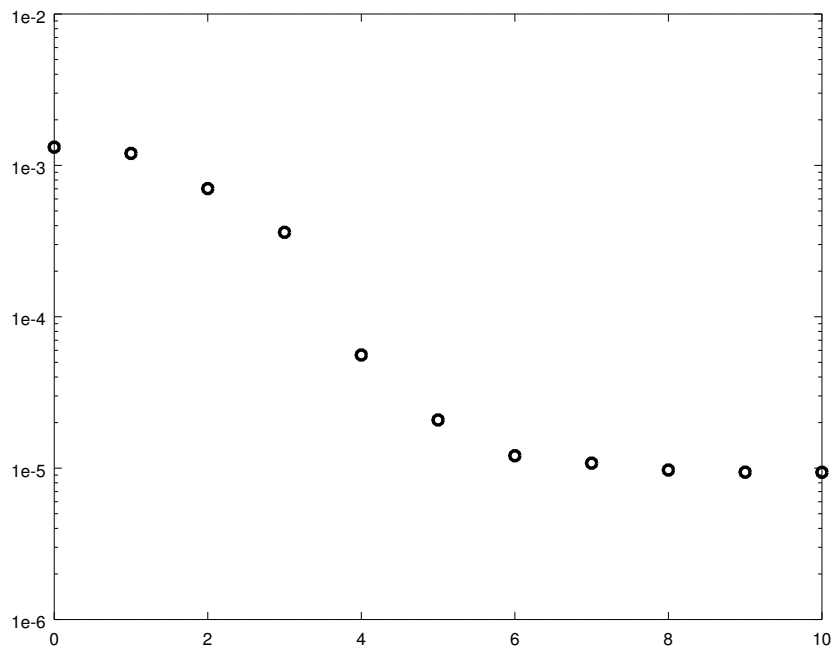
For our situation (with only domain functionals), the topological derivative actually matches the shape derivative in some sense. In particular, if the shape derivative is given by (118), then the topological derivative at some point x is

$$d_T J(\Omega; x) = f(x, \Omega).$$

A heuristic argument to see why this is the case is the following: Consider the situation that $x \in \Gamma$ and $F(x) = 1$. The contribution of the particular point x to the shape derivative (118) is then precisely

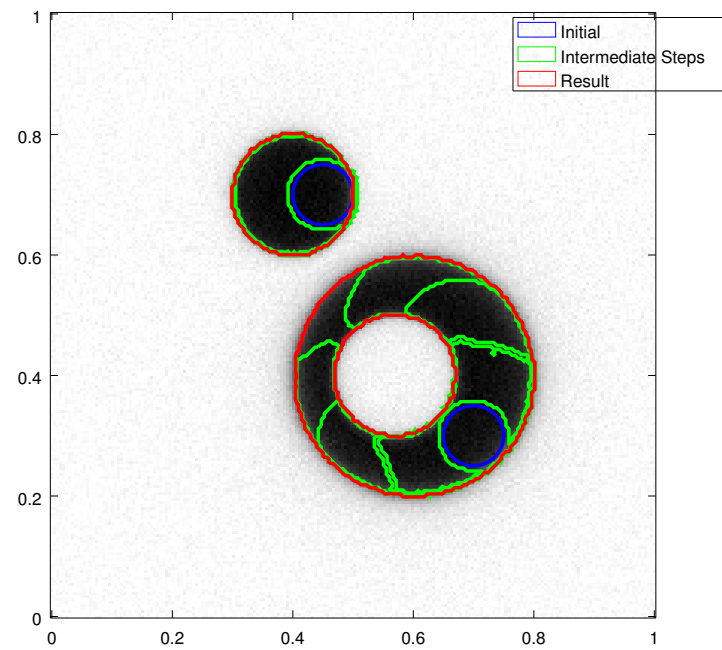


(a) Initial (blue), intermediate (green) and final (red) shapes.

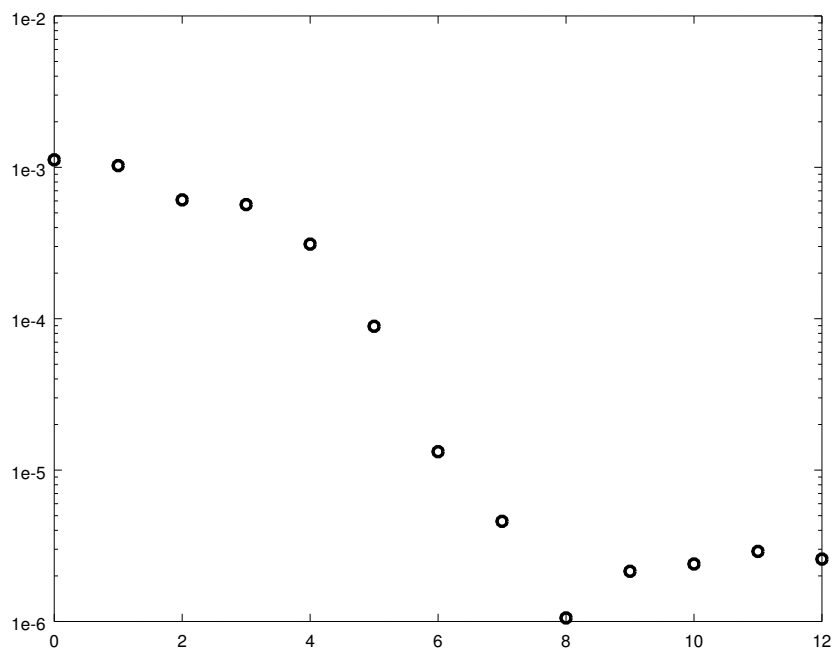


(b) Evolution of the cost.

Figure 57: Application of the multi-step self-consistent gradient-flow method to our image-segmentation problem. Compare also Figure 39.



(a)



(b)

Figure 58: Continuation of Figure 57 for an image with sharper edges. Compare also Figure 41.

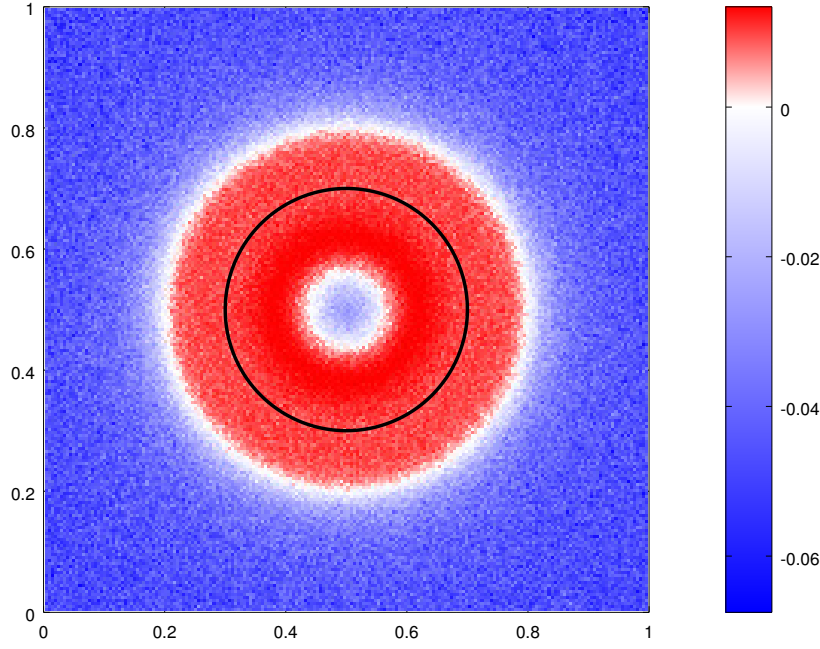


Figure 59: The self-consistent speed field for the image-segmentation example discussed in Section 7.5.

$f(x, \Omega)$. Furthermore, $F(x) > 0$ with $x \in \Gamma$ means that, from a local point of view, x is being added to Ω . This, in turn, is roughly just the meaning of the topological derivative at x .

Now, assume that we have found a self-consistent gradient flow F according to Definition 24. In this case, $F(x) = -f(x, \Omega(x)) = -d_T J(\Omega(x); x)$. Instead of evolving Ω_0 along F to get the next iterate Ω_1 of the geometry, we can instead use the following idea: Whenever $F(x) > 0$, this means that the topological derivative is negative at x . Consequently, it is beneficial for decreasing the cost to include those x into the domain. Similarly, we want to exclude all x where the topological derivative is positive. Thus, we can simply *define*

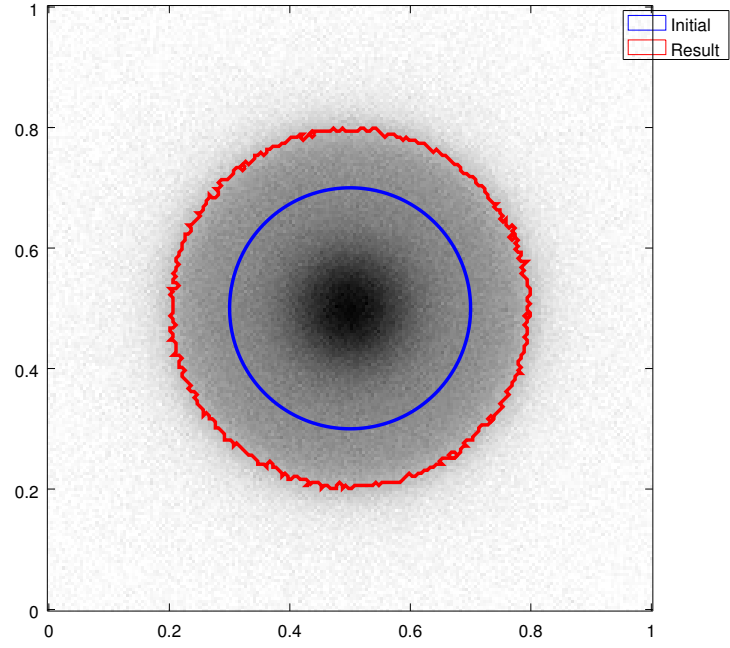
$$\Omega_1 = \{x \in \mathbb{R}^n \mid F(x) > 0\} = (-F)^{-1}((-\infty, 0)). \quad (137)$$

This can be achieved by just interpreting $-F$ as the level-set function for Ω_1 , similar in spirit to Lemma 51. Depending on the problem at hand, one can build a suitable heuristic to decide when to use (137) instead of a shape evolution. For instance, whenever the descent seems to be converged, one can try a step with (137) to check whether this is really the case or it is just stuck in a local minimum. This approach matches the strategy suggested in Subsection 3.4 of [69].

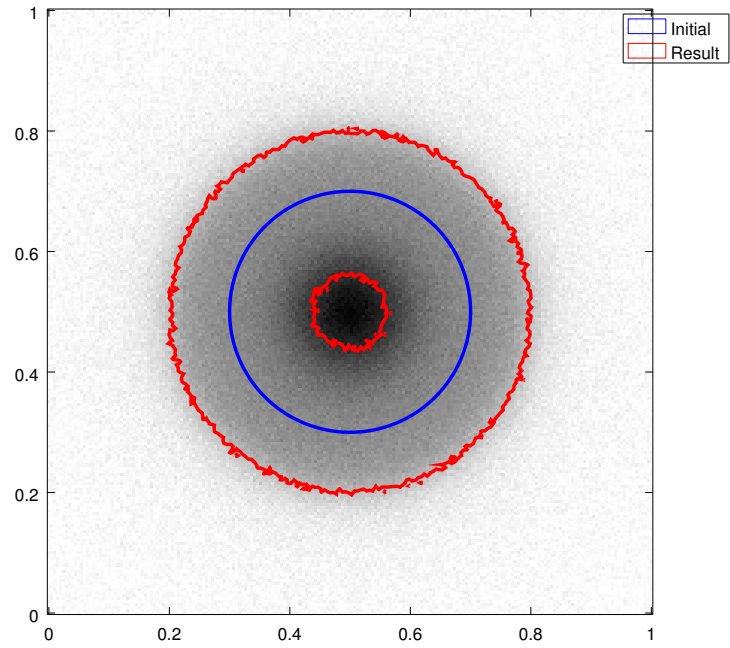
To conclude this section, let us demonstrate this idea on a simple example. We use the image-segmentation problem in Figure 40 but define the initial geometry as a circle that is symmetric around the inner black area. For this situation, both the gradient-descent and the gradient-flow method lead to a suboptimal shape that does not exclude the centre. The corresponding speed field resulting from our fixed-point iteration is plotted in Figure 59. One can clearly see that it (and thus the topological derivatives) are negative where the hole needs to be created. The geometry that results by evolving Ω_0 along the speed field is shown in Figure 60a. In contrast, the domain according to (137) can be seen in Figure 60b. For the situation at hand, the latter is the superior solution.

7.6 Boundary Length and Mean-Curvature Flow

In the last section of this chapter, we would like to discuss how the idea of “a single speed field for the whole evolution” can also be applied to other problems. In particular, an important generalisation of the model problem (102) includes the perimeter of Ω as an additional regularisation term. This prevents



(a) Shape evolution of Ω_0 according to the speed field.



(b) Definition of the new shape via (137).

Figure 60: The shapes that result after taking one step based on the speed field in Figure 59. Compare also Figure 40, where a different initial shape is used together with gradient descent.

the effect of an irregular boundary that we have seen in Figure 57a and Figure 58a. Going even further, if the cost function is *just* the perimeter, it is well-known that the shape evolution corresponding to the gradient flow is the so-called *mean-curvature flow*. It has been widely studied both theoretically and from the point of view of applications. See, for instance, [43]. The description of mean-curvature flow with level-set methods is discussed, among others, in [41] and [67]. In particular, the normal speed F is given by the (negative) *mean curvature* κ of the evolving surface. The mean curvature can be computed from a sufficiently smooth level-set function ϕ by the expression

$$\kappa(x) = \operatorname{div} \left(\frac{\nabla \phi(x)}{|\nabla \phi(x)|} \right). \quad (138)$$

(For a derivation, see (1.4.9) on page 29 of [41].) Thus, we can modify our level-set equation (2) to read:

$$0 = \dot{\phi} + F(x) |\nabla \phi| = \dot{\phi} - \kappa |\nabla \phi| = \dot{\phi} - \operatorname{div} \left(\frac{\nabla \phi}{|\nabla \phi|} \right) \cdot |\nabla \phi| \quad (139)$$

While this equation has a singularity at $\nabla \phi = 0$, one can still establish a suitable solution theory based on viscosity solutions. This was pioneered by Evans and Spruck in a series of papers starting with [38]. It is also discussed in great detail in [41]. For numerical methods, we refer to [28].

Our discussion is focused on a new approach instead: We would like to compute the mean-curvature flow based on an Eikonal equation similar to Chapter 3. This method, of course, has a major drawback: Since it is based on the ideas described in this chapter, it only works as long as the evolution of the shape is *monotone*. This is, for instance, the case for mean-convex geometries (meaning that κ is positive all over the surface). However, also many interesting cases are excluded by that requirement. On the other hand, we believe that our new approach also has advantages that make it, nevertheless, interesting to study: First, it may lead to more efficient methods for the computation of the mean-curvature flow. This needs some further algorithmic work besides what we will describe below, but it is definitely an interesting subject for further research. Second, a description of the mean-curvature flow in terms of an Eikonal equation allows to apply new analytical tools just like our Hopf-Lax formula introduced in Section 3.4 allowed us to draw new theoretical conclusions in Chapter 4. And third, this can be used as a starting point to apply self-consistent gradient-flow methods to problems which have regularisation terms based on the boundary length. Here, one can hope that the restriction to monotone evolutions can be circumvented with a multi-step procedure similar to the one demonstrated in Section 7.4. This idea will be discussed briefly at the end of this section and is also an interesting area for further research. Note that this section is intended only to demonstrate the ideas. No rigorous analysis will be done.

The basic idea of our method is the same as described in Section 7.1: We want to define a speed field corresponding to the steepest descent and make sure that it is self-consistent with respect to shape-dependent quantities. For the case of mean-curvature flow, we have to set $F(x) = -\kappa(x)$. As before, this value depends on the shape $\Omega(x)$. In contrast to the situation analysed above, however, the shape dependence is *local* this time: The curvature depends only on the shape of the boundary in a neighbourhood of x . It does not depend on things like the volume of Ω or other global quantities. Let us now assume that some speed field F is fixed. We use (47) to describe the shape evolution. Excluding the stationary case $F(x) = 0$, this implies that a level-set function for the domain evolution is given by

$$\phi(x, t) = D(x) \pm t. \quad (140)$$

Note specifically that the spatial dependence of ϕ is precisely the term $D(x)$. Thus, *the mean curvature $\kappa(x)$ can be computed from D alone without any time-dependent terms*. In particular, (138) implies

$$\kappa(x) = \operatorname{div} \left(\frac{\nabla \phi(x, t)}{|\nabla \phi(x, t)|} \right) = \operatorname{div} \left(\frac{\nabla D(x)}{|\nabla D(x)|} \right).$$

Recall also (37): The distance D depends on the speed field F via the Eikonal equation

$$F(x) |\nabla D(x)| = 1.$$

Consequently, we can conclude for a self-consistent situation:

$$-\kappa |\nabla D| = -\operatorname{div} \left(\frac{\nabla D}{|\nabla D|} \right) \cdot |\nabla D| = 1 \quad (141)$$

In other words, the distance that defines the shape evolution for the mean-curvature flow solves the *mean-curvature Eikonal equation* (141).

A possible way to solve (141) numerically is to introduce a pseudotime and evolve towards a stationary situation. For this, we introduce an artificial time dependence of D and propagate the parabolic equation

$$\frac{D_\tau}{|\nabla D|} = \operatorname{div} \left(\frac{\nabla D}{|\nabla D|} \right) + \frac{1}{|\nabla D|}$$

in time (denoted by the variable τ). We can hope that it converges towards a stationary state D_∞ for $\tau \rightarrow \infty$, which then solves (141). Note that this equation is the same as the mean-curvature level-set equation (139) except for the additional forcing term. Thus, we can apply the methods of [28] to solve it: As a first step, let us introduce $\epsilon > 0$ as a small regularisation parameter. In order to avoid singularities for $\nabla D = 0$, we consider the regularised equation

$$\frac{D_\tau}{\sqrt{|\nabla D|^2 + \epsilon^2}} = \operatorname{div} \left(\frac{\nabla D}{\sqrt{|\nabla D|^2 + \epsilon^2}} \right) + \frac{1}{\sqrt{|\nabla D|^2 + \epsilon^2}}. \quad (142)$$

We solve this equation with finite elements and a semi-implicit time-stepping scheme (see also Subsection 8.2.2 for a description of our implementation of finite elements). In particular, let $D^i = \sum_k c_k^i u_k$ be the finite-element discretisation of D at some time t_i . Here, $(u_i)_i$ is the finite-element basis and $(c_k^i)_{ik}$ are the time-dependent coefficients. With

$$D_\tau \approx \frac{D^{i+1} - D^i}{\Delta\tau} = \frac{1}{\Delta\tau} \sum_k (c_k^{i+1} - c_k^i) u_k,$$

we see that the discrete version

$$\frac{1}{\Delta\tau} \sum_k (c_k^{i+1} - c_k^i) \int \frac{u_k v}{\sqrt{|\nabla D^i|^2 + \epsilon^2}} dx = - \sum_k c_k^{i+1} \int \frac{\langle \nabla u_k, \nabla v \rangle}{\sqrt{|\nabla D^i|^2 + \epsilon^2}} dx + \int \frac{v}{\sqrt{|\nabla D^i|^2 + \epsilon^2}} dx$$

of the weak form of (142) must hold for all test functions v . To simplify notation, let us assemble all coefficients $(c_k^i)_k$ to a vector c^i and define

$$M_{kl}^i = \int \frac{u_k u_l}{\sqrt{|\nabla D^i|^2 + \epsilon^2}} dx, \quad K_{kl}^i = \int \frac{\langle \nabla u_k, \nabla u_l \rangle}{\sqrt{|\nabla D^i|^2 + \epsilon^2}} dx, \quad f_k^i = \int \frac{u_k}{\sqrt{|\nabla D^i|^2 + \epsilon^2}} dx.$$

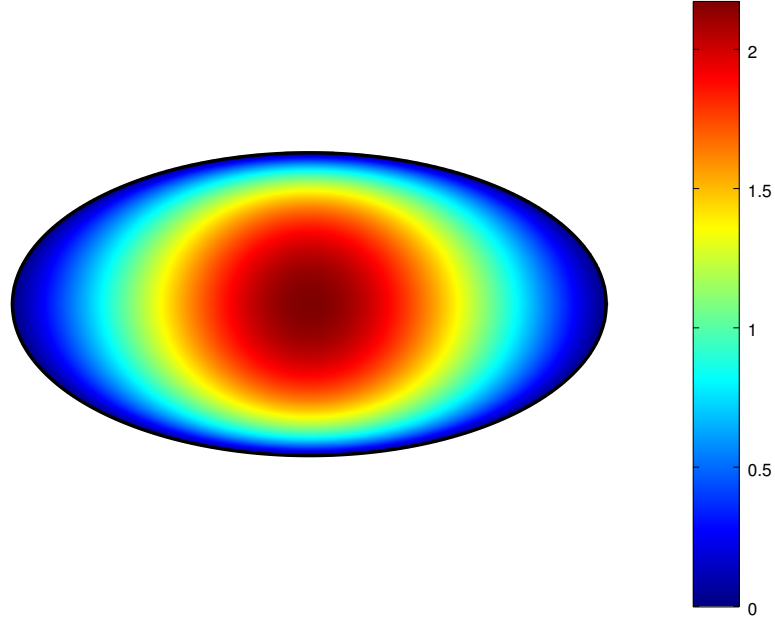
Note that the matrices M and K can be computed by scaling the standard mass and stiffness matrices accordingly. For linear elements, ∇D^i and thus also the weights are constant on each mesh triangle. Then, each time step corresponds to solving the linear system

$$(M^i + \Delta\tau \cdot K^i) c^{i+1} = M^i c^i + \Delta\tau \cdot f^i.$$

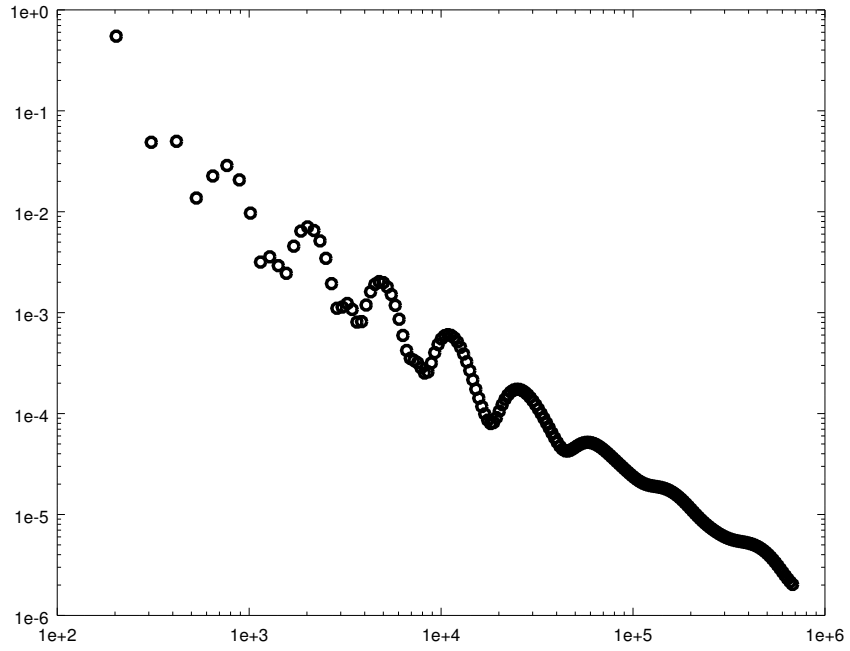
Let us demonstrate the viability of this method: We use an elliptic initial domain Ω_0 and solve (141) on it with the method described above. The resulting distance D , which is the stationary state of (142), is shown (inside of Ω_0) in Figure 61a. Its contour lines correspond to the shape at various times (as per (140)). One can clearly see that the shape first turns into a circle and later vanishes. This is the expected behaviour according to [43]. The relative difference in L^2 -norm between consecutive pseudotime steps is plotted in Figure 61b. This clearly shows that the pseudotime iteration converges, indeed, to a stationary state and thus a solution of (141).

To conclude this discussion, let us now consider how the shape-optimisation idea introduced in the beginning of this section can be combined with the mean-curvature approach. A combined method promises a way to solve shape-optimisation problems that include perimeter terms as regularisation. Let us, again, consider a base problem whose shape derivative is of the form (118). If we add $P(\Omega)$ as additional term to the cost, the new shape derivative is

$$dJ(\Omega; F) = \int_\Gamma F(f(x, \Omega) + \kappa(x)) d\sigma.$$



(a) The resulting distance D .



(b) Relative L^2 -difference between consecutive time steps during the pseudotime evolution.

Figure 61: Solution of the mean-curvature Eikonal equation (141) for an elliptic initial geometry.

Thus, the steepest-descent direction is

$$F(x) = -f(x, \Omega(x)) - \kappa(x).$$

As before, κ depends on the distance D , which, in turn, can be computed from the initial speed field F_0 by solving (37). In order to find a self-consistent gradient flow in this situation, we have to find a solution (F, D) to the mixed algebraic-differential equation

$$F = \psi(F) - \operatorname{div} \left(\frac{\nabla D}{|\nabla D|} \right), \quad F |\nabla D| = 1. \quad (143)$$

Here, ψ denotes the fixed-point iteration mapping without perimeter regularisation as it was discussed in Section 7.1 and analysed in Section 7.2. Of course, a first idea to solve (143) is the following: As before, do a fixed-point iteration. Instead of ψ , we could iterate with the extended right-hand side of (143) this time. This is possible, since one can compute D and then κ from a given F . Unfortunately, however, this method does not work. In practice, the numerical computation of κ as a second derivative of D is too unstable. To circumvent this issue, it was a crucial to switch to the weak form and an implicit solution method when solving (141). That way, we can exploit the smoothing effect of the *inverse* Laplacian instead of computing explicit derivatives. It seems necessary to apply such a rewrite also for (143). We can, however, not present a complete method that does this yet.

8 PDE-Constrained Shape Optimisation

A lot of the classical shape-optimisation problems considered in applications (such as, e. g., structural optimisation) involve partial differential equations. For a general introduction, we refer to [44]. With our image-segmentation problem analysed in Chapter 6 and Chapter 7, we have avoided the difficulties that appear with these types of problems. This simplification allowed us to concentrate on and better understand other, more general aspects of level-set based shape optimisation. In this last chapter, we want to discuss how the gradient-descent method of Chapter 6 can be applied to shape-optimisation problems with PDE constraints. The results presented are based on our work in [58]. Let us also refer to [53]; this paper is based on the same level-set fundamentals (and our code in [59]), but uses a slightly different optimisation method. Note that PDE-constrained shape optimisation is a very challenging field, such that a lot of “loose ends” remain for further research. Rigorous analysis of all involved difficulties has been done only recently for selected problems, as in [16]. For this reason, the content of this chapter is formulated only in an informal way, assuming necessary regularity as we go along.

Throughout this chapter, we consider a simple elliptic equation and a tracking-type cost functional. Let $D \subset \mathbb{R}^2$ be compact, $B \subset D$, $f \in L^2(D)$ and $u_d \in L^2(B)$. For a given domain Ω , let $u = u(\Omega)$ satisfy the state equation

$$-\Delta u + u = f \text{ in } \Omega, \quad \frac{\partial u}{\partial \nu} = 0 \text{ on } \Gamma = \partial\Omega. \quad (144)$$

Standard theory for the analysis of equations of this type is based on the *weak form* of (144): It is well-known that the unique solution $u \in H^1(\Omega)$ satisfies

$$\int_{\Omega} (\langle \nabla u, \nabla v \rangle + uv) \, dx = \int_{\Omega} f v \, dx \quad (145)$$

for all test functions $v \in H^1(\Omega)$. For a thorough discussion of the underlying theory, see [36]. Thus, it is justified to consider

$$J(\Omega) = \frac{1}{2} \|u(\Omega) - u_d\|_{L^2(B)}^2 + R(\Omega) \quad (146)$$

as a cost functional depending on Ω . The term $R(\Omega)$ is an appropriate regularisation term. We use the boundary length to enforce a smooth boundary of Ω , i. e., we set

$$R(\Omega) = \alpha \cdot P(\Omega) = \alpha \cdot \mathcal{H}^1(\Gamma)$$

with $\alpha \geq 0$. We want to minimise (146) over all sufficiently regular domains Ω with $B \subset \Omega \subset D$. This inclusion constraint ensures that Ω is inside the hold-all domain D and fully contains the area of measurement B . See [53] and Section 6.6 for a discussion of geometric constraints. Note, though, that these constraints are not the main focus of our interest in this chapter. They are inactive for almost all situations considered below.

8.1 Computation of the Shape Derivative

Our goal is to apply the gradient-descent method described in Chapter 6 to the minimisation problem (146). For this, we have to compute the shape derivative of the new cost function as a first step. Let us, as usual, assume that we have a speed field F and denote the evolving domain at time $t \geq 0$ by Ω_t . Formally differentiating $J(\Omega_t)$ with respect to t , we obtain the Eulerian derivative

$$dJ(\Omega_0; F) = \lim_{t \rightarrow 0^+} \frac{J(\Omega_t) - J(\Omega_0)}{t} = \int_B (u - u_d) \cdot u'(x; F) \, dx + dR(\Omega_0; F). \quad (147)$$

Here, we have assumed that the shape-dependent solution u of the state equation is shape differentiable. In particular, let

$$u'(x; F) = \lim_{t \rightarrow 0^+} \frac{u(x; \Omega_t) - u(x; \Omega_0)}{t}$$

exist for all $x \in \Omega_0$. Before we analyse this term further, let us consider the derivative of the regularisation term first. According to classical results (see, for instance, Section 2.33 of [78]), it can be expressed in terms of the mean curvature κ of the propagating surface as

$$dR(\Omega_0; F) = \alpha \cdot \int_{\Gamma_0} \kappa F \, d\sigma.$$

Let us now discuss the shape derivative $u'(x; F)$ of the state. We follow the classical idea as it is also described in Section 3.2 of [78], but use our *scalar* speed method and Corollary 7. Note that $H^1(\Omega)$ can be considered as a “subset” of $H^1(D)$ when we restrict the functions to $\Omega \subset D$. Thus, we can consider the weak equation (145) with $u, v \in H^1(D)$. Assume now that the shape derivative $u'(\cdot; F)$ exists and is, furthermore, in H^1 itself. Let us also assume that u and v are regular enough to possess a weak derivative on Γ_0 in the sense of traces. For u , this follows from elliptic regularity as discussed below. In this situation, we can apply Corollary 7 to both sides of (145) to deduce

$$\int_{\Gamma_0} (\langle \nabla u, \nabla v \rangle + uv) F d\sigma + \int_{\Omega_0} (\langle \nabla u'(x; F), \nabla v \rangle + u'(x; F) \cdot v) dx = \int_{\Gamma_0} f v F d\sigma. \quad (148)$$

Since this equality holds for all sufficiently regular $v \in H^1(D)$, we have found a weak equation that characterises $u'(\cdot; F)$. It corresponds to a differential equation similar to (144), but has a right-hand side with support on Γ_0 . Hence, given a direction F , we can evaluate $u'(\cdot; F)$ and thus the shape derivative $dJ(\Omega_0; F)$ by solving the variational problem (148).

While this is a perfectly valid characterisation of $u'(\cdot; F)$, it is not the most practical. In particular, recall that we need the mapping $F \mapsto dJ(\Omega_0; F)$ in order to apply the method described in Section 6.3. With (148), we have to solve a PDE for *each* direction F when evaluating $dJ(\Omega_0; F)$. Luckily, this is not necessary. An alternative is the so-called *adjoint approach*, as it is discussed also in Section 1.6 of [47]. In particular, let us assume that $p \in H^1(D)$ solves the *adjoint equation*

$$\int_{\Omega_0} (\langle \nabla w, \nabla p \rangle + wp) dx = \int_B (u - u_d) w dx \quad (149)$$

for each $w \in H^1(D)$. This is the weak form of the equation

$$-\Delta p + p = (u - u_d)\chi_B \text{ in } \Omega_0, \quad \frac{\partial p}{\partial \nu} = 0 \text{ on } \Gamma_0 = \partial\Omega_0. \quad (150)$$

Using the adjoint equation (149) together with (148), we can express the first term on the right-hand side of (147), which gives

$$\int_B (u - u_d) \cdot u'(x; F) dx = \int_{\Omega_0} (\langle \nabla u'(x; F), \nabla p \rangle + u'(x; F) \cdot p) dx = \int_{\Gamma_0} (fp - \langle \nabla u, \nabla p \rangle - up) F d\sigma.$$

This yields the full shape derivative (with regularisation) as

$$dJ(\Omega_0; F) = \int_{\Gamma_0} (fp - \langle \nabla u, \nabla p \rangle - up + \alpha\kappa) F d\sigma. \quad (151)$$

In this form, it is enough to solve the state and adjoint equations for u and p whenever the geometry changes. Then, evaluation of the shape derivative in some direction is only a matter of integrating along the boundary Γ_0 . Furthermore, (151) makes it clear that the shape derivative $dJ(\Omega_0; \cdot)$ is a linear functional in the direction F .

Thus, we can proceed to implement a gradient descent method in the way described in Section 6.3. In particular, we are looking for $G \in H^1(D)$ such that

$$\int_D (FG + \beta \langle \nabla F, \nabla G \rangle) dx = \int_{\Gamma_0} ((f - u)p - \langle \nabla u, \nabla p \rangle + \alpha\kappa) F d\sigma \quad (152)$$

holds for all $F \in H^1(D)$. Recall that u and p are the weak solutions of the elliptic equations (144) and (150) with right-hand sides in $L^2(\Omega_0)$. Assuming a sufficiently smooth domain Ω_0 , standard results about boundary regularity (see, for instance, Theorem 4 on page 317 of [36]) imply that $u, p \in H^2(\Omega_0)$. Consequently, ∇u and ∇p are in $L^2(\Gamma_0)$ by the trace theorem (e. g., Theorem 1 on page 258 of [36]). If we further assume that the boundary is smooth enough for the curvature term, this means that the right-hand side of (152) is a functional in $H^{-1}(D)$. Thus, (152) is well-posed. This variational problem allows us to compute a shape gradient G and with it a descent direction.

8.2 Aspects of the Numerical Computation

Before we present numerical results in Section 8.3, we want to describe some aspects of our numerical solvers. In particular, Subsection 8.2.1 describes how a triangulation of Ω is computed from its level-set representation. The basic finite-element discretisation used for the state and adjoint equations is presented in Subsection 8.2.2. For the shape derivative (151), additional difficulties arise. They are discussed in Subsection 8.2.3 and Subsection 8.2.4. In combination with the methods for shape propagation described in Section 3.5, this is everything that we need to apply the gradient-descent method of Section 6.3 to the PDE-constrained problem (146).

8.2.1 Generation of a Triangular Mesh

In contrast to the square grid that is used for the discrete level-set function (see Section 3.5), we use a *triangle mesh* for numerical computations involving the state and adjoint equations. This is the most common approach for finite-element discretisations. Furthermore, in this way we are able to resolve the moving boundary of the level-set domain more precisely. The boundary is approximated by a polygonal curve, whose construction is the first step when generating our mesh. Whenever the level-set function ϕ changes its sign between two neighbouring points of the rectangular grid, there exists an intersection between Γ as the zero level set of ϕ and the edge connecting the points. We approximate these intersection points using an affine model for ϕ along each edge of the grid. The polygonal approximation of Γ is then found by connecting all intersection points in the appropriate order. This computation is implemented in `ls.find_geometry` of our package [59]. Also note that we can define an *orientation* for the boundary polygon. We do this such that Ω is always on the left-hand side when traversing the polygon.

Once the boundary polygon is found, it remains to split the domain into triangles in an appropriate way. This is done by `ls.build_mesh`, which can be used in two modes: The first one only constructs a mesh on the interior of Ω . This is what we need for solving the state and adjoint equations. The “global” mode, on the other hand, constructs a triangle mesh of the whole hold-all domain D . This is done in a way that still resolves the boundary Γ correctly. We need this mesh in order to compute shape gradients as Riesz representatives as discussed in Section 6.2. For this, we have to solve (106) on the *global* mesh. In both cases, squares of the original grid that are not intersected by Γ are easy: They can just be split into a pair of triangles along a diagonal. The triangulation of *boundary elements*, i. e., squares intersected by the boundary Γ , is more challenging. As a first step, we look for edges of the square where Γ *enters* according to its orientation. These are, of course, only half the number of all intersected edges. Following the edges of the square clockwise from such an intersection point, we traverse grid points inside of Ω until we find another intersection point at which the boundary edge leaves the square again. Then, we have to distinguish four possible cases:

Inner Triangle There is only one entrance point and also only one inner point. In this case, the boundary element is cut into a triangle inside of Ω and a pentagon outside.

Inner Trapezoid There is only one entrance point followed by two inner points. Here, Γ cuts through the square at parallel sides to produce two trapezoids.

Inner Pentagon Opposite to the *inner triangle* case, we can have one entrance point and three inner points. Only one vertex of the square is outside of Ω .

Narrow Pair It is also possible that ϕ has the same sign for points diagonal to each other. In this case, we find *two* entrance points, each followed by a single inner point. This situation is ambiguous, such that the values of ϕ on the grid alone do not allow us to determine whether the two points in Ω are connected through a narrow channel or not. Our implementation of mesh building assumes that they are *not* connected.

These four cases are illustrated in Figure 62. The entrance points are marked with red dots and the grey parts correspond to the interior of Ω . For each case, we indicate how the parts are split into triangles.

An example mesh generated with this technique is shown in Figure 63. Taking all triangles together, we get a global mesh for D . The mesh for Ω alone consists of only the green triangles. The polygonal approximation of Γ is shown in red as the interface between both regions. The depicted situation includes all of the four cases. In particular, a narrow pair appears at the centre where the two circles nearly touch

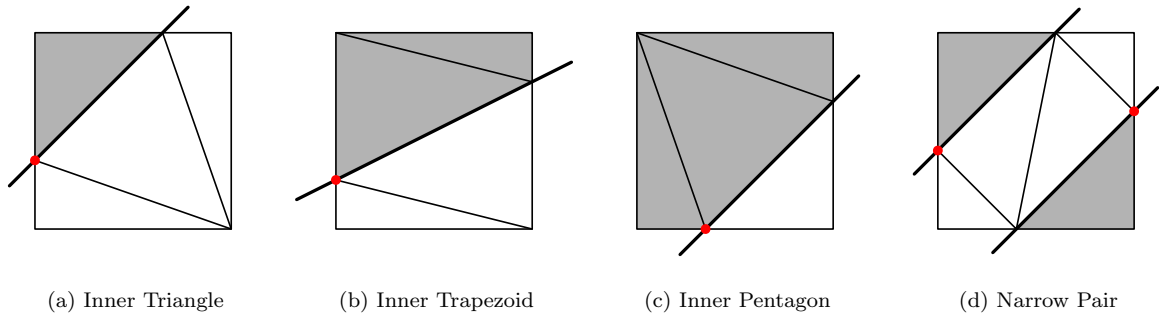


Figure 62: Possibilities for splitting boundary elements into triangles. The interior of the Ω is grey, the exterior white. Red dots indicate the entrance points of Γ .

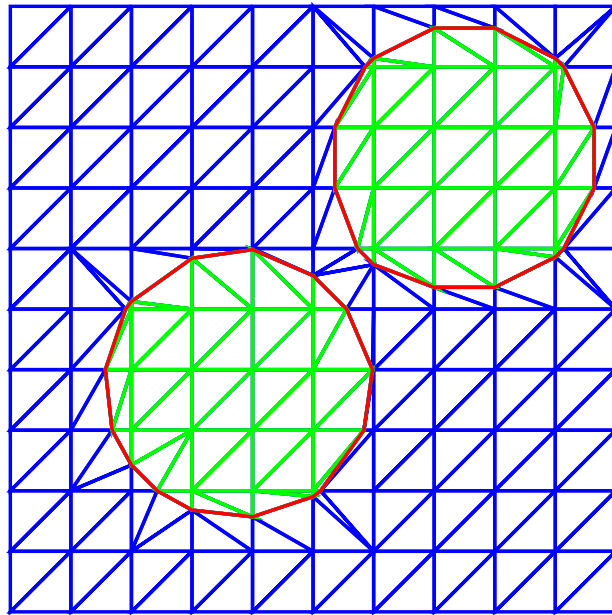


Figure 63: Example mesh constructed for a level-set domain. The triangles inside of Ω are green, those for the hold-all domain blue. The approximation of the boundary Γ is indicated in red.

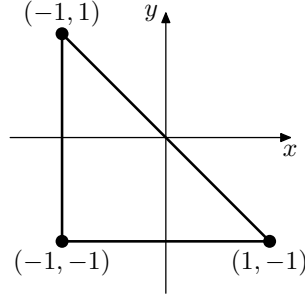


Figure 64: The reference triangle used to construct the FEM basis functions.

each other. Note that the generated triangles may be quite distorted. This is a result of the simple mesh-generation strategy that we employ. In order to prevent numerical issues with triangles that are too degenerate, we enforce a certain minimum ratio between the side lengths of each triangle. I. e., if an intersection point between Γ and the grid is too close to a grid point, it is slightly pushed away.

8.2.2 FEM Discretisation of the State and Adjoint Equations

The state and adjoint equations (145) and (149) are solved numerically with linear finite elements in a nodal basis. While there exist various libraries for the numerical solution of PDEs like these with finite elements, most of them are built and optimised under the assumption that the geometry of the domain is fixed and, if anything, the coefficients of the equation change. This is, of course, not the case for our shape-optimisation problem. Thus, we decided to use our own custom-made solver. It follows mostly the standard procedure described, for instance, in Section 4.3 of [31]. Let us, nevertheless, briefly mention some of the key concepts as they are useful later on in Subsection 8.2.3 as well.

We use the reference element $R \subset \mathbb{R}^2$ depicted in Figure 64 and define the Lagrange basis on it:

$$p_0(x, y) = -\frac{x+y}{2}, \quad p_1(x, y) = \frac{x+1}{2} \quad \text{and} \quad p_2(x, y) = \frac{y+1}{2} \quad (153)$$

For an arbitrary triangle $T \subset \mathbb{R}^2$ of our mesh, there exists an affine transformation $\psi_T: R \rightarrow T$ that maps the reference triangle to T in a bijective way. Thus, we can define basis functions on T by

$$r_i^T(x) = p_i(\psi_T^{-1}(x)), \quad i = 0, \dots, 2.$$

It is now easy to compute the local mass and stiffness matrices

$$(M_T)_{ij} = \int_T r_i^T(x) r_j^T(x) dx \quad \text{and} \quad (K_T)_{ij} = \int_T \langle \nabla r_i^T(x), \nabla r_j^T(x) \rangle dx \quad \text{for } i, j = 0, \dots, 2$$

on the mesh triangle T . This computation can be done by first integrating the reference basis functions (153) symbolically on R and then including the Jacobian of ψ_T to transform the integrals according to the change-of-variables formula. The right-hand side of (145) can be approximated in a similar way by a vector $f_T \in \mathbb{R}^3$.

As the next step, we have to use the local basis functions on each mesh triangle to build a *global* basis. For this, we use *node condensation* with an assembly matrix $A \in \mathbb{R}^{3K \times N}$. Here, K is the number of mesh triangles and N the number of vertices of the mesh. In general, $N < 3K$ so that the matrix A is tall. Each column of A corresponds to a mesh vertex and each row to a local basis function on one of the triangles. The matrix A now contains a one for each position where the vertex of a local triangle corresponds to a particular mesh vertex. This construction ensures that local basis functions are combined to global ones in such a way that continuity across the edges of adjacent triangles is enforced. Let us assemble the local matrices and right-hand side into block-diagonal matrices $M_g, K_g \in \mathbb{R}^{3K \times 3K}$ and the vector $f_g \in \mathbb{R}^{3K}$. Then, the finite-element system corresponding to the state equation (145) is

$$A^\top (M_g + K_g) A \cdot u = A^\top f_g. \quad (154)$$

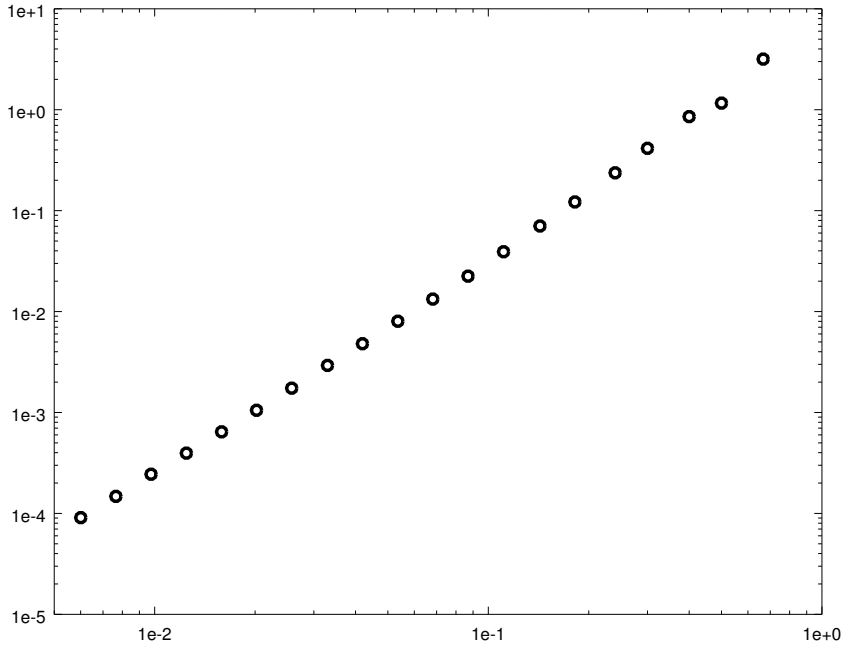


Figure 65: Relative L^2 -error of the approximated solution of the state equation (144) with our FEM solver. We compute a manufactured solution on different grid sizes. The x -axis shows h .

We have to solve it to get the coefficients u_i of the approximate state. Since we use the Lagrange basis, these coefficients correspond directly to the values of u on the mesh vertices, i. e., $u_i = u(x_i)$, $i = 1, \dots, N$, for each node x_i of the mesh. To test our solver, we apply it to a manufactured solution of (144) for various grid sizes h . (The grid size, in turn, is mostly proportional to the size of the mesh triangles.) The result is shown in Figure 65. One can clearly see that it matches the expected $O(h^2)$ behaviour of the L^2 -error (see Theorem 4.21 on page 130 of [31]).

The adjoint equation (149) can be solved in the same way. The only difference is the right-hand side. Instead of $\int_{\Omega} f v \, dx$ we now have an integral over $B \subset \Omega$. For simplicity, let us assume that B is resolved exactly by the chosen mesh. Then, we have to evaluate the right-hand side $\int_B g u_i \, dx$ for a global basis function u_i and with $g = u - u_d$ being a known function. In contrast to the previous situation, the integral is not over the full domain Ω but only over a subset of all mesh triangles. This can be computed by masking out all triangles that are not in B . Note, though, that this has to be done *before assembly*, since at this stage the basis functions can still be associated to individual triangles. Global basis functions that live on the boundary of B contribute partially to this integral, and can thus neither be masked out completely nor included completely after assembly.

Let us conclude this subsection with two remarks about solving (154) in the context of shape optimisation: Most of the time during an optimisation descent, the boundary is moved only slightly from one iteration to the next. In order to resolve the boundary and these steps accurately, we have to use a fine enough grid. It may, however, not be necessary to use such a fine grid for solving (154) with reasonable accuracy. Thus, one can try to develop an *adaptive strategy* that uses a fine grid only near the boundary. It may be possible to implement such an approach relatively easily if the level-set method is still performed on a uniform, fine grid, but the triangular mesh is made coarser in the interior (controlled by some error estimator) when solving the FEM systems.

Another idea based on the same observation is the following: If the boundary is, indeed, moved only slightly, the sparse system matrix is also only changed in “a few” places. In particular, for an $M \times M$ grid, we may expect to have $O(M^2)$ triangles while a slight change to the boundary only perturbs $O(M)$ of them (namely along the boundary Γ). With this in mind, one can try to exploit this structure. In particular, when a sparse Cholesky decomposition is known already for the last domain, one can try to

update it with the methods introduced in [27] instead of fully computing a new decomposition. This works, but it comes at a cost: In order to make the updates viable, one has to choose the order of the unknowns in the linear system in a particular way. For a complete factorisation, on the other hand, the order can be chosen arbitrarily to reduce the number of non-zeros in the factor. See, for instance, [71]. It turns out that the *approximate minimum degree* algorithm employed by GNU Octave [35] is so powerful that the complete factorisation with this additional freedom is, in our tests, more efficient than the update strategy. Nevertheless, we believe that it may still be possible to turn the update idea into a more efficient solver with additional research and optimisations.

8.2.3 Approximation of the Shape Derivative

Once u and p are computed, the next step is to find the shape gradient and use it as descent direction. For this, we have to solve (152) numerically. Let us, for now, assume $\alpha = 0$. The case $\alpha > 0$ will be discussed in the following Subsection 8.2.4. We use linear finite elements as before, and the left-hand side of (152) can be discretised with standard mass and stiffness matrices as described in Subsection 8.2.2. This subsection is dedicated to the discretisation of the trace functional on the right-hand side. If we denote the normal and tangential vectors to the boundary Γ by ν and τ , respectively, we can split the gradient ∇u into these two components:

$$\nabla u = \frac{\partial u}{\partial \tau} \cdot \tau + \frac{\partial u}{\partial \nu} \cdot \nu$$

Note that u solves (144) with homogeneous Neumann boundary conditions. Exploiting this fact, we find

$$\langle \nabla u, \nabla p \rangle = \frac{\partial u}{\partial \tau} \cdot \langle \tau, \nabla p \rangle + \frac{\partial u}{\partial \nu} \cdot \langle \nu, \nabla p \rangle = \frac{\partial u}{\partial \tau} \cdot \frac{\partial p}{\partial \tau}.$$

Thus, the right-hand side of (152) becomes

$$\int_{\Gamma} \left((f - u)p - \frac{\partial p}{\partial \tau} \cdot \frac{\partial u}{\partial \tau} \right) F d\sigma. \quad (155)$$

Here, u , p and f are known already by their coefficients in the FEM basis. Note that the choice of linear finite elements implies that these discrete functions are still continuous and piecewise linear when restricted to the boundary polygon approximating Γ . Furthermore, the tangential derivatives of u and p can be computed from their coefficients *just along the boundary polygon*. This is in contrast to the normal derivative and full gradient, which require knowledge of all coefficients on a whole mesh triangle and thus also for basis functions supported on the *interior* of the domain. We can do this because of the a-priori information on the normal derivatives that we have from the state and adjoint equations.

In order to assemble the right-hand side of the discrete FEM system, we have to evaluate the expression (155) along a boundary edge $E \subset \Gamma$ and with F set to one of the basis functions corresponding to the end points of E . Up to rigid transformations, we may assume that $E = [0, \lambda]$ and that the two basis functions on E are

$$q_1(s) = 1 - \frac{s}{\lambda} \quad \text{and} \quad q_2(s) = \frac{s}{\lambda}.$$

Due to symmetry, it is enough to consider one of them; say, $F = q_1$. All that remains now is to evaluate

$$\int_0^\lambda \left((\tilde{f} - \tilde{u})\tilde{p} - \frac{\partial \tilde{u}}{\partial \tau} \cdot \frac{\partial \tilde{p}}{\partial \tau} \right) q_1(s) ds$$

with $\tilde{u}(s) = u_1 q_1(s) + u_2 q_2(s)$ for some coefficients $u_1, u_2 \in \mathbb{R}$. The discrete functions \tilde{p} and \tilde{f} are defined similarly. This integral can be computed symbolically. The result then allows us to assemble the FEM right-hand side for (152) based on the coefficients of u , p and f .

Let us demonstrate numerically that this scheme works: Figure 66 shows the relative errors made when computing (155) on grids of various sizes h . We use the unit square as domain and have chosen the functions u , p , f and F in such a way that the integral (155) can be computed exactly. Furthermore, u and p satisfy homogeneous Neumann boundary conditions. Besides the total error (blue), we also show the error for just the term involving tangential derivatives (red) and the remaining part of the integral (green). One can clearly see that all three terms converge with $O(h^2)$. The derivative term still dominates the total error.

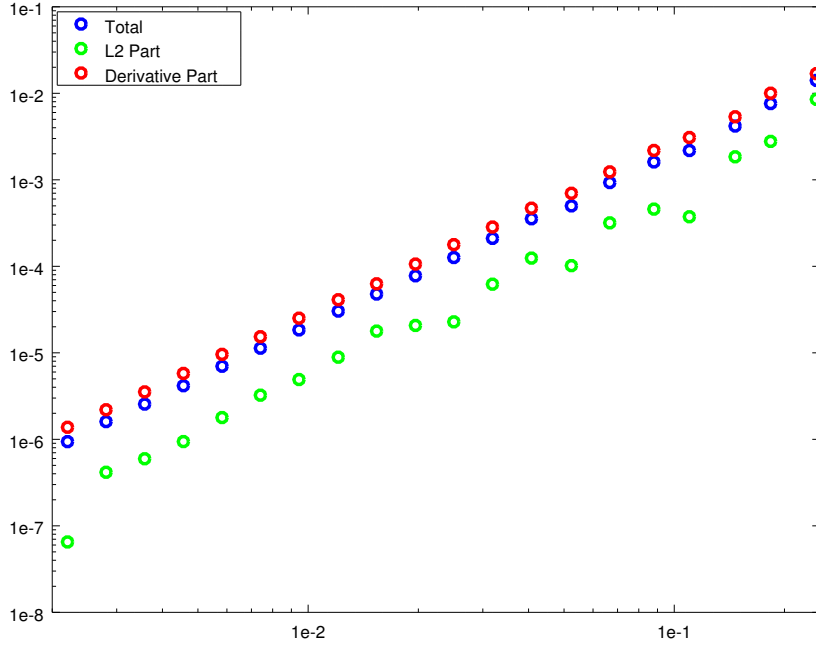


Figure 66: Relative error made by approximating (155) numerically for different grid sizes. The error is also computed separately for the L^2 - and derivative terms. The x -axis shows h .

8.2.4 Discretisation of the Curvature Term

The last remaining piece to discuss for the numerics is handling of the regularisation term in the shape derivative. In particular, we have to approximate the integral

$$\int_{\Gamma} \kappa F d\sigma \quad (156)$$

with κ being, as before, the mean curvature. In order to complete the FEM right-hand side of (152), we have to compute this expression for a polygonal Γ and a FEM basis function F . The key ingredient here is a suitable way to express κ . For our situation of a curve in the plane, the mean curvature is just the standard curvature of this curve. It can be defined (in magnitude) as the derivative of the unit tangential vector of the curve with respect to the arc length s as parameter:

$$|\kappa(s)| = \left| \frac{\partial \tau(s)}{\partial s} \right| = |\dot{\tau}(s)|$$

For a basic introduction into the geometry of curves, see [33]. In particular, Remark 1 on page 21 deals with the curvature of plane curves. Let us rewrite $|\kappa|$ now in terms of the angle $\omega(s)$ which the tangential direction has with respect to some fixed reference direction. Choosing the x -axis as reference, we get

$$\tau(s) = \begin{pmatrix} \sin \omega(s) \\ \cos \omega(s) \end{pmatrix} \Rightarrow \kappa(s)^2 = \left| \begin{pmatrix} \cos \omega(s) \\ -\sin \omega(s) \end{pmatrix} \cdot \dot{\omega}(s) \right|^2 = |\dot{\omega}(s)|^2.$$

In this form, we can even take the orientation into account to define the curvature with the proper sign. Henceforth, let us use $\kappa(s) = \dot{\omega}(s)$ as the curvature.

We have to employ this expression now in the discrete setting of our boundary polygon. Let us use the notation depicted in Figure 67 for this: At some boundary point x_i , we denote the approximated curvature by κ_i . The preceding and following edges are numbered $i-1$ and i . The length of an edge j

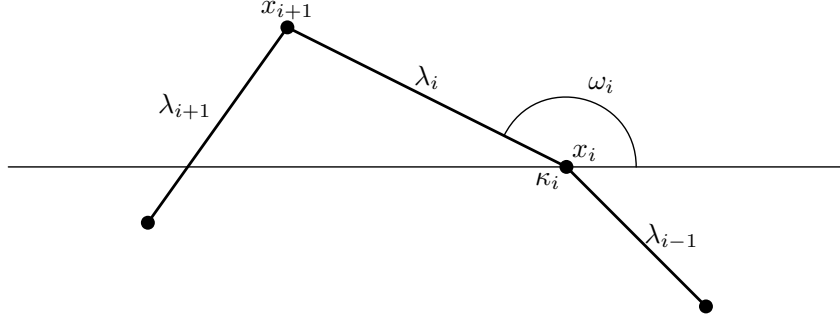


Figure 67: Notation used for the boundary polygon in Subsection 8.2.4.

is λ_j and its angle to the reference axis is ω_j . A straight-forward approximation gives

$$\kappa_i \approx 2 \frac{\omega_i - \omega_{i-1}}{\lambda_i + \lambda_{i-1}}.$$

Thus, for the Lagrangian basis function r_i corresponding to x_i , we may use the approximation

$$\int_{\Gamma} \kappa r_i d\sigma \approx \frac{\kappa_i}{2} (\lambda_{i-1} + \lambda_i) = \omega_i - \omega_{i-1}.$$

It is interesting to note that we can arrive at exactly the same conclusion via a different approach: Using $\kappa = \dot{\omega}$ and integration by parts, we may rewrite (156) to

$$\int_{\Gamma} \kappa F d\sigma = \int_{\Gamma} \dot{\omega} F d\sigma = - \int_{\Gamma} \omega \frac{\partial F}{\partial \tau} d\sigma.$$

The boundary term vanishes since Γ consists only of closed curves. For the FEM basis function r_i in the place of F , this integral and the tangential derivative can be evaluated as described above in Subsection 8.2.3. This yields

$$- \int_{\Gamma} \omega \frac{\partial r_i}{\partial \tau} d\sigma = - \left(\frac{\omega_{i-1}}{\lambda_{i-1}} \lambda_{i-1} - \frac{\omega_i}{\lambda_i} \lambda_i \right) = \omega_i - \omega_{i-1}$$

and thus an approximation equivalent to the result of the previous calculation. It is, of course, straight-forward to evaluate this expression for the boundary polygon and compute (156) with it.

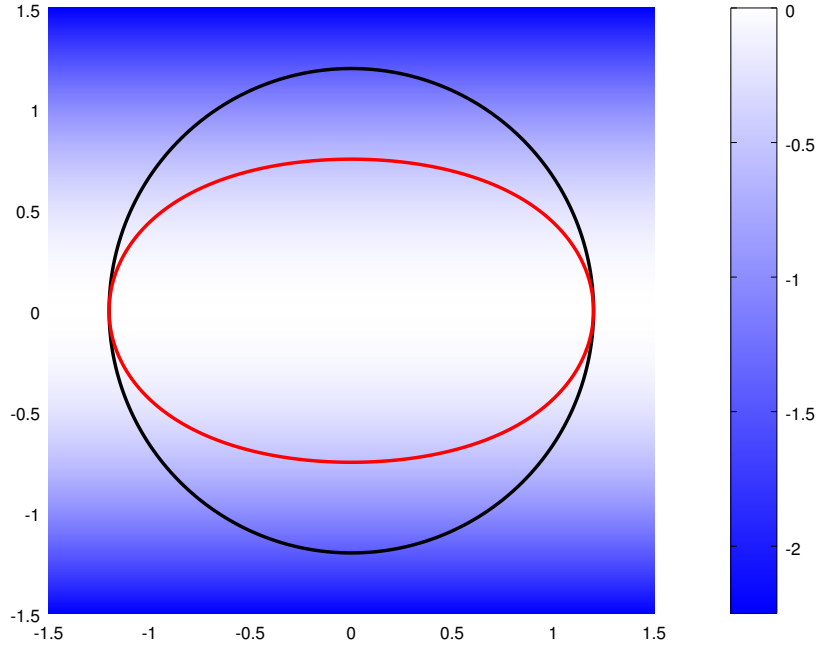
8.3 Numerical Results

We implemented the methods and solver described above in GNU Octave [35]. For the time evolution of shapes, we used our `level-set` package [59] and the methods described in Chapter 3. All computations were done on a desktop computer of the `amd64` architecture.

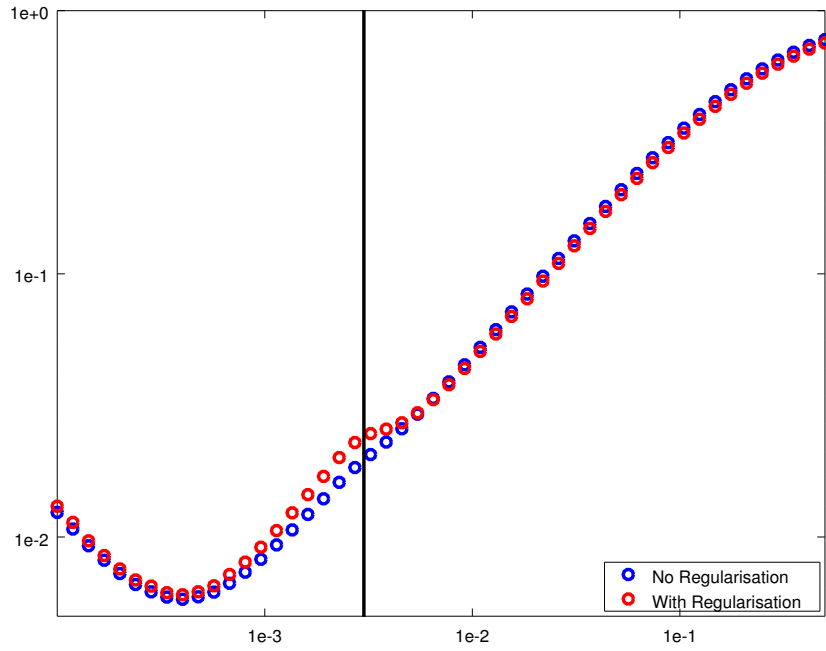
8.3.1 Shape Derivative and Finite Differences

First, let us validate our methods for computing shape derivatives. For this, we compare the derivative computed with (151) to a finite-difference approximation. The shape derivative is computed based on Subsection 8.2.3 and Subsection 8.2.4 on a very fine $1,000 \times 1,000$ grid. In addition, we also evolve the domain for a short time and compute the changes to the cost directly. We use the speed field shown in Figure 68a as direction, which transforms a spherical initial domain into an ellipse. The relative difference between both values is shown in Figure 68b. One can clearly see the typical behaviour of a finite-difference approximation: The difference quotient converges to the exact derivative as the step length goes to zero, until it reaches a minimum value when the approximation gets worse again due to numerical errors. We get almost the same result with and without the regularisation term.

The vertical line indicates the grid spacing h . Since our speed field has, very roughly, magnitude one, this corresponds at least by order of magnitude to the time step at which the boundary is moved



(a) The speed field defining the direction together with the initial domain (black) and the evolved domain for a large time step (red).



(b) Relative error between (151) and finite differences for various lengths of the time step.

Figure 68: Comparison between the shape derivative computed with (151) and a finite-difference approximation. The computation has been done both with ($\alpha = 1$) and without ($\alpha = 0$) regularisation. The vertical line in the bottom plot indicates the grid spacing h . See the discussion in Subsection 8.3.1.

about one grid cell. This is the step where one can intuitively expect the approximation to break down. Interestingly, it even continues to work well for step lengths smaller by almost a factor of ten. All in all, the results show that our implementations work as expected and are, indeed, able to compute shape derivatives with good precision.

8.3.2 Regularisation of an Inverse Problem

Let us consider the effect of the regularisation parameter α next. As test problem, we use

$$u_d(x, y) = (x^2 + y^2) - \frac{(x^2 + y^2)^3}{3}.$$

One can trivially compute a forcing function f from (144) such that u_d is an exact solution on the domain $\Omega_{\text{ex}} = B_1(0, 0)$. For our computation, we chose a square as initial domain and added 10% of Gaussian noise to u_d . Additional choices were $t_{\min} = 10^{-6}$ for the minimum step length, 1,000 descent iterations for all runs, a 500×500 grid and

$$B = \left\{ (x, y) \in \mathbb{R}^2 \mid |x| \leq \frac{1}{2} \text{ and } |y| \leq \frac{1}{2} \right\}.$$

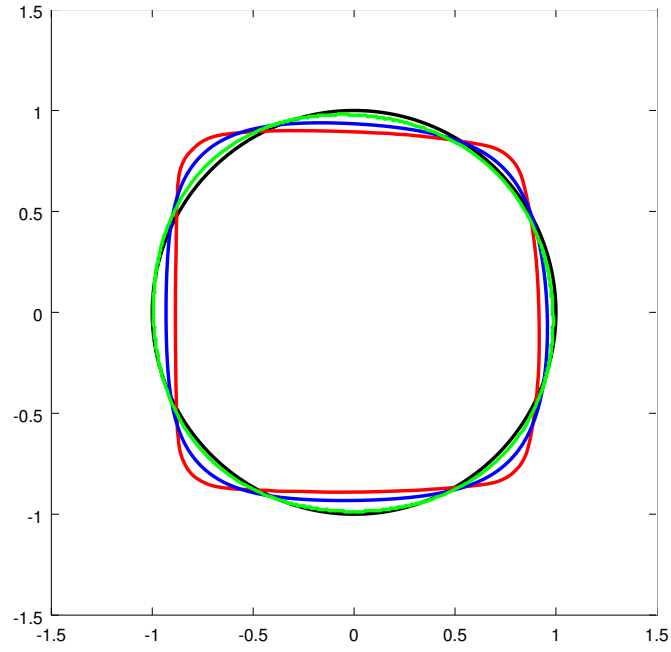
Figure 69 shows how well we are able to reconstruct Ω_{ex} from the noisy data for different regularisation parameters α . The plot in Figure 69a shows the reconstructed domains for selected parameter values. Figure 69b, in particular, shows the Hausdorff distance between the desired Ω_{ex} and the reconstructions as a function of α . Note that our cost functional is relatively insensitive to changes in the shape, so that there is a wide range of shapes that bring the cost down to almost the same minimal value (non-zero due to the noise). Thus, one can see that the resulting shape without regularisation (red) and also with small α is still quite far from Ω_{ex} . With increasing regularisation, the shape gets closer (blue and green in the plots). However, if α is increased too much, the results become worse again; over-regularisation forces the optimal shape to be too small. Of course, it is important to keep in mind that the regularisation term we use (the boundary length) is, of course, very favourable for the reconstruction of the *circle* Ω_{ex} .

Note that the regularisation creates additional numerical difficulties. Take a look at Figure 70: It shows the evolution of the cost, gradient norm and the used step lengths for a particular descent run. As one expects from such a run, the first few iterations are very effective at reducing the cost and gradient. After that, the decrease continues, but only at a much slower pace. The step length is roughly constant (around 10^{-1} in the example) throughout this phase. Two consecutive speed fields for this part of the descent are shown in Figure 71. One can see that they try to move the domain in the right direction, but the zig-zag behaviour already discussed in Section 6.5 makes the descent inefficient. Compare, in particular, Figure 42. The difference with Figure 70, however, is that a final phase follows afterwards: There, the iteration gets completely stuck with mostly the minimum step length enforced. A typical speed field is shown in Figure 72. Here, no longer any zig-zag movement happens. Instead, the force due to the tracking term in the cost functional has decreased so much that the numerical approximation of the curvature is the dominant driving force. This, however, can become unstable when no other forces are present anymore. Small but sharp corners form (in the figure to the north east), which force the line search to accept only the minimum step length. These corners have the additional detrimental effect of actually *decreasing* boundary smoothness (although the regularisation should, in theory, increase it), which leads to an *increase* of the cost and gradient going forward.

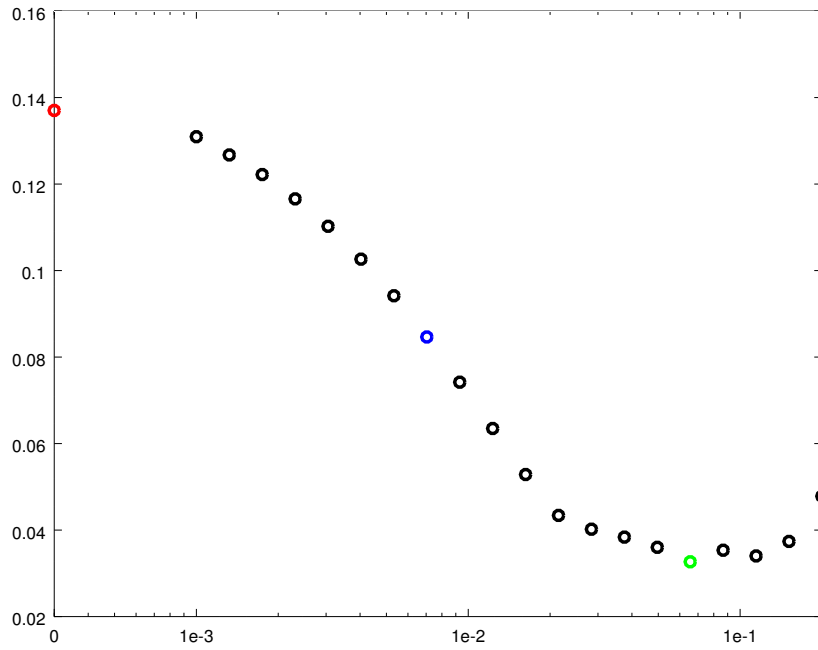
Obviously, this effect gets worse the larger α is. It also gets worse when β is chosen smaller, because this leads to less smoothing of the speed fields. Hence, one has to find a good balance between α and β . This is illustrated in Figure 73: For fixed $\alpha = 10^{-2}$ and descent runs with various choices of β , the accepted step lengths are shown. The smaller β is, the earlier the minimum step length is enforced. The best costs achieved throughout each of these runs are also smaller for larger values of β .

8.3.3 Convergence of the Gradient Descent

Let us now show numerical results for a more interesting problem of shape optimisation. For the computations here, we have turned off regularisation (i. e., $\alpha = 0$) completely. This allows us to focus on the behaviour of the optimisation algorithm in terms of decreasing the actual cost functional (146) and,



(a) Reconstructed domains in comparison to Ω_{ex} (black).



(b) Hausdorff distance between Ω_{ex} and the reconstruction for various regularisation parameters.

Figure 69: Quality of the reconstruction of the exact shape Ω_{ex} from noisy data for various regularisation parameters. The reconstructed domains (top) correspond to the values of α marked with the respective colour in the bottom plot.

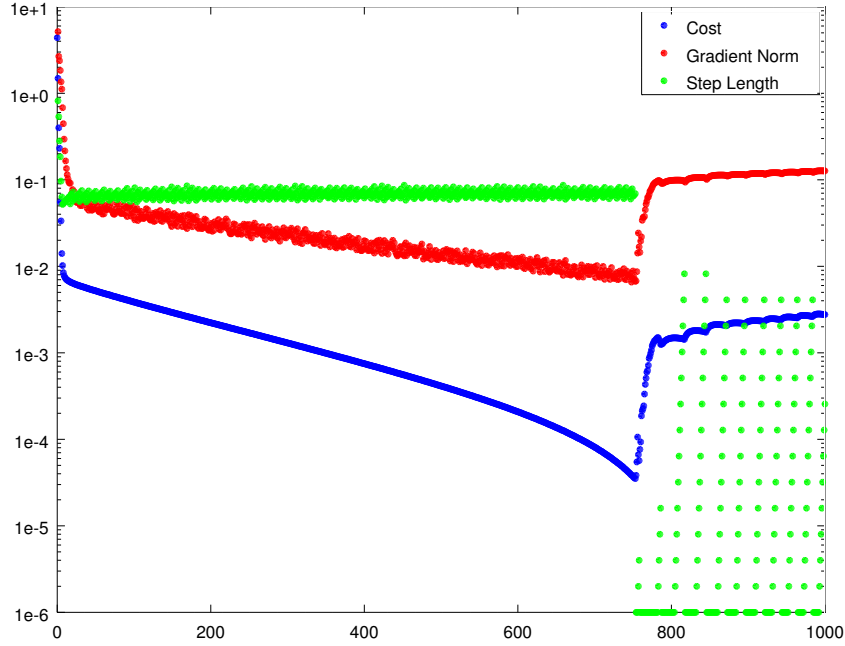
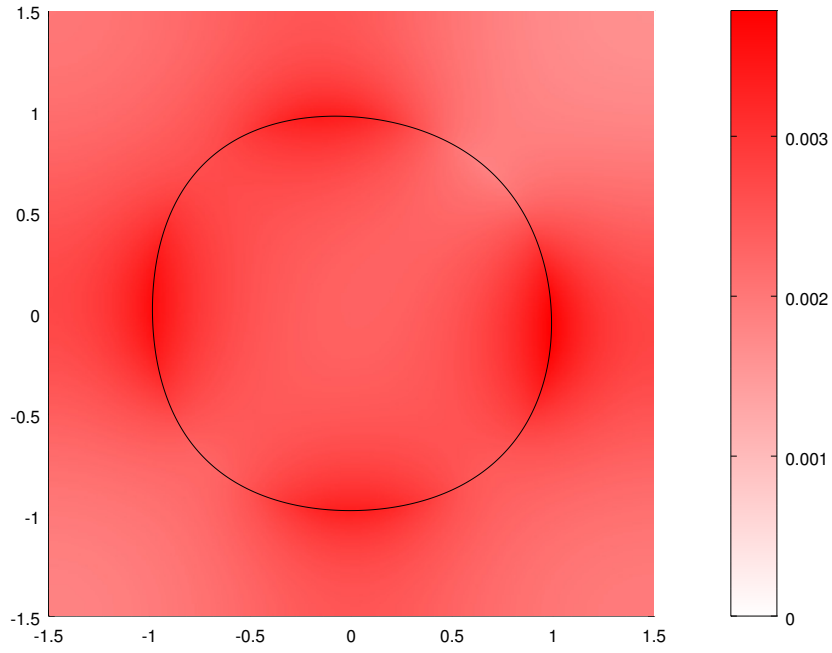


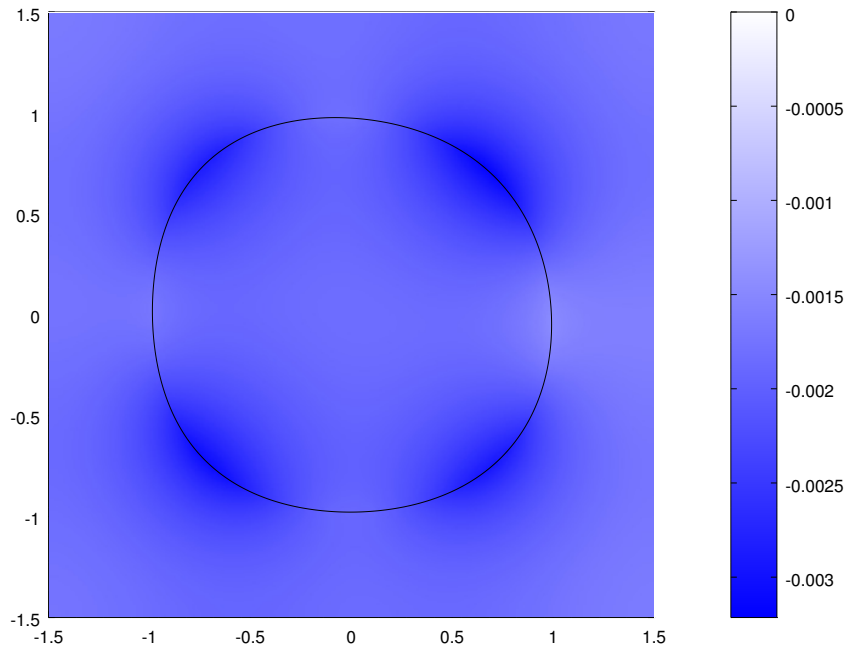
Figure 70: Behaviour of a typical descent iteration with regularisation turned on.

in particular, tracking u_d . The basic situation is shown in Figure 74a. For our choice of Ω_{ex} and some f , we computed an exact solution as u_d with **fem-fenics** [79] based on FEniCS [63]. This ensures that the data generation is done independently from our own solver. To this “exact” u_d , we added 10% of Gaussian noise. The forcing function f was chosen in such a way that it strongly penalises the domain inside the hole of Ω_{ex} . We use $t_{\min} = 10^{-3}$ here to avoid getting stuck in the gradient descent, and performed 2,000 descent iterations on a 500×500 grid.

The final shapes for different choices of β are shown in Figure 74b. The corresponding cost evolutions are plotted in Figure 75 for the first 1,000 steps. One can clearly see that the choice of β matters: The best result is achieved with $\beta = 10^{-2}$. For $\beta = 1$, the speed fields are too smooth and thus not flexible enough to provide an efficient descent. Many more iterations would be needed to converge to an optimal shape. With $\beta = 10^{-3}$, on the other hand, the resulting shape is quite irregular. The descent is converged in this case, but $\beta = 10^{-2}$ leads to a better result. We also tried $\beta = 10^{-1}$. In this case, the descent converges within our 2,000 descent steps, but more slowly than with $\beta = 10^{-2}$. Apart from that, the descent behaviour and final shape are similar to the situation with $\beta = 10^{-2}$. Figure 76, finally, shows two typical speed fields as they appear in the descent for $\beta = 10^{-2}$: More often, the speed looks like Figure 76a. The domain grows slowly towards the bottom, following the geometry of Ω_{ex} . From time to time, however, a speed like Figure 76b is used when the domain is too far inside the hole and the strongly penalising f forces it out again.



(a) Iteration 750



(b) Iteration 751

Figure 71: Speed fields at two consecutive iteration steps for the descent of Figure 70. They still correspond to the situation with step length around 10^{-1} .

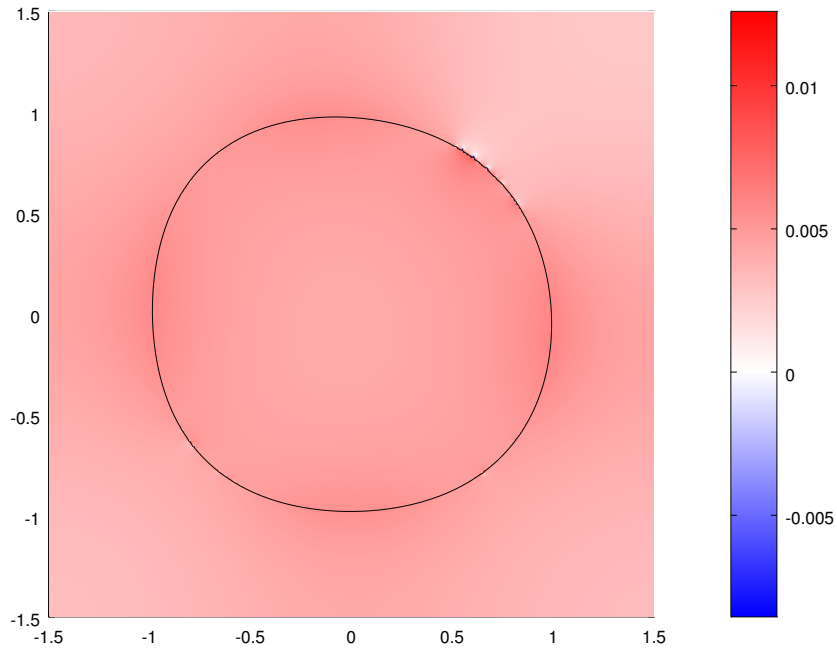


Figure 72: Continuation of Figure 71. This is at iteration 775 and shows a typical speed field where the minimum step length is enforced.

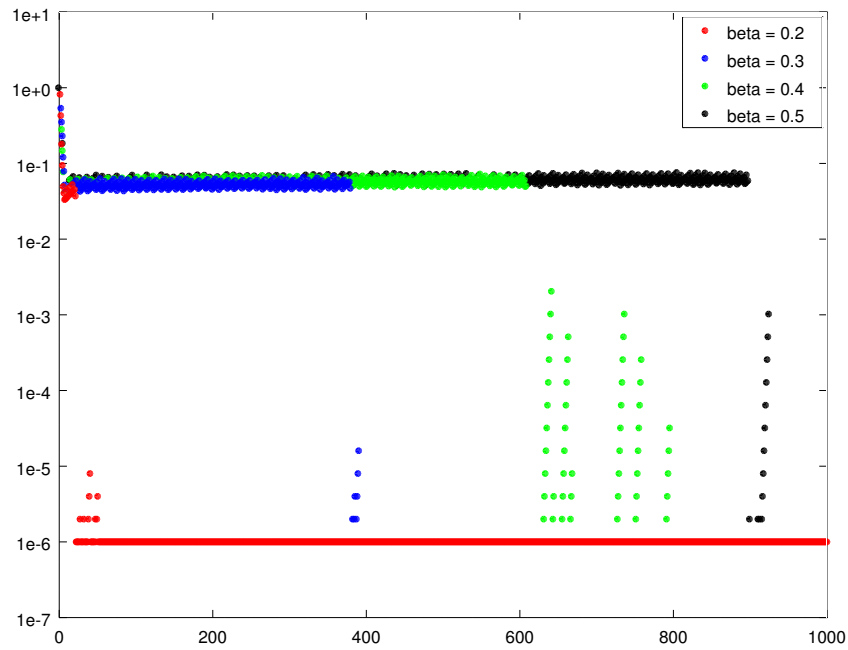
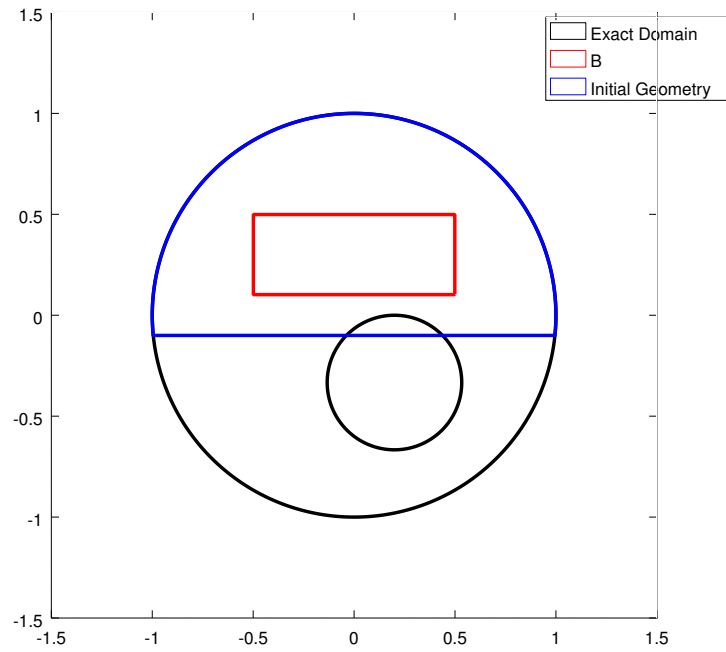
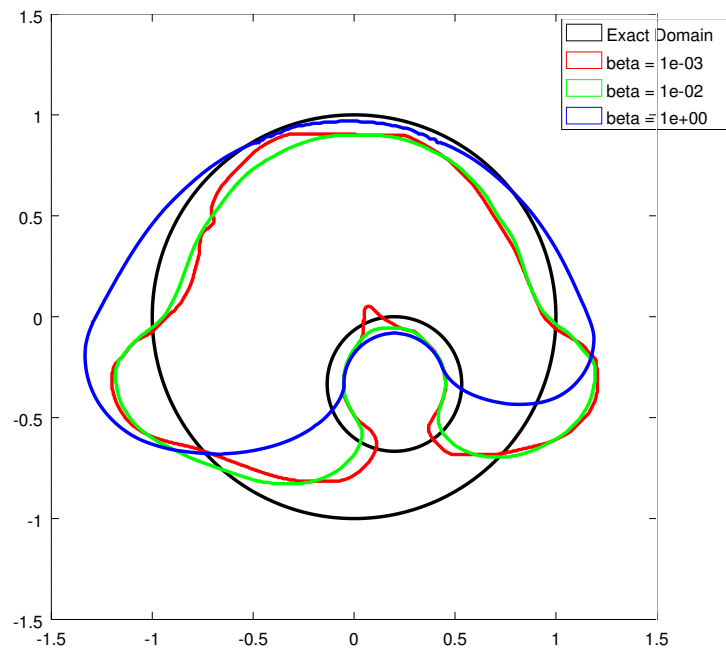


Figure 73: Step lengths accepted by the line search for different choices of the descent parameter β in the situation of Subsection 8.3.2.

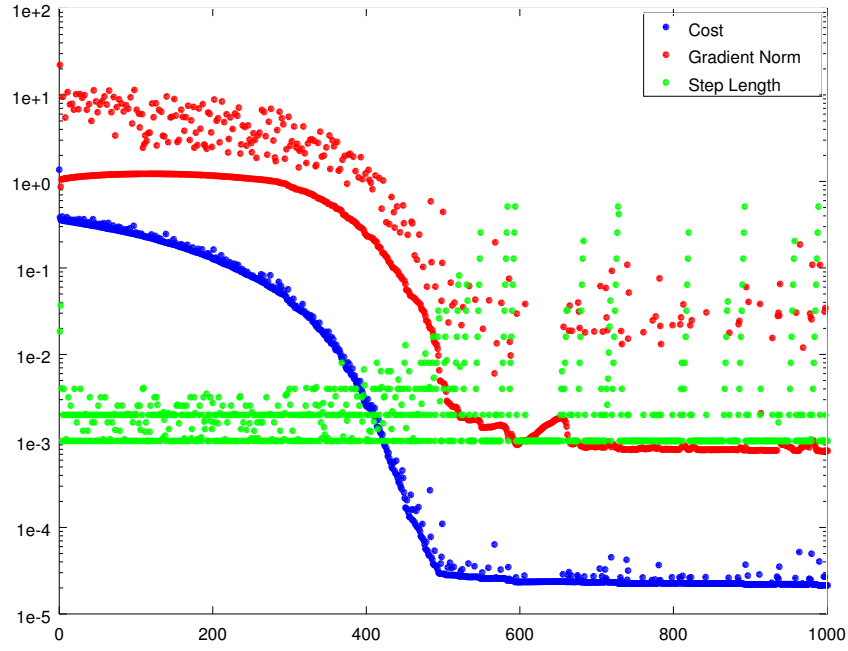


(a) Basic situation with Ω_{ex} , B and Ω_0 .

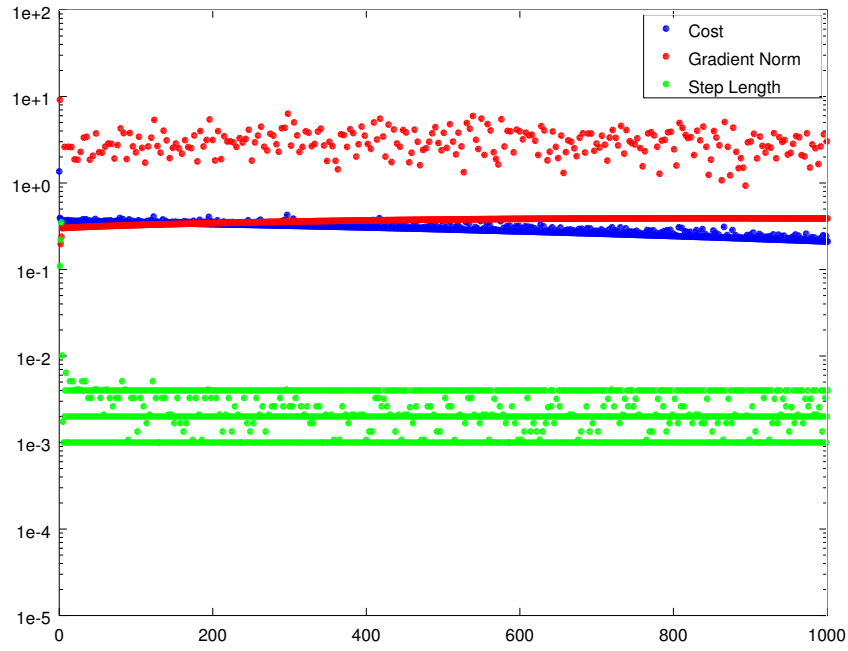


(b) Final shapes for various choices of β .

Figure 74: The example problem for shape optimisation discussed in Subsection 8.3.3.

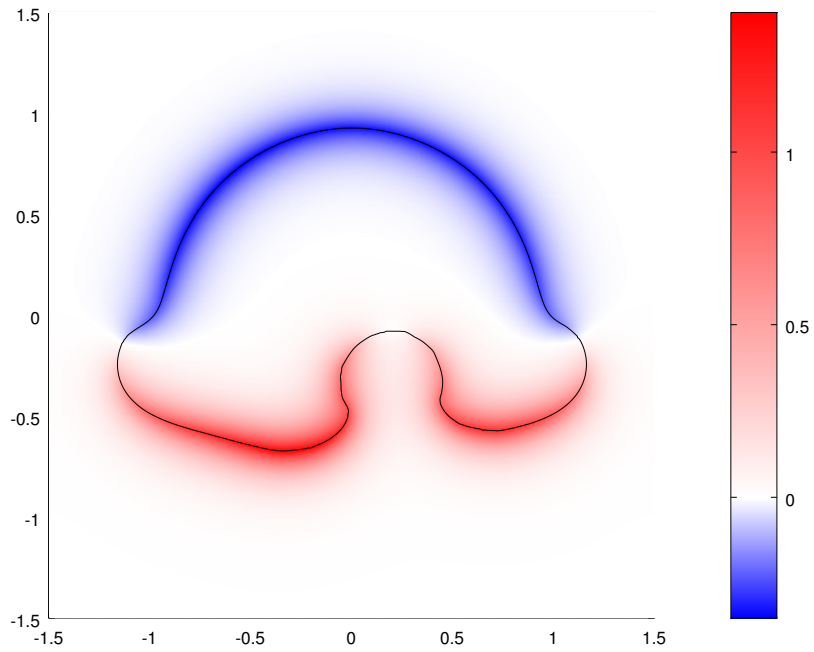


(a) $\beta = 10^{-2}$

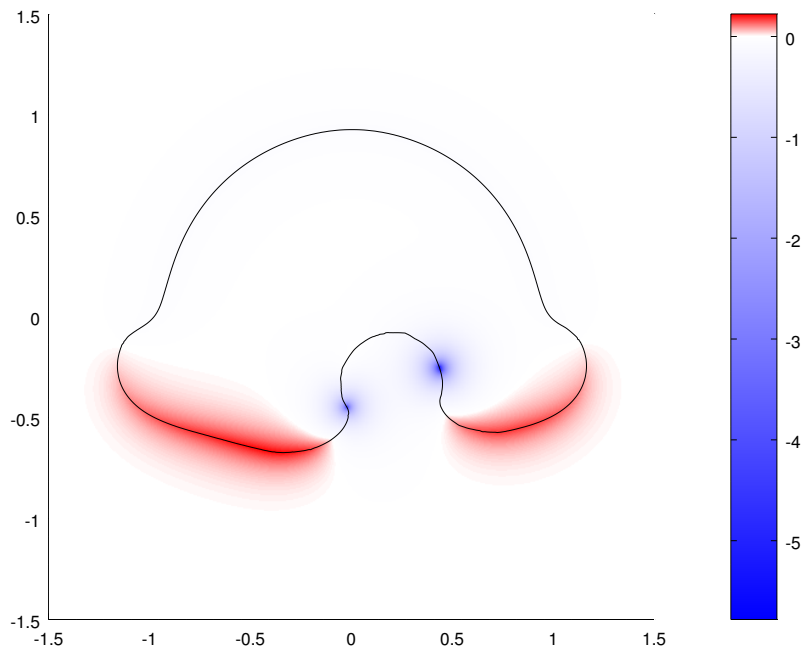


(b) $\beta = 1$

Figure 75: Continuation of Figure 74. Evolution of the cost, gradient norm and step length.



(a) Iteration 308



(b) Iteration 309

Figure 76: Continuation of Figure 74. The two kinds of typical speed fields during the descent.

References

- [1] Giovanni Alberti, Stefano Bianchini, and Gianluca Crippa. Structure of Level Sets and Sard-Type Properties of Lipschitz Maps. *Annali della Scuola Normale Superiore di Pisa - Classe di Scienze*, 12(4):863–902, 2013.
- [2] Grégoire Allaire, François Jouve, and Anca-Maria Toader. A Level-Set Method for Shape Optimization. *Comptes Rendus Mathématique*, 334(12):1125–1130, 2002.
- [3] Fred Almgren, Jean E. Taylor, and Lihe Wang. Curvature-Driven Flows: A Variational Approach. *SIAM Journal on Control and Optimization*, 31(2):387–437, March 1993.
- [4] Luigi Ambrosio, Nicola Fusco, and Diego Pallara. *Functions of Bounded Variation and Free Discontinuity Problems*. Oxford Mathematical Monographs. Oxford Science Publications, 2000.
- [5] J. Andreas Bærentzen. On the Implementation of Fast Marching Methods for 3D Lattices. Technical Report IMM-REP-2001-13, Department of Mathematical Modelling, Technical University of Denmark, 2001.
- [6] Martino Bardi and Italo Capuzzo-Dolcetta. *Optimal Control and Viscosity Solutions of Hamilton-Jacobi-Bellman Equations*. Systems & Control: Foundations & Applications. Birkhäuser, 1997.
- [7] Martino Bardi and Francesca Da Lio. On the Strong Maximum Principle for Fully Nonlinear Degenerate Elliptic Equations. *Archiv der Mathematik*, 73:276–285, 1999.
- [8] G. Barles, H. M. Soner, and P. E. Souganidis. Front Propagation and Phase Field Theory. *SIAM Journal on Control and Optimization*, 31(2):439–469, March 1993.
- [9] Richard Bellman. On the Theory of Dynamic Programming. *Proceedings of the National Academy of Sciences*, 38(8):716–719, 1952.
- [10] Richard Bellman. *Dynamic Programming*. Princeton University Press, 1957.
- [11] Dimitri P. Bertsekas. *Dynamic Programming and Optimal Control*. Athena Scientific, 1995.
- [12] L. E. Blumenson. A Derivation of n -Dimensional Spherical Coordinates. *The American Mathematical Monthly*, 67(1):63–66, January 1960.
- [13] Dorin Bucur and Jean-Paul Zolésio. Free Boundary Problems and Density Perimeter. *Journal of Differential Equations*, 126:224–243, 1996.
- [14] Martin Burger. A Framework for the Construction of Level Set Methods for Shape Optimization and Reconstruction. *Interfaces and Free Boundaries*, 5:301–329, 2003.
- [15] Martin Burger, Benjamin Hackl, and Wolfgang Ring. Incorporating Topological Derivatives into Level Set Methods. *Journal of Computational Physics*, 194:344–362, 2004.
- [16] Martin Burger, Norayr Matevosyan, and Marie-Therese Wolfram. A Level Set Based Shape Optimization Method for an Elliptic Obstacle Problem. *Mathematical Models and Methods in Applied Sciences*, 21(4):619–649, April 2011.
- [17] Italo Capuzzo-Dolcetta. A Generalized Hopf-Lax Formula: Analytical and Approximations Aspects. In Fabio Ancona, editor, *Geometric Control and Nonsmooth Analysis*, volume 76 of *Series on Advances in Mathematics for Applied Sciences*, pages 136–150. World Scientific, 2008.
- [18] David G. Caraballo. Areas of Level Sets of Distance Functions Induced by Asymmetric Norms. *Pacific Journal of Mathematics*, 218(1), January 2005.
- [19] E. Carlini, M. Falcone, N. Forcadell, and R. Monneau. Convergence of a Generalized Fast-Marching Method for an Eikonal Equation with a Velocity-Changing Sign. *SIAM Journal of Numerical Analysis*, 46(6):2920–2952, 2008.

- [20] Vicent Caselles, Francine Catté, Tomeu Coll, and Françoise Dibos. A Geometric Model for Active Contours in Image Processing. *Numerische Mathematik*, 66:1–31, 1993.
- [21] Tony F. Chan and Luminita A. Vese. Image Segmentation Using Level Sets and the Piecewise-Constant Mumford-Shah Model. Technical Report 00-14, UCLA CAM, 2000.
- [22] Chong Chen, Juelin Leng, and Guoliang Xu. A General Framework of Piecewise-Polynomial Mumford-Shah Model for Image Segmentation. Technical Report 13-50, UCLA CAM, 2013.
- [23] Thomas H. Cormen, Charles E. Leiserson, Ronald L. Rivest, and Clifford Stein. *Introduction to Algorithms*. The MIT Press and McGraw-Hill Book Company, second edition, 2001.
- [24] R. Courant, K. Friedrichs, and H. Lewy. Über die partiellen Differenzengleichungen der mathematischen Physik. *Mathematische Annalen*, 100:32–74, 1928.
- [25] Michael G. Crandall. Viscosity Solutions: a Primer. In *Viscosity Solutions and Applications*, volume 1660 of *Lecture Notes in Mathematics*, pages 1–43. Springer, 1997.
- [26] Michael G. Crandall, Hitoshi Ishii, and Pierre-Louis Lions. User’s Guide to Viscosity Solutions of Second Order Partial Differential Equations. *Bulletin of the American Mathematical Society*, 27(1):1–67, July 1992.
- [27] Timothy A. Davis and William W. Hager. Multiple-Rank Modifications of a Sparse Cholesky Factorization. *SIAM Journal on Matrix Analysis and Applications*, 22(4):997–1013, 2001.
- [28] Klaus Deckelnick and Gerhard Dziuk. Numerical Approximation of Mean Curvature Flow of Graphs and Level Sets. In P. Colli and J. F. Rodrigues, editors, *Mathematical Aspects of Evolving Interfaces*, volume 1812 of *Lecture Notes in Mathematics*, pages 53–87. Springer, 2003.
- [29] Michel C. Delfour and Jean-Paul Zolésio. The New Family of Cracked Sets and the Image Segmentation Problem Revisited. *Communications in Information and Systems*, 4(1):29–52, 2004.
- [30] Michel C. Delfour and Jean-Paul Zolésio. *Shapes and Geometries: Metrics, Analysis, Differential Calculus, and Optimization*. Advances in Design and Control. SIAM, second edition, 2011.
- [31] Peter Deufhard and Martin Weiser. *Adaptive Numerical Solutions of PDEs*. De Gruyter, 2012.
- [32] Edsger W. Dijkstra. A Note on Two Problems in Connexion with Graphs. *Numerische Mathematik*, 1:269–271, 1959.
- [33] Manfredo P. do Carmo. *Differential Geometry of Curves and Surfaces*. Prentice-Hall, 1976.
- [34] Marc Droske and Wolfgang Ring. A Mumford-Shah Level-Set Approach For Geometric Image Registration. *SIAM Journal on Applied Mathematics*, 66(6):2127–2148, 2006.
- [35] John W. Eaton, David Bateman, Søren Hauberg, and Rik Wehbring. GNU Octave version 4.0.0 manual: a high-level interactive language for numerical computations, 2015. <https://www.gnu.org/software/octave/doc/interpreter/>.
- [36] Lawrence C. Evans. *Partial Differential Equations*, volume 19 of *Graduate Studies in Mathematics*. American Mathematical Society, 1998.
- [37] Lawrence C. Evans and Ronald F. Gariepy. *Measure Theory and Fine Properties of Functions*. Studies in Advanced Mathematics. CRC Press, 1992.
- [38] Lawrence C. Evans and Joel Spruck. Motion of Level Sets by Mean Curvature, I. *Journal of Differential Geometry*, 33(3):635–681, 1991.
- [39] M. Falcone, T. Giorgi, and P. Loreti. Level Sets of Viscosity Solutions: Some Applications to Fronts and Rendez-Vous Problems. *SIAM Journal on Applied Mathematics*, 54(5):1335–1354, 1994.
- [40] Herbert Federer. *Geometric Measure Theory*. Springer, 1969.

- [41] Yoshikazu Giga. *Surface Evolution Equations: A Level Set Approach*, volume 99 of *Monographs in Mathematics*. Birkhäuser, 2006.
- [42] David Gilbarg and Neil S. Trudinger. *Elliptic Partial Differential Equations of Second Order*, volume 224 of *Grundlehren der mathematischen Wissenschaften*. Springer, 1998.
- [43] Matthew A. Grayson. The Heat Equation Shrinks Embedded Plane Curves to Round Points. *Journal of Differential Geometry*, 26(2):285–314, 1987.
- [44] Jaroslav Haslinger and Raino A. E. Mäkinen. *Introduction to Shape Optimization: Theory, Approximation, and Computation*. Advances in Design and Control. SIAM, 2003.
- [45] Lester L. Helms. *Potential Theory*. Springer, second edition, 2014.
- [46] Antoine Henrot and Michel Pierre. *Variation et optimisation de formes: Une analyse géométrique*, volume 48 of *Mathématiques & Applications*. Springer, 2005.
- [47] Michael Hinze, Rene Pinnau, Michael Ulbrich, and Stefan Ulbrich. *Optimization with PDE Constraints*, volume 23 of *Mathematical Modelling: Theory and Applications*. Springer, 2009.
- [48] Hitoshi Ishii. Perron’s Method for Hamilton-Jacobi Equations. *Duke Mathematical Journal*, 55(2):369–384, June 1987.
- [49] Michael Kass, Andrew Witkin, and Demetri Terzopoulos. Snakes: Active Contour Models. *International Journal of Computer Vision*, 1(4):321–331, January 1988.
- [50] Bernhard Kawohl and Nikolay Kutev. Comparison Principle and Lipschitz Regularity for Viscosity Solutions of Some Classes of Nonlinear Partial Differential Equations. *Funkcialaj Ekvacioj*, 43:241–253, 2000.
- [51] Stephen L. Keeling and Leonie Knittelfelder. Image Segmentation Based upon Piecewise Polynomials on Connected Sets. Draft, University of Graz, 2015.
- [52] Moritz Keuthen. *Second Order Shape Optimization with Geometric Constraints*. PhD thesis, Technical University of Munich, 2015.
- [53] Moritz Keuthen and Daniel Kraft. Shape Optimization of a Breakwater. *Inverse Problems in Science and Engineering*, September 2015.
- [54] Moritz Keuthen and Michael Ulbrich. Moreau-Yosida Regularization in Shape Optimisation with Geometric Constraints. *Computational Optimization and Applications*, May 2014.
- [55] Donald E. Knuth. *Sorting and Searching*, volume 3 of *The Art of Computer Programming*. Addison-Wesley, second edition, 1998.
- [56] Daniel Kraft. A Hopf-Lax Formula for the Time Evolution of the Level-Set Equation and a New Approach to Shape Sensitivity Analysis. Preprint IGDK-2015-18, https://igdk1754.ma.tum.de/foswiki/pub/IGDK1754/Preprints/Kraft_2015A.pdf.
- [57] Daniel Kraft. Computing the Hausdorff Distance of Two Sets from Their Signed Distance Functions. Preprint IGDK-2015-03, https://igdk1754.ma.tum.de/foswiki/pub/IGDK1754/Preprints/Kraft_2015.pdf.
- [58] Daniel Kraft. A Hopf-Lax Formula for the Level-Set Equation and Applications to PDE-Constrained Shape Optimisation. In *Proceedings of the 19th International Conference on Methods and Models in Automation and Robotics*, pages 498–503. IEEE Xplore, 2014.
- [59] Daniel Kraft. The `level-set` Package for GNU Octave. Octave Forge, 2014–2015. <http://octave.sourceforge.net/level-set/>.
- [60] Daniel Kraft. Measure-Theoretic Properties of Level Sets of Distance Functions. *Journal of Geometric Analysis (accepted)*, 2015.

- [61] Randall J. LeVeque. *Finite Difference Methods for Ordinary and Partial Differential Equations: Steady-State and Time-Dependent Problems*. SIAM, 2007.
- [62] Pierre-Louis Lions. *Generalized Solutions of Hamilton-Jacobi Equations*, volume 69 of *Research Notes in Mathematics*. Pitman Advanced Publishing Program, 1982.
- [63] Anders Logg, Kent-Andre Mardal, Garth N. Wells, et al. *Automated Solution of Differential Equations by the Finite Element Method*. Springer, 2012.
- [64] François Murat and Jacques Simon. Sur le contrôle par un domaine géométrique. Technical Report 76015, Laboratoire d'Analyse Numérique, Université de Paris VI, 1976.
- [65] Jorge Nocedal and Stephen J. Wright. *Numerical Optimization*. Springer Series in Operation Research and Financial Engineering. Springer, second edition, 2006.
- [66] Stanley J. Osher and Fadil Santosa. Level Set Methods for Optimization Problems Involving Geometry and Constraints: I. Frequencies of a Two-Density Inhomogeneous Drum. *Journal of Computational Physics*, 171(1):272–288, 2001.
- [67] Stanley J. Osher and James A. Sethian. Fronts Propagating with Curvature-Dependent Speed: Algorithms Based on Hamilton-Jacobi Formulations. *Journal of Computational Physics*, 79:12–49, 1988.
- [68] Olivier Pironneau. *Optimal Shape Design for Elliptic Systems*. Springer Series in Computational Physics. Springer, 1984.
- [69] Ronny Ramlau and Wolfgang Ring. A Mumford-Shah Level-Set Approach for the Inversion and Segmentation of X-Ray Tomography Data. *Journal of Computational Physics*, 221:539–557, 2007.
- [70] C. W. Rhee, L. Talbot, and James A. Sethian. Dynamical Behaviour of a Premixed Turbulent Open V-Flame. *Journal of Fluid Mechanics*, 300:87–115, October 1995.
- [71] Donald J. Rose. A Graph-Theoretic Study of the Numerical Solution of Sparse Positive Definite Systems of Linear Equations. In Ronald C. Read, editor, *Graph Theory and Computing*, pages 183–217. Academic Press, 1972.
- [72] Elisabeth Rouy and Agnès Tourin. A Viscosity Solutions Approach to Shape-from-Shading. *SIAM Journal on Numerical Analysis*, 29(3):867–884, June 1992.
- [73] George I. N. Rozvany. *Structural Design via Optimality Criteria: The Prager Approach to Structural Optimization*, volume 8 of *Mechanics of Elastic and Inelastic Solids*. Kluwer Academic Publishers, 1989.
- [74] Walter Rudin. *Real and Complex Analysis*. McGraw-Hill Book Company, third edition, 1987.
- [75] Fadil Santosa. A Level-Set Approach for Inverse Problems Involving Obstacles. *ESIAM: Control, Optimisation and Calculus of Variations*, 1:17–33, January 1996.
- [76] James A. Sethian. A Fast Marching Level Set Method for Monotonically Advancing Fronts. *Proceedings of the National Academy of Sciences*, 93(4):1591–1595, 1996.
- [77] James A. Sethian. *Level Set Methods and Fast Marching Methods: Evolving Interfaces in Computational Geometry, Fluid Mechanics, Computer Vision, and Materials Science*. Cambridge University Press, second edition, 1999.
- [78] Jan Sokolowski and Jean-Paul Zolésio. *Introduction to Shape Optimization: Shape Sensitivity Analysis*, volume 16 of *Springer Series in Computational Mathematics*. Springer, 1992.
- [79] Marco Vassallo. The fem-fenics Package for GNU Octave. Octave Forge, 2015. <http://octave.sourceforge.net/fem-fenics/>.
- [80] B. C. Vemuri, J. Ye, Y. Chen, and C. M. Leonard. Image Registration via Level-Set Motion: Applications to Atlas-Based Segmentation. *Medical Image Analysis*, 7:1–20, 2003.

- [81] Luminita A. Vese and Tony F. Chan. A Multiphase Level Set Framework for Image Segmentation Using the Mumford and Shah Model. *International Journal of Computer Vision*, 50(3):271–293, 2002.
- [82] Wolfgang A. Wall, Moritz A. Frenzel, and Christian Cyron. Isogeometric Structural Shape Optimization. *Computer Methods in Applied Mechanics and Engineering*, 197:2976–2988, 2008.
- [83] Michael Yu Wang, Xiaoming Wang, and Dongming Guo. A Level Set Method for Structural Topology Optimization. *Computer Methods in Applied Mechanics and Engineering*, 192:227–246, 2003.
- [84] Philip Wolfe. Convergence Conditions for Ascent Methods. *SIAM Review*, 11(2), April 1969.
- [85] James Yeh. *Real Analysis: Theory of Measure and Integration*. World Scientific, second edition, 2006.
- [86] Laurent Younes. *Shapes and Diffeomorphisms*, volume 171 of *Applied Mathematical Sciences*. Springer, 2010.
- [87] Hong-Kai Zhao, Tony F. Chan, B. Merriman, and Stanley J. Osher. A Variational Level Set Approach to Multiphase Motion. *Journal of Computational Physics*, 127:179–195, 1996.